UNDERSTANDING LAMIN A/C

AND ITS ROLES IN DISEASE PATHOLOGIES

AUDREY WANG SHIMEI

BSC (HONS.), NANYANG TECHNOLOGICAL

UNIVERSITY

A THESIS SUBMITTED

FOR THE DEGREE OF DOCTOR OF PHILOSOPHY

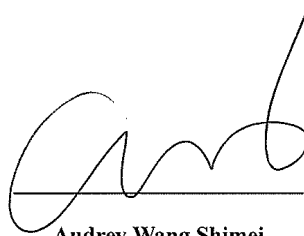## DEPARTMENT OF BIOLOGICAL SCIENCES

NATIONAL UNIVERSITY OF SINGAPORE

2014

DECLARATION

I hereby declare that the thesis is my original work and it has been written by me in its entirety. I have duly acknowledged all the sources of information which have been used in this thesis.

This thesis has also not been submitted for any degree in any university previously.

Audrey Wang Shimei

28th November 2014

ACKNOWLEDGEMENTS

TABLE OF CONTENTS

SUMMARY

The nuclear lamina, comprised of the A and B-type lamins, is important in maintaining nuclear shape and regulating key nuclear functions such as chromatin organization and transcription. Deletion of the A-type lamins results in genome instability and many cancers show altered levels of A-type lamin expression. Loss of function mutations in the *Lmna* gene result in early postnatal lethality, usually within 3-6 weeks of birth making analysis of the role of *Lmna* in carcinogenesis difficult. To circumvent early lethality and determine the role of the A-type lamins in specific tissues in older mice, a "floxed" conditional allele of *Lmna* gene, *Lmna*$^{FL/FL}$, was derived. It has the flexibility to be crossed with different *Cre* deletors to generate constitutive or tissue-specific *Lmna* knockouts. Constitutive deletion of *Lmna* with *Zp3-Cre* was efficient at the genomic and proteomic level. *Lmna*$^{FL/FL}$ mice were then used to generate tissue-specific *Lmna* knockout mice to investigate the physiological and oncogenic roles of *Lmna* in two highly proliferative tissues: the intestines and skin.

Lmna was specifically deleted in the gastrointestinal (GI) epithelium by crossing the *Lmna*$^{FL/FL}$ mice with Villin-Cre mice. *Lmna*$^{\Delta/\Delta/Vil-Cre}$ mice are overtly normal with no effects on overall growth, longevity or GI morphology. On a GI-specific sensitized (*Apc*$^{Min/+}$) background, polyp numbers are unchanged, but polyp size is increased in the duodenum. These findings reveal that although A-type lamins are dispensable in the postnatal GI epithelium,

loss of *Lmna* under malignant conditions enhances polyp size, suggesting that A-type lamins regulate cell proliferation.

The skin is affected in laminopathies such as progeria and restrictive dermopathy. Altered LMNA levels are also observed in human skin cancers. However the exact role of LMNA/C in skin has yet to be elucidated. Through the introduction of *Keratin 14-cre*, a mouse line ($Lmna^{\Delta/\Delta/K14\text{-}Cre}$) was derived where *Lmna* was specifically ablated in keratinocytes. $Lmna^{\Delta/\Delta/K14\text{-}Cre}$ mice show epidermal thickening in the skin due to hyperplasia. In addition, $Lmna^{\Delta/\Delta/K14\text{-}Cre}$ mice also show aberrant hair cycles where the onset of the second hair growth phase is greatly accelerated. Human $LMNA^{KD}$ keratinocytes also exhibit a pronounced acceleration in growth. Consistently, loss of *Lmna* altered expression of genes associated with hyperproliferation and malignant transformation of keratinocytes. Collectively, these results indicate that A-type lamins are important in keratinocyte growth and hair cycle regulation.

In collaboration with Solovei and colleagues, we show that lamin A/C and LBR are important in the regulation of peripheral heterochromatin positioning in mammalian cells. Absence of both lamin A/C and LBR results in the loss of peripheral heterochromatin and pronounced inversion of nuclei. Furthermore, loss of lamin A/C results in prolonged LBR expression, indicating that lamin A/C plays a significant role in regulating LBR expression during differentiation. During muscle development, lamin A/C and LBR have opposing effects with lamin A/C increasing and LBR decreasing muscle gene

transcription. Taken together, lamin A/C and LBR have important roles in regulation of chromatin organization and cellular differentiation.

LIST OF TABLES

LIST OF FIGURES

LIST OF SYMBOLS

AD-EDMD	Autosomal-dominant Emery-Dreifuss muscular dystrophy
ADLD	autosomal dominant leukodystrophy
BAF	barrier-to-autointegration factor
BCC	basal cell carcinoma
BMP	bone morphogenetic protein
bp	base pair
BSA	bovine serum albumin
CB	Cajal Body
CDKs	cyclin-dependent kinases
cDNA	complementary DNA
CMT2B1	Charcot-Marie-Tooth syndrome type 2B1
CNS	central nervous system
CO_2	carbon dioxide
CRC	colorectal cancer
Cre	cyclization recombination
DCM	Dilated Cardiomyopathy
DMBA	7,12-dimethylbenz[*a*]anthracene
EDMD	Emery-Dreifuss muscular dystrophy
EDTA	Ethylenediaminetetraacetic acid
EGF	epidermal growth factor
ER	endoplasmic reticulum
ESCs	embryonic stem cells

FISH	fluorescent in situ hybridization
FBS	fetal bovine serum
FGF	fibroblast growth factors
FPKM	fragments per kilobase
FPLD	familial partial lipodystrophy
GFP	green fluorescent proteins
GI	gastrointestinal
GOC	Gene Ontology Consortium
GT	gene-trapped
H&E	hematoxylin and eosin
HBSS	Hank's Balanced Salt Solution
HCL	hydrochloric acid
HDAC	histone deacetylase
HEM	hydrops-ectopic calcification-moth-eaten
HFs	hair follicles
HGPS	Hutchinson-Gilford progeria syndrome
hMSCs	human mesenchymal stem cells
i.p.	intraperitoneal
IACUC	Institutional Animal Care and Use Committee
ICMT	isoprenylcysteine carboxyl methyltransferase
IECs	intestinal epithelial cells
IF	intermediate filaments
Ig	immunoglobulin
IGF	insulin-like growth factor

ING1	inhibitor of growth 1
INM	inner nuclear membrane
IPA	Ingenuity Pathway Analysis
iPSC	induced pluripotent stem cells
KASH	Klarsicht, Anc-1, Syne homology
KD	knockdown
KGF	keratinocyte growth factor
K-SFM	keratinocyte serum free media
LAPs	Lamina-associated polypeptides
LBR	Lamin B Receptor
LEM	Lap2, emerin, man1
LINC	Linker of Nucleoskeleton and Cytoskeleton
LMG1B	Limb-girdle muscular dystrophy type 1B
MAD	Mandibuloacral dysplasia
MAFs	mouse adult fibroblasts
MEFs	mouse embryonic fibroblasts
MSR	Major satellite repeats
NaOH	sodium hydroxide
NBF	Neutral Buffered Formalin
NE	nuclear envelope
NGPS	Nestor-Guillermo progeria syndrome
NLS	nuclear localization signal
NPCs	nuclear pore complexes
ONM	outer nuclear membrane

ORS	outer root sheath
PAGE	polyacrylamide gel electrophoresis
PBS	phosphate buffered saline
PCA	Principal component analysis
PCNA	proliferating cell nuclear antigen
PFA	paraformaldehyde
PML	promyelocytic leukaemia
PNS	perinuclear space
PP2A	protein phosphatase 2A
pRb	phosphorylated retinoblastoma protein
PTMs	post-translational modifications
qRT-PCR	quantitative real time-PCR
Rb	retinoblastoma
RBBP4/7	retinoblastoma binding protein 4/7
RD	restrictive dermopathy
SA	splice acceptor
SCC	squamous cell carcinoma
SEM	standard error of the mean
SFC	splicing-factor compartments
SUN	Sad1p/Unc-84
TGF-β	transforming growth factor-beta
TPA	12-O-tetradecanoylphorbol 13-acetate
UTR	untranslated region
WT	wild-type

Zp3   zona pellucida 3

Chapter 1 - Introduction

1.1 The nuclear envelope and lamina proteins

1.1.1 <u>The nuclear envelope</u>

The nucleus is a characteristic hallmark in all eukaryotic cells and comprises of the nucleoplasm and nuclear envelope (NE). The nucleoplasm houses the genetic material of the cell and various structural subcompartments such as the nucleolus, splicing-factor compartments (SFCs), the Cajal body (CB) and promyelocytic leukaemia (PML) body (Dundr and Misteli, 2001). The NE encloses and separates the nucleoplasm from cytoplasm. The NE was originally thought to largely function as a selective barrier to regulate the entry and exit of macromolecules, but this view is changing due to immense data that it is involved in the maintenance of nuclear architecture, organization of chromatin, control of DNA replication, transcription and cellular signaling (Burke and Stewart, 2014).

The NE consists of three important elements: the nuclear membranes, nuclear pore complexes (NPCs) and nuclear lamina. The nuclear membranes consist of two lipid bilayers membranes. The outer nuclear membrane (ONM), facing the cytoplasm, is continuous with the rough endoplasmic reticulum (ER) and associates with ribosomes and a variety of other ONM-specific proteins (Stewart et al., 2007b) (Fig. 1.1). The inner nuclear membrane (INM), facing the nucleoplasm, contains some 70 or more unique transmembrane proteins that are anchored to the INM during interphase (Schirmer et al.,

2003). The ONM and INM are separated by a 40-50 nm perinuclear space (PNS) (Stewart et al., 2007b), but periodically connected where they are transversed by NPCs that are important in moving macromolecules between the cytoplasm and nucleus (Grossman et al., 2012). Underlying the INM is the 10-20 nm thick nuclear lamina, a proteinaceous meshwork comprised of the type V intermediate filaments (IF) collectively termed the lamins (Dwyer and Blobel, 1976; Fisher et al., 1986), which are found exclusively in the nucleus (Gerace and Huber, 2012) (Fig. 1.1).
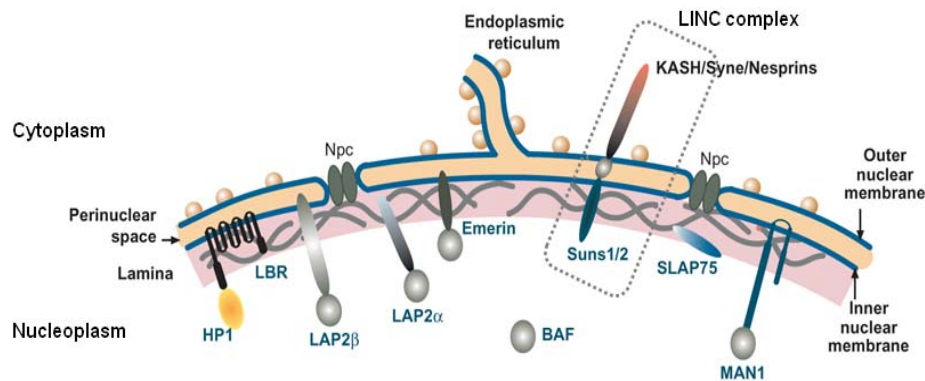
Figure 1.1: The NE consists of three important elements: the nuclear membrane, nuclear pore complexes (NPCs) and the nuclear lamina. The nuclear membrane consists of an outer nuclear membrane (ONM) contiguous with the endoplasmic reticulum (ER) and faces the cytoplasm, and an inner nuclear membrane (INM), which faces the nucleoplasm. Underlying the INM is a meshwork of intermediate filaments comprised of the A-type and B-type lamins known as the nuclear lamina. The nuclear lamina and the integral INM proteins (including LBR, emerin, MAN1) that it harbors have important functions such as chromatin organization and gene regulation. The LINC (linker of nucleoskeleton and cytoskeleton) complex (dashed box) comprising of SUN and KASH proteins has important connections to the cytoskeleton. Illustration was adapted and modified with permission (Burke and Stewart, 2014).

1.1.2 <u>The nuclear lamins</u>

Lamins are the major structural components of the proteinaceous nuclear lamina. Nuclear lamin isoforms are divided into two major classes

based on their sequence homologies, structural similarities, isoelectric points, expression patterns and behavior during disassembly and assembly on the NE during cell division (Broers et al., 2006). The B-type lamins have acidic isoelectric points and are membrane associated throughout the cell cycle, whereas A-type lamins have neutral isoelectric points and are solubilized during mitosis (Burke and Ellenberg, 2002; Gerace and Blobel, 1980).

1.1.3 Genes encoding lamins

A-type lamins (lamin A, lamin C, lamin C2 and lamin AΔ10) are encoded by a single *LMNA* gene on human chromosome 1q21.2 (Furukawa et al., 1994; Lin and Worman, 1993; Machiels et al., 1996) and generated by alternate splicing at exon 10. Lamins A and C are the major A-type lamins: lamin A contains 12 exons while lamin C is identical except for lacking part of exons 10 to 12 of the *LMNA* gene (Lin and Worman, 1993) (Fig. 1.2). Lamin C2 is a minor splice variant of *LMNA,* with an identical sequence to lamin C but lacking the N-terminal head (Furukawa et al., 1994). Lamin AΔ10 is an alternatively spliced product that lacks all of the residues encoded by exon 10 of the *LMNA* gene (Machiels et al., 1996).

There are three mammalian B-type lamins. *LMNB1* on human chromosome 5q23.3-q31.1 encodes lamin B1, *LMNB2* on human chromosome 19p13.3 encodes lamin B2 (Furukawa and Hotta, 1993; Hoger et al., 1988; Zewe et al., 1991). Lamin B3 is a minor variant that arises from alternate splicing of *LMNB2* (Biamonti et al., 1992; Furukawa and Hotta, 1993).

3

1.1.4 Structure of lamins

Lamins have a highly conserved tripartite domain organization typical of type V IF. They have a short globular head domain, a central α-helical rod consisting of 4 coiled-coil segments separated by linker regions, and a globular COOH-terminal tail domain (Fisher et al., 1986; Herrmann and Aebi, 2004) (Fig. 1.2). The central rod domain is essential for the formation of parallel coiled-coil lamin dimers that are required for the assembly into higher order structures (Aebi et al., 1986). The tail domain contains an approximately 120 residue immunoglobulin (Ig) fold (Krimm et al., 2002) and both the head and tail domains of the lamins are highly positively charged which is important for their potential interaction with DNA and other proteins (Stierle et al., 2003). Lamins also contain a nuclear localization signal (NLS) located between the rod domain and the Ig fold (Frangioni and Neel, 1993) and mutations in the NLS cause mislocalization of nuclear lamins to the cytoplasm (Loewinger and McKeon, 1988). The tail domains of lamin A (but not lamin C) and B-type lamins contain a CAAX motif ("C" is Cysteine, "A" is an aliphatic residue and "X" can be any amino acid, but usually is a Methionine) (Fig. 1.2), that is involved in numerous post-translational modifications (PTMs) important for the efficient targeting of lamins to the INM (Dechat et al., 2007).
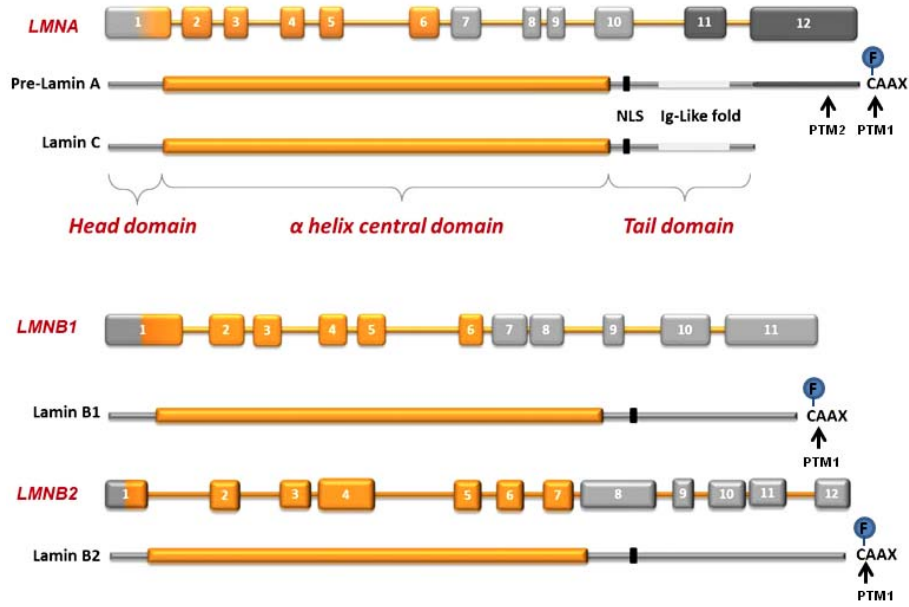
Figure 1.2: A- and B-type lamins have similar structural domains and undergo post-translational modifications (PTMs) to produce mature lamins. Lamin A and C are encoded by the same gene (*LMNA*) and arise through alternate RNA splicing while B-type lamins are encoded by two separate genes (*LMNB1* and *LMNB2*). Lamins have a conserved tripartite structure consisting of a short globular head, a α-helical central rod and a tail domain. Both A and B-type lamins contain a nuclear localization signal (NLS, black rectangle) and immunoglobulin (Ig) fold (light grey regions) at their tail domains. Immature pre-lamin A undergoes two PTMs (PTM1 and PTM2, black arrows) to release a mature lamin A protein while lamin C lacks the CAAX motif and does not undergo PTMs. Lamin B1 and B2 undergo only one PTM (black arrows) and stay farnesylated (blue circle F). Illustration was adapted and modified with permission (Mendez-Lopez and Worman, 2012).

1.1.5 Post-translation processing of lamins

Lamin A and the B-type lamins are synthesized as precursors prelamin A, prelamin B1 and prelamin B2. These prelamins undergo a series of four enzymatic post-translational processing steps to yield mature and functional lamin proteins. First, the cytosolic enzyme farnesyl transferase catalyzes the farnesylation of cysteine of the CaaX motif. ZMPSTE24/FACE1, a membrane zinc metalloproteinase, removes the –aaX amino acids. The newly exposed farnesyl-cysteine is then methylated by a membrane methyltransferase,

isoprenylcysteine carboxyl methyltransferase (ICMT) (Casey, 1992; Casey and Seabra, 1996; Clarke, 1992; Davies et al., 2009). Farnesylation is important in targeting the newly synthesized lamins to the NE by enhancing protein hydrophobicity (Holtz et al., 1989). At the nuclear lamina, prelamin A undergoes the final proteolytic cleavage by ZMPSTE24/FACE1, which releases the last 15 amino acids of the protein to generate a mature lamin A containing 646 amino acids. B-type lamins, on the other hand, remain permanently farnesylated (Gerace et al., 1984; Pendas et al., 2002; Weber et al., 1989) (Fig. 1.2). Other PTMs of lamins include phosphorylation (Stuurman et al., 1998) and sumoylation (Zhang and Sarge, 2008); defects in these PTMs can hinder proper assembly of the nuclear lamina. Lamin C (562 amino acids) does not contain the CaaX motif at the C-terminus nor undergoes PTMs and may rely on the presence of lamin A to incorporate into the nuclear lamina (Vaughan et al., 2001) although a lamin C only mouse has been derived and is overtly normal (Fong et al., 2006).

1.1.6 Expression profile of lamins

The A- and B-type lamins are differentially expressed in mammalian tissues (Broers et al., 1997). Studies tracing the expression of A-type lamins from embryonic stage to birth indicate that expression of lamin A is developmentally regulated in a tissue-specific manner (Rober et al., 1989; Stewart and Burke, 1987). All cells express either one or both of the B-type lamins. In contrast, expression of A-type lamins, though present in the fertilized egg, disappear during pre-implantation development and only start to

reappear, initially in the trophoblast and visceral endoderm and then in the embryo proper at around E10 to E12, when basic organogenesis and tissue differentiation occur (Rober et al., 1989; Stewart and Burke, 1987). The onset of lamin A/C expression is not simultaneous in all tissues of the embryo proper, as its expression is first detected at E10 in skeletal and smooth muscle but does not appear until after birth in other organs such as the heart, liver, lungs and intestine. Furthermore, brain cells and undifferentiated lymphoid cells of the spleen, thymus, blood and bone marrow from postnatal day 15 (P15) mice show little or no expression of lamin A/C. However, once the lamin A/C expression sets in, it persists and becomes increasingly prominent.

These studies by Stewart and Burke and then Rober *et al.* were the first to establish that lamin A/C is expressed in differentiated adult cells, but absent from embryonic stem cells (ESCs). It has since been confirmed that A-type lamins are not expressed in either human or mouse ESCs (Butler et al., 2009; Constantinescu et al., 2006), suggesting that A-type lamins are non-essential at the cellular level during development. Indeed, mice lacking lamin A/C are indistinguishable from their wild-type (WT) littermates at birth. However at about 2-3 weeks after birth, they present defects in skeletal muscle and heart which lead to early lethality (Sullivan et al., 1999). Therefore, A-type lamins may be dispensable for uterine development but appear to serve specialized functions in different postnatal tissues and may be implicated in terminal tissue differentiation during postnatal development (Broers et al., 1997; Goldman et al., 2002; Hutchison et al., 2001). The other lamin A family members are lamin C2 that is uniquely expressed in the testis and lamin AΔ10

is expressed in the human placental, colon and leukocytes as well as a variety of carcinoma cell lines (e.g. lung and neuroblastoma) (Furukawa et al., 1994; Machiels et al., 1995; Machiels et al., 1996).

B-type lamins (lamin B1 and B2) are expressed in embryos and all adult cell types (Broers et al., 1997), while lamin B3 is expressed only in spermatocytes (Furukawa and Hotta, 1993). Since at least one B-type lamin is expressed in all cell types throughout development, it was thought that they may perform essential functions of the lamina (Burke and Stewart, 2013). But despite the dogma that B-type lamins are essential for cell survival, growth and development (Harborth et al., 2001; Vergnes et al., 2004), there have been contradicting reports. Mice deficient in *Lmnb1* undergo prenatal development, but die at birth due to abnormal development of the central nervous system (CNS) and with no evidence of diseased nuclear phenotypes in the skin, liver, heart and skeletal muscle (Vergnes et al., 2004). Deletion of both *Lmnb1* and *Lmnb2* in mouse keratinocytes did not result in overt pathologies in the skin, hair and nails, indicating that complete absence of B-type lamins does not affect keratinocytes development and proliferation (Yang et al., 2011a). Similarly, mice with deletion of both *Lmnb1* and *Lmnb2* in hepatocytes had normal liver development and function (Yang et al., 2011b). In contrast, forebrain-specific deletion of *Lmnb1* and/or *Lmnb2* resulted in mice with a smaller cranium, abnormal neuronal migration and cortical layering defects, indicating that B-type lamins are critical in the survival of neurons and proper development of the CNS (Coffinier et al., 2011). Collectively, these studies indicate that B-type lamins might not be obligatory in cell survival but instead

may exhibit different levels of importance in different cell types. Another explanation is that abundant expression of lamin A/C in skin and liver may compensate and contribute to survival of keratinocytes and hepatocytes. However as lamin A/C expression is low/absent in the brain, the effect of the absence of B-type lamins is more profound in neurodevelopment (Coffinier et al., 2011; Yang et al., 2011a; Yang et al., 2011b).

More interestingly, mouse ESCs and keratinocytes lacking all nuclear lamins are able to proliferate normally (Jung et al., 2014; Kim et al., 2013). Lamin-null ESCs injected into nude mice were capable of teratoma formation, giving rise to endodermal, mesodermal and ectodermal structures (Kim et al., 2013).

1.1.7 <u>Integral membrane proteins of the INM</u>

The INM harbors approximately 70 to 100 unique membrane-associated and integral proteins (Fig. 1.1). The functions of most of these proteins are still poorly understood (Schirmer et al., 2003). Moreover, expression of many INM proteins may also be tissue-specific (Korfali et al., 2012; Solovei et al., 2013). Proteins are localized to the INM via their selective retention that is mediated via interaction with components of the nuclear lamina and chromatin (Powell and Burke, 1990). This interaction is crucial in modulating signaling pathways within and outside the nucleus. Mutations in many of these proteins and complexes are undesirable as they can cause severe human diseases (Burke and Stewart, 2014).

1.1.7a <u>LEM domain-containing proteins</u>

A group of lamin-interacting proteins share a 40 amino acid bi-helical structural motif known as the LEM domain (Lin et al., 2000). Members of the LEM domain-containing protein family include lamina-associated polypeptides (LAP) 2, emerin, MAN1, LEM2, LEM3, LEM4 and LEM5 (Brachner et al., 2005; Cai et al., 2001; Lee and Wilson, 2004; Lin et al., 2000). At the nucleoplasmic side, the LEM domain interacts with a small DNA-binding protein barrier-to-autointegration factor (BAF/BANF1) that binds to and compacts DNA in a sequence-independent manner (Cai et al., 2001; Shumaker et al., 2001). LEM domain proteins anchor heterochromatin to the NE in yeast, which has no lamins, and in *Caenorhabditis elegans (C. elegans)*, which has a single lamin (Ikegami et al., 2010; Mattout et al., 2011).

The LAP family comprises of LAP1 and LAP2. LAP1 does not contain the LEM domain and has three major isoforms (LAP1A, LAP1B and LAP1C) (Martin et al., 1995). LAP1 interacts with Torsin A, a poorly understood nuclear membrane AAA ATPases, through a perinuclear domain (Sosa et al., 2014). LAP1 also specifically associates with B-type lamins (Maison et al., 1997). LEM domain-containing LAP2 consists of a family of 6 isoforms (α, β, δ, γ, ε, ζ) (Berger et al., 1996; Dorner et al., 2007) and interacts with chromatin and lamins (Gant et al., 1999; Yang et al., 1997). All LAP2 isoforms are INM-bound proteins except for LAP2α, which lacks the transmembrane domain, localizes to the nucleoplasm and binds specifically nucleoplasmic A-type lamins (Dechat et al., 2000a; Dechat et al., 2000b). Adult mouse

10

fibroblasts (MAFs) and epidermal progenitor cells deficient in LAP2α display loss of the nucleoplasmic lamin A, indicating that LAP2α associates with A-type lamins (Gotic et al., 2010). *LAP2α*-null mice exhibit hyperproliferation of erythroid and epidermal precursors, an increased myofiber stem cell pool and eventually develop impaired systolic function and extensive fibrosis due to dysregulation of tumour suppressor retinoblastoma (Rb) protein (Gotic et al., 2010; Naetar et al., 2008). Hence, the association of LAP2α, lamin A/C and Rb may be essential in the cell cycle control (Dorner et al., 2007). LAP2α is also expressed during final stage of spermatogenesis and may be involved in chromatin remodeling (Alsheimer et al., 1998). LAP2β specifically binds to B-type lamins (Foisner and Gerace, 1993; Furukawa et al., 1998) and chromosomes and has important functions in lamin assembly and nuclear organization (Gant et al., 1999).

Emerin, encoded by *EMD* gene on chromosome X, binds to all lamins but displays a stronger binding to lamin C (Clements et al., 2000; Fairley et al., 1999; Vaughan et al., 2001). Lamin A binds to the middle of the emerin protein at residue 70-178 (Lee et al., 2001) and is essential for the localization of emerin to the INM (Sullivan et al., 1999; Vaughan et al., 2001). Emerin is ubiquitously expressed in almost all human cell types (Tunnah et al., 2005). While mutations in emerin result in a form of muscular dystrophy (X-linked Emery Dreifuss) in humans (Bione et al., 1994), it is dispensable for cell survival and normal development in mice as *Emd*-null mice are overtly normal with mild retardation in muscle regeneration (Melcon et al., 2006; Ozawa et al., 2006). However, lethality occurs when both LAP1 and emerin are

simultaneously deleted in skeletal muscle, indicating that emerin and LAP1 work together and are essential in skeletal muscle function and maintenance (Shin et al., 2013).

MAN1, encoded by *LEMD3* gene, is a double pass transmembrane INM protein with a nucleoplasmic LEM motif in its N- and C-terminal domain (Lin et al., 2000; Paulin-Levasseur et al., 1996). Both emerin and MAN1 have essential and overlapping functions in chromosomal segregation during cell division (Liu et al., 2003). *Lemd3*-null mice die during embryogenesis due to defective vascularization of the yolk sac (Cohen et al., 2007; Ishimura et al., 2006) and display abnormal heart morphogenesis (Ishimura et al., 2008). MAN1 interacts with receptor regulated SMAD (rSMAD) so antagonizing transforming growth factor-β (TGF-β) and bone morphogenetic proteins (BMP) signaling pathways (Hellemans et al., 2004; Lin et al., 2000; Osada et al., 2003; Pan et al., 2005). Loss of MAN1 results in increased phosphorylation and hyperactivity of SMAD2/3 (Cohen et al., 2007).

1.1.7b <u>Lamin B Receptor (LBR)</u>

LBR protein binds to the B-type lamins via its nucleoplasmic N-terminal domain (Worman et al., 1988). The Tudor domain at the N-terminus of LBR selectively interacts with heterochromatin (Hirano et al., 2012; Makatsori et al., 2004; Olins et al., 2010), heterochromatin protein HP1 (Ye et

al., 1997) and RNA helicase A binding protein HA95 (Martins et al., 2000). It possesses a short hydrophobic C-terminal domain with 8 transmembrane segments that exhibit sterol reductase activity (Fig. 4.1) (Holmer et al., 1998; Silve et al., 1998). During human fetal development, LBR and its sterol reductase activity is critical for normal chondro-osseous calcification and loss of LBR results in fetal lethality (Waterham et al., 2003).

Mice with mutations in their *Lbr* gene (*ic^J* and *Lbr$^{Gt/Gt}$*) display overt phenotypes such as ichthyosis with dry skin and alopecia, syndactyly, severe growth retardation and often early postnatal death. Non-segmented nuclei and abnormal chromatin organization are also observed in neutrophils and eosinophils in the *ic^J* and *Lbr$^{Gt/Gt}$* mice (Cohen et al., 2008; Shultz et al., 2003). Recent evidence has revealed that LBR may have close proximity with lamin A (Roux et al., 2012) and they both function in retaining heterochromatin at the nuclear periphery (Solovei et al., 2013). In chapter 4 of this thesis, we show that LMNA/C and LBR sequentially tether heterochromatin to the nuclear periphery and loss of both proteins results in the displacement of heterochromatin to the nuclear interior resulting in nuclear inversion (Solovei et al., 2013).

1.1.7c <u>SUN and KASH proteins</u>

The SUN (Sad1p/Unc-84) family consists of at least six proteins and the two most widely expressed isoforms, SUN1 and SUN2, localize to the

13

INM (Starr and Han, 2002). In mice, SUN1 is required for gametogenesis hence both male and female mice lacking SUN1 are infertile (Chi et al., 2009; Ding et al., 2007). The N-terminal regions of SUN1 and SUN2 proteins extend into the nucleoplasm and interact with lamins and other nucleoplasmic factors. The C-terminal regions of SUN1 and SUN2 proteins extend into the PNS and bind KASH (Klarsicht, Anc-1, Syne homology) proteins by interactions between the SUN and KASH domains respectively (Burke and Stewart, 2013; Crisp et al., 2006; Haque et al., 2006; Sosa et al., 2013; Sosa et al., 2012). Therefore, SUN1 and SUN2 function as bridge proteins connecting the nuclear lamins and other components of the nuclear interior to the cytoskeleton networks via KASH proteins and this assembly is known as the LINC (linker of nucleoskeleton and cytoskeleton) complex (Fig. 1.1) (Crisp et al., 2006; Padmakumar et al., 2005).

The KASH (Syne/Nesprins) family consists of six mammalian proteins that contain the conserved 50-60 amino acids C-terminal KASH domain with them being mostly localized to the ONM (Crisp et al., 2006). The members include Nesprins 1-4, KASH 5 and lymphoid-restricted membrane protein (LRMP) (Horn et al., 2013b; Lindeman and Pelegri, 2012; Zhang et al., 2001). KASH proteins are important in the control of cell polarization (Roux et al., 2009), centrosome positioning (Zhang et al., 2009), neuronal cell migration (Tsai and Gleeson, 2005), nuclear positioning (Horn et al., 2013a) and maintenance of cytoskeleton architecture (Warren et al., 2005). The LINC complex mechanically couples the lamina/nucleoplasm to the cytoplasmic cytoskeleton including the 3 different cytoskeletal networks, namely the actin,

14

microtubule and intermediate filaments. Except LRMP, all nesprin proteins interact with different components of the cytoskeleton (Burke and Stewart, 2014). Both Nesprins 1 and 2 connect the nucleus to actin cytoskeleton to anchor or move nuclei. Nesprin 3 binds to plectin which acts as a link to the intermediate filament network. Nesprin 2, Nesprin 4 and KASH5 interact with the microtubule network via Kinesin 1 and/or dynein during nuclear migration (Burke and Stewart, 2013; Starr and Fischer, 2005).

Disruption in the LINC complex results in disease phenotypes. For example, mice lacking SUN1 or KASH4 show progressive hearing loss as outer hair cells of the cochlea display impaired nuclear positioning and cell motility (Horn et al., 2013a). KASH5 forms a meiotic complex with SUN1 and is required for male and female gametogenesis in mice (Horn et al., 2013b). Together with the nuclear lamina, LINC complex forms a structural and functional connection between the nucleus and cytoplasm that may be important for maintaining nuclear architecture, high-order chromatin arrangement (Ding et al., 2007; Sato et al., 2009), nuclear migration (Mosley-Bishop et al., 1999; Zhang et al., 2009), and proper nuclear anchorage and positioning (Luxton et al., 2010).

1.2 Functions of Lamins

The NE was originally thought to largely function as a selective barrier to regulate the entry and exit of macromolecules and the nuclear lamina being

an inert scaffolding structure providing mechanical support to the nucleus and for maintaining nuclear shape. However emerging data now shows that the nuclear lamina and INM proteins are also critical to processes such as chromatin organization, DNA synthesis, transcription control, cellular differentiation, cell migration, signal transduction and cell cycle control. Lamins directly and/or indirectly participate in the fundamental functions of striated and cardiac muscles, fat, glucose metabolism, bone formation and even aging and cancer (Burke and Stewart, 2014).

1.2.1 <u>Maintenance of the nuclear architecture</u>

The nuclear lamina is an important determinant of nuclear architecture and has an essential role in the NE integrity. It determines the overall shape and size of the interphase nucleus and provides structural stability to the nucleus. In particular, A-type lamins are the principal contributors to the biophysical properties of the lamina, providing mechanical strength and stiffness to the nuclei (Lammerding et al., 2006). Loss of lamin A/C in mouse embryonic fibroblasts (MEFs) causes the nucleus to lose its rounded morphology, and become defective in shape with increased numbers of nuclear blebs. This also makes the nucleus more prone to damage arising from physical mechanical stress (Lammerding et al., 2004; Sullivan et al., 1999). When compared to nuclei in soft tissues (e.g. fat and brain), higher expression levels of A-type lamins are detected in stiff tissues (e.g. cartilage and bone) with the A-type lamins contributing to nuclear stiffness and preventing nuclear distortion in these tissues (Swift et al., 2013). In contrast, fibroblasts deficient

in lamin B1, though displaying nuclear deformations, did not lose nuclear stiffness (Lammerding et al., 2006).

Besides providing structural support, the NE with the lamina, also functions as a scaffold for the proper localization of nuclear membrane proteins, NPCs and peripheral chromatin (Burke and Stewart, 2014). In particular, A-type lamins mediate the localization and form an interconnected network with LEM domain proteins such as emerin, LEM2 and LAP2 at the INM (Dechat et al., 2000a). In *C.elegans (Ce)*, *Ce*-lamin is central in the formation of a complex involving *Ce*-MAN1, *Ce*-BAF and *Ce*-emerin as RNAi knockdown of *Ce*-lamin resulted in mislocalization of *Ce*-emerin, *Ce*-MAN1 and *Ce*-BAF, together with defects in chromatin segregation during mitosis and aneuploidy (Liu et al., 2003; Liu et al., 2000; Zheng et al., 2000). Loss of lamin A/C causes the relocalization of emerin to the ER (Raharjo et al., 2001; Sullivan et al., 1999), with minor effects on MAN1 (Liu et al., 2003; Mansharamani and Wilson, 2005), nesprins (Zhang et al., 2005) and abnormal aggregation of LAP2α (Pekovic et al., 2007). The lamina anchors NPCs and maintains their normal distribution within the NE via the interaction with Nup153 (Hutchison, 2002; Lenz-Bohme et al., 1997; Smythe et al., 2000).

Lamins contribute to normal chromatin organization and functions. Electron microscopy revealed partial loss of heterochromatin from the lamina in MEFs and cardiomyocytes derived from *Lmna*-deficient mice (Galiova et al., 2008; Nikolova et al., 2004; Sullivan et al., 1999). Fibroblasts from patients with various *LMNA* mutations showed detachment or/and

redistribution of heterochromatin at the nuclear periphery (Capanni et al., 2003; Columbaro et al., 2005; Goldman et al., 2004; Sabatelli et al., 2001). Expression of LMNA/C and LBR is coordinated in a temporally synchronized manner, and important in tethering heterochromatin to the nuclear periphery. Indeed, absence of both LMNA/C and LBR results in chromatin inversion, with heterochromatin being displaced from nuclear periphery to the interior (*see Chapter 4*) (Solovei et al., 2013).

Lamins also contribute to the regulation of the epigenetic signature of chromatin through regulating the stability, localization and/or activity of chromatin associated proteins (Scaffidi and Misteli, 2005; Shumaker et al., 2006). Cells lacking or carrying mutations in *LMNA* exhibit mislocalization and reduced levels of histones binding protein ING1 (inhibitor of growth 1) (Han et al., 2008) and RBBP4/7 (retinoblastoma binding protein 4/7) (Pegoraro et al., 2009). Furthermore, displacement of chromosome 18 was also observed in cells with *LMNA* mutations (Meaburn et al., 2007) and *Lmnb1*-null MEFs (Malhas et al., 2007), suggesting that the lamins play an important role in chromosome positioning and may consequently impact transcriptional regulation of genes located on such chromosomes.

1.2.2 <u>Cytoskeleton organization and function</u>

Lamins interacts with the LINC complex consisting of the SUN/KASH domains to the maintain nuclear shape and cytoskeleton organization (Tzur et al., 2006). This connection is essential in establishing connections between the

nucleoskeleton and cytoskeleton through the binding to actin, microtubules, and cytoplasmic intermediate filaments (Burke and Stewart, 2014). Mutations in lamins affect localization of SUN/KASH proteins and cellular behavior. For example, $Lmna^{Sul-/-}$ MEFs showed defective nuclear mechanotransduction, attenuated NF-kB regulated gene transcription (Lammerding et al., 2004), reduced mechanical stiffness and cytoskeletal disorganization (Broers et al., 2005). Loss of $Lmna$ also resulted in the mislocalization of NE-bound Sun2 and since the ONM localization of Nesprin 2 is dependent on SUN domains, the loss of $Lmna$ may also affect nesprin localization to the ONM (Crisp et al., 2006). When $Lmna^{Sul+/-}$ MEFs expressing $Lmna$ point mutations were exposed to mechanical strain *in vitro*, they displayed greater deformities and impaired nuclear stability compared to $Lmna^{Sul+/-}$ MEFs expressing wild-type $Lmna$. Loss of one copy of $Lmna$ allele is therefore enough to induce defects in the maintenance of proper nucleo-cytoskeleton connection (Zwerger et al., 2013). The nuclear lamina therefore contributes to the maintenance of physical and functional connections throughout the cell.

1.2.3 <u>Involvement in cellular signaling and functions</u>

Other than merely maintaining nuclear integrity, the lamina also has complex roles in the maintenance of fundamental cellular physiology. Lamins are implicated in DNA replication and transcription, regulation of gene expression and signaling, apoptosis, and maintenance of genomic stability (Andres and Gonzalez, 2009; Gerace and Burke, 1988; Goldman et al., 2002; Moir et al., 1994; Stuurman et al., 1998; Sullivan et al., 1999).

1.2.3a <u>Lamins in DNA replication</u>

Roles of lamins in DNA replication surfaced when lamin B1 was found at proliferating cell nuclear antigen (PCNA) positive replication foci in late S-phase (Moir et al., 1994) while lamin A localized to replication sites in early S-phase (Kennedy et al., 2000). Experiments using *Xenopus* egg interphase extracts to study nuclear assembly showed that nuclei assembled in a lamin-depleted extract were unable to replicate their DNA (Meier et al., 1991; Newport et al., 1990). When dominant negative *Lmna* mutants were added to *Xenopus* interphase nuclear extracts, redistribution of endogenous lamins into intranuclear foci and inhibition of DNA replication were observed (Ellis et al., 1997; Spann et al., 1997), with lamin A being critical during the chain elongation phase of replication (Moir et al., 2000). *Lmna*-null MEFs showed defective DNA replication and introduction of lamin A in the mutant cells restored the normal rate of DNA replication to that of WT cells (Johnson et al., 2004).

1.2.3b <u>Lamins in gene regulation</u>

B-type lamins bind to RNA polymerase II (pol II) to regulate basic processes of mRNA synthesis (Spann et al., 2002). Both RNAi inhibition of *LMNB1* (Tang et al., 2008) or overexpression of LMNA/C in Hela cells (Kumaran et al., 2002) caused a significant decrease in pol II transcription. A-type lamins may bind the zinc finger transcription factor MOK2 (Dreuillet et al., 2002), sterol response element binding protein SREBP1 (Lloyd et al.,

2002) and c-Fos (Ivorra et al., 2006) to regulate transcription. Lamin A/C is important in the stability, localization and activity of Rb, a tumour suppressor protein which restricts the cell's ability to replicate DNA by preventing its progression from the G1 to S phase by repression of E2F gene activity (Johnson et al., 2004; Ozaki et al., 1994). Loss of A-type lamins and/or LAP2α in MEFs results in the loss of Rb activity and an accelerated S-phase entry (Johnson et al., 2004; Markiewicz et al., 2002). Loss of lamin A also affects downstream effects of TGF-β signaling via alteration of Rb phosphorylation and nuclear protein phosphatase 2A (PP2A) resulting in hyperproliferation of MEFs (Van Berlo et al., 2005). Lamin A may also regulate transcription through its interaction with MAN1, which binds and inhibits SMADs 2/3/4, disrupting TGF-β/BMP signaling (Bengtsson, 2007; Pan et al., 2005; Van Berlo et al., 2005). In the $Lmna^{\Delta9/\Delta9}$ mouse line which expresses a truncated and farnesylated form of lamin A (progerin), MAFs exhibit reduced proliferative capacity and impaired extracellular matrix formation due to reduced transcriptional activity of Wnt signaling components Tcf-1 and Lef1 (Hernandez et al., 2010).

By tethering reporter genes to emerin and Lap2β to monitor their subnuclear localization, it was suggested that the lamina participates in the repositioning of genes to the lamina, which then leads to partial to full transcriptional repression (Finlan et al., 2008; Reddy et al., 2008). Conversely, tethering lamin B1 showed that the nuclear lamina may not be a transcriptionally repressive environment (Kumaran and Spector, 2008).

Taken together, the lamina contributes to signaling platforms at both nuclear periphery and nucleoplasm by providing binding sites for regulatory molecules such as transcription cofactors and by creating an environment of active and inactive transcriptional regions through gene repositioning (Burke and Stewart, 2006; Wilson and Foisner, 2010).

1.2.3c <u>Regulation of genomic stability</u>

NE components are also important for proper cell proliferation and mitosis. Disruption of lamins and its interacting partners such as emerin, BAF and MAN1 can result in abnormal mitosis, defective chromosomal segregation and cell death (Liu et al., 2003; Zheng et al., 2000). Loss of lamin A/C in MAFs results in aneuploidy, increased frequency of chromosome and chromatid breaks, telomere shortening, defects in telomere structure and function and defective DNA repair mechanisms as A-type lamins may be important for the recruitment of DNA repair proteins such as p53 binding protein 1 (53BP1), BRCA1 and Rad51 to the sites of DNA damage (Gonzalez-Suarez et al., 2009b; Redwood et al., 2011). Fibroblasts from patients with a truncated form of LMNA (progerin) exhibit increased genomic instability such as nuclear defects, abnormal chromatin structure and increased DNA damage (Bridger and Kill, 2004; Goldman et al., 2004). MEFs and bone marrow cells from *Zmpste24*-deficient mice, a model of premature aging due to disrupted PTM of lamin A, also show increased DNA damage and sensitivity to DNA-damaging agents, delayed checkpoint response and compromised DNA repair due to impaired recruitment of 53BP1 and Rad51 to sites of DNA lesions (Liu

et al., 2005) and defective chromatin remodeling after DNA damage (Liu et al., 2013).

Apoptosis is the process of programmed cell death. Characteristic hallmarks include cell shrinkage, blebbing, DNA fragmentation, presence of micronuclei and chromatin condensation. During apoptosis, chromatin condensation is followed by proteolytic lamin degradation and DNA fragmentation (Neamati et al., 1995; Oberhammer et al., 1994). The presence of degradation-resistant lamins delayed apoptosis, indicating that lamins are important in facilitating cellular apoptotic events (Rao et al., 1996).

In fibroblasts lacking lamin A/C, the nuclear lamina is weakened causing the nuclear envelope to be more susceptible to tearing by ROCK I/Rho kinase compared to WT fibroblasts. This indicates that both a weakened lamina and an intact cytoskeletal actin-myosin-based contraction are required for disruption of nuclear integrity during apoptosis (Croft et al., 2005). In *Lmna*-null mice, spermatocytes exhibited characteristics of apoptosis leading to impaired spermatogenesis (Alsheimer et al., 2004) whereas fibroblasts subjected to mechanical stress displayed increased nuclear deformation and defective NF-κB regulated transcription which has anti-apoptotic roles (Lammerding et al., 2004)..

Introduction of *FACE1/Zmpste24* siRNA to HeLa cells resulted in accumulation of prelamin A and cells displayed apoptotic phenotypes such as nuclear hyperlobulations, increased frequency of micronuclei and mitotic

arrest (Gruber et al., 2005). Dermal fibroblasts from patients with various different *LMNA* mutations also displayed increased micronuclei and apoptosis (Meaburn et al., 2007). These studies show that mutations in *LMNA* result in nuclear deformities, dysregulated signaling pathways culminating to apoptosis, reinforcing the importance of lamin A in the maintenance of genomic stability and its potential role in tumorigenesis.

1.2.3d <u>Regulation of adult stem cell differentiation</u>

While B-type lamins are ubiquitously expressed in all cell types, A-type lamins are absent or expressed in very low levels in ESCs and later upregulated in differentiated cell types, indicating that A-type lamins are critical in postnatal tissue homeostasis in both mouse and human (Constantinescu et al., 2006). An emerging body of evidence suggests that A-type lamins are involved in regulating cell type-specific gene expression and adult stem cells differentiation (Gotzmann and Foisner, 2006; Pekovic and Hutchison, 2008).

Human and mouse progeria fibroblasts exhibit accelerated growth at early passage but undergo premature senescence at later passages (Bridger and Kill, 2004; Mounkes et al., 2003). Introduction of *Lmna* mutants (R453W) in mouse C2C12 myoblasts significantly inhibited differentiation into myotubes while overexpression of WT lamin A delayed the process (Favreau et al., 2004). In adipocytes, lamin A acts as a differentiation antagonist as *Lmna*-null mouse fibroblasts differentiated into adipocytes more readily (Boguslavsky et

al., 2006). In human mesenchymal stem cells (hMSCs), lack of lamin A/C inhibited osteoblast differentiation but instead favoured adipocyte differentiation (Akter et al., 2009). Furthermore, expression of progerin in patients' fibroblast may activate the Notch signaling pathway, resulting in accelerated aging and progressive deterioration of tissue functions (Scaffidi and Misteli, 2008). However, the components of the Notch signaling pathway were not affected when induced pluripotent stem cells (iPSC) differentiated derivatives from HGPS (Hutchinson-Gilford Progeria Syndrome) dermal fibroblasts were analyzed (Zhang et al., 2011).

Zmpste24-null mice exhibit increased numbers, but with a reduced proliferative capacity of epidermal stem cells in their skin, aberrant nuclear structure in the bulge cells and increased apoptotic hair bulb cells. Wnt signaling was also impaired in *Zmpste24*-null mice as both total and activated (nuclear bound) β-catenin were decreased and cyclin D1, a target of the Wnt/ β-catenin pathway, was also significantly reduced (Espada et al., 2008). Disrupted Wnt signaling was also present in cells derived from a progeriod mouse model and in HGPS progeria fibroblasts (Hernandez et al., 2010).

Increases in the progenitor cells proliferation were detected in various tissues such as skin, colon, skeletal muscle and in the hematopoietic system of *LAP2α*-null mice (Gotic and Foisner, 2010; Gotic et al., 2010; Naetar and Foisner, 2009; Naetar et al., 2008). Loss of LAP2α ameliorates the muscular dystrophy resulting from *Lmna* loss possibly through promoting muscle growth, due to increased Smad activity, suggesting an involvement of a

complex containing both lamin A, LAP2α and Smads in the differentiation of tissue progenitor cells and tissue homeostasis (Cohen et al., 2013).

Collectively, these reports indicate that lamin A participates in adult stem cell homeostasis and *Lmna* mutations cause dysfunction in maintenance and differentiation of epidermal, adipogenic and muscle stem cells via disruption of key signaling pathways.

1.3 <u>Diseases associated with the nuclear lamina</u>

The interest in studying the functions of the nuclear lamina was stimulated by the findings that approximately 30 different inherited diseases affecting different organs and tissues had been reported (Worman, 2012; Worman et al., 2010). Defects in nuclear envelope proteins and lamins, including defective post-translational processing of prelamin A, give rise to a wide variety of diseases including muscular dystrophy, lipodystrophy, neuropathy and progeroid syndromes. These diverse and often severe genetic disorders are collectively called the 'laminopathies' (when mutations arise in genes encoding lamins) or 'nuclear envelopathies' (when mutations arise from genes encoding INM and/or NPC proteins) (Worman et al., 2010).
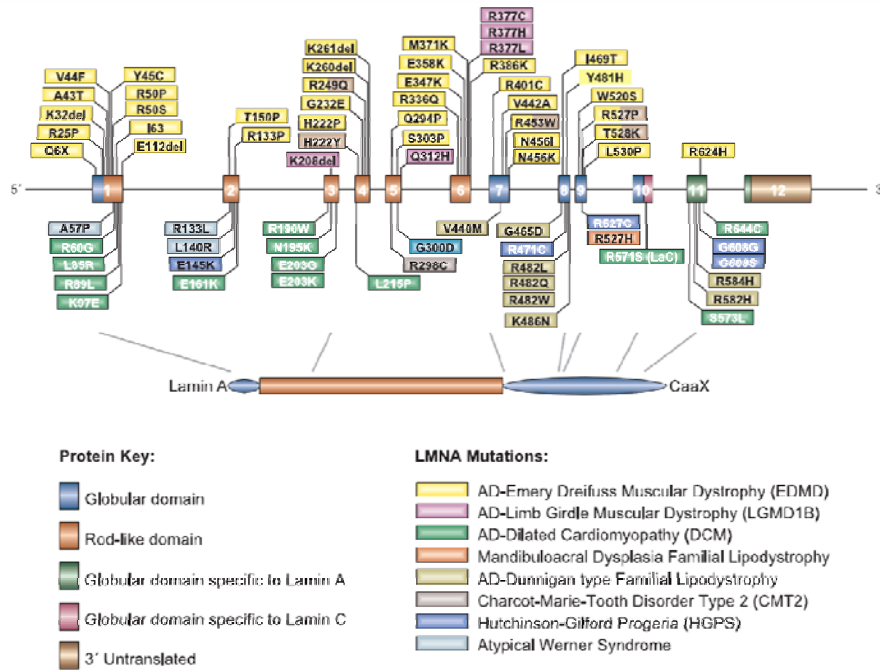
Figure 1.3: Mutations in the *LMNA* gene give rise to a group of severe diseases known as laminopathies. Over 460 different and randomly distributed mutations have been identified in *LMNA*, resulting in diseases affecting various tissues such as the skeletal muscles, cardiac muscles, fat distribution and peripheral nerves. Diagram reproduced with permission (Burke and Stewart, 2006).

1.3.1 Laminopathies

The most significant finding that has catalyzed the increased interest in the lamins has been the discovery that some 13 different diseases are caused by over 460 different mutations throughout the *LMNA* gene (Worman, 2012) (Fig. 1.3). *LMNA* has the largest and most diverse number of disease-linked mutations in the human genome (Burke and Stewart, 2013). These mutations are usually missense mutations scattered across the *LMNA* gene causing the expression of mutated LMNA proteins that have undergone a single amino acid exchange. The diseases associated with mutations in lamins can be classified as primary or secondary laminopathies when mutations arise in

27

LMNA or *ZMPSTE24* gene respectively (Stewart et al., 2007a) and grouped into three broad classes based on the affected tissues.

The first and largest group of laminopathies comprises 60% of all reported cases and primarily affects striated muscle function. Autosomal-dominant Emery-Dreifuss muscular dystrophy (AD-EDMD) is characterized by early joint contractures of the elbows and posterior neck, rigidity of the spine, progressive muscle weakness and wasting in the upper arms and lower legs, and dilated cardiomyopathy which eventually results in heart failure (Bonne et al., 2000; Muchir and Worman, 2007). Limb-girdle muscular dystrophy type 1B (LMG1B) patients suffer from slow progressive muscle weakness in proximal skeletal muscles and dilated cardiomyopathy (Muchir et al., 2000) while isolated Dilated Cardiomyopathy 1A (DCM) patients present cardiovascular defects but minimal to no effects on skeletal muscle (Fatkin et al., 1999). Charcot-Marie-Tooth syndrome type 2B1 (CMT2B1), a form of peripheral neuropathy that results in demyelination of motor nerves and muscle wasting of the limbs, is also included in this first group (Chaouch et al., 2003; De Sandre-Giovannoli et al., 2002).

The second group of laminopathies comprises of Dunnigan-type familial partial lipodystrophy (FPLD) and Mandibuloacral dysplasia (MAD). The development, homeostasis and distribution of adipose tissues are primarily affected in this group of laminopathies. FPLD is autosomal-dominantly inherited with clinical features such as a marked acral loss of subcutaneous white adipose tissue with increased accumulation around the

neck and trunk. It usually manifests with the onset of puberty suggesting that hormonal changes may participate in the initiation of the disease. Hyperlipidemia, insulin resistance followed by type 2 diabetes and increased susceptibility to atherosclerotic heart disease subsequently develops (Vigouroux et al., 2000). Approximately 90% of mutations that cause FPLD are due to a missense mutation in exon 8 of *LMNA* and lead to arginine substitution that changes the surface charge of the Ig-like fold domain in the carboxyl tail of LMNA (Cao and Hegele, 2000; Shackleton et al., 2000). MAD is an autosomal-recessively inherited condition that causes abnormalities in fat distribution and bone formation. Patients present loss of adipose tissues in their extremities with excessive fat accumulation around the neck and face, delayed closure of the cranial sutures, joint contractures and retarded growth. 94% of mutations causing MAD are a missense mutation (R527H) (Novelli et al., 2002).

The third group of laminopathies is principally comprised of Hutchinson-Gilford Progeria Syndrome (HGPS) and atypical Werner's syndrome. They affect multiple systems including the skin, hair, skeleton and especially the vascular system with signs of accelerated aging or progeria syndromes (Burke and Stewart, 2002; Worman and Bonne, 2007). HGPS is a rare (1 in 4 million births), dominantly inherited disease where patients show severe growth retardation, loss of subcutaneous fat, alopecia, skin atrophy, wrinkling, osteoporosis and poor muscle development with an average lifespan of 12 to 15 years, due to fatal arteriosclerotic vascular disease (Merideth et al., 2008; Sarkar and Shinton, 2001). The majority of HGPS

cases are due a de novo point mutation in exon 11 of the *LMNA* gene (c.1824C>T, p.G608G), which introduces a cryptic splice site resulting in an in-frame deletion of 50 amino acids. Consequently, a truncated and farnesylated LMNA protein known as progerin is synthesized while LMNC is unaffected (De Sandre-Giovannoli et al., 2003; Eriksson et al., 2003). Atypical Werner's syndrome arises from missense mutations mostly towards the 5' end of the *LMNA* gene. They are characterized by age-related features such as thinning and graying hair, skin atrophy, myopathy, atherosclerosis and mandibuloacral dysplasia symptoms such as short stature, lipodystrophy, and osteoporosis (Bonne and Levy, 2003; Chen et al., 2003).

Disruption of prelamin A processing to mature lamin A by other mutations also results in progeroid disorders and these diseases are classified as secondary laminopathies as they involve mutations in metalloproteinase *ZMPSTE24/FACE1* (Burke and Stewart, 2006). Complete loss of ZMPSTE24 causes a rare disorder known as Restrictive dermopathy (RD), a perinatal fatal disorder where newborns present severe symptoms such as tight, rigid and erosive skin, epidermal hyperkeratosis, pulmonary hypoplasia, bone density reduction and sparse eyebrows and eyelashes. These newborns usually die within the first week of birth. A study on RD patients revealed that 2 out of 9 patients showed a heterozygous splicing mutation in *LMNA*, leading to a truncated, non-functional prelamin A protein. In the other patients, mutations were found in *ZMPSTE24*, resulting in loss of mature LMNA and mislocalization of lamin B1 and emerin (Navarro et al., 2004).

It is also interesting to note that while different mutations in *LMNA* manifest diverse pathologies, only one disease adult onset autosomal dominant leukodystrophy (ADLD) has been linked to defective duplication of *LMNB1* (Padiath et al., 2006). ADLD is characterized by symmetric demyelization of the central nervous system. Similarly, only one adipose tissue disorder, Acquired Partial Lipodystrophy, has been linked to mutations in *LMNB2* (Hegele et al., 2006). There are no reports of human diseases due to loss of function mutations in lamin B genes, hence it is possible that complete absence of either B-type lamins is embryonic lethal (Vergnes et al., 2004). One study identified 2 unique missense mutations in the *LMNB1* gene in patients with neural tube defects (NTD). These mutations resulted in compromised stability of the LMNB1 protein, and therefore may contribute to the defects in CNS development in these patients (De Castro et al., 2012; Robinson et al., 2013).

1.3.2 <u>Nuclear envelopathies</u>

Nuclear envelopathies refer to diseases that arise due to defects in other proteins in the NE, such as emerin, MAN1, LBR and nesprins. X-linked Emery-Dreifuss muscular dystrophy (EDMD) is caused by mutations in Emerin gene (*EMD*) and patients present very similar clinical features to AD-EDMD patients (Bione et al., 1994). Mutations in *LEMD3* gene that encodes for MAN1 cause disorders such as Buschke-Ollendorff Syndrome with an increase in bone density resulting in osteopoikilosis, a form of sclerosing bone dysplasia which also affects the skin in the form of connective tissue nevi

(skin growths) (Chigira et al., 1991; Hellemans et al., 2004). Melorheostosis also occurs and is characterized by excessive growth of the tubular bone cortex accompanied by abnormalities of adjacent soft tissues such as joint contractures, scleorodermatous skin lesions, muscle atrophy and hemangiomas (Rozencwaig et al., 1997). Mutations in BAF have been linked to atypical Nestor-Guillermo Progeria Syndrome (NGPS) where patients exhibit multiple system disorders such as dry atrophic skin, lipoatrophy and osteoporosis (Cabanillas et al., 2011; Puente et al., 2011). It is plausible that mutations in these INM proteins disrupt the interaction with lamin A/C causing diseases with clinical phenotypes similar to that of laminopathies.

LBR has been implicated in regulating sterol metabolism (Kelley, 2000; Porter, 2003; Waterham et al., 2003) and chromatin organization (Hoffmann et al., 2002; Solovei et al., 2013). Mutations in LBR can lead to mild or severe diseases depending on the site of mutation. Heterozygous *LBR* mutations lead to Pelger-Huët anomaly, a benign condition associated with hypolobulation of granulocyte nuclei and altered chromatin structure (Best et al., 2003; Hoffmann et al., 2002) while the homozygous form of the same disease results in more severe blood phenotype and clinical manifestations such as impaired cognitive development, epilepsy and heart defects (Hoffmann et al., 2007; Oosterwijk et al., 2003). Homozygous *LBR* mutations lead to Greenberg Dysplasia, also known as hydrops-ectopic calcification-moth-eaten (HEM) skeletal dysplasia, due to a "moth-eaten" ectopic skeletal calcifications clinical presentation which is associated with lack of 3-beta-hydroxysterol delta-14 reductase. Clinical manifestations include dwarfism,

polydactyly, disorganization of cartilage and it is characterized by fetal lethality due to fetal hydrops (Waterham et al., 2003). Reynolds syndrome, an autoimmune disorder, can also be caused by missense mutations in *LBR* resulting in primary biliary cirrhosis and limited cutaneous systemic sclerosis (Gaudy-Marqueste et al., 2010).

Mutations in *SYNE1* and *SYNE2*, genes encoding Nesprins 1 and 2 respectively, cause a form of EDMD (Zhang et al., 2007) and cerebellar ataxia (Gros-Louis et al., 2007). A truncated form of the *SYNE4,* gene encoding for Nesprin 4, results in a progressive sound-induced high frequency hearing loss implicating the LINC complex in being essential for hearing (Horn et al., 2013a).

1.3.3 <u>Mechanisms of disease</u>

Studying the laminopathies has stimulated much interest into the roles of lamins and other INM proteins, but the complete understanding of the disease mechanisms still lags. The nuclear lamina functions as a large scaffold and provides docking sites and an organization center for chromatin and other INM proteins. A straightforward explanation of the disease mechanism is that mutations in *LMNA* can disrupt the assembly of lamins into the lamina and when cells are exposed to physical stress, nuclear fragility and cellular damage happen culminating in cell death (Lammerding et al., 2004; Prokocimer et al., 2009). Furthermore, mutations in *LMNA/Lmna* lead to changes in localization and expression of other NE proteins such as emerin (Dechat et al., 2000b;

Raharjo et al., 2001; Sullivan et al., 1999), LAP2α (Dorner et al., 2007; Pekovic et al., 2007), LINC complex (Crisp et al., 2006; Zhang et al., 2005) and chromatin (Capanni et al., 2003; Columbaro et al., 2005; Goldman et al., 2004; Sabatelli et al., 2001; Solovei et al., 2013), thus disrupting the NE composition, nucleo-cytoskeleton network (Zwerger et al., 2013) and chromosome positioning (Meaburn et al., 2007). Hence, mutations in lamin A and/or other INM proteins resulting in disruption of lamin A complexes may be the molecular cause of laminopathies.

However, a large body of evidence revealed that lamin A have roles far beyond nuclear scaffolding, and mutations in lamin A can affect various nuclear functions such as cell cycle progression and differentiation via disruption of Rb (Johnson et al., 2004; Markiewicz et al., 2002; Ozaki et al., 1994), Wnt or TGF-β signaling (Dechat et al., 2007; Hernandez et al., 2010; Van Berlo et al., 2005). Since mutations in INM proteins such as MAN1 cause enhanced TGF-β signaling (Cohen et al., 2007; Hellemans et al., 2004), it is also possible that mutations in lamin A and emerin may cause diseases by altering MAN1 function in certain cell types resulting in tissue-specific alterations in TGF-β signaling (Bengtsson, 2007; Van Berlo et al., 2005). Loss of LAP2α leads to dysregulation of pRb and affects cell cycle control in several cell types such as MAFs, EDMD and HGPS human fibroblasts (Cohen et al., 2013; Dorner et al., 2007; Gotic et al., 2010; Naetar et al., 2008; Pekovic and Hutchison, 2008). Accumulation of prelamin A caused by the loss of *Zmpste24,* as well as progeric mutations, impaired Wnt signaling and altered

34

the proliferative capacity and function of epidermal progenitor stem cells (Espada et al., 2008; Hernandez et al., 2010).

Taken together, lamin A/C together with its potentially large number of interactors, may well be important in the maintenance of an intricate balance between cell proliferation, self-renewal and differentiation. Hence, mutations in the nuclear lamina and/or lamin associated proteins may disrupt several aspects of normal cellular physiology culminating in the drastic phenotypes in the laminopathies. However, the understanding of tissue-specific functions of lamin A and tissue-specific disease mechanisms in laminopathies still lags thus I hope to address this aspect in this thesis.

1.4 <u>Lamins and cancer</u>

Emerging data has indicated that changes in the nuclear lamina not only cause rare occurring laminopathies but may contribute to other diseases particularly cancer (Worman and Foisner, 2010). Alterations in nuclear morphology and architecture are associated with human diseases and are classic hallmarks of cancer cells. Morphological changes in nuclear shape, size, lobulations and heterochromatin appearance are commonly used to identify and evaluate cancer cells, and determine the stage of tumor development to help make a prognosis (Zink et al., 2004).

In recent years, increased interest into the roles of lamins and changes to nuclear structure in malignancy has arisen, since cells with defective lamins

show altered nuclear morphology such as misshapen nucleus, increased incidence of nuclear blebs and lobulations (Broers et al., 1993; Goldman et al., 2004; Tilli et al., 2003). Hence, the role of the nuclear lamina in maintenance of nuclear architecture and flexibility in relation to cell metastasis (Rowat et al., 2013), interactions with cancer gene pathways through regulation of signal transduction pathways such as Rb, Wnt and TGF-β signaling and role in chromosomal segregation and genome stability (Andres and Gonzalez, 2009; Broers et al., 2006; Foster et al., 2010; Gonzalez-Suarez et al., 2009a; Zink et al., 2004) has led to speculations that nuclear lamins have important roles in tumorigenesis (Prokocimer et al., 2009). However, the understanding of specific functions of lamins in the transformation of cells to cancer states remains an enigma and requires further study.

Alterations, including the absence, reduction, or increase in lamin expression and localization, especially lamin A/C, have been reported in leukemias (Kaufmann, 1992), lymphomas (Agrelo et al., 2005), lung (Broers et al., 1993; Machiels et al., 1995), colon (Belt et al., 2011; Willis et al., 2008), skin (Tilli et al., 2003; Venables et al., 2001), ovarian (Capo-chichi et al., 2011), breast and prostate cancers (Capo-chichi et al., 2011; Helfand et al., 2012), suggesting that abnormal lamins expression is closely related to carcinogenesis. However, analysis of lamin expression patterns in different forms of cancer showed that there is no simple trend in expression in one type of human cancer, as expression profiles of the lamins change with tumor subtypes, differentiation and metastatic stages (Prokocimer et al., 2009). Interestingly, even though HGPS patients exhibit dramatically high levels of

DNA damage, only 1 incidence of osteosarcoma (bone cancer), has been reported in a progeria patient diagnosed with Werner syndrome (Fernandez et al., 2014; Goto et al., 1996).

1.5 <u>Mouse models of *Lmna* mutations</u>

Over the past 15 years, mouse models had been created by introducing the same human mutations into the mouse *Lmna* gene (as their nucleotide sequence are more than 95% conserved) to attempt to mimic the phenotypic pathologies. To date, more than 10 lines of mice targeting *Lmna* have been established, many of which present an early postnatal lethality due to detrimental effects in their skeletal and cardiac muscles (Stewart et al., 2007a; Zhang et al., 2013). These mouse models have provided valuable information on effects of mutations in different components of the lamina on various tissues and more importantly, the participation of lamins in various signaling pathways.

The first *Lmna* knockout mouse was created by Sullivan and colleagues, whereby targeted deletion of *Lmna* exons 8 to 11 was performed via homologous recombination (Sullivan et al., 1999). Homozygous *Lmna*-null ($Lmna^{Sul-/-}$) mice developed normally and at birth, did not present any distinguishable phenotype that differs from their heterozygous and WT littermates. However, at 2-4 weeks, $Lmna^{Sul-/-}$ mice showed severe growth retardation, weak limbs and stiff walking posture, and had an average lifespan

of 3-5 weeks. Histological observations of the musculature of the *Lmna$^{Sul-/-}$* mice revealed dystrophic perivertebral muscles, increased nuclear number within muscle fibres and atrophic cardiac myocytes in the heart (Nikolova et al., 2004; Sullivan et al., 1999), which closely resembles the human EDMD pathology (Bonne et al., 2000; Muchir and Worman, 2007).

Since *Lmna$^{Sul-/-}$* mice have no or little pathology at birth, it was evident that lamin A/C may not be important during embryogenesis but becomes increasingly crucial in the postnatal control of tissue homeostasis. Moreover, *Lmna$^{Sul-/-}$* mice displayed only muscle and heart tissue-specific pathologies despite lamin A/C being ubiquitously expressed in most adult tissues (Sullivan et al., 1999). Striated muscle cells are frequently subjected to mechanical stress thus in *Lmna*-deficient cells, increased nuclear deformation and cell injury culminating to cell death was observed (Lammerding et al., 2004). Although mice heterozygous for *Lmna* appear phenotypically normal, they developed dilated cardiomyopathy after 1 year (Wolf et al., 2008). However, a recent reexamination of the *Lmna$^{Sul-/-}$* mice revealed that it is not completely deficient for A-type lamins as a truncated form of *Lmna* gene product (lamin AΔ8-11) at both transcript and protein level was detected at very low levels in the *Lmna$^{Sul-/-}$* mice. It was suggested that this truncated form of lamin A could act as a toxic molecule with a gain-of-function effect, similar to progerin and farnesylated prelamin A, but to a lesser extent based on comparing phenotypes of *Lmna$^{Sul-/-}$* mouse to another mouse model (*Lmna$^{HG/+}$*) with progerin (Jahn et al., 2012).

Other *Lmna*-null mouse lines include *Lmna*$^{\Delta K32/+}$ (Bertrand et al., 2012)*, Lmna*$^{Gt/-}$ (Kubben et al., 2011) and Disheveled Hair and Ear *(Dhe)* - a spontaneous *Lmna* L52R mutation (Odgren et al., 2010). These *Lmna*-null mice develop normally till birth but within 2 weeks of postnatal development, start to present growth retardation, skeletal deformities, defective skeletal and cardiac muscle development, and die by 3 weeks of birth. Heterozygous *Dhe* mice exhibit mild skin and hair anomalies such as sparse and scruffy hair coat, smaller ear pinnae, flaky skin, abnormal skull and bone morphology inferior and reduced body fat while homozygous null mice exhibit multinucleated and apoptotic epidermal cells in the skin along with defective skull growth and mineralization deficiencies (Odgren et al., 2010).

H222P (Arimura et al., 2005) and *N195K* (Mounkes et al., 2005) mutant mice mimic human laminopathies AD-EDMD and DCM respectively. *H222P* mice exhibit a stiff walking posture, cardiac fibrosis with conduction defects and die around 9 months of age. Cardiac and skeletal muscles from these mice showed accumulation of phosphorylated Smad2 and Smad3 in their nuclei (Arimura et al., 2005). Mice homozygous for *N195K* mutation do not exhibit skeletal muscle defects but die around 3 months of age due to cardiac conduction defects and arrhythmia (Mounkes et al., 2005). In a model where mice express only lamin C but not lamin A, mutant mice do not display any overt skeletal, cardiac or skin abnormalities, indicating that the presence of either, not both, lamin A or C is essential for survival (Fong et al., 2006).

A number of different mutant mouse lines had also been established as models for progeria. The *Lmna*$^{\Delta 9/\Delta 9}$ mouse line, to some extent mimics the most common form of HGPS, by introducing a splicing defect in *Lmna* intron 9, resulting in the deletion of *Lmna* exon 9 and consequential in-frame deletion of 40 amino acids resulting in a truncated and farnesylated lamin A. *Lmna*$^{\Delta 9/\Delta 9}$ mice are grossly normal at birth but gradually display pathological phenotypes associated with progeria such as growth retardation, weight loss, lipodystrophy, alopecia, and bone defects. These mice did not survive beyond 4 weeks after birth (Mounkes et al., 2003).

Lmna$^{\Delta 9/\Delta 9}$ MAFs show misshapen nuclei, accelerated senescence and death, similar to phenotypes characteristic to HGPS patients' fibroblasts (Bridger and Kill, 2004; Mounkes et al., 2003). Reduced expression of extracellular matrix components and disrupted Wnt signaling were observed in these MAFs (Hernandez et al., 2010). Increased levels of SUN1 are present in *Lmna*-null MEFs and it accumulates at the NE and Golgi causing abnormal nuclear shape and blebs. Loss of SUN1 rescues the weight loss and shortened lifespan in both *Lmna*$^{Su1-/-}$ and *Lmna*$^{\Delta 9/\Delta 9}$ mice as compound mutants exhibit a longer lifespan possibly due to a rescue of cardiac and skeletal muscle pathologies (Chen et al., 2012). Another mouse model of progeria is the *Zmpste24*-null mouse that unlike humans, do not develop RD or die at birth. Mice deficient in *Zmpste24* are normal at birth but gradually display growth retardation, reduced incisor development, hair loss, skeletal muscle weakness, bone deformities leading to fractured ribs and they eventually die by 6 months of age (Navarro et al., 2005; Pendas et al., 2002).

Although current mouse models of laminopathies have provided tremendous amount of information in the molecular mechanisms of lamin A/C, these constitutive *Lmna* knockout mouse models exhibit early postnatal lethality due to severe phenotypes in the cardiac and skeletal muscles (Bertrand et al., 2012; Mounkes et al., 2003; Mounkes et al., 2005; Sullivan et al., 1999; Yang et al., 2006). Hence it is difficult to study the manifestation of disease phenotypes in other tissues and cell types. The short lifespan of the current models also hinder the possibility to study the association of lamin A/C to cancer. Therefore, it is essential to develop a conditional, true *Lmna*-null mouse model to better understand the roles of lamin A/C in homeostasis and development of tissues, maintenance of genomic stability and involvement in cancer. Through tissue-specific deletion of *Lmna*, it will be more insightful to study the roles of lamin A/C in tissues with less mechanical stress and a milder deleterious effect.

1.6 <u>Cre-lox technology</u>

The Cre-lox technology was used to create conditional *Lmna* tissue-specific mouse lines. It is now a well-characterized tool that allows close regulation of the location and timing of genetic manipulation in yeast, bacteria, mammalian cells and mice (Araki et al., 1997). It is based on the ability of the P1 bacteriophage cyclization recombination (Cre) recombinase gene to catalyze recombination between two 34 base pair (bp) loxP sites (Sauer and Henderson, 1988; Sternberg and Hamilton, 1981). By breeding a

Cre mouse line (containing a *Cre* recombinase transgene under the control of a ubiquitous or tissue-specific promoter) to a loxP line (containing a pair of *loxP* sites flanking critical exons of the gene of interest), "Cre-lox" mice are produced. The orientation and location of the loxP sites determine whether the floxed gene of interest is deleted, inverted or translocated while the regulatory elements that are driving the Cre recombinase determine the location and timing of gene recombination. A general (constitutive) or tissue-specific (conditional) promoter drives the activation of Cre to produce constitutive or tissue-specific knockouts. There are also inducible Cre mice where deletion of the target gene occurs by introducing inducing agents such as doxycycline or tamoxifen at desired developmental stages (Nagy, 2000; Utomo et al., 1999).

Cre-lox conditional mice therefore offer the opportunity to study tissue-specific cell functions of *Lmna* as it allows the analysis of the consequences of deleting *Lmna* in a specific cell type, which may be otherwise obscured by the early lethality of the mice, which occurs when the *Lmna* is deleted in all tissues.

1.7 <u>Aims and objectives</u>

Mutations in *LMNA* result in laminopathies, a group of diseases which show tissue specificities. This has led to the question on how different mutations in a single *LMNA* gene that is almost ubiquitously expressed in adult tissues can lead to different tissue-specific diseases. Since mice completely null for *Lmna* usually die between 3-5 weeks after birth due to muscular dystrophy and cardiomyopathy (Bertrand et al., 2012; Kubben et al., 2011; Sullivan et al., 1999), this may not be long enough to allow for pathologies to manifest in other tissues. Thus, to increase current understanding of the requirement for *Lmna* in other tissues and the various tissue-specific diseases it causes, I sought to employ the Cre-lox system to derive mouse lines with tissue-specific deletions of the *Lmna* gene to investigate the physiological roles of *Lmna* in two highly proliferative tissues: the skin and intestinal epithelium.

Furthermore, the availability of a conditional *Lmna* knockout mouse provides a major opportunity to study cancer formation in tissues such as the intestinal epithelium and skin epidermis where lamin A/C levels were shown to be altered during cancer (Foster et al., 2010). Lamin A/C has important roles in nuclear dynamics, chromatin organization, gene regulation and DNA repair (Prokocimer et al., 2009; Redwood et al., 2011), all of which are critical events that can impact cancer development and progression. Therefore, I hypothesized that loss of *Lmna* may lead to increased tumorigenesis. This

thesis aims to test this hypothesis using *Lmna* mutant mouse lines generated in the laboratory.

In this thesis, I report the generation and characterization of a conditional *Lmna* mouse model, which has the flexibility to be crossed with ubiquitous or tissue-specific promoter-driven Cre deletors to generate mouse lines lacking *Lmna* in specific tissues. As a start, I determined the success of deleting *Lmna* using a global zona pellucida 3-Cre (*Zp3-Cre*) deletor and characterized this constitutive *Lmna* knockout mouse line. I aimed to investigate the roles of lamin A/C in two tissues characterized by high levels of cell turnover: the skin and intestinal epithelium. I bred Villin-Cre (*Vil-Cre*; driven by the villin promoter in the intestinal epithelium) (Madison et al., 2002) and Keratin 14-Cre (*K14-Cre*; driven by human keratin 14 promoter in the skin epidermis) (Vasioukhin et al., 1999) mice to floxed *Lmna* mice to specifically delete *Lmna* in the gastrointestinal (GI) epithelium and skin epidermis respectively, and studied the effects of its absence thereafter.

Utilizing the non-lethal $Lmna^{\Delta/\Delta Vil\text{-}Cre}$ mouse model where *Lmna* is ablated in the GI epithelium, I aimed to evaluate the effects *Lmna* has on the morphology and proliferation of normal GI epithelium. Then, to test whether loss of *Lmna* contributes to tumorigenesis or become more resistant to formation of intestinal adenomas, I generated $Lmna^{\Delta/\Delta/Vil\text{-}Cre}/Apc^{Min/+}$ mice and analyzed polyp formation in the mice.

Since different mutations in *LMNA* lead to laminopathies affecting the skin, it is evident that lamin A/C has an important role in the proper homeostasis of the skin and hair. Therefore, utilizing the non-lethal keratinocyte-specific *Lmna* knockout mice, I aimed to investigate the requirement for lamin A/C in epidermal homeostasis and maintenance of genomic stability. In particular, I am interested to elucidate the mechanisms of lamin A/C in keratinocyte proliferation, skin homeostasis, hair formation, hair cycling, and carcinogenesis. To investigate whether *Lmna* loss accelerates tumor formation in skin, I will also perform cutaneous two-stage chemical carcinogenesis on *Lmna*-deficient mice to induce papillomas formation.

In addition, the $Lmna^{\Delta/\Delta}$ and $Lbr^{GT/GT}$ mutant mouse lines (also generated in our laboratory) were used to study the regulation of chromatin organization. Eukaryotic cells contain heterochromatin that underlines the NE with the exception of photoreceptor rod cells of nocturnal animals. Rod cells lack peripheral heterochromatin and exhibit inversion of euchromatin and heterochromatin positions to reduce light loss to the retina and adapt to nocturnal vision (Solovei et al., 2009). Rod cells with inverted nuclei lack both LMNA/C and LBR, whereas cells with a conventional chromatin pattern express either LBR or LMNA/C, indicating that the presence of either protein is enough for proper heterochromatin distribution (Solovei et al., 2013).

Therefore to expand our knowledge on how NE proteins LMNA/C and LBR can regulate chromatin distribution, a collaboration was established with Dr. Irina Solovei to investigate chromatin organization in the $Lmna^{\Delta/\Delta}$ and

Lbr^{GT/GT} mouse lines. We sought to understand the spatio-temporal expression patterns of LMNA/C and LBR in different mammalian cell types and whether they serve distinct functional roles in terms of cellular differentiation. Then, we also investigated if absence of both LMNA/C and LBR results in nuclear inversion in cell types other than rods and ultimately hope to elucidate the mechanisms of LMNA/C and LBR in the regulation of chromatin organization in mammalian cells.

Chapter 2 - Materials and Methods

2.1 Mouse husbandry

Mice were kept and bred in cages with 12 hour light periods at the animal facility in Biological Research Centre, A-STAR, Singapore. Mice were supplied with Altromin standard diet pellets and drinking water *ad libitum*. Sex determination and weaning of pups were performed from postnatal day 20 (P20) onwards, and 2mm tail tip tissues were collected for genotyping. Mice were sacrificed by CO_2 euthanasia when tissues were harvested. All experiments in this thesis were approved by the Institutional Animal Care and Use Committee (IACUC) review board.

2.2 Generation of *Lmna*$^{\Delta/\Delta}$ knockout mice

To obtain global deletion of the floxed *Lmna* allele (*Lmna*$^{FL/FL}$), *Lmna*$^{FL/FL}$ mice were bred to mice with Cre recombinase driven by the regulatory sequences of the mouse zona pellucida 3 (*Zp3*) gene (JAX stock 003651) (de Vries et al., 2000). Subsequently, female mice with *Lmna*$^{FL/+}$ *Zp3-Cre*$^+$ alleles were bred to C57BL6 WT mice that then give heterozygous (*Lmna*$^{\Delta/+}$) offspring. In the third round of mating, heterozygous male and female breeding were set up to obtain constitutive homozygous knockout (*Lmna*$^{\Delta/\Delta}$) mice. The colony is subsequently maintained by mating heterozygous male and female *Lmna*$^{\Delta/+}$ mice. The body weight of the mice

was measured at P12-14 and quantitative statistical analysis of body weight and survival rate was performed using Graphpad Prism software.

2.3 Genotyping of mutant mice

At weaning, tail tip tissues of the mice were collected and DNA was extracted by alkaline lysis. Tail tips were incubated in 25mM NaOH, 0.2mM EDTA solution for 30 mins at 95°C followed by neutralization with 40mM Tris-HCL solution. To test for the presence of loxP sites ($Lmna^{FL}$) and deleted $Lmna$ allele ($Lmna^{\Delta}$), DNA was PCR amplified using MangoMix (Bioline). The sequences of primers used for the genotyping are listed in Table 2.1.

2.4 RNA extraction and quantitative real time-PCR (qRT-PCR)

Mouse tissues and cell lines were harvested, put in Trizol® reagent and immediately snap frozen. Total RNA was extracted using QIAGEN RNeasy kit according to manufacturer's instructions. The quality and quantity of total RNA was determined with NanoDrop spectrophotometer (Thermo Scientific). Subsequently, 10ug of RNA was reverse transcribed to cDNA using the High Capacity cDNA Reverse Transcription Kit (Applied Biosystems) and qRT-PCR was performed on the 7500 Fast Real-Time PCR system (Applied Biosystems) with Fast Sybr Green Master Mix Kit (Applied Biosystems) or TaqMan® Fast Universal PCR Master Mix (Applied Biosystems). The

48

sequences of primers used for all the qRT-PCR experiments are listed in Table 2.2.

2.5 <u>Immunoblot analysis of tissues and cell lines</u>

Mouse tissues and cell lines were harvested, homogenized in RIPA lysis buffer (150mM NaCl, 1.0% NP-40, 0.5% sodium deoxycholate, 0.1% SDS, 50mM Tris, pH 8.0 supplemented with protease inhibitors) and spun at 13,200g, 10 mins, 4°C. Total cell lysate was subjected to polyacrylamide gel electrophoresis (PAGE), transferred to PVDF membrane and blocked with Odyssey Blocking Buffer (Li-Cor Biosciences). The membrane was then incubated with primary antibodies for 1-2h at room temperature or overnight at 4°C. After, the membrane was washed in Tris buffered saline with 0.1% Tween 20 (TBST) washing solution and incubated in Odyssey IR Dye secondary antibodies for 0.5-1h before visualization on the Odyssey Infrared Imaging System (Li-Cor Biosciences). The primary and secondary antibodies used for immunoblot analysis are listed in Table 2.3. The primary antibodies used for detection of LMNA/C are N-18 (goat, 1:200, Santa Cruz) that is specific to an epitope in the first 50 amino acids in LMNA/C.

2.6 <u>Histological studies and immunofluorescence microscopy</u>

Mouse tissues were extracted and fixed in 4% paraformaldehyde (PFA) in phosphate buffered saline (PBS) or 10% Neutral Buffered Formalin (NBF)

for 16-20h, then dehydrated in 70% for at least 24h and processed through conventional tissue processing protocols before they were embedded in paraffin (Leica Microsystems). For histological studies, tissue sections (4-5um) were de-waxed in 100% xylene and rehydrated through sequential steps of 100%, 70% and 30% ethanol, then stained in hematoxylin and eosin (H&E) and imaged using Zeiss Axio Imager Upright Microscope.

For immunofluorescence, sections were de-waxed in 100% xylene and rehydrated through sequential steps of 100%, 70% and 30% methanol before washing with PBS. Antigen retrieval was performed in sodium citrate buffer (DAKO) in a pressure cooker and quenched in 10mg/ml sodium borohydride in PBS for 15 mins. Next, tissue sections were blocked with normal donkey serum, incubated with primary antibodies overnight at 4°C. The next day, the tissue sections were incubated in secondary antibodies and DAPI for 1h, before washing in 100mM copper sulphate dissolved in 50mM ammomium acetate buffer and finally, mounted in Prolong-Gold Anti-fade reagent (Invitrogen). Washes between and after incubation with antibodies were done with PBS (2 x 15mins, rtp). Immunofluorescence images were taken on the Olympus LSM510 confocal laser scanning microscope equipped with Plan Apo 20x-, 40x-, 63x/1.4 NA oil immersion objective and lasers with excitation lines 405, 488, 561 and 594nm.

For immunofluorescence of cryosections, tissues were excised and fixed in 4% PFA for 12-24 hr, infiltrated with 30% sucrose, and embedded in Jung tissue freezing medium (Leica Microsystems). Cryosections (16-20μm)

were prepared and immediately stored at −80°C. Immunostaining was performed as described in (Eberhart et al., 2012). Before immunostaining, tissue sections were dried at room temperature for 30 min, rehydrated in sodium citrate buffer, and subjected to antigen retrieval by heating up to 80-85°C in a microwave. After antigen retrieval, tissue sections were incubated in 0.5% Triton X-100 for 1 hr. Primary and secondary antibodies were diluted in blocking solution (1% BSA, 0.1% Triton X-100, 0.1% Saponin in PBS) and applied for 12-24 hr under glass chambers at room temperature. Washes between and after incubation with antibodies were done with 0.01% Triton X-100, 3 × 30 mins, at 37°C. The primary and secondary antibodies used for immunofluorescence are listed in Table 2.3.

2.7 <u>Extraction and cell culture of mouse adult fibroblasts (MAFs)</u>

2 weeks old $Lmna^{\Delta/\Delta}$ mice and their WT littermates were sacrificed and all four limbs were cut off, muscles were removed from the bones and washed for 20 mins in 2% Penicillin /Streptomycin antibiotic solution, then transferred in Hank's Balanced Salt Solution (HBSS). Next, sterile dispase (2.4U/ml) and collagenase type II (1%) enzyme solution (1:1 volume to tissue weight) was added and tissues were digested at 37°C for 30 mins. Equal volume of DMEM supplemented with 10% FBS (D10) was added and the solution was filtered through a 70 μm filter, then through a 40 μm sterile filter. Cells were centrifuged at 1200 rpm for 5 mins and the pellet was rinsed with D10. Cells were cultured in collagen-plated T75 flasks overnight at 37°C. After 2 days,

cells were passaged onto new flasks and whenever it reached 70-80% confluency.

MAFs were plated onto 100mm petri dishes and harvested when it reached required confluency. D10 media was removed and cells were washed twice with cold PBS. Total RNA extraction was performed by Trizol® extraction and RNAesy kit (QIAGEN) as mentioned in 2.4. For immunofluorescence of cells, during passaging, cells were plated onto glass cover slips in a 6-well dish. After 2 days, D10 was removed and cover slips were fixed with 100% methanol at -20°C followed incubation of primary antibodies at room temperature for 1-2h and secondary antibodies and DAPI for 30 mins and finally, mounted in Prolong-Gold Anti-fade reagent (Invitrogen). Washes after methanol fixation, between and after incubation with antibodies were done with PBS (2x, 5mins). The primary and secondary antibodies used for immunofluorescence are listed in Table 2.3.

2.8 <u>Generation of the *Lbr*$^{GT/GT}$ mice</u>

To obtain *Lbr*$^{GT/GT}$ mice (Cohen et al., 2008), heterozygous breeding of *Lbr*$^{GT/+}$ mice were set up. The sequences of the primers used for genotyping are listed in Table 2.1.

2.9 <u>Microscopy and image acquisition and analysis for chromocenters</u>

Single optical sections or stacks of optical sections were obtained using Leica TCS SP5 confocal microscope equipped with Plan Apo 63x/1.4 NA oil immersion objective and lasers with excitation lines 405, 488, 561, 594 and 633 nm. Dedicated plug-ins in ImageJ program were used to compensate for axial chromatic shift between fluorochromes in confocal stacks, to create RGB stacks/images and to arrange them into galleries (Ronneberger et al., 2008; Walter et al., 2006). Chromocenter number in rod cells was scored on confocal image stacks using ImageJ program.

2.10 <u>Transcriptome analysis of *Lmna*$^{\Delta/\Delta}$ and *Lbr*$^{GT/GT}$ myoblast cultures</u>

Myoblasts cultures were derived from limb muscles of P15/P16 WT, *Lmna*$^{\Delta/\Delta}$ and *Lbr*$^{GT/GT}$ mice using the method described in 2.7. Myoblasts were collected at passage number 2 at 40-50% confluency to avoid tissue culture artifacts. RNA was extracted using Trizol® and QIAGEN RNeasy kit. The transcriptomes of two biological replicate knockouts (*Lmna*$^{\Delta/\Delta}$, *Lbr*$^{GT/GT}$) myoblast transcriptomes were compared to the transcriptomes of their WT littermates.

Starting from 100ng of total RNA, double-stranded cDNA was generated by the Ovation RNA-Seq v2 Kit (Nugen, San Carlos, CA) according to the manufacturer's protocol for myoblast samples. Briefly, total RNA was

reversely transcribed into cDNA using a tagged random primer. The purified double-stranded cDNA was amplified by isothermal amplification enabled by RNase H cleavage of a chimeric RNA-DNA primer that allows for repeated re-priming and strand displacement (Dafforn et al., 2004). 200ng of the resulting double stranded cDNA were random-sheared by sonication (30 on/off cycles of 30 secs each) and subjected to end-repair and adaptor ligation to generate sequencing libraries for the Illumina Genome Analyzer. Each library was barcoded by a distinct 4 nucleotides sequence located at the 5′ end of each library insert in order to allow multiplex sequencing. Six barcoded libraries representing duplicates of $Lmna^{\Delta/\Delta}$, $Lbr^{GT/GT}$ and WT control were pooled and single-end sequenced on 6 lanes on the Illumina Genome Analyzer GAIIx yielding 217 million raw reads with a length of 84 bp. After demultiplexing, barcode trimming and quality filtering each library retained 25 to 30 million reads.

For limb muscle samples, 100ng of total RNA were used to generate strand-specific cDNA libraries using the Encore complete RNA-Seq Kit (Nugen, San Carlos, CA) according to the manufacturer's protocol. Briefly, after first strand synthesis with semi-random hexamers, depleted for rRNA priming sequences, second strand cDNA was tagged with dUTP and selectively digested after library generation. Six barcoded libraries representing duplicates of $Lmna^{\Delta/\Delta}$, $Lbr^{GT/GT}$ and WT control were pooled and single-end sequenced on 2 lanes on the Illumina Genome Analyzer GAIIx yielding 86 million raw reads with a length of 90 bp. After demultiplexing, barcode trimming and quality filtering each library retained around 10 million

reads. Sequencing depth was 35 Mio reads per RNA sample for myoblasts and 7.5 Mio reads per sample for limb muscles.

Reads were mapped to the mouse genome using the splice-junction mapper Tophat (Trapnell et al., 2009). The program module Cuffdiff from the Cufflinks package (Trapnell et al., 2010) was used to obtain normalized FPKM (fragments per kilobase) values and to identify differentially expressed genes by accounting for biological replicates (n = 2) and setting a false discovery rate of 0.05. For assessment of repeat expression, a RepeatMasker file was obtained from UCSC genome browser (http://genome.ucsc.edu), restricted to region not overlapping with annotated genes and the FPKM values were summarized to the different repeat classes using Cuffdiff. All data handling steps were performed on a client-cluster grid with a local instance of the GALAXY platform (Goecks et al., 2010). Gene Ontology analysis was performed using GOrilla (Eden et al., 2009) and GSEA (Subramanian et al., 2005) software.

2.11 Deleting *Lmna* in the intestinal epithelial cells (IECs)

To obtain an intestinal epithelial specific deletion of floxed *Lmna* allele, I used mice (JAX 004586) in which Cre expression is regulated by promoter sequences of mouse Villin (*Vil*) gene (Madison et al., 2002). To obtain *Lmna*$^{\Delta/\Delta/Vil\text{-}Cre}$ mice, male *Lmna*$^{FL/FL}$ mice were bred to female *Vil-Cre* mice. Subsequently, female mice with *Lmna*$^{FL/+}$ *Vil-Cre*$^+$ alleles were bred

55

Lmna$^{FL/+}$ male mice that then give *Lmna$^{\Delta/\Delta/Vil\text{-}Cre}$* offspring. The colony is subsequently maintained by mating *Lmna$^{\Delta/\Delta/Vil\text{-}Cre}$* mice to *Lmna$^{FL/FL}$* mice. The sequences of primers used for genotyping the mice are listed in Table 2.1.

2.12 <u>Isolation of intestinal epithelial cells (IECs)</u>

3 month old *Lmna$^{\Delta/\Delta/Vil\text{-}Cre}$* mice and their WT littermates were sacrificed and their GI tracts (small and large intestines) were removed. Intestines were cut open longitudinally and into smaller pieces, then incubated in pre-warmed PBS containing 30mM EDTA for 10min at 37°C. Intestine pieces were then transferred into ice cold PBS containing Mg^{2+} and Ca^{2+} and shook vigorously. Intestine pieces were again transferred back to fresh pre-warmed PBS containing 30mM EDTA and these steps were repeated twice to obtain IECs (E1 and E2) and the remaining lamina propria and muscularis mucosa (T). IECs were pelleted, homogenized in RIPA lysis buffer and western analysis was performed as mentioned in 2.5. The membrane was first probed with LMNA/C and tubulin antibodies, and then subsequently probed with villin antibody.

2.13 <u>Deriving a tumour-sensitized mouse line lacking *Lmna*</u>

To derive a tumour-sensitized mouse line, *Lmna$^{\Delta/\Delta/Vil\text{-}Cre}$* and *Apc$^{Min/+}$* (Su et al., 1992) mice were intercrossed. The sequences of primers for detection of *Apc* alelles are listed in Table 2.1. Two cohorts of mice

$Lmna^{\Delta/\Delta/Vil\text{-}Cre}/Apc^{Min/+}$ and $Lmna^{WT/WT}/Apc^{Min/+}$ were derived and maintained for 17-30 weeks for intestinal tumours to develop.

2.14 Preparation and scoring of intestinal polyps

$Lmna^{\Delta/\Delta/Vil\text{-}Cre}/Apc^{Min/+}$ and $Lmna^{WT/WT}/Apc^{Min/+}$ mice were sacrificed by CO_2 euthanasia and their GI tract removed, and divided into 5 equal parts- duodenum, proximal jejunum, distal jejunum, ileum and colon. Intestines were fixed in Methacarn fixative (Methanol: Chloroform: Glacial Acetic Acid – 6:3:1) overnight for the visualization of polyps (Kongkanuntn et al., 1999). The next day, the polyps were visualized under a light microscope, and scored according to 3 categories by sizes (0-2mm, 2-5mm and >5mm). Quantitative statistical analysis was performed using Graphpad Prism software.

2.15 Deleting *Lmna* in the intestinal stem cells

To derive an inducible *Cre* deletion of *Lmna*, I crossed $Lmna^{FL/FL}$ mice to *Lgr5-EGFP-IRES-CreERT2* mice (Barker et al., 2007) where deletion of *Lmna* only occurs in the intestines and colon following tamoxifen induction. Tamoxifen (Sigma-Aldrich) was dissolved in 100% ethanol as a 10mg/ml stock. For administration, fresh tamoxifen was prepared daily by centrifugal evaporation into corn oil (Sigma-Aldrich) and a final concentration of 20mg/ml tamoxifen was obtained. $Lmna^{FL/FL/Lgr5\text{-}CreERT}$ mice were injected

with tamoxifen (40mg/kg body weight) via intraperitoneal (i.p.) administration for 3 consecutive days.

Subsequently, to derive alternative tumor-sensitized mouse lines, I bred $Lmna^{FL/FL/Lgr5\text{-}CreERT}$ mice to $Apc^{FL/FL}$ (Cheung et al., 2010) and $p53^{FL/FL}$ mice (Marino et al., 2000) and derived another two lines of double mutant mice ($Lmna^{FL/FL}Apc^{FL/FL/Lgr5\text{-}CreERT}$ and $Lmna^{FL/FL}p53^{FL/FL/Lgr5\text{-}CreERT}$). The efficiency of $Lmna$ deletion was confirmed by genotyping and immunofluorescence staining for lamin A/C in the intestines. The sequences of the primers used for genotyping are listed in Table 2.1.

2.16 Deleting *Lmna* in the keratinocytes of skin and tongue epithelium

To obtain keratinocyte-specific deletion of floxed $Lmna$ allele, I used mice (JAX 004782) in which Cre expression is driven by the human epithelial keratin 14 ($K14$) promoter (Dassule et al., 2000). To obtain $Lmna^{\Delta/\Delta/K14\text{-}Cre}$ mice, female $Lmna^{FL/FL}$ mice were bred to male $K14\text{-}Cre$ mice. Subsequently, male mice with $Lmna^{FL/+}$ $K14\text{-}Cre^{+}$ alleles were bred $Lmna^{FL/+}$ female mice that then gave $Lmna^{\Delta/\Delta/K14\text{-}Cre}$ and $Lmna^{FL/FL}$ offspring. Subsequently, the mouse colony is maintained by mating female $Lmna^{FL/FL}$ mice to male $Lmna^{\Delta/\Delta/K14\text{-}Cre}$ mice. The Cre gene was never introduced through the mother as maternally inherited $K14\text{-}Cre$ was reported to be active in oocytes and resulted in loxP flanked sequences to be deleted ubiquitously (Hafner et al., 2004).

$Lmna^{\Delta/\Delta/K14\text{-}Cre}$ mice on a FVB/N background were also established by backcrossing both $Lmna^{FL/FL}$ and $K14\text{-}Cre$ mouse lines to WT FVB/N females for 3 generations. Then, female $Lmna^{FL/+}$ mice were bred to male $K14\text{-}Cre$ mice for another two crosses to obtain $Lmna^{\Delta/\Delta/K14\text{-}Cre}$ (FVB/N) mice. The mouse colony is maintained by mating female $Lmna^{FL/FL}$ mice to male $Lmna^{\Delta/\Delta/K14\text{-}Cre}$ mice. This line of mice was used for two-stage chemical carcinogenesis experiments as mentioned in 2.22 since mice on C57/BL6 background has been reported to be resistant to chemical-induced cutaneous carcinogenesis (Hennings et al., 1993).

2.17 <u>Measurement of epidermis thickness in $Lmna^{\Delta/\Delta/K14\text{-}Cre}$ mice</u>

$Lmna^{\Delta/\Delta/K14\text{-}Cre}$ mice and their WT littermates were sacrificed and their hair on the dorsal back and ventral side was shaved, and a small piece of dorsal and ventral skin (0.5cm x 0.5cm), tongue, and hind paws were removed. Tissues were fixed in 4% PFA or 10% NBF overnight and tissue processing was performed as mentioned in 2.6. H&E staining was performed on tissue sections and images were captured by light microscopy. To measure the thickness of the epidermis in the different parts of the skin, the images were processed on Adobe Photoshop CS4 and the thickness of the epidermis was measured by taking the average of at least 20 widths at random locations along the length of epidermis. This was repeated for at least 3 biological replicates for both $Lmna^{\Delta/\Delta/K14\text{-}Cre}$ and WT mice for all tissues examined.

Quantitative statistical analysis was performed using Graphpad Prism software.

2.18 Analysis of hair cycle in $Lmna^{\Delta/\Delta/K14\text{-}Cre}$ mice

At P16, $Lmna^{\Delta/\Delta/K14\text{-}Cre}$ mice and their WT littermates were anesthetized with 250mg/kg body weight Avertin (12.5 mg 2,2,2 Tribromoethanol/ml, i.p.) and their hair on the dorsal back was shaved. Dorsal skin pigmentation was recorded and subsequently, mice were checked on thrice a week for their hair regrowth and change in skin pigmentation. Hair cycles of mice were monitored throughout their first two synchronized cycles up to 16 weeks. To study the histomorphology of the hair follicles, 1 x 1cm dorsal skin specimens were obtained at desired hair growth stages (P16, 19, 32, 42, 49, 67, 84, 101) from $Lmna^{\Delta/\Delta/K14\text{-}Cre}$ mice and their WT littermates. Samples were processed as mentioned in 2.6 and histolomorphological assessment was performed.

2.19 Analysis of wound healing capacity of $Lmna^{\Delta/\Delta/K14\text{-}Cre}$ mice

7 weeks old $Lmna^{\Delta/\Delta/K14\text{-}Cre}$ mice and their WT littermates were anesthetized with 250mg/kg body weight Avertin (12.5mg 2,2,2 Tribromoethanol/ml, i.p.) and their hair on the dorsal back was shaved. A 4mm wound was administered on the dorsal skin with a sterile tissue biopsy punch (Miltex Inc., Germany). The wounds were allowed to heal for 48h before the

mice were sacrificed to harvest the dorsal skin around the wound area (approximately 1.5cm x 1.5cm). The dorsal skin was fixed in 10% NBF for 24h before being processed as mentioned in 2.6 for histological analysis. Immediately after harvesting, the skin was laid flat, photographed and the area of each wound was subsequently demarcated and calculated on ImageJ software. Quantitative statistical analysis was performed using Graphpad Prism software.

2.20 Isolation of keratinocytes from mouse dorsal skin

$Lmna^{\Delta/\Delta/K14-Cre}$ mice and their WT littermates were sacrificed and their hair on the dorsal back was shaved, and the dorsal skin was removed. The skin was washed in 2 x ice-cold 70% ethanol for 1 min, followed 1-2 mins in ice-cold PBS. Then, the dorsal skin was placed dermis side up and the muscles and fat were removed by scraping with scalpels, leaving only the dermis and epidermis. Next, the skin was placed onto a clean 100mm petri dish with the dermis side down and 8ml of 0.25% trypsin in Keratinocyte Serum Free Media (K-SFM) was added to the dish such that the skin floated on the trypsin solution. The skin was incubated with the media overnight at 4°C. The next day, the epidermis was scraped off the dermis with scalpels and incubated in 0.25% trypsin solution for 15 mins at 37°C, with intermittent pipetting. 2x volume of DMEM 10% FBS (D10) was added to neutralize the trypsin and the solution was filtered through a 70μm sterile filter, then through a 40μm filter. The keratinocytes were centrifuged at 1000 rpm for 8 min and the pellet was

rinsed twice with K-SFM (Jensen et al., 2010). The keratinocytes were then processed for extraction of RNA, immunoblots or immunofluorescence as mentioned in 2.4, 2.5 and 2.6 respectively.

2.21 Gene expression microarray analysis of *Lmna*-null keratinocytes

4 months old *Lmna*$^{\Delta/\Delta/K14\text{-}Cre}$ mice and their WT littermates were sacrificed and their dorsal skin were harvested and keratinocytes were extracted as mentioned in 2.19. Total RNA was extracted from keratinocytes using Trizol® and QIAGEN RNeasy kit as mentioned in 2.4. The quality and quantity of total RNA was determined with an Agilent RNA 6000 Nano Kit and Agilent Bioanalyzer 2100. Samples with RNA integrity number (RIN) above 7 were used for microarray analysis, which was performed using MouseWG-6 v2.0 Expression BeadChip (Illumina). Each experimental group consisted of 3 mice, and RNA from each biological sample was performed in triplicate. The samples were randomly assigned to different chips and microarray was performed as described (Rosario et al., 2014). 500ng RNA was first amplified into cRNA using Illumina TotalPrep-96 RNA Amplification Kit (Applied Biosystems/Ambion) according to the manufacturer's protocol. 1.5ug of amplified cRNA was hybridized to each chip, scanned using BeadArray Reader (Illumina) and analyzed with Genome Studio Software (Illumina).

Partek Genome Studio version 6.6 was used to analyze the generated data where background subtraction, quantile normalization and removal of

batch effects were performed across all the chips. Principal component analysis (PCA) was performed to monitor the reproducibility of isolation with chip-to-chip and remove inter-animal variations. Hierarchical cluster analysis was also performed to validate the data. Three-way analysis of variance (ANOVA) was applied with a false discovery rate of 0.05. Subsequently, the gene list with >1.5 fold change in expression was then analyzed using Ingenuity Pathway Analysis (IPA) software (Ingenuity Systems). Genes identified in the microarray analysis were verified by qRT-PCR and the sequences of the primers used are listed in Table 2.2.

2.22 <u>Two-stage chemical carcinogenesis in *Lmna*$^{\Delta/\Delta/K14\text{-}Cre}$ mouse skin</u>

6 weeks old female *Lmna*$^{\Delta/\Delta/K14\text{-}Cre}$ (FVB/N) mice and their WT littermates were anesthetized with 250mg/kg body weight Avertin (12.5mg 2,2,2 tribromoethanol/ml, i.p.) and their dorsal hair was shaved. One week later, a single dose of 100nmol 7,12-dimethylbenz[*a*]anthracene (DMBA) (dissolved in 100ul acetone; Sigma-Aldrich) was topically applied to the dorsal skin of the mice. After another week, 10nmol 12-O-tetradecanoylphorbol 13-acetate (TPA) (in 100ul acetone, Sigma-Aldrich) was topically applied to the dorsal skin of mice every 48h to induce skin papillomas (Abel et al., 2009).

2.23 Cell culture of N/TERT-1 keratinocytes, viral infection and knockdown assay to obtain $LMNA^{KD}$

Human N/TERT-1 keratinocyte cells were cultured in K-SFM supplemented with 0.1mg/ml penicillin/streptomycin, 25ug/ml bovine pituitary extract, 0.2ng/ml epidermal growth factor, 0.3mM $CaCl_2$. N/TERT-1 keratinocyte cells were infected with lentiviral vectors with *LMNA* shRNA targeting exon 7 of *Lmna* as described previously (Dreesen et al., 2013b). The target sequence for *LMNA* knockdown was 5'-TGC GCT TTT TGG TGA CGC T-3', targeting exon 7 of the *LMNA* gene. Selection of infected cells was performed with 1ug/ml puromycin (Sigma Aldrich) for 14 days. Cells were split every 4 days or when they were approximately 70% confluent. The keratinocytes were then processed for extraction of RNA and immunoblots as mentioned in 2.4 and 2.5 respectively.

2.24 Cell proliferation assay of $LMNA^{KD}$ N/TERT-1 keratinocytes

The proliferation rate of $LMNA^{KD}$ N/TERT-1 keratinocytes was determined with xCELLigence RTCA System (ACEA Biosciences). Firstly, the microelectrode assay plate containing 100µl of supplemented K-SFM per well was equilibrated at 37°C and the electrical microimpedance signal (cell index) was set to zero in these conditions. Then, 750 or 1000 of $LMNA^{KD}$ or sham control N/TERT-1 keratinocytes were added to each well (n=3 cell lines per group with 5 technical replicate per cell line). Then, the plate was placed

in the 37°C incubator with 5% CO_2 content. Electrical microimpedance signal was measured every hour for 14 days. 75% of the media was replaced every 3-4 days. Data from 4 experimental sets was tabulated and analyzed with RTCA software. Statistical analysis was performed using Graphpad Prism software.

Alleles	Primer name	Sequence (5' - 3')
Lmna^{FL}	Lmna_F2	TCC TTG CAG TCC CTC TTG CAT C
	Lmna_R	AGG CAC CAT TGT CAC AGG GTC
Lmna^Δ	Lmna_F1	CCA GCT TAC AGA GCA CCG AGC T
	Lmna_R	AGG CAC CAT TGT CAC AGG GTC
Zp3-Cre	Cre_F	ATC TGG CAT TTC TGG GGA TT
	Cre_R	TTA TTC GGA TCA TCA GCT ACA C
Vil-Cre	Vil_F	ATC AAA GCC GGG TGG GCA GG
	Cre_R	CCT GGC GAT CCC TGA ACA TGT C
Apc^{min}	Apc_F	TTC TGA GAA AGA CAG AAG TCA
	Apc_R	TTC CAC TTT GGC ATA AGG C
K14-Cre	Krt14_F1	TGG ATG TTA AAG GCC CAT TC
	Cre_R2	CCT GGC GAT CCC TGA ACA TGT C
Lgr5-CreERT	Lgr5_KI_F	CAC TGC ATT CTA GTT GTG G
	Lgr5_KI_R	CGG TGC CCG CAG CGA G
Apc^{FL}	Apc_F	CAC TCA AAA CGC TTT TGA GGG TTG ATT C
	Apc_R	GTT CTG TAT CAT GGA AAG ATA GGT GGT C
p53^{FL}	p53_F	GGT TAA ACC CAG CTT GAC CA
	p53_R	GGA GGC AGA GAC AGT TGG AG
LBR	LBR-WT-F	TTC CTA TGG ACT GGG TGT GGA G
	LBR-WT-R	GCC TGA AAC TGG GTC AAA TAA GG
	LBR-Mut-R	TCA AAC CTG AAC CCC GAC TTC

Table 2.1: List of primer sequences for genotyping mice.

Gene		Sequence (5' - 3')
Sybr Green		
Lmna (exon 3)	For	GGA GGA GCT TGA CTT CCA GAA G
(mouse)	Rev	CCA CAA GCC GCG TCT CAT
Lmna (exon 10)	For	CGC ACC GCT CTC ATC AAC T
(mouse)	Rev	CCT CAT TGT CCT CAA CCA TGG T
Lmnb1	For	GAATCGCTGTCAGAGCCTTACTG
(mouse)	Rev	CCACCAAGCGGGTCTCAT
Lmnb2	For	GATGCTGGACGCTAAGGAACA
(mouse)	Rev	GAGAGATGGTGATCCGTGATGA
Klk6	For	GAG GCC CGT GTT TGA AGG A
(mouse)	Rev	CCC CAC CAC ACA GCA AGT G
Tgfb1	For	CTC CCG TGG CTT CTA GTG C
(mouse)	Rev	GCC TTA GTT TGG ACA GGA TCT G
TGFB1	For	GGC CAG ATC CTG TCC AAG C
(human)	Rev	GTG GGT TTC CAC CAT TAG CAC
Tgfb2	For	TCG ACA TGG ATC AGT TTA TGC G
(mouse)	Rev	CCC TGG TAC TGT TGT AGA TGG A
TGFB2	For	CAG CAC ACT CGA TAT GGA CCA
(human)	Rev	CCT CGG GCT CAG GAT AGT CT
TgfbR1	For	TCT GCA TTG CAC TTA TGC TGA
(mouse)	Rev	AAA GGG CGA TCT AGT GAT GGA
TgfbR2	For	CCG CTG CAT ATC GTC CTG TG
(mouse)	Rev	AGT GGA TGG ATG GTC CTA TTA CA
Smad2	For	ATG TCG TCC ATC TTG CCA TTC
(mouse)	Rev	AAC CGT CCT GTT TTC TTT AGC TT
Smad3	For	AGG GGC TCC CTC ACG TTA TC
(mouse)	Rev	CAT GGC CCG TAA TTC ATG GTG
Smad4	For	ACA CCA ACA AGT AAC GAT GCC
(mouse)	Rev	GCA AAG GTT TCA CTT TCC CCA
Ppid/ PPID	For	TGT GC CAG GGT GGT GAC TT
(mouse / human)	Rev	TCA AAT TTC TCT CCG TAG ATG GAC TT

Taqman		**Assay ID**
E-cadherin	*Cdh1*	Mm01247357_m1
Beta-catenin	*Ctnnb1*	Mm00483039_m1
Hypoxanthine guanine phosphoribosyltransferase	*HPRT1*	Mm000439307_m1

Table 2.2: List of primer sequences used for qRT-PCR.

Primary antibodies			
Name	**Source**	**Dilution (WB)**	**Dilution (IF)**
Emerin	Novocastra	1:500	1:100
GAPDH	Abcam	1:500	N.A.
Green Fluorescent Protein	Abcam	N.A.	1:100
H4K20me3	Abcam (ab9053)	N.A.	1:100
H4K8ac	Millipore (06-866)	N.A.	1:100
Keratin 10	Pierce Thermo Scientific	N.A.	1:100
Keratin 14	Covance	N.A.	1:1000
Ki67	Abcam	N.A.	1:100
Lamin A	H. Hermann's lab	N.A.	1:10
Lamin A (N18)	Santa Cruz	1:1000	1:100-200
Lamin B1	Yenzyme	1:500	1:200
Lamin B2	Yenzyme	1:500	N.A.
Lamin B-Receptor	H. Hermann	N.A.	1:100
Lap2-alpha	Santa Cruz	1:200	N.A.
Loricrin	Birgit Lane's lab	N.A.	1:500
Tubulin	Abcam	1:1000	N.A.
Villin	Santa Cruz	1:200	N.A.
Secondary antibodies			
Name	**Source**	**Dilution (WB)**	**Dilution (IF)**
Alexa Fluor® 488 Donkey Anti-Goat IgG	Molecular Probes	N.A.	1:500
Alexa Fluor® 568 Donkey Anti-Goat IgG	Molecular Probes	N.A.	1:500
Alexa Fluor® 488 Donkey Anti-Rabbit IgG	Molecular Probes	N.A.	1:500
Alexa Fluor® 568 Donkey Anti-Rabbit IgG	Molecular Probes	N.A.	1:500
Alexa Fluor® 488 Donkey Anti-Mouse IgG	Molecular Probes	N.A.	1:500
Rabbit anti-Chicken IgY (H+L)FITC	Pierce Thermo Scientific	N.A.	1:500
Donkey Anti-Guinea Pig IgG (H+L)	Jackson Immuno Research	N.A.	1:700
IRDye® 680CW Donkey anti-Rabbit IgG (H + L)	Licor	1:2500	N.A.
IRDye® 800CW Donkey anti-Goat IgG (H + L)	Licor	1:2500	N.A.

Table 2.3: List of antibodies for western blot and immunofluorescence.

Chapter 3- Deriving and characterizing a conditional lamin A/C knockout mouse model

Loss of function mutations in the *Lmna* gene result in early postnatal lethality in mice, usually within 3 to 6 weeks of birth (Bertrand et al., 2012; Sullivan et al., 1999). This makes the analysis of tissue-specific roles of lamins difficult. To circumvent this issue and provide a means to determine the role of the A-type lamins in specific tissues and in older mice, a conditional allele of *Lmna* was derived. The generation and extensive characterization of this conditional *Lmna* mouse line will facilitate analysis of the consequences of lamin A/C loss in specific tissues and in postnatal stages.

3.1 The conditional lamin A mouse model (*Lmna*$^{FL/FL}$)

A conditional *Lmna* allele (*Lmna*^{FL}) was generated in which exons 10 and 11 of *Lmna* were flanked by 2 loxP sites located upstream of exon 10 and in the 3' untranslated region (UTR) before exon 12 (Fig. 3.1A). Mice are on C57BL6 background and on homozygous genotype (*Lmna*$^{FL/FL}$), they are healthy, do not present any overt phenotypes and breed normally. Presence of loxP sites can be detected via genomic DNA PCR amplification to differentiate between wild-type (WT) *Lmna*$^{+/+}$, heterozygous *Lmna*$^{FL/+}$ and homozygous *Lmna*$^{FL/FL}$ mice. WT *Lmna* allele was amplified as a 579 bp band and floxed *Lmna* allele (*Lmna*^{FL}) was amplified as a larger 645 bp band (Fig. 3.1B).

3.2 Creating and validating the global lamin A/C knockout mice (*Lmna*$^{\Delta/\Delta}$)

For the constitutive deletion of the 3' terminus of *Lmna*, conditional *Lmna*$^{FL/FL}$ mice were crossed with oocyte-specific Cre recombinase deletor mice, where Cre deletion is driven by the regulatory sequences of zona pellucida 3 (*Zp3*) (de Vries et al., 2000). Deletion of *Lmna* was confirmed by multiplex PCR of genomic DNA, where approximately 1.5kb of the 3' terminus of *Lmna* is deleted and a resultant 460bp band (*Lmna*$^{\Delta}$) was detected (Fig. 3.1C).
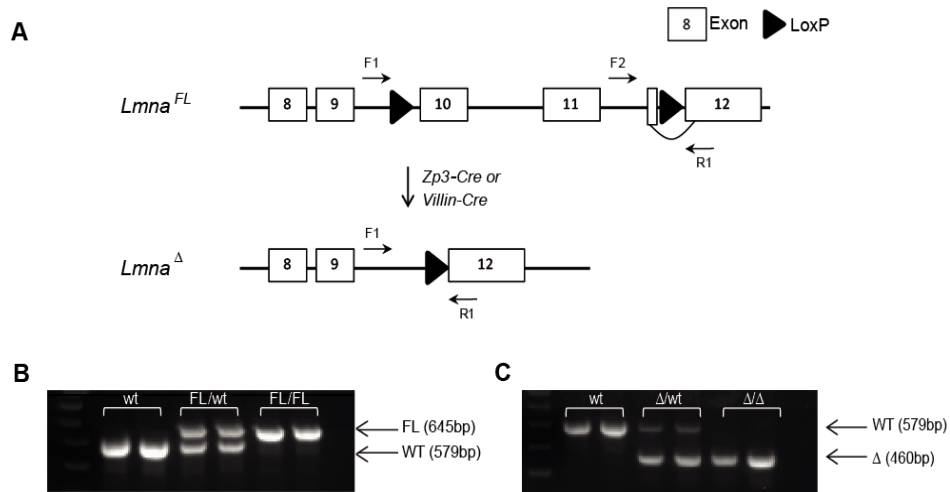
Figure 3.1: Generation of the *Lmna*^{FL} and *Lmna*$^{\Delta}$ mice. (A) A pair of 34-bp loxP sites (black triangle) flanks exon 10 to 11 of *Lmna* gene, which can be removed by a Cre recombinase to obtain a null allele (*Lmna*$^{\Delta}$). (B) PCR amplification of genomic DNA from tail-clips of wild-type *Lmna* (WT, 579bp) and floxed *Lmna* (FL, 645bp) alleles with primers F2 and R1. (C) Duplex PCR amplification of WT *Lmna* (579bp) and null *Lmna*$^{\Delta}$ (Δ, 460bp) alleles with primers F1, F2 and R1.

3.3 <u>Lamin A/C transcripts and proteins are depleted in *Lmna*^{Δ/Δ} mice</u>

Tissues such as skin, heart, duodenum, muscles and kidneys were harvested from P14 *Lmna*$^{\Delta/\Delta}$ mice and analyzed by quantitative real-time-PCR (qRT-PCR) for *Lmna* mRNA transcript levels. Using primers specific for *Lmna* exons 9 to 10, no *Lmna* mRNA transcripts were detected in various tissues such as skin, heart, duodenum, kidney and liver (>99% absent). Primers specific for *Lmna* exons 3 to 4 showed a 30% (duodenum) to 65% (skin) reduction in transcript levels (Fig. 3.2). Hence, *Lmna*$^{\Delta/\Delta}$ mice do not make any full-length *Lmna* transcripts.
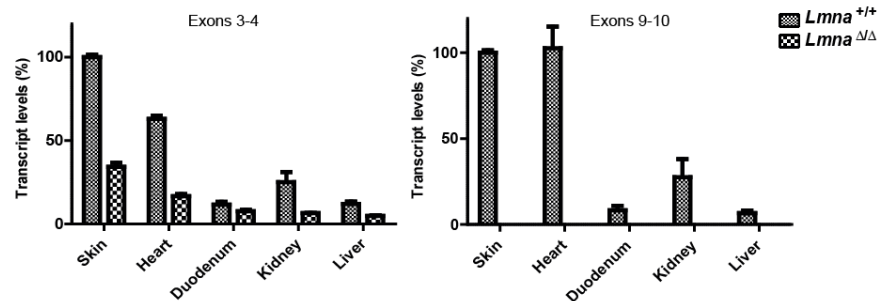
Figure 3.2: *Lmna* transcripts are abolished in *Lmna*$^{\Delta/\Delta}$ mice. qRT-PCR of mRNA at exons 3 to 4 and 9 to 10 showed that *Lmna* was depleted in various tissues such as the skin, heart, duodenum, kidney and liver.

To study the expression of LMNA/C protein, I used an antibody that recognizes the first 50 amino acids in the N-terminus of LMNA/C protein. Immunofluorescence staining of lamin A and C was evident in WT mice as a distinct staining around the nuclear rim. In *Lmna*$^{\Delta/\Delta}$ mice, the expression of LMNA/C was absent in all the cells in tissues such as the skeletal quadriceps muscle, lung and heart (Fig. 3.3A). Western blot analysis also showed that LMNA/C protein is abolished in tissues such as skin, skeletal quadriceps

muscles, heart and duodenum (Fig. 3.3B). Previous reports have shown the presence of smaller truncated LMNA bands in the $Lmna^{Sul-/-}$ mouse (Sullivan et al., 1999, Jahn et al., 2012). In some tissues of the $Lmna^{\Delta/\Delta}$ mice, a faint low-molecular weight band was detected, but it was present in both $Lmna^{+/+}$ and $Lmna^{\Delta/\Delta}$ tissues and therefore it is unlikely to represent an aberrant truncated form of LMNA/C as a result of $Lmna$ deletion.
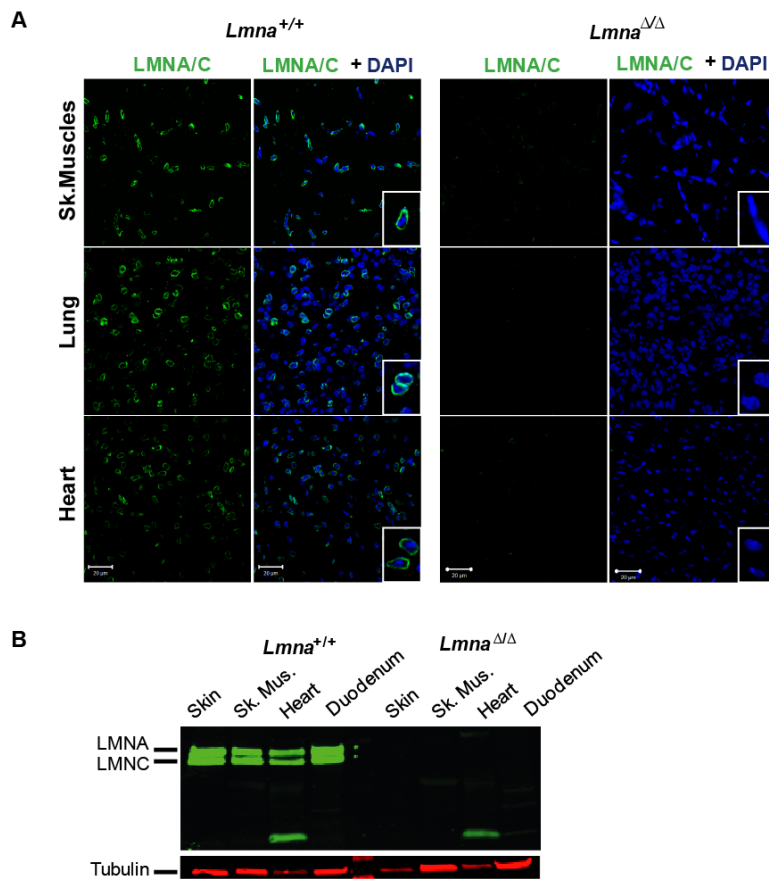
Figure 3.3: LMNA/C proteins are completely abolished in $Lmna^{\Delta/\Delta}$ mice. Protein analysis via (A) immunofluorescence and (B) western blot confirmed that expression of LMNA/C is completely abolished in skin, skeletal muscles (sk. mus.), heart, duodenum and lung. Nuclear rim staining of LMNA/C is observed in cells of $Lmna^{+/+}$ mouse tissues, but absent in $Lmna^{\Delta/\Delta}$ cells (inset). (Scale bars, 20µm).

3.4 Characterization of the $Lmna^{\Delta/\Delta}$ knockout mice

Heterozygote breeding of $Lmna^{\Delta/+}$ mice was set up and from 21 litters, $Lmna^{\Delta/\Delta}$ mice were born according to Mendelian ratios (Table 3.1), indicating that $Lmna$ is not essential for embryonic development. $Lmna^{\Delta/\Delta}$ mice appear to be slightly smaller at birth and have a slower postnatal growth rate so that by P12-14, $Lmna^{\Delta/\Delta}$ mice are approximately 50% of the weight of their WT or heterozygous littermates (4.089g vs. 7.637g, $p<0.001$) (Table 3.1).

Genotype	Mendelian ratio *(%)*	Weight (g)
$Lmna^{+/+}$	24.6% *(n=46)*	7.637 ±1.64 *(n=38)*
$Lmna^{\Delta/+}$	51.3% *(n=96)*	7.613 ±1.40 *(n=65)*
$Lmna^{\Delta/\Delta}$	24.1% *(n=45)*	4.089 ±0.77 *(n=35)* ***(p<0.001)*

Table 3.1: Loss of *Lmna* is not embryonic lethal but *Lmna*$^{\Delta/\Delta}$ mice show severe growth retardation. $Lmna^{+/+}$, $Lmna^{\Delta/+}$ and $Lmna^{\Delta/\Delta}$ mice were born according to Mendelian ratios at 24.6%, 51.3% and 24.1% respectively (n=187). By P14, $Lmna^{\Delta/\Delta}$ mice (4.089 ±0.77g) are significantly smaller than their $Lmna^{+/+}$ (7.637 ±1.64g) and $Lmna^{\Delta/+}$ (7.613g ±1.40) littermates. ***($p<0.001$).* Data represents mean ± SEM.

By P8-10, $Lmna^{\Delta/\Delta}$ mice are distinguishable from their WT littermates as they present signs of muscular dystrophy such as stiff walking posture and a kink in their tail (Fig. 3.4A). $Lmna^{\Delta/\Delta}$ mice generally survive to P12-18 while $Lmna^{\Delta/+}$ mice survive for more than 1 year and are indistinguishable from their WT littermates (Fig. 3.4B). I did not observe weight difference between male and female mice of the same genotype (Fig. 3.4C), indicating that effects caused by loss of $Lmna$ are not gender specific. The lifespan of $Lmna^{\Delta/\Delta}$ mice

is shorter than the original constitutive $Lmna^{Sul-/-}$ line that dies around P35-42 (Sullivan et al., 1999), with the difference in longevity possibly being influenced by genetic background (129/JXC57Bl6 vs. C57/B6) (B. Kennedy pers comm) and/or the presence of low levels of a truncated LMNA fragment that has been reported (Jahn et al., 2012).
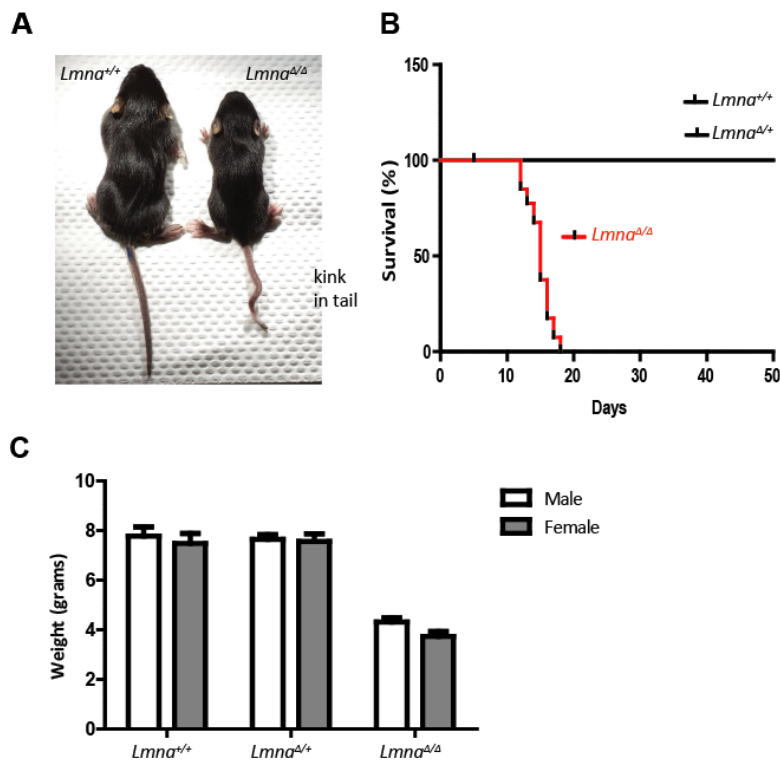
Figure 3.4: $Lmna^{\Delta/\Delta}$ mice have decreased lifespan and present non-gender specific weight loss. (A) At P13, $Lmna^{\Delta/\Delta}$ mice are smaller compared to their $Lmna^{+/+}$ littermates, with a kinked tail. (B) $Lmna^{\Delta/\Delta}$ mice generally die before P18, having a significantly shorter lifespan compared to their $Lmna^{+/+}$ and $Lmna^{\Delta/+}$ littermates. (C) Male (white bars) and female (grey bars) mice within each genotype have similar weights. Data represents mean ± SEM.

3.5 Histological analysis of $Lmna^{\Delta/\Delta}$ tissues

Pathological assessment showed that $Lmna^{\Delta/\Delta}$ mice had a smaller heart size compared to their WT littermates and histological analysis confirmed that $Lmna^{\Delta/\Delta}$ mice have a smaller heart with thinner heart walls, indicative of cardiomyopathy (Fig 3.5A). Histological analysis of skeletal quadriceps muscle showed significantly smaller diameter myofibrils and increased incidence of centrally located nuclei (Fig 3.5B), which could be indicative of slower muscle growth and immaturity. Hence, our $Lmna^{\Delta/\Delta}$ mouse model is similar to other $Lmna$ mutant lines that present muscular dystrophy and cardiomyopathy symptoms (Arimura et al., 2005; Sullivan et al., 1999). The smaller muscle mass in $Lmna^{\Delta/\Delta}$ mice contribute to the severe weight difference. More interestingly, $Lmna^{\Delta/\Delta}$ mice showed anomalies in skin histology with a seemingly increase in the number of hair follicles in the dorsal skin (Fig 3.5C). The effect of the loss of $Lmna$ on skin will be discussed further in chapter 6 where I analyzed $Lmna$ loss in skin epidermis.

3.6 Redistribution of emerin in $Lmna^{\Delta/\Delta}$ MAFs

Lamin A/C is essential for the proper localization of INM proteins such as emerin. MAFs and tongue epithelium cells in $Lmna^{Sul-/-}$ mice showed emerin relocalization (Raharjo et al., 2001; Sullivan et al., 1999). In $Lmna^{\Delta/\Delta}$ mice, MAFs showed more irregularly shaped nuclei and emerin relocalization from the nuclear periphery into the cytoplasm and ER (Fig. 3.6).

75

A *Lmna$^{+/+}$* *Lmna$^{\Delta/\Delta}$*

Heart

B *Lmna$^{+/+}$* *Lmna$^{\Delta/\Delta}$*

Skeletal Muscle

C *Lmna$^{+/+}$* *Lmna$^{\Delta/\Delta}$*

Dorsal skin
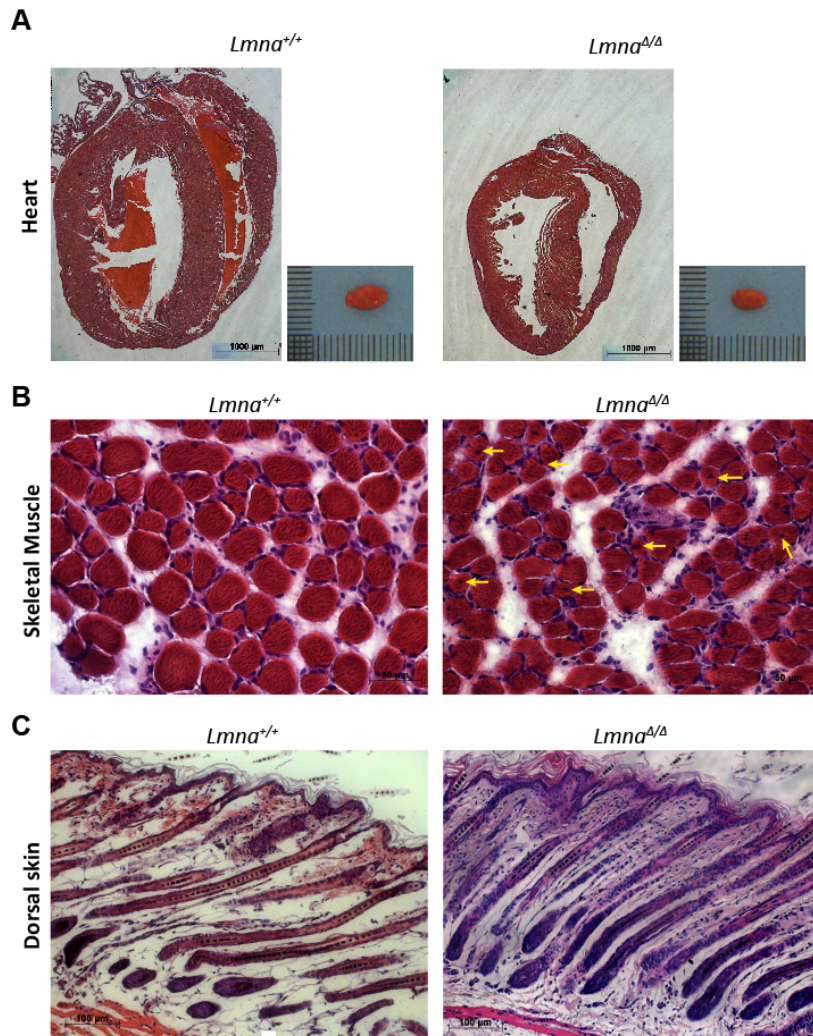
Figure 3.5: Histological analysis of P13 *Lmna*$^{\Delta/\Delta}$ male mice revealed anomalies in heart, skeletal muscles and skin. (A) During necropsy, *Lmna*$^{\Delta/\Delta}$ mice have smaller heart size compared to WT mice (inset) and histological analysis showed that *Lmna*$^{\Delta/\Delta}$ mice have thinner heart walls (Scale bars, 1000µm). (B) Skeletal muscles of *Lmna*$^{\Delta/\Delta}$ mice show smaller myofibrils and have increased frequency of centrally located nuclei (yellow arrows), indicative of defects in muscle growth and maturation (Scale bars, 50µm). (C) Dorsal skin of *Lmna*$^{\Delta/\Delta}$ mice showed a slightly thickened epidermis with striking increase in number of hair follicles (Scale bars, 100µm).
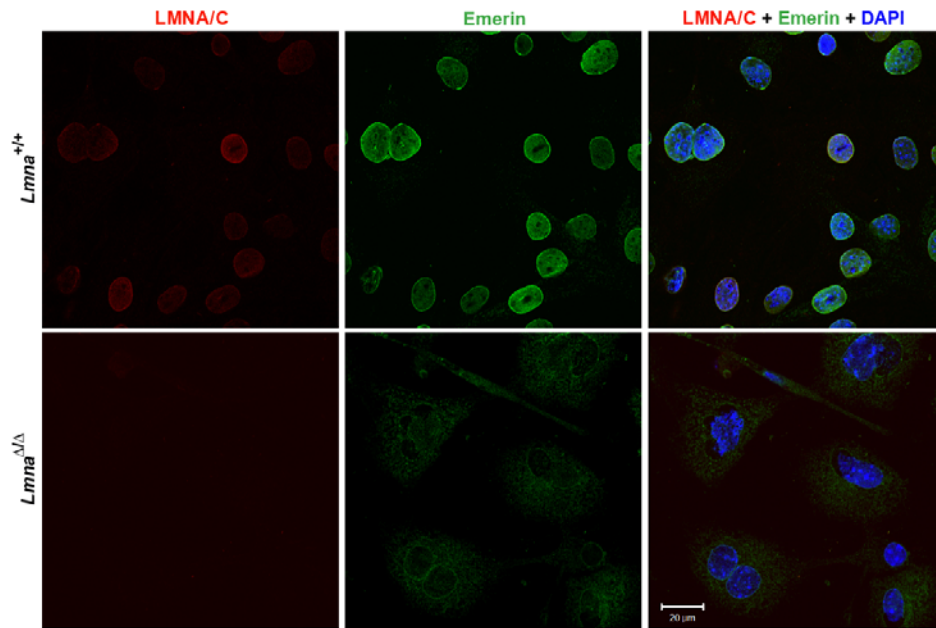
Figure 3.6: Emerin is relocalized in *Lmna*$^{Δ/Δ}$ mice fibroblasts. Immunostaining of emerin showed that emerin localization was more diffused and relocated from NE to the ER due to loss of *Lmna*. (Scale bars, 20µm).

3.7 Conclusions

In conclusion, I characterized a conditional (floxed) allele of the *Lmna* gene and show that mice with ubiquitous deletion of *Lmna* die within 3 weeks of birth. By means of PCR and qRT-PCR, no full-length *Lmna* mRNA transcripts were detected. Through immunoblot analysis and immunofluorescence studies with an antibody specific to the N-terminal 50 amino acids of LMNA/C protein, I confirm that no full-length or aberrant truncated LMNA/C protein as a result of *Lmna* deletion of *Lmna*. Homozygous null *Lmna*$^{Δ/Δ}$ mice have a reduced life span, stiff walking gait, and severely retarded growth from P10 onwards, whereas heterozygous mice show no overt phenotypic abnormalities. Histological assessment of the heart

and quadriceps muscle revealed that $Lmna^{\Delta/\Delta}$ mice have a smaller heart with thinner heart muscles and smaller diameter myofibrils in skeletal muscles, with an increased percentage of centrally located nuclei, indicative of either retarded or defective muscle growth and maturation, which contributes to the severe weight loss in the knockout mice. A striking observation in the increased number of hair follicles in the $Lmna^{\Delta/\Delta}$ mice was also made and will be further discussed in chapter 6.

Chapter 4 – Lamin B receptor (LBR) and lamin A/C sequentially tether peripheral heterochromatin and inversely regulate differentiation

4.1 The *LBR^GT* mouse line

Mutations in the *LBR* gene result in nuclear envelopathies such as Pelger-Huët anomaly, Greenberg/HEM skeletal dysplasia and Reynolds syndrome (Gaudy-Marqueste et al., 2010; Hoffmann et al., 2002; Waterham et al., 2003). LBR is essential for regulating sterol metabolism during fetal development (Holmer et al., 1998; Waterham et al., 2003) and chromatin organization (Ye et al., 1997). To study the functional roles of LBR, a mouse line was derived where a gene trap (GT) cassette, consisting of *en2* splice acceptor (SA) sequences, neomycin resistance selection marker and *β*-galactosidase reporter marker (β-geo), was inserted within exon 9 of the *Lbr* gene (*Lbr^GT*) (Fig 4.1A) (Cohen et al., 2008). WT LBR protein possesses a N-terminal DNA and HP1 binding domain and a C-terminal hydrophobic domain with 8 transmembrane segments important in the regulation of sterol metabolism (Holmer et al., 1998; Silve et al., 1998). In the hybrid LBR^GT protein, the first 366 amino acids containing the N-terminus and transmembrane domains 1 to 4 is fused to β-geo and since it lacks the last 4 transmembrane domains and C-terminus (Fig. 4.1B), mutant LBR^GT protein relocalizes from the nuclear lamina to the ER (Cohen et al., 2008).
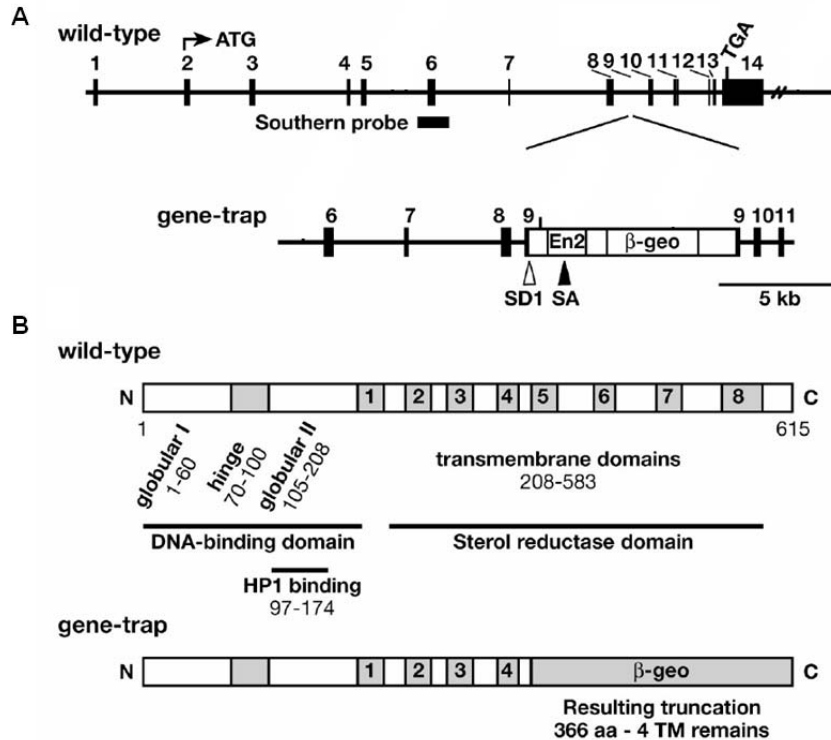
Figure 4.1: *Lbr* **mouse line was derived by the insertion of a gene-trapped (GT) cassette.** (A) The WT *Lbr* gene consists of 14 exons (black rectangles). The GT cassette consisting of *en2* splice acceptor (SA) sequences, neomycin resistance and *β*-galactosidase cDNA sequences (β-geo) was inserted into exon 9 of the *Lbr* gene.
(B) WT LBR protein has DNA and HP1 binding domains as well as 8 transmembrane (TM) domains (grey numbered boxes) that are important for sterol metabolism regulation. LBR[GT] is a 366 amino acid protein containing the N-terminus and the first 4 TM domains fused to β-geo. Diagram was adapted and modified with permission (Cohen et al., 2008).

While heterozygous (*Lbr*[GT/wt]) mice are phenotypically normal, some *Lbr*-null (*Lbr*[GT/GT]) mice exhibit embryonic lethality while some display incomplete penetrance and survive to postnatal stages. These latter mice however have decreased lifespan with multiple pathologies including hyperkeratosis, alopecia, hydrocephaly, scoliosis, syndactyly, apoptotic thymus, clogged nasolacrimal duct and anomalies in hematopoetic cells such as hypolobulations in the granulocytes but with no effects on its anti-bacterial

functions. *Lbr* is transcriptionally regulated by CCAAT/enhancer-binding protein epsilon (C/EBPε) which is important in the morphological differentiation of granulocyte nuclei (Cohen et al., 2008).

Lbr$^{GT/GT}$ MEFs exhibited altered nuclei morphologies including misshapen nuclei, wrinkly nuclear lamina, large nucleoplasmic foci associated with HP1α and increased numbers of micronuclei. Expression of emerin was also enriched at the nuclear lamina. During embryogenesis, LBR is strongly expressed in thymus, spleen and testis but its expression in other tissues becomes elevated postnatally. LBR is also expressed in outer root sheath of hair follicles and matrix cells in the hair bulb hence disruption of LBR results in overt pathologies in the skin and hair in *Lbr*$^{GT/GT}$ mice (Cohen et al., 2008).

4.2 *Lbr*$^{GT/GT}$ mice exhibit anomalies in skin morphology

In our laboratory, *Lbr*$^{GT/GT}$ mice generally survive to P18 while a small percentage (<5%) survive to P145. *Lbr*$^{GT/GT}$ mice are smaller in size compared to their *Lbr*$^{wt/wt}$ (WT) littermates (Fig. 4.2A). *Lbr*$^{GT/GT}$ mice also display gross abnormalities such as syndactyly where digits fuse together in both front and hind paws (Fig. 4.2B), alopecia with sparse and wavy hair, hardened dorsal and ventral skin, and loss of skin elasticity. Gross anatomy and microscopic analysis also show that *Lbr*$^{GT/GT}$ mice vibrissae and dorsal hair appears lighter and wavier with increased fragments in hair shafts compared to WT mice (Fig. 4.2C). Histological analysis of P15 *Lbr*$^{GT/GT}$ mice skin revealed epidermal and

dermal thickening as well as thicker keratinized squames in dorsal skin (Fig.

4.2D). These anomalies are similar as previously reported (Cohen et al., 2008).
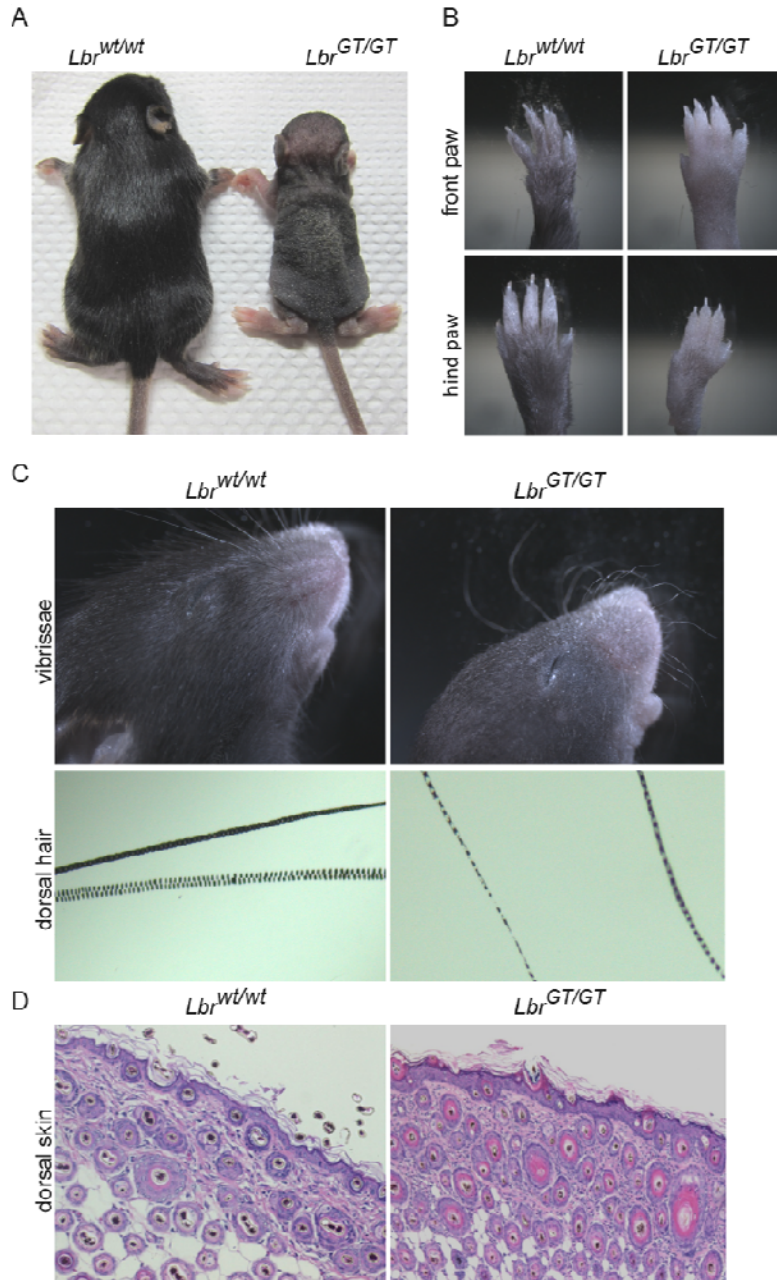
Figure 4.2: $Lbr^{GT/GT}$ mice are smaller, exhibited syndactyly and anomalies in hair and skin. (A) At P15, $Lbr^{GT/GT}$ mice are smaller than their WT littermates. (B) Syndactyly is observed in the front and hind paws of $Lbr^{GT/GT}$ mice. (C) Vibrissae of $Lbr^{GT/GT}$ mice are short and curly and hair shafts of body hair are thinner and fragmented. (D) Dorsal skin of $Lbr^{GT/GT}$ mice show a thickened epidermis and dermis, with lighter hair shafts in the hair follicles.

4.3 Mammalian rod cells with inverted nuclei do not express both lamin A/C and LBR

The NE with its lamina functions as a nuclear scaffold for the correct localization of INM proteins and NPCs as well as performs critical processes in chromatin organization (Burke and Stewart, 2014). Nuclear localization of the chromatin regions is highly ordered and plays an important role in functional organization of the nucleus (Cremer and Cremer, 2010). Majority of eukaryotic nuclei have a conventional chromatin architecture consisting of euchromatin that predominantly occupies internal nuclear regions while heterochromatin primarily lines the NE between the NPCs and also surrounds the nucleolus. Euchromatin is predominately juxtaposed to the NE with only small islands of heterochromatin being present at the periphery (Kizilyaprak et al., 2011; Solovei et al., 2009).

A unique exception to chromatin organization in eukaryotes is found in photoreceptor rod cells of nocturnal animals (Solovei et al., 2009). Rod cells lack peripheral heterochromatin and exhibit inversion of euchromatin and heterochromatin positions in order to reduce light loss in the retina and adapt to nocturnal vision (Solovei et al., 2009). In Dr. Irina Solovei's laboratory in Ludwig-Maximilians University Munich, the analysis of retinas in 39 diurnal and nocturnal mammalian species with conventional and inverted rod nuclei showed that inverted rod nuclei expressed neither LMNA/C nor LBR, whereas all rod cells with a conventional chromatin pattern expressed either LBR or LMNA/C, indicating that a lack of either protein was not enough for nuclear

inversion (Solovei et al., 2013). To expand our knowledge on how chromatin distribution is regulated by LMNA/C and LBR, a collaboration was established with Dr. Irina Solovei and colleagues to investigate the chromatin organization in our mutant $Lmna^{\Delta/\Delta}$ and $Lbr^{GT/GT}$ mouse lines.

4.4 <u>Expression of LMNA/C and LBR is temporally coordinated</u>

In the developing retina, the expression of both LMNA/C and LBR in neuronal nuclei is temporarily coordinated (Fig. 4.3A, B). At first, retinal neurons only express LBR. LMNA/C then appears and replaces LBR 10–14 days after the birth of the respective neuronal cell type (i.e., after the last division of the cell-type specific progenitor cells (Rapaport et al., 2004)). In rod cells, LBR expression ceases after P14 without initiation of LMNA/C expression (Fig. 4.3A).

Timelines for other representative tissues and cell types are shown in Fig. 4.3C. In contrast to neurons and cardiomyocytes (grouped as non-renewed cells), other cell types are constantly renewed by the differentiation of stem cells (renewed cells). In the intestinal epithelium and stratified epidermis of the lip, the positions of cells at successive stages of differentiation are spatially ordered in a linear fashion. A graded staining pattern of LBR and LMNA/C observed in these tissues (Fig. 4.3D, E) clearly reveals temporal changes in expression of the two proteins.

Timelines for renewed cells (Fig. 4.3C) actually show the differences in expression between cells that are at the same (differentiated) state but in mice of different ages rather than differences in the same cells arising with age, as in non-renewed cells. For instance, differentiated absorptive and goblet cells of the small intestine are LMNA/C negative until P14, whereas in older mice, differentiated cells of these types express both LBR and LMNA/C (Fig. 4.3D1). The crypt cells renewing the intestinal epithelium express only LBR at all ages (Fig. 4.3D1). The nuclei of hepatocytes and myotubes (striated muscle) lose most LBR around P9–P14 and P0, respectively. These cells retain a weak LBR signal even as adults, whereas satellite cells that renew myotubes have a lifelong strong expression of LBR. The nuclei of cardiomyocytes lose most LBR by P9, retaining only residual LBR expression. Differentiated lymphoid and myeloid blood cells do not express LMNA/C (Rober et al., 1989) but persistently express LBR. These results corroborate the role of LBR and LMNA/C in maintaining peripheral heterochromatin: all cell types except rods always express at least one of these two proteins.

Figure 4.3: Coordinated expression of LBR and LMNA/C in WT mice. Temporal coordination in retinal (A and B) and non-retinal (C) cell types. The stages at which a cell type cannot be identified are shown in gray; initial low LMNA/C expression level is shown in pink, and light green marks a very low residual LBR level, hatched pattern symbolizes variation between nuclei in mixed populations. (D and E) Spatio-temporal coordination of LBR and LMNA/C expression in the intestinal epithelium of the duodenum (D) and stratified epidermis of the lip (E) tissues at low magnification (D1 and E1) and representative nuclei (D2 and E2). During differentiation, cells are shifted in the apical direction, therefore a clear LBR (green) to LMNA/C (red) gradient is observed. In D1, arrowheads mark the entrances of three crypts. In (E), arrows mark basal keratinocytes; arrowheads indicate suprabasal keratinocytes expressing both LBR and LMNA/C (solid arrowheads) or only LMNA/C (apical strata, empty arrowheads). Bars: B and D2, 2 μm; D1, 50 μm; E1,

86

10 μm; and E2, 5 μm. In all panels, LBR is shown in green, and LMNA/C (LA/C) is shown in red.
4.3D1).

4.4 Nuclei not expressing LMNA/C undergo nuclear inversion in $Lbr^{GT/GT}$ mice

Since onset of LMNA/C expression occurs postnatally in some tissues, we reasoned that cells not expressing LMNA/C in $Lbr^{GT/GT}$ mice, thus lacking both proteins, would be expected to exhibit nuclear inversion. To search for inversion, we screened tissues from P5, P12–14, and adult (AD) $Lbr^{GT/GT}$ mice. Out of 34 cell types assayed, several cell types such as thymic and splenic lymphocytes, microglia and Kupffer cells showed advanced inversion and were astonishingly similar to mature or maturating rod nuclei (Fig. 4.4A, B). In all cases, inversion coincided with the absence of LMNA/C that was confirmed by a LMNA/C signal in adjacent cells of other types (Fig. 4.4). For a semiquantitative description of the degree of inversion in non-retinal cells, we compared them to rods of different stages of differentiation. P14, P21, P28, and AD rods (Fig. 4.4A) were used to describe the state of inversion in non-rod cell nuclei.

Non-rod cells with advanced inversion (Fig. 4.4B) had nuclei with one to five large dense aggregates of heterochromatin regions (chromocenters) surrounded by AT-rich/long interspersed nuclear element (LINE) -rich chromatin, with little or no contact with the NE; they corresponded to P21-AD

87

rods. A representative example is lymphocytes, which do not express LMNA/C in WT mice (Rober et al., 1989). WT lymphocytes usually either have none or only one internal chromocenters (Fig. 4.4C). In $Lbr^{GT/GT}$ lymphocytes, all chromocenters were internal (Fig. 4.4B, C, 4.5A, B).

For quantitative analysis, we compared inverted and non-inverted nuclei (from $Lbr^{GT/GT}$ and WT mice) in P5 and P46 thymic lymphocytes and P5 cerebellar granular cells. Peripheral chromocenters adjoin the nuclear border and have a hemispherical or discoid shape while internal chromocenters are spherical (Fig. 4.4C and 4.5B). Hence, using the numbers of peripheral and internal chromocenters as coordinates, we found that inverted and conventional nuclei occupy two non-overlapping regions in the respective two-dimensional diagram indicating that inverted and conventional nuclei have different numbers of internal and peripheral chromocenters (Fig. 4.5B-D). Such differences were observed even for the moderately inverted lymphocyte nuclei and cerebellar granular neurons from P5 mice, showing that, if inversion occurs in a cell type, it affects all nuclei. These data also show that the essence of inversion is the loss of heterochromatin association with the NE (which also facilitates chromocenter fusion). In these cells lacking both LMNA/C and LBR, chromocenter numbers also decrease approximately 1.5-fold in average, whereas the sizes of the two largest chromocenters increase.

The relationship between inversion and the dynamics of LBR and LMNA/C expression during differentiation is directly visible in the hair

follicle (Fig. 4.4E). In the central part of a hair bulb, matrix cells do not express LMNA/C and exhibit pronounced nuclear inversion (comparable to P14–21 rods) in $Lbr^{GT/GT}$ mice. During differentiation, the cells migrate along the hair follicle toward its opening. Differentiated cells at the border of the bulb are LMNA/C positive and display a conventional nuclear architecture, as do the nuclei of cells situated closer to the hair follicle opening.

In several cell types, LMNA/C expression does not start by P5 (Fig. 4.4D and 4.5). At P5, these cells from $Lbr^{GT/GT}$ mice have fewer chromocenters and a nuclear architecture corresponding to the P14/P21 stage of inversion in rods (Fig. 4.4A, D). This was observed in the granular cells of the cerebellum, bipolar cells in the retina, and absorptive cells of the small intestine (Fig. 4.4D, 4.5E). By P14, LMNA/C expression commences in these cell types, and in adult $Lbr^{GT/GT}$ mice, nuclei of these cells do not differ from their WT counterparts. Inverted nuclei were also present in the niches of the least differentiated and most rarely dividing stem cells (Greco and Guo, 2010), which presumably have enough time for inversion. We observed inverted nuclei in the hair bulge (Fig. 4.4F) and at the bottom of the crypts of the small intestine in $Lbr^{GT/GT}$ mice (Fig. 4.4G).
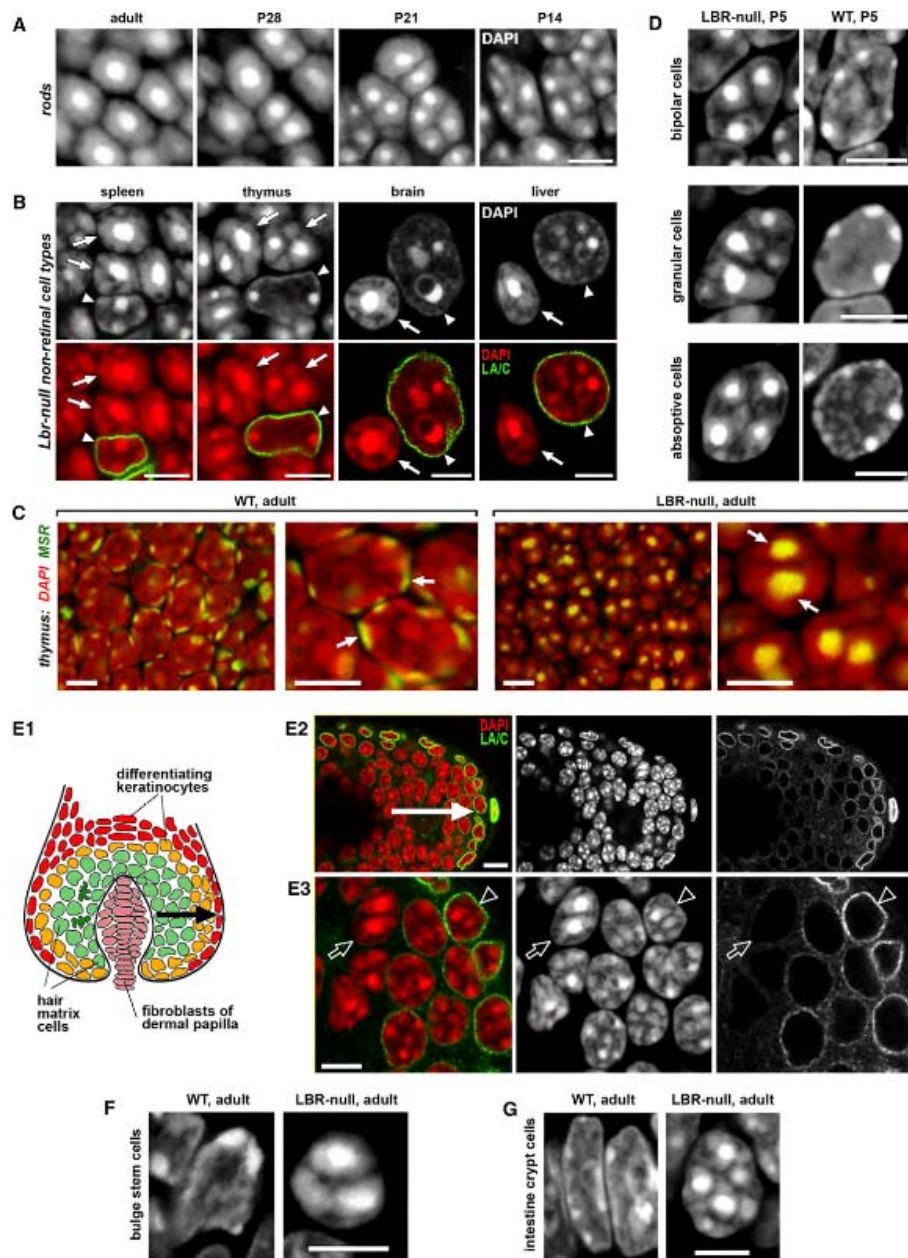
Figure 4.4: Nuclear inversion occurs in *Lbr^{GT/GT}* cells not expressing LMNA/C.
(A) Representative images showing landmark stages of nuclear inversion in WT rods.
(B) Inverted nuclei in thymic and splenic lymphocytes, microglia (brain), and
Kupffer (liver) cells. Inverted nuclei lack LMNA/C (arrows), whereas neighboring
nuclei expressing LMNA/C (green) retain a normal nuclear architecture
(arrowheads). (C) Thymic lymphocytes, fluorescent in situ hybridization (FISH) with
major satellite repeat (MSR) probe specific for chromocenters (arrows). (D) Transient
inversion in bipolar cells (retina), granular cells (cerebellum), and absorptive cells
(duodenum) from P5 *Lbr^{GT/GT}* mice. (E) Inversion and rescue of the nuclear
architecture in the hair bulb matrix cells. (E1) Illustration of the hair bulb structure:
Dividing cells of the hair matrix (green) and differentiating keratinocytes (orange and
red) are shifted peripherally during differentiation (arrow). (E2) A section through
hair bulb showing LMNA/C-positive cells at the periphery, with the arrow showing

the direction of centrifugal migration. Note the much stronger LMNA/C staining in a fibroblast abutting the hair bulb. (E3) Representative region of a hair bulb: inverted nucleus not expressing LMNA/C (arrow) and conventional architecture in nuclei expressing LMNA/C (arrowhead). (F and G) Inverted nuclei from hair bulge (F) and crypt (G). Bars, 5 μm.
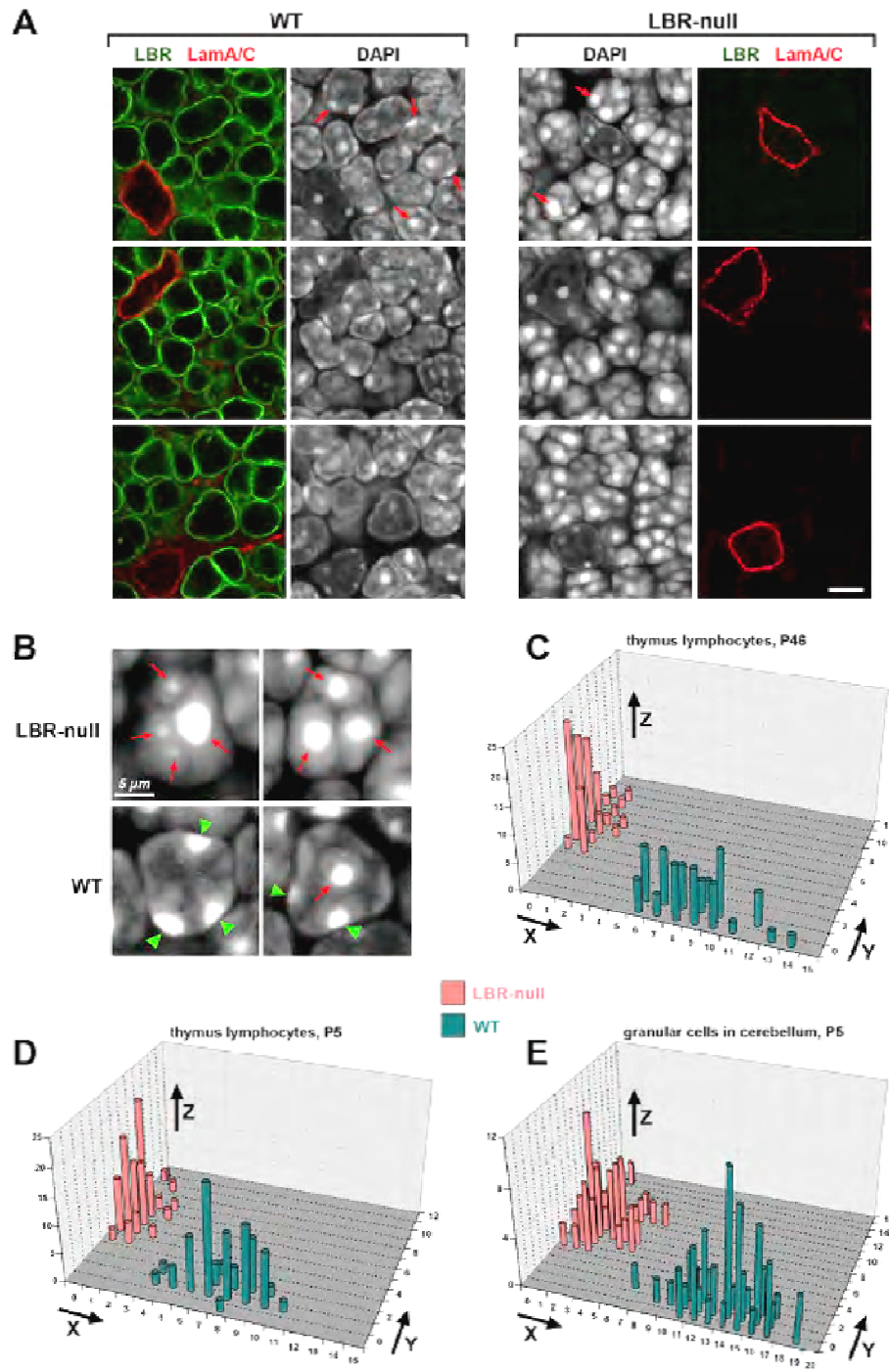
Figure 4.5: Comparison of the organization of inverted and conventional nuclei. (A) Lymphocytes only express LBR (green) while neighbouring stromal cells express LMNA/C (red). Compared to WT cells, LBR null ($Lbr^{GT/GT}$) lymphocytes have a smaller number of larger chromocenters. Nuclei of stromal cells have a conventional architecture and are not different between WT and LBR null. (B) WT lymphocytes have none or only one internal chromocenter (red arrow) and several peripheral chromocenters (green arrowheads) while LBR null lymphocytes have only spherical internal chromocenters (red arrows). Bars: 5μm. (C–E) 2-dimensional distribution of frequency of internal and peripheral chromocenters in thymic lymphocytes and cerebellar granular cells. x axis: the number of peripheral chromocenters; y axis: the number of internal chromocenters; z-axis: percent of nuclei with the respective numbers of peripheral and internal chromocenters. (C) Lymphocytes from adult (P46) mice. (D) Lymphocytes from P5 mice. (E) Granular cells from P5 mice; these cells experience transient inversion during early postnatal development. As inverted nuclei from LBR null (pink) and conventional nuclei from WT (blue) mice have different numbers of internal and peripheral chromocenters, they populate two non-overlapping regions of the diagram.

4.4 Loss of LMNA/C either induces nuclear inversion or is compensated by prolonged expression of LBR

In P13 and P16 $Lmna^{\Delta/\Delta}$ mice, we examined all cell types that, by this age express LMNA/C but not LBR (Fig. 4.3C and Table 4.1). Fibroblasts of the dermal papilla, lacking both LBR and LMNA/C, presented pronounced chromatin inversion (Fig. 4.6A). In other cell types such as reticulocytes in the spleen, cortical neurons in the brain and epithelial cells in the thymus, we observed a different phenotype where the expression of LBR persisted longer in $Lmna^{\Delta/\Delta}$ than WT mice. Prolonged LBR expression rescued nuclear inversion and maintained normal nuclear architecture in these cells (Table 4.1, 4.6B1, and 4.7). Using a tissue-specific knockout mouse line ($Lmna^{\Delta/\Delta/K14\text{-}Cre}$; discussed in chapter 6) where LMNA/C is deleted only in keratinocytes but not in dermal fibroblasts, persistent LBR expression is observed only in

LMNA/C null keratinocytes. We observed that the compensatory phenomenon

of LBR expression persisted for at least 3 months (Fig. 4.6B2 and 4.7B).

tissue	cell type		WT		nuclear pattern in LBR-null mice P5 and AD (P46)	nuclear pattern in *Lmna*-KO mice P16
			LBR	LA/C		
brain	microglial cells		+	-	inverted	conventional
spleen	lymphocytes		+	-	inverted	conventional
	granulocytes		+	-	inverted	conventional
thymus	lymphocytes		+	-	inverted	conventional
intestine	crypt cells		+	-	inverted	conventional
hair	matrix keratinocytes		+	-	inverted	conventional
liver	Kupffer cells		+	-	inverted	conventional
retina	rod cells	(P5)	+	-	inverted	conventional
		(AD)	-	-	inverted	inverted
cerebellum	granular cells	(P5)	+	-	moderate inversion	conventional, rescued
		(AD)	-	+	conventional	
retina	bipolar cells	(P5)	+	-	moderate inversion	conventional, rescued
		(AD)	-	+	conventional	
intestine	absorptive cells	(P5)	+	-	moderate inversion	conventional, rescued
		(AD)	+	+	conventional	
kidney	podocytes	(P5)	+	-	moderate inversion	not studied
		(AD)	+	+	conventional	
retina	amacrine cells	(P5)	+	-	enhanced CC fusion	conventional, rescued
		(AD)	-	+	conventional	
	cone cells [1]	(P5)	+	-	enhanced CC fusion	conventional, rescued
		(AD)	-	+	enhanced CC fusion	
brain	cortical neurons		-	+	conventional	conventional, rescued
cerebellum	Purkinje cells		-	+	conventional	conventional, rescued
retina	ganglion cells		-	+	conventional	conventional, rescued
	horizontal cells		-	+	conventional	conventional, rescued
spleen	reticulocytes		-	+	conventional	conventional, rescued
thymus	epithelial cells		-	+	conventional	conventional, rescued
skin	keratinocytes [2]		+/-	+	conventional	conventional, rescued
	dermal fibroblasts		-	+	conventional	conventional, rescued
hair	fibroblasts of dermal papilla		-	+	conventional	inverted
kidney	epithelial cells of proximal and distal convoluted tubes		-	+	conventional	not studied
liver	hepatocytes		+ (w)	+	conventional	conventional, rescued
skeletal muscles	myotubes		+ (w)	+	conventional	conventional, rescued
	satellite cells		+	+	conventional	conventional
spleen	erythroblasts		+	+	conventional	conventional
	megacaryocytes		+	+	conventional	conventional
small intestine	Paneth cells (indiscernible in P5)		+	+	conventional	conventional
	smooth muscle cells		+	+	conventional	conventional
blood vessels	endothelial cells		+	+	conventional	conventional
heart	cardiomyocytes	(P5)	+	+	conventional	conventional, rescued
		(AD)	+ (w)	+	conventional	
connective tissue	chondroblasts / chondrocyte	(P5)	+	+	conventional	conventional, rescued
		(AD)	-	+	conventional	
	osteoblasts / osteocytes	(P5)	+	+	conventional	conventional, rescued
		(AD)	-	+	conventional	

Table 4.1: Correlation of LBR and LMNA/C expression with the nuclear architecture in 34 cell types from WT, *Lmna*$^{\Delta/\Delta}$, and *Lbr*$^{GT/GT}$ mice. LMNA/C staining in cones[1] is notably weaker than in the majority of other retinal cells. Cone nuclei are comparable to a moderate inversion in WT retina, and chromocenter

93

fusion tends to be enhanced in LBR null cones compared to WT. However, in difference to rod nuclei, peripheral heterochromatin is retained in cones. A proportion of basal keratinocytes[2] are LBR positive; other basal and all suprabasal keratinocytes are LBR negative. In P46 adult WT mice, the nuclei of hepatocytes, cardiomyocytes, and myotubes[w] retain a very low level of LBR expression. In $Lmna^{\Delta/\Delta}$ mice, LBR expression is dramatically enhanced.
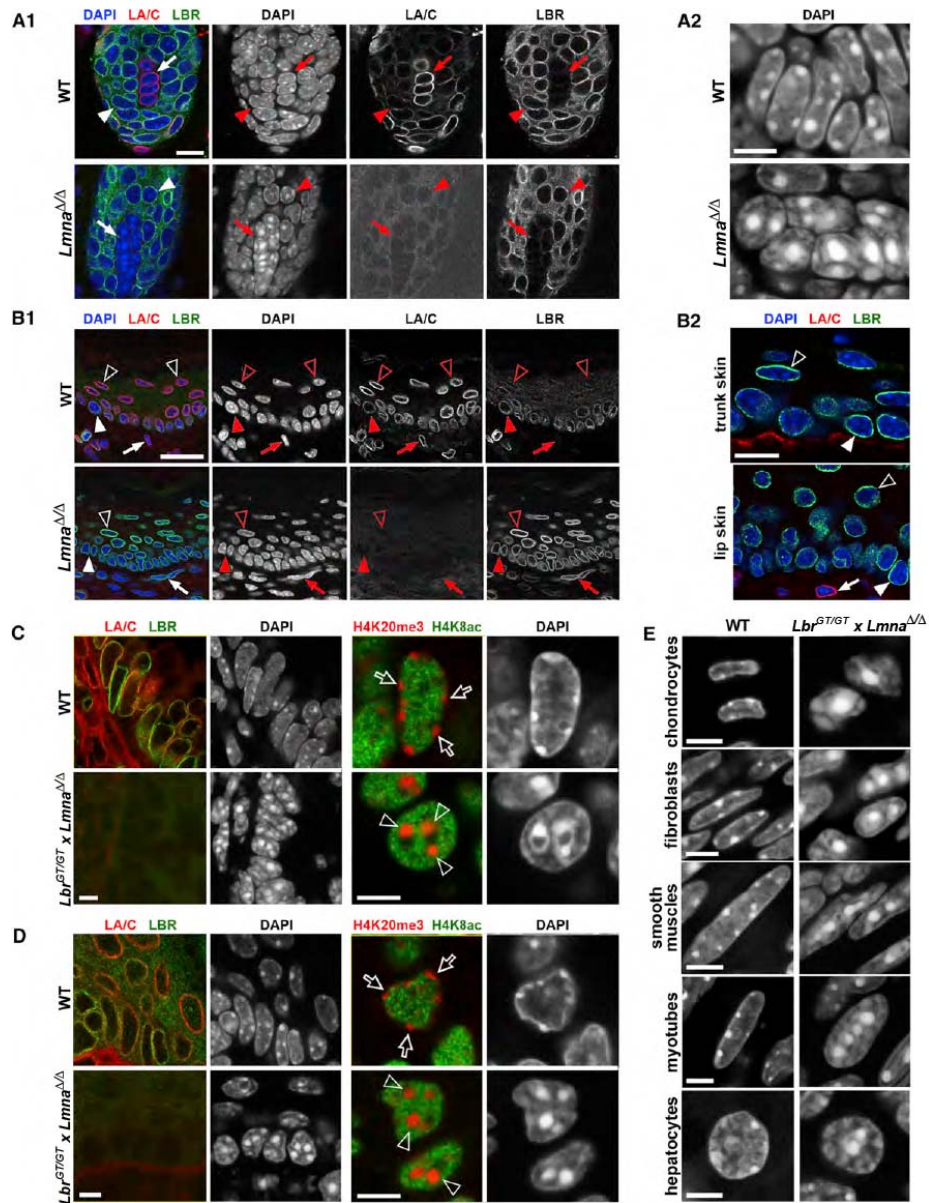
Figure 4.6: Nuclear organization in $Lmna^{\Delta/\Delta}$ and $Lbr^{GT/GT} x Lmna^{\Delta/\Delta}$ double null mice. (A1, A2) Nuclear inversion in the hair bulb of P16 $Lmna^{\Delta/\Delta}$ mice. In contrast to the matrix cells (arrowheads), the fibroblasts of the dermal papilla (arrows) do not express LBR and nuclei invert. (B1) Compensation for loss of LMNA/C by persistent expression of LBR in lip skin of P16 $Lmna^{\Delta/\Delta}$ mouse. Basal keratinocytes (solid arrowhead) express both LBR and LMNA/C, whereas suprabasal keratinocytes

94

(empty arrowheads) and dermal fibroblasts (arrow) express only LMNA/C. (B2) Compensation in suprabasal keratinocytes in both trunk (top) and lip skin (bottom) from a 3-month-old $Lmna^{\Delta/\Delta/K14\text{-}Cre}$ mice. Note a fibroblast expressing LMNA/C (arrow). (C and D) Epithelial cells in the colon (C) and epidermal keratinocytes (D) of $Lbr^{GT/GT}$ x $Lmna^{\Delta/\Delta}$ double null mice have a smaller number of chromocenters that are internal and larger (due to fusion) than in WT. Differences in the position and size of chromocenters are emphasized by differential staining of eu- and hetero-chromatin (H4K8ac and H4K20m3, respectively; right). (E) Increased size and internalization of chromocenters in several postmitotic cell types from $Lbr^{GT/GT}$ x $Lmna^{\Delta/\Delta}$ double knockout mice. Bars: A1 and B2, 10 μm; A2 and C–E, 5 μm; B1, 25 μm.

4.5 $\underline{Lbr^{GT/GT}\,x\,Lmna^{\Delta/\Delta}\text{ mice show inversion in all postmitotic cell types}}$

Despite the absence of overt morphological defects, compound double null $Lbr^{GT/GT}$ x $Lmna^{\Delta/\Delta}$ pups died shortly after birth, and therefore, only P0 animals were studied. We focused attention on cell types that do not invert in any of the two single gene knockouts ($Lbr^{GT/GT}$ and $Lmna^{\Delta/\Delta}$) (Table 4.1), in particular, the colon epithelium and skin epidermis. Both cell types express LBR and LMNA/C at birth. In $Lbr^{GT/GT}$ x $Lmna^{\Delta/\Delta}$ double null mice, cells show a clear increase in chromocenter size (chromocenter fusion) and relocation of chromocenters from the periphery to the nuclear interior (Fig. 4.6C, D). Similar changes occurred in all postmitotic cell types such as chondrocytes, myotubes and hepatocytes (Figure 4.6E).

As expected, inversion is not complete in the nuclei of P0 double null cells because full inversion needs several weeks after cell cycle exit (Solovei et al., 2009). The levels of inversion observed in double null nuclei were comparable to that of the transient inversion in P5 LBR null mice (Fig. 4.4D). The level of inversion varies between nuclei because some cells in P0 pups are postmitotic and some are cycling. Nevertheless, all identified postmitotic cell

95

types showed a clear inversion, confirming that peripheral heterochromatin cannot be maintained in postmitotic cells in absence of both LMNA/C and LBR.
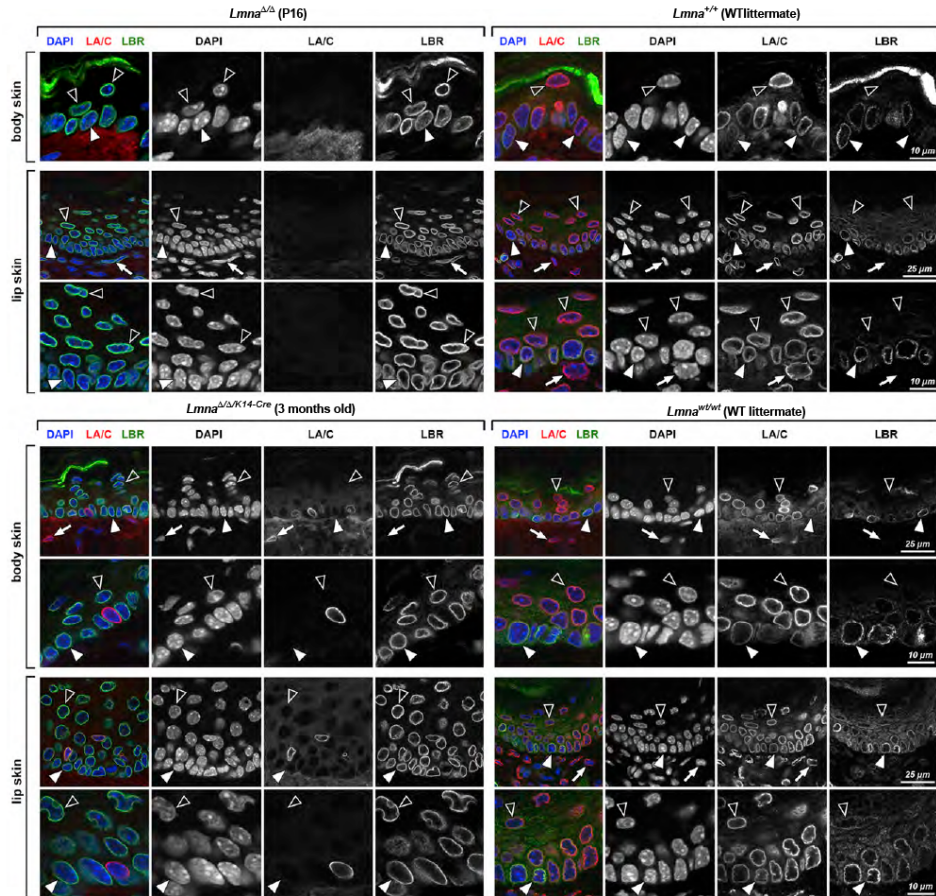
Figure 4.7: Compensation of LMNA/C deletion by prolonged expression of LBR. Basal keratinocytes (solid arrowheads), suprabasal keratinocytes (empty arrowheads), and dermal fibroblasts (arrows). In both body skin and lip skin from P16 $Lmna^{\Delta/\Delta}$ mice and 3 month old $Lmna^{\Delta/\Delta/K14-Cre}$ mice, deletion of LMNA/C results in prolonged and enhanced expression of LBR in all keratinocytes. Single cells situated between basal keratinocytes but expressing LMNA/C are melanocytes. Basal cells not expressing LBR probably are cells that already exited cell cycle but still have not moved apically.

4.6 <u>**Loss of LBR and LMNA/C inversely affects transcription in a proportion of muscle genes in early myogenic cells, but not in differentiated muscle**</u>

To determine the functional roles of the two temporally distinct heterochromatin tethers by LMNA/C and LBR, we analyzed the genome-wide effects of LBR and LMNA/C deficiency on the transcriptome. Primary cultures of myogenic cells were derived from limb muscles of P15–P16 $Lbr^{GT/GT}$ and $Lmna^{\Delta/\Delta}$ mice with WT littermates as controls. To minimize artifacts due to culture, myoblasts were harvested at passage 2. Transcription profiles confirmed the early myogenic nature of the cells in our cultures (Table 4.2).

Gene Ontology (GO) enrichment analysis using GOrilla suggested that the loss of Lbr or $Lmna$ tends to have opposite effects on muscle-related genes, reducing their expression in $Lmna^{\Delta/\Delta}$ and increasing it in $Lbr^{GT/GT}$ myoblasts. To test this finding, we analyzed expression levels of all genes covered by two Gene Ontology Consortiums (GOCs) most relevant for our experiments: structural constituent of muscle (GO: 0008307) and striated muscle cell differentiation (GO: 0051146) (Gene list available in Appendix A and B). This provided us with two relevant gene sets for statistical analysis, which we restricted to genes that had a non-zero expression level (FPKM > 0; frequency of reads per Kb per Mio) in all studied transcriptomes to facilitate uniform comparison of genotypes and cell types.

97

Nearly 60% of the genes from the GOC structural constituent of muscle (41 genes with non-zero expression in our data) were strongly and similarly deregulated in myoblasts; expression was reduced by the loss of *Lmna* and slightly increased by the loss of *Lbr* (Fig. 4.8A1). This pattern was also reproduced by nearly all genes individually deregulated in one or both knockouts at a statistically significant level ($p < 0.05$; marked by colored bullets in Fig. 4.8A1). More than 2-fold deregulation was observed in a large proportion of genes, irrespective of their expression level (Fig. 4.8B1). In contrast to myoblasts, differences in expression levels in differentiated muscles were much smaller and without the reverse effect of *Lmna* and *Lbr* loss (Fig. 4.8A2, B2). Deletion of *Lbr*, which is anyway nearly silenced during myotube differentiation (Fig. 4.3C), had very little effect on their transcriptome. GOC striated muscle cell differentiation revealed the same trends (Fig. 4.8C) as the GOC structural constituent of muscle. From a statistical perspective, the differences (i) between the myoblasts of $Lbr^{GT/GT}$ and $Lmna^{\Delta/\Delta}$ mice and (ii) between myoblasts and muscles of the same genotype were significant at the levels $p < 0.001$ for the first GOC and $p = 0.013$ or better for the second GOC (signed rank test). The differences between the two knockouts in limb muscle transcriptomes were not statistically significant for either GOC.

Myoblasts

	$Lmna^{\Delta/\Delta}$	WT littermates	$Lbr^{GT/GT}$	WT littermates
CD34	2.45954	5.80351	4.92951	2.80275
Pax3	0.165364	0.227697	0.122594	0.110527
Pax7	0.161318	0.152383	0.273316	0.253432
Myf5	0.191151	0.440881	0.377228	0.241417
MyoD1	2.0922	5.34758	5.50964	2.45502
Myog	2.88662	7.46752	10.4954	2.94114
Des	18.708	32.8722	85.1552	23.2916
Mef2c	2.50152	5.44563	13.288	6.61753
Mir-682	1301.71	1087.62	559.289	557.579
Dek	49.8429	54.8952	98.054	93.0605

Limb muscles

	$Lmna^{\Delta/\Delta}$	$Lbr^{GT/GT}$	WT littermates	
CD34 *	44.7451	50.2645	47.221	
Pax3	0.404821	0.334161	0.184962	
Pax7	1.28372	2.10147	1.70659	
Myf5	3.69195	3.20587	3.75945	
MyoD1	16.4394	17.8303	18.1321	
Myog	28.6889	48.6182	42.8943	
Des	909.125	791.968	730.555	
Mef2c	67.4002	71.1844	69.0648	
Mir-682	40.3143	34.8678	34.802	
Dek	14.7152	13.5977	13.1896	

(green)	statistically significantly upregulated (P < 0.05 or better)
(pink)	statistically significantly downregulated (P < 0.05 or better)

Table 4.2: Expression (FPKM) of marker genes of myogenic differentiation in myoblasts and limb muscles. Transcription profiles with expression of quiescent satellite cells and myoblasts markers such Pax3, CD34, Pax7 confirmed the early-myogenic nature of the cells in our cultures. Markers relating to more advanced stages of myogenic differentiation such as Myogenic factor 5 (Myf5), MyoD, myogenin (Myog) was also observed but this diversity is typical of myogenic cell cultures (Zammit et al., 2006). Myoblasts cultures showed also a high level of the oncogene *Dek* and microRNA *Mir682* which is upregulated on activation of satellite cells (Cheung et al., 2012) and proliferation of muscle progenitor cells (Chen et al., 2011) respectively.
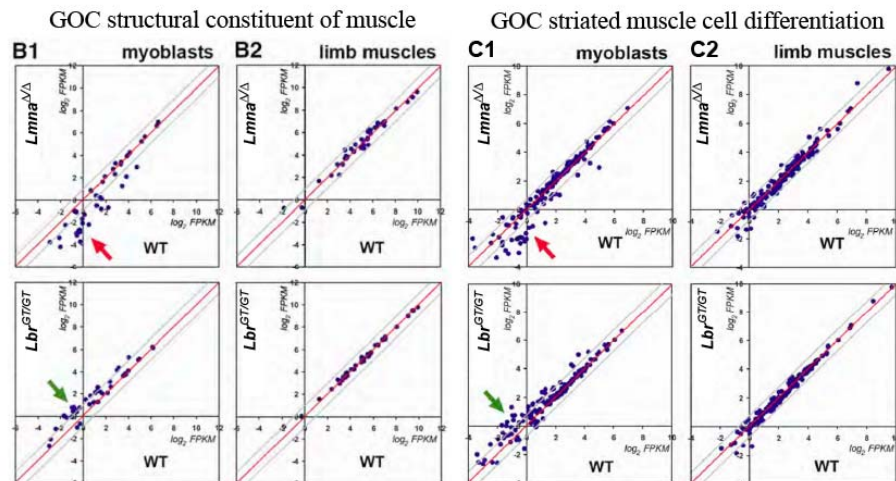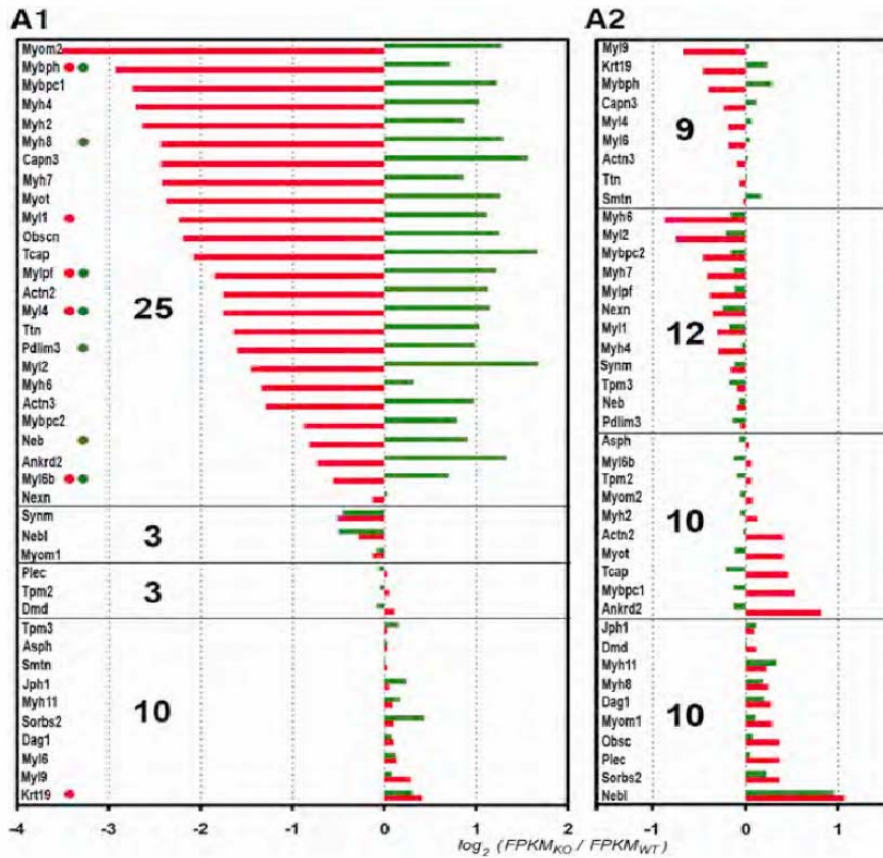
Figure 4.8: The effect of loss of *Lbr* and *Lmna* on the transcription of muscle-related genes in myoblasts and differentiated myotubes. (A) Genes from the GOC structural constituent of muscle: myoblasts (A1) and limb muscles (A2). The difference in transcription level (x axis) is expressed as logarithm of the fold change, ln (FPKM$_{KO}$/FPKM$_{WT}$), for *Lmna* (red) and *Lbr* (green). Numbers of genes with each of the four possible deregulation patterns are shown in bold. Green and red bullets mark genes that are statistically significantly deregulated (p < 0.05 or better) in *Lmna* (red) and *Lbr* (green) knockouts. (B) Genes from the GOC structural constituent of

100

muscle: myoblasts (B1) and limb muscles (B2). Each point represents a gene, with its expression levels (log$_2$ FPKM). Gray lines mark a 2-fold reduction in expression (below the red line) and increased expression (above the red line). Arrows emphasize deregulation trends for *Lmna* (red) and *Lbr* (green). (C) Genes from the GOC striated muscle cell differentiation: myoblasts (C1) and limb muscles (C2). The results are very similar to (B). The proportion of genes strongly deregulated in myoblasts is smaller, which may be explained by the fact that this GOC covers numerous genes (157 with non-zero expression in our data), many of which are not muscle-specific (e.g., Dicer1, Ezh2, Notch1, Rb1).
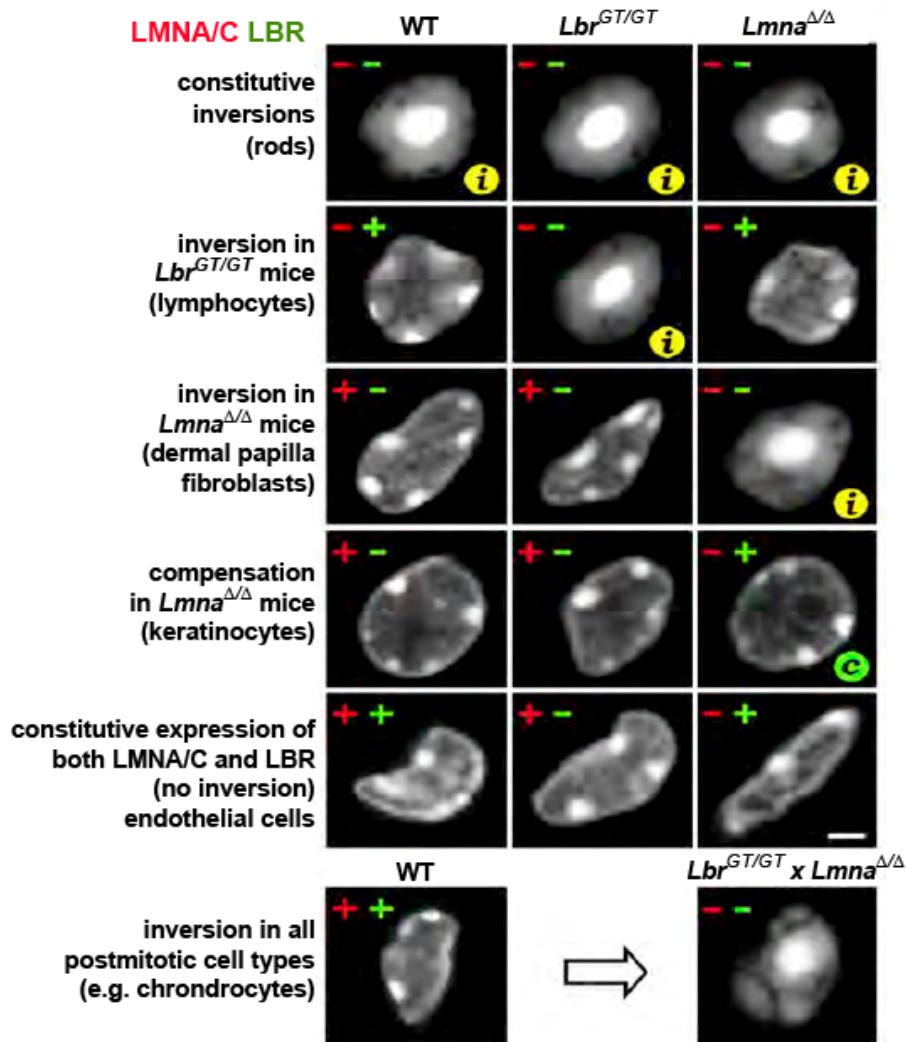
Figure 4.9: Summary of the effects of LMNA/C and LBR on the nuclear architecture. Presence and absence of LBR and LMNA/C in individual cell types are shown with green and red pluses and minuses; i, inversion; c, compensation by prolonged LBR expression. Bar, 2 μm.

4.7 <u>Conclusions</u>

By analyzing more than 30 cell types from WT, $Lbr^{GT/GT}$ and $Lmna^{\Delta/\Delta}$ mouse tissues (and 4 other transgenic lines based on other collaborators' work), we showed that LBR and/or lamin A/C are essential for tethering heterochromatin to the nuclear periphery. Absence of both proteins in postmitotic cells results in inversion of the nuclear architecture with heterochromatin relocalizing from the nuclear envelope to nuclear interior. During development and cellular differentiation, expression of LBR and LMNA/C is sequential and coordinated. Initially, only LBR is expressed and is later replaced by LMNA/C, with a few differentiated cell types expressing both proteins. In most cell types, deletion of $Lmna$ is compensated by prolonged expression of LBR. Deletion of both Lbr and $Lmna$ causes inversion in all differentiated cell types in newborn mice (summarized in Fig. 4.9). Comparison of WT, $Lbr^{GT/GT}$ and $Lmna^{\Delta/\Delta}$ myoblast transcriptomes revealed that a sequential temporal usage of LBR and LMNA/C tethers during development correlates with their opposite effects on the transcription of muscle specific genes: a decrease and increase, respectively. However, in terminally differentiated muscle, the differences between transcriptomes were almost non-existent.

Although both LBR and LMNA/C are indispensable for heterochromatin tethering, the roles of these proteins are different. LBR is an integral protein of the INM, which preferentially binds to B-type lamins. The Tudor domain of LBR selectively interacts with heterochromatin (Hirano et

al., 2012; Makatsori et al., 2004; Olins et al., 2010). LBR, B-type lamins and INM are sufficient to build a heterochromatin tether (Fig. 4.10) (Clowney et al., 2012). However, B-type lamins seem to be dispensable because mouse cells lacking both *Lmnb1* and *Lmnb2* retain a conventional nuclear architecture in the absence of LMNA/C (Kim et al., 2011; Yang et al., 2011a); this may be due to the retention of LBR, which has eight transmembrane domains at the INM.
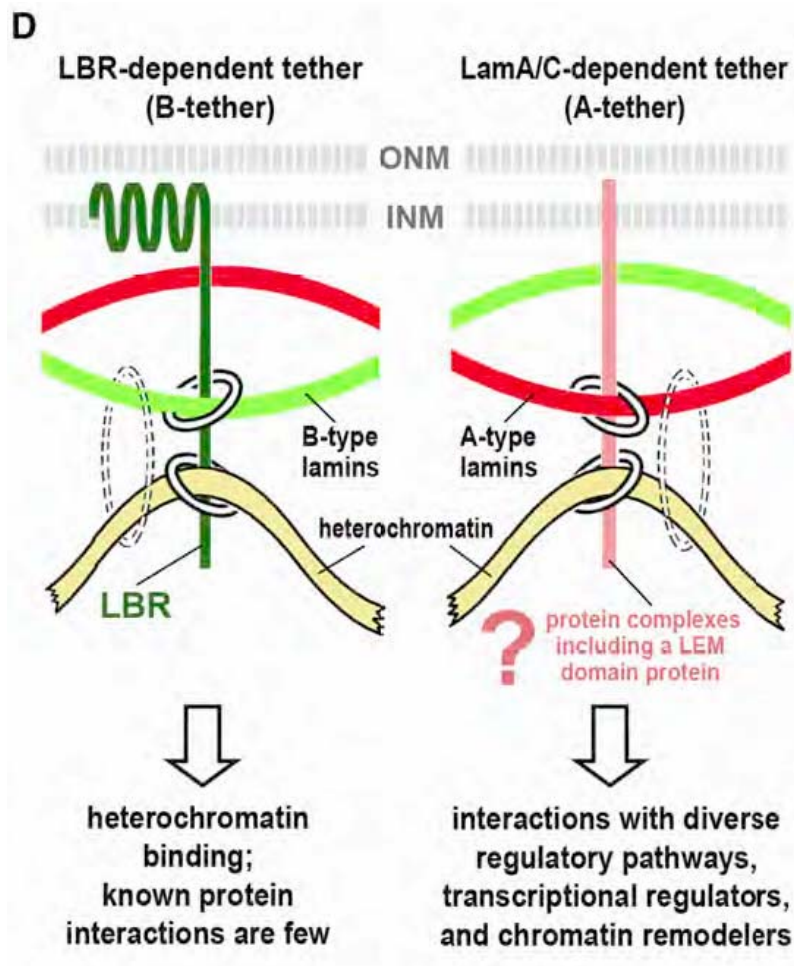
Figure 4.10: Proposed organization of the two tethers maintaining peripheral heterochromatin. Chromatin/DNA binding by lamins (dotted circles) is not sufficient for heterochromatin tethering but might synergistically enhance binding.

In contrast to LBR, exogenous A-type lamins expression does not counteract inversion in rods (Solovei et al., 2013). Although LMNA/C may bind chromatin directly (Andres and Gonzalez, 2009; Kubben et al., 2012), it typically functions as a scaffold for other chromatin-interacting proteins, such as LEM-domain proteins in particular. The latter share three important properties with LBR: they are anchored in the INM, interact with lamins, and bind to chromatin and/or DNA through their binding partners (Brachner and Foisner, 2011). LEM domain proteins anchor heterochromatin to the NE in yeast, which have no lamins, and in *C. elegans*, which has a single lamin (Ikegami et al., 2010; Mattout et al., 2011; Towbin et al., 2012).

The LEM domain protein Lap2β was recently implicated in gene silencing at the nuclear periphery in mammals (Zullo et al., 2012). It forms a complex with histone deacetylase (HDAC3) and cKrox, a protein binding to stretches of GA dinucleotides. While HDAC3 promotes heterochromatinization, the LEM domain protein binds the whole complex to the NE. The activity of the complex is cell-type- and developmental-stage-specific (Zullo et al., 2012), which probably depends on PTMs known to strongly affect the properties of LEM domain proteins (Tifft et al., 2009). Lap2β doubtlessly contributes to peripheral heterochromatin tethering in differentiated cells but cannot completely account for all tethering. Lap2β does not target, to the nuclear periphery, all lamina-associated DNA sequences analyzed (Zullo et al., 2012). NE-associated isoforms of Lap2 (neLap2) does not prevent inversion occurring in WT rods lacking both LBR and LMNA/C. Also, in rods, neLap2 does not counteract inversion in combination with

transgenically expressed LMNC (and native B-type lamins) (Solovei et al., 2013). Also, B-type lamins are dispensable for maintaining peripheral heterochromatin in the absence of LBR in nuclei from mice lacking both *Lmnb1* and *Lmnb2* (Kim et al., 2011; Yang et al., 2011a).

These facts emphasize the importance of LMNA/C and also suggest a role for other LEM domain proteins in the LMNA/C tether. Notably, emerin also binds to HDAC3, and its deletion reduces the level of HDAC3 at the nuclear periphery (Demmerle et al., 2012), whereas HDAC3 regulates heterochromatin levels (Bhaskara et al., 2010). The other LEM domain proteins have not yet been studied in this respect. In dermal papilla cells (also affected by *Lmna* deletion), loss of emerin results in increased expression of neLap2, supporting a possible role for both emerin and neLap in peripheral heterochromatin tethering. However, even the absence of both emerin and neLap2 does not result in inversion in striated muscle. It was also shown that the pattern of LEM domain protein expression is cell type specific, with none of the LEM domain proteins being universally expressed in mammalian cells (Solovei et al., 2013). This is in agreement with the reported broad functional overlap between LEM domain proteins in all organisms studied so far (Barkan et al., 2012; Huber et al., 2009; Mattout et al., 2011).

Clearly, the composition of the LMNA/C-dependent peripheral heterochromatin tether requires further analysis. Nevertheless, our data corroborates with published data and supports the notion that LEM-domain proteins cooperate with LMNA/C in tethering peripheral heterochromatin to

the NE in mammals (Fig. 4.10). Available data also suggest that different LEM domain proteins (probably combinations of these proteins) mediate heterochromatin binding to LMNA/C, depending on the cell type and developmental stage. Indeed, in *C.elegans*, heterochromatic chromosome arms are targeted to the nuclear lamina by a complex of lamin with any of the two LEM domain proteins (Ikegami et al., 2010; Mattout et al., 2011). Targeting depends on histone methylation (Towbin et al., 2012) —that is, using the same repressive epigenetic marks that LBR binds to in mammals. This suggests that complexes of lamin and LEM domain proteins in mammals should also include proteins recognizing histone methylation.

LMNA/C is a known marker of the differentiated state (Zhang et al., 2011), whereas our data primarily link LBR expression to undifferentiated or early differentiated states. This difference in the timing of expression of LBR and LMNA/C conforms to the opposite effects of *Lbr* and *Lmna* loss on transcription of many muscle-specific genes during the early stages of myotube differentiation. Loss of *Lbr* increases, whereas loss of *Lmna* decreases expression of these genes. This is consistent with the earlier findings on the delayed maturation of satellite and myotubes with myopathogenic mutations in *Lmna* (Bertrand et al., 2012; Melcon et al., 2006; Park et al., 2009). In agreement with previous studies (Kubben et al., 2011; Verhagen et al., 2012), loss of *Lbr* and *Lmna* had little effect on the transcriptomes of mature, fully differentiated skeletal muscle, though transgenic expression of LBR deregulates the differentiation of olfactory neurons (Clowney et al., 2012).

The same sequential pattern of LBR and LMNA/C expression in diverse cell types suggests that peripheral heterochromatin tethers regulate differentiation in a broad range of tissues, e.g., mesodermal (osteogenic and adipogenic) or perhaps in all cell types. In mammalian cells, targeting chromatin to the NE mediates its silencing in a histone-deacetylation-dependent manner (Finlan et al., 2008), which concurs with HDAC3 associating with LEM domain proteins. Tellingly, the proximity of the myogenic master regulator gene MyoD to the nuclear periphery directly affects its binding to alternative transcription factors in mammalian cells (Melcon et al., 2006; Yao et al., 2011). This illustrates how changes in gene position can switch between regulatory pathways and regulate cellular differentiation. The versatility of chromatin binding by the LMNA/C tether, suggested by our results, may explain how LMNA/C contributes to the regulation of diverse genes and developmental processes, resulting in a plethora of phenotypically different syndromes when this protein is mutated.

Chapter 5 – Determining the role of lamin A/C in gastrointestinal (GI) epithelium

Increased interest in the roles of lamins in changes to nuclear structure and link to malignancy has emerged. A great body of evidence indicates that alterations in lamins affect a variety of processes that can impact cancer development and progression, such as changes in nuclear flexibility in relation to cell metastasis (Rowat et al., 2013), gene regulation, proliferation, apoptosis, chromatin organization and genome stability (Broers et al., 2006; Foster et al., 2010; Gonzalez-Suarez et al., 2009a; Zink et al., 2004).

Expression of A-type lamins is altered in colorectal, lung, skin, ovarian, breast, thyroid cancers as well as in some leukemias (Agrelo et al., 2005; Belt et al., 2011; Broers et al., 1993; Capo-chichi et al., 2011; Foster et al., 2010; Helfand et al., 2012; Kaufmann, 1992; Machiels et al., 1995; Tilli et al., 2003; Venables et al., 2001; Willis et al., 2008). However, there are conflicting reports as to the significance of LMNA levels in GI tumors. In a study by Willis *et al.*, the increased expression of LMNA, but not LMNC, was linked to tumor progression in colorectal cancer (CRC). Patients with high levels of LMNA expression were more likely to die of CRC than similarly staged patients with low LMNA expression. Thus, LMNA was suggested to be a potential risk biomarker in CRC. Expression of LMNA in CRC cell lines up-regulated the expression of actin bundling protein T-plastin, resulting in reduced expression of cell adhesion molecule E-cadherin. It was proposed that loss of cell adhesion led to increased cell motility and resulted in metastasis of

tumor cells via reorganization of the actin cytoskeleton, and hence suggested that cancer cells with increased levels of LMNA were responsible for increased progression of CRC. In the same study, LMNA was highly expressed in the basal region of colonic crypt, a region suggested as the stem cell niche (Willis et al., 2008), contrary to previous evidence that LMNA is expressed only in differentiated somatic cells. In another study, low expression of LMNA/C in colonic epithelial cancer cells correlated to increased disease recurrence in stage II and III colon cancer patients (Belt et al., 2011). Therefore, while these studies implicate that alteration in LMNA expression levels is involved in oncogenesis in the intestines, the exact role of A-type lamins in intestinal tumor formation and progression remains to be elucidated.

I was interested to examine the roles of *Lmna* in highly proliferative murine intestinal epithelial cells (IECs) and in particular, its role in oncogenesis in the GI tract (restricted to the small and large intestines). Utilizing the conditional *Lmna*$^{FL/FL}$ mouse model that I described in chapter 3 and Villin-Cre recombinase (*Vil-Cre*) mice (Madison et al., 2002), I generated an IEC-specific *Lmna*-null mouse model where *Lmna* is deleted in epithelial cells in the GI tract but remains expressed in other cell types of the GI tract and all other organs.

5.1 <u>Expression of LMNA/C in the GI tract</u>

The expression of LMNA/C in the GI tract was examined in WT mice by immunofluorescence and western analysis. In the small intestine (duodenum, jejunum and ileum), expression of LMNA/C is higher in the central lamina propria than in the IECs (Fig. 5.1A and B). Expression of LMNA/C progressively increases as IECs migrate to the villous tip as they differentiate. Expression was weak or absent in most cells in the basal colonic crypts (Fig. 5.1A). LMNA/C expression in the murine GI is similar to the human GI where LMNA/C was strongly expressed in the functionally differentiated epithelial layers and also strongly expressed in surrounding stromal tissue and underlying muscle, with weaker or no expression in the majority of cells in the colonic crypts (Willis et al., 2008).

It is well documented that A-type lamins are expressed in differentiated cells but are usually absent in human and mouse stem cells (Constantinescu et al., 2006). LBR, but not LMNA/C, is expressed in the crypt cells in the duodenum (Fig. 4.3D) (Solovei et al., 2013). However, one study reported LMNA to be expressed in the stem cell niche of the human colon (Willis et al., 2008). To further determine whether LMNA/C is expressed in murine GI stem cells, I used a reporter line expressing green fluorescent proteins (GFP) under control of the stem cell marker Lgr5 (*Lgr5-EGFP-IRES-creERT2*) (Barker et al., 2007), to determine if LMNA/C co-localizes with Lgr5 in the duodenum. I did not find any co-expression of LMNA/C with the Lgr5-positive GI stem cells in the duodenum crypts (n=25) of 7-weeks old mice (Fig. 5.2).
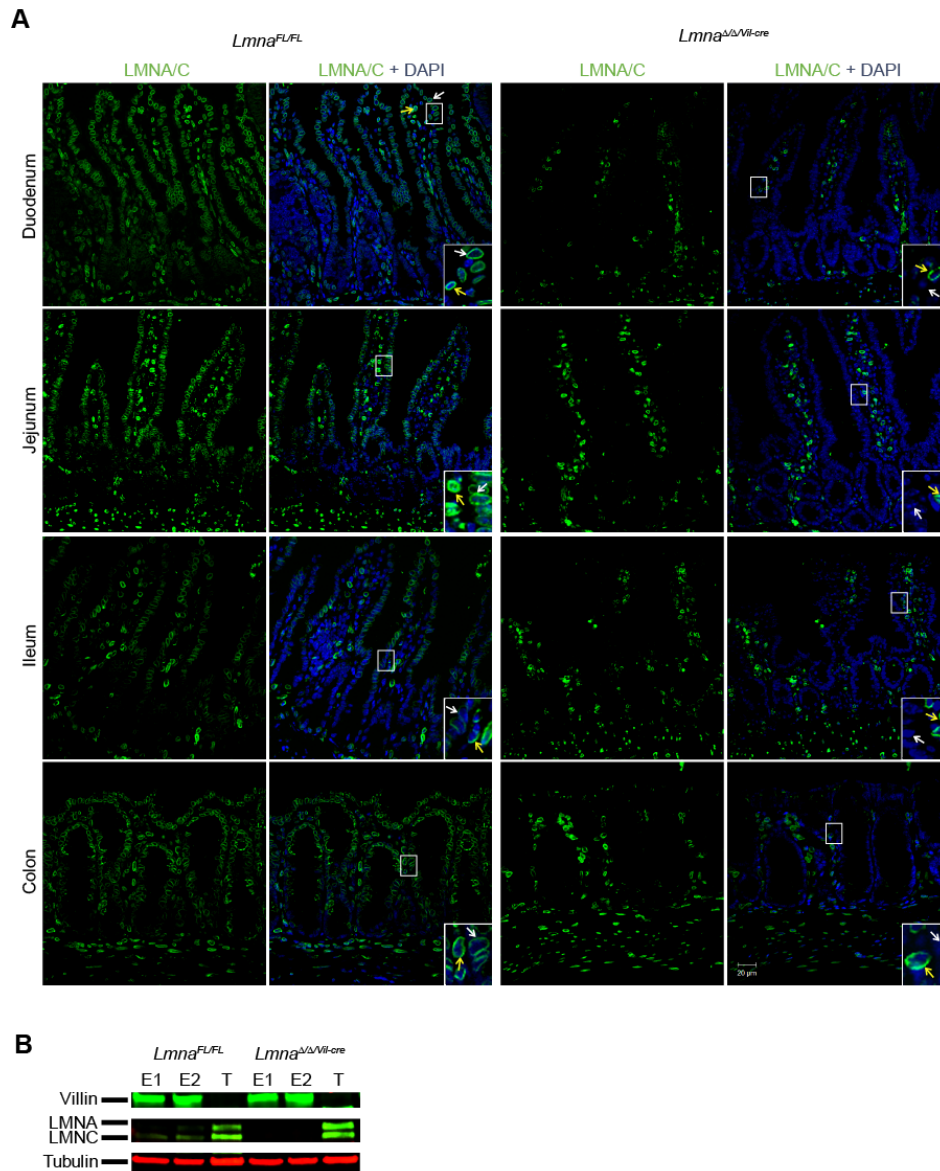
Figure 5.1: LMNA/C is abolished in _Lmna^Δ/Δ/Vil-Cre_ mice IECs. (A) Immunofluorescence staining of LMNA/C in _Lmna^Δ/Δ/Vil-Cre_ mouse GI tract (duodenum, jejunum, ileum and colon) showed that in WT mice, LMNA/C was detected in lower levels in the IECs (white arrows) compared to cells of the lamina propria (yellow arrows) and muscularis mucosa. Upon introduction of _Vil-Cre_, no LMNA/C was detected in the IECs in _Lmna^Δ/Δ/Vil-Cre_ mice but remains in lamina propria cells (inset) (Scale bars, 20 µm). (B) Western blot for LMNA/C indicated that in _Lmna^FL/FL_ mice, less LMNA/C was detected in IECs (E1, E2) compared to lamina propria cells and muscularis mucosa (T) and upon introduction of _Vil-Cre_, complete loss of LMNA/C was observed.
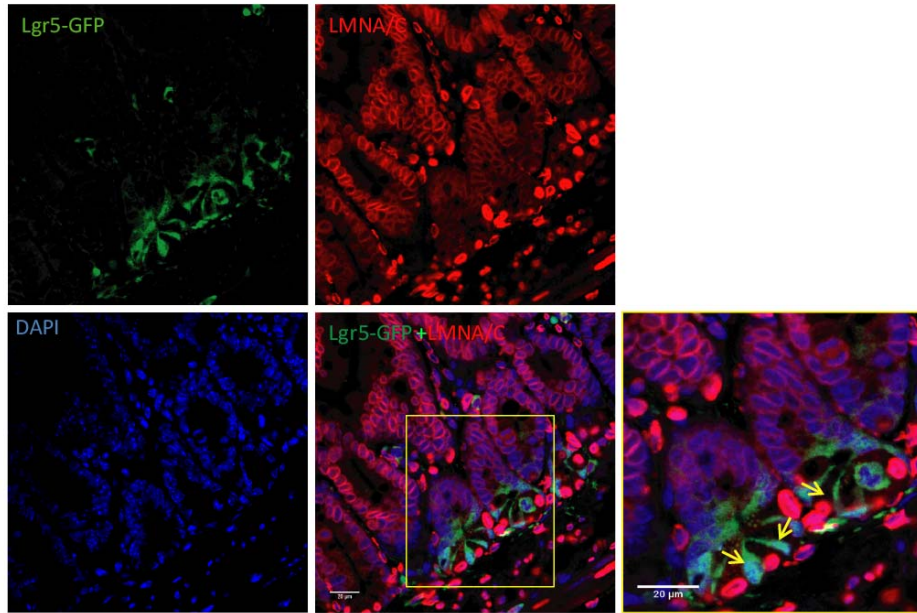
Figure 5.2: LMNA/C is not expressed in murine Lgr5-positive intestinal stem cells. In *Lgr5-eGFP-IRES-creERT2* reporter mouse duodenum, there was no co-localization of LMNA/C (red) and Lgr5-eGFP (green), indicating that LMNA/C is not expressed in the adult stem cell populations in the crypts (yellow arrows) of the murine duodenum. (Scale bars, 20 μm)

5.2 Deleting *Lmna* in the GI epithelium using *Vil-Cre* recombinase

To study the effects of loss of *Lmna* in the highly proliferative IECs, I used *Vil-Cre* mice to delete the *Lmna* gene and derive GI IEC-specific *Lmna* null mice (*Lmna*$^{\Delta/\Delta/Vil-Cre}$). Immunofluorescence and western analysis of *Lmna*$^{\Delta/\Delta/Vil-Cre}$ GI confirmed that LMNA/C was ablated in the epithelial layer throughout the GI tract, but not in the lamina propria or muscularis mucosa (Fig. 5.1A and B). *Vil-Cre* mediated deletion is generally efficient and continuous but a residual amount of mosaicism may remain (Madison et al., 2002). We observed occasional IECs still expressing LMNA/C in the *Lmna*$^{\Delta/\Delta/Vil-Cre}$ GI, but estimated this is in less than 1% of the total number of IECs.

5.3 *Lmna*$^{\Delta/\Delta/Vil\text{-}Cre}$ mice appear phenotypically normal

Lmna$^{\Delta/\Delta/Vil\text{-}Cre}$ mice were born at expected Mendelian ratios, and were indistinguishable from their WT littermates. They survived for more than 1 year without presenting any gross phenotypic abnormalities, such as shortened lifespan, reduced weight or spontaneous adenoma formation in their GI tract. Histological analysis of the GI at 10 weeks showed no overt disparities in intestinal morphology between control *Lmna*$^{FL/FL}$ and *Lmna*$^{\Delta/\Delta/Vil\text{-}Cre}$ mice (Fig. 5.3). Examination of 3 one year old *Lmna*$^{\Delta/\Delta/Vil\text{-}Cre}$ mice revealed no overt consequences on intestinal morphology. Although renal cortex and testes epithelial cells also expresses villin (Maunoury et al., 1992), minimal Cre recombination was observed in kidneys or testes of this Villin-Cre line (Madison et al., 2002). I also did not observe any gross morphological abnormalities in the kidneys or testes of *Lmna*$^{\Delta/\Delta/Vil\text{-}Cre}$ mice, and reasoned that deletion of *Lmna* occurred exclusively in the IECs or at least, did not contribute to non-GI specific phenotypes in *Lmna*$^{\Delta/\Delta/Vil\text{-}Cre}$ mice.
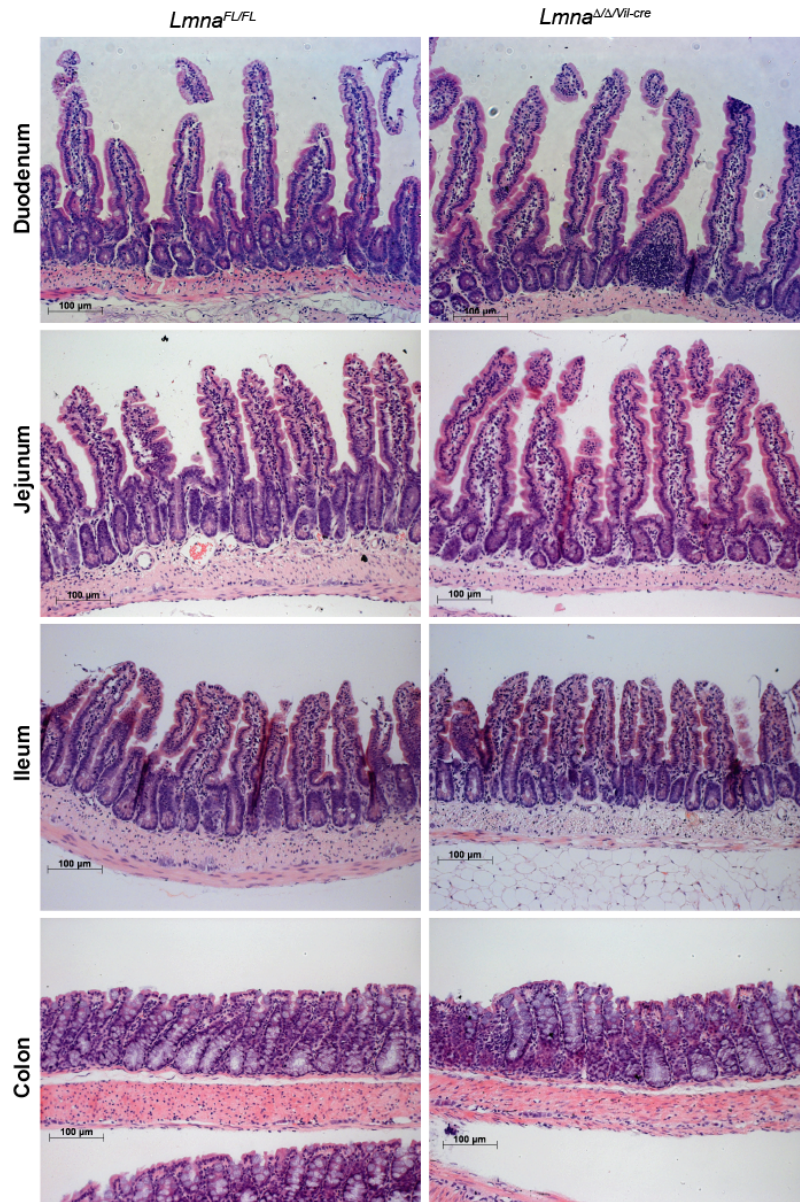
Figure 5.3: No observable histological differences were detected in *Lmna*^{Δ/Δ}*Vil-Cre* mice intestines. H&E staining of the different regions of the GI tract (duodenum, jejunum, ileum and colon) showed that at 10-weeks old, $Lmna^{\Delta/\Delta/Vil\text{-}Cre}$ mice were healthy and comparable to their WT littermates (Scale bars, 100 µm).

5.4 $Lmna^{\Delta/\Delta/Vil\text{-}Cre}$ mice do not show differences in GI epithelial proliferation

Since previous studies on human samples showed that there is no consistent pattern of LMNA expression in GI tumorigenesis, I investigated the effects of loss of *Lmna* on the proliferative capacity of the GI epithelium. Analysis of Ki-67 expression of the different segments of the intestines showed that Ki-67 positive cells were located in the crypt, mainly in the transit amplifying cells of the GI with no difference in the numbers of Ki-67 positive nuclei between control $Lmna^{FL/FL}$ and $Lmna^{\Delta/\Delta/Vil\text{-}Cre}$ (Fig. 5.4A and B). These findings are similar to previous reports where CRC lines not expressing LMNA showed no differences in proliferation rates compared to cells expressing LMNA (Willis et al., 2008).
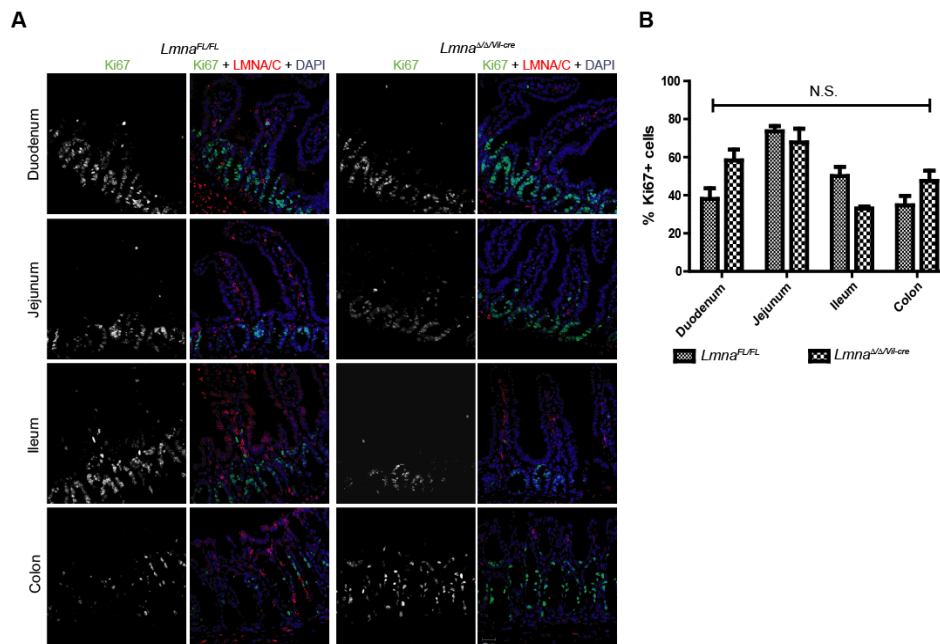
Figure 5.4: *Lmna*-null IECs do not show any differences in proliferation rate. (A) Ki-67 positive cells (white/green) were mainly located in the transit amplifying cells in the crypts, where LMNA/C (red) was not expressed. No difference in the number of Ki-67 positive cells was observed in *Lmna*$^{\Delta/\Delta/Vil\text{-}Cre}$ mice compared to their wild-type littermates (Scale bars, 20 µm). (B) Ki-67 positive cells in the crypts of duodenum, jejunum, ileum and colon were counted and tabulated. No statistical difference was observed between *Lmna*$^{\Delta/\Delta/Vil\text{-}Cre}$ mice and their WT littermates.

5.5 Loss of *Lmna* in the GI increases papilloma size

To investigate a potential link of LMNA/C to carcinogenesis, I bred *Lmna*$^{\Delta/\Delta/Vil\text{-}Cre}$ mice to mice carrying a mutation in the adenomatous polyposis coli gene (*Apc*$^{Min/+}$). *Apc*$^{Min/+}$ mice have a germ-line nonsense mutation in the adenomatous polyposis coli (Apc) gene and spontaneously develop intestinal adenomatous polyps in the GI tract around 10-12 weeks (Su et al., 1992). Immunofluorescence analysis of polyps obtained from *Lmna*$^{wt/wt}$/*Apc*$^{Min/+}$ and *Lmna*$^{\Delta/\Delta/Vil\text{-}Cre}$/*Apc*$^{Min/+}$ mice GI revealed that the polyps originated from IECs in both genotypes (Fig. 5.6). A comparison of the number and size of polyps throughout the GI tract was made between *Lmna*$^{wt/wt}$/*Apc*$^{Min/+}$ (n=14) and *Lmna*$^{\Delta/\Delta/Vil\text{-}Cre}$/*Apc*$^{Min/+}$ (n=16) mice aged between 17-30 weeks. The total number of polyps in the GI tract was only slightly elevated in *Lmna*$^{\Delta/\Delta/Vil\text{-}Cre}$/*Apc*$^{Min/+}$ mice (77.56 ±13.17 vs. 58.79 ±11.96, Fig. 5.5A), although I found an increased frequency of large polyps (2-5mm) in the duodenum (1.5-fold larger, *p<0.05*) and proximal jejunum (3-fold larger, *p<0.01*) compared to *Lmna*$^{wt/wt}$/*Apc*$^{Min/+}$ mice (Fig. 5.5B). These results indicate that in the absence of *Lmna*, polyp growth is accelerated, though possibly only in specific segments of the GI tract.
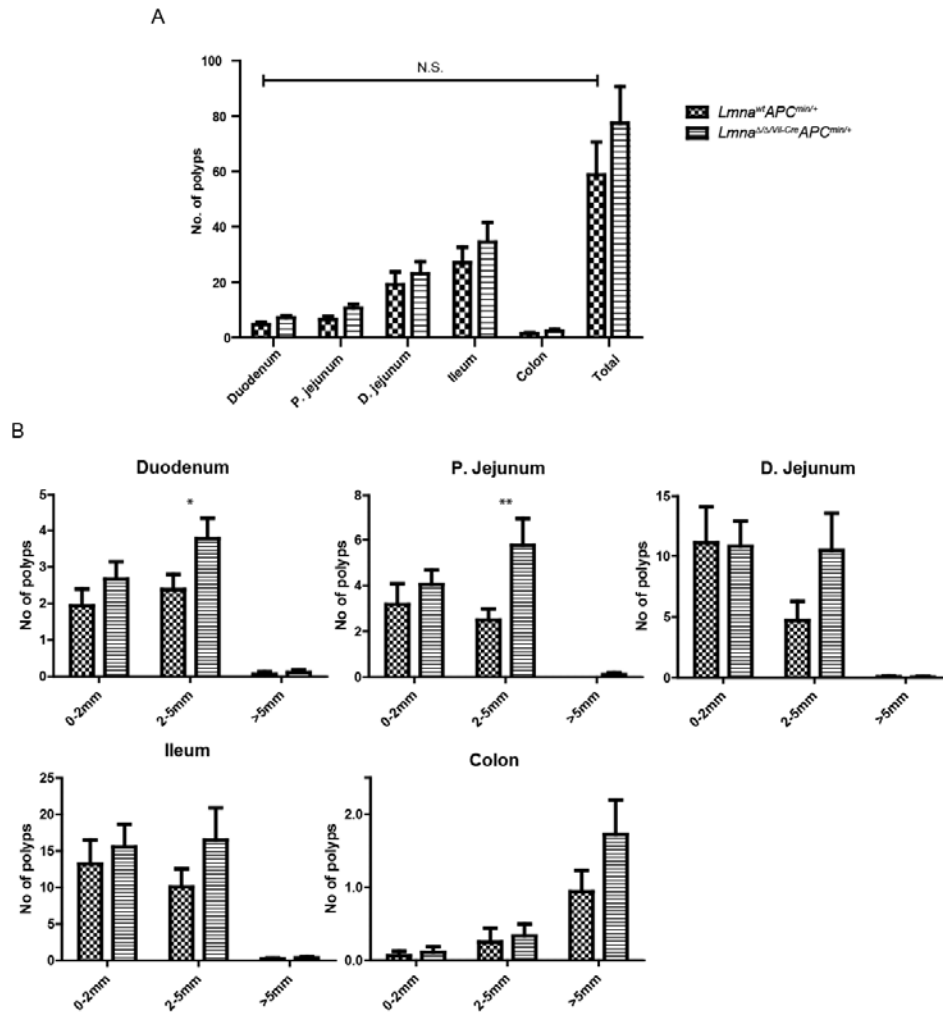
Figure 5.5: When exposed to *APC^min* mutation, the total number of polyps was unchanged but polyp size was enhanced in *Lmna^ΔΔ/Vil-Cre* mice GI. (A) The total number of polyps observed in the GI tract (duodenum, proximal and distal jejunum, ileum and colon) was not changed in *Lmna^wt/wt^/APC^Min/+* (n=14) compared to *Lmna^ΔΔ/Vil-Cre^/APC^Min/+* (n=16) mice. (B) Increased frequency of larger polyps (2-5mm) was observed in the duodenum (* *p<0.05*) and proximal jejunum of *Lmna^ΔΔ/Vil-Cre^*/APC^Min/+ mice. (** *p<0.01*) compared to their WT littermates. Data represents mean ± SEM.

5.6 Prolonged expression of LBR in *Lmna*-null IECs and polyps

In chapter 4, I showed that LMNA/C and LBR expression is coordinated in a temporally synchronized manner and that loss of both LBR and LMNA/C results in chromatin inversion (Solovei et al; 2013). In the GI epithelium, LBR is strongly expressed in the basal colonic crypts and as IECs progress up the vilum, LMNA/C replaces LBR in the nuclei (Fig. 5.6A). I analyzed LBR expression in $Lmna^{\Delta/\Delta/Vil-Cre}/APC^{Min/+}$ GI and found LBR expression was enhanced in *Lmna*-null IECs (Fig. 5.6A). LBR was also highly expressed in *Lmna*-null IECs-derived polyps in $Lmna^{\Delta/\Delta/Vil-Cre}/Apc^{Min/+}$ mice compared to *Lmna* positive IECs in the polyps of $Lmna^{wt/wt}/Apc^{Min/+}$ mice (Fig. 5.6B).
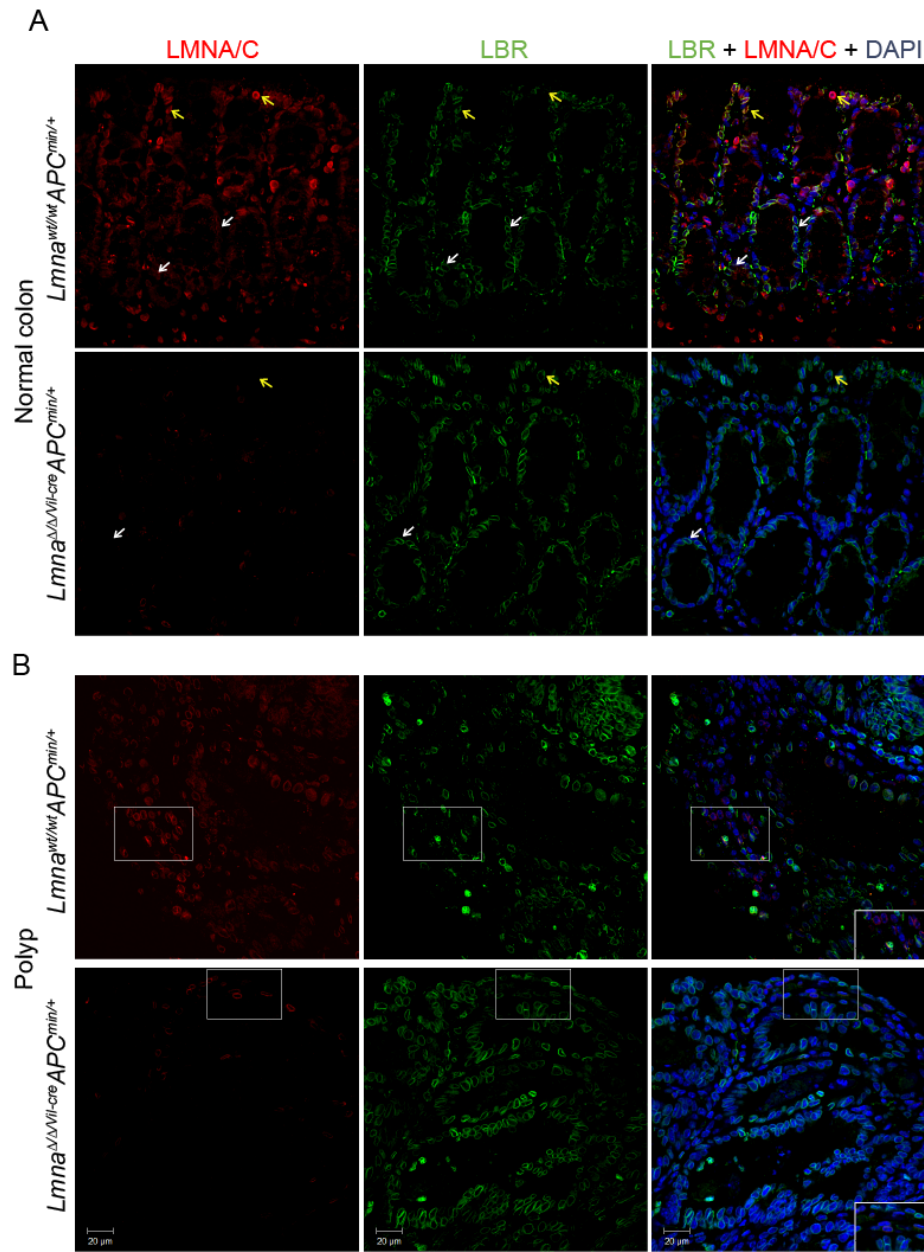
Figure 5.6: Increased expression of LBR in *Lmna*-null IECs. Immunofluorescence co-staining of LMNA/C and LBR showed that (A) in the normal regions of *Lmna*$^{wt/wt}$/APC$^{Min/+}$ colon, expression of LMNA/C and LBR was coordinated such that LMNA/C is highly expressed at villous tip (indicated as yellow arrows) while LBR is abundantly expressed in the basal colonic crypt IECs (indicated as white arrows). In *Lmna*$^{\Delta/\Delta/Vil-Cre}$/APC$^{Min/+}$ colon IECs, expression of LBR was uniform. (B) In the *Lmna*$^{wt/wt}$/APC$^{Min/+}$ polyp, IECs expressing LMNA/C exhibited none/lower expression of LBR whereas in *Lmna*$^{\Delta/\Delta/Vil-Cre}$/APC$^{Min/+}$ polyp, LMNA/C-null cells exhibited higher expression of LBR in contrast to neighboring cells with LMNA/C expression and low LBR expression (see inset) (Scale bars, 20 μm).

5.7 Conclusions

In conclusion, by employing the conditional $Lmna^{FL/FL}$ mouse model, I generated a mouse line ($Lmna^{\Delta/\Delta/Vil-Cre}$) where $Lmna$ was ablated in the IECs but remains intact in the lamina propria and other tissues. Mice lacking $Lmna$ throughout the GI epithelium survived more than 1 year without presenting gross abnormalities or spontaneous development of GI tumors. Histological analysis of the GI tract lacking LMNA/C showed no abnormalities in morphology and proliferation. Hence, the creation of our mouse model allows us to bypass the early lethality due to global loss of lamin A/C, and evaluate tissue-specific loss of $Lmna$ in the GI and the consequences on tumorigenesis.

To elucidate the role of lamin A/C in GI oncogenesis, we investigated the effect of loss of $Lmna$ on the proliferative capacity of murine GI epithelial cells. Our findings reveal that, although A-type lamins appear to be dispensable in the GI epithelium, loss of $Lmna$ in the IECs increased the frequency of larger polyps (2-5mm) in the duodenum and proximal jejunum, but have no significant effect on overall number of papillomas. Although the statistical significance is marginal, my data suggests that loss of $Lmna$ leads to accelerated polyp growth indicating that $Lmna$ may serve as a tumor suppressor gene.

Loss of $Lmna$ in our conditional $Lmna^{\Delta/\Delta/Vil-Cre}/Apc^{Min/+}$ mice possibly resulted in defective control of genomic stability in highly proliferative intestinal epithelial cells, resulting in occurrence of bigger polyps. Therefore, I

took another approach to confirm our hypothesis. p53, apart from *APC*, is one out of three genes most frequently mutated in CRC (Fearon and Vogelstein, 1990). p53 is a tumor suppressor gene that has an important role in regulating the cell cycle and apoptosis. In p53-null mice, cancer begins to develop at 4 to 6 months of age (Donehower et al., 1992; Jacks et al., 1994). Therefore, I attempted to obtain an inducible Cre deletion of *Lmna* specifically in the intestinal stem cells that will subsequently proliferate and differentiate into IECs. I crossed *Lmna*$^{FL/FL}$ mice to *Lgr5-EGFP-IRES-CreERT2* mice (Barker et al., 2007) where deletion of floxed *Lmna* occurs in GI following tamoxifen induction. This would allow me to investigate if loss of *Lmna* shortens the period or increase the incidence of cancer of the intestine and help further elucidate the role of *Lmna* in cancer formation in the highly proliferative intestine. However, I found that *Lgr5-EGFP-IRES-CreERT2* mediated deletion of *Lmna* was inefficient and mosaic. Tumour sensitized double mutant mouse lines containing floxed *Apc* (Cheung et al., 2010) and floxed *p53* alleles (Marino et al., 2000) that result in the deletion of *Lmna* as well as APC and p53 respectively (*Lmna*$^{FL/FL}$*Apc*$^{FL/FL/Lgr5-CreERT}$ and *Lmna*$^{FL/FL}$*p53*$^{FL/FL/Lgr5-CreERT}$), were also analyzed for tumor formation. However, due to mosaic deletion of *Lmna*, I was unable to obtain conclusive results on disparities in lifespan or polyps formation between *Lmna*-null and WT mice.

LMNA/C is important in tethering chromatin to the nuclear periphery in terminally differentiated cells while LBR does the same in less differentiated cells (Solovei et al., 2013). Furthermore, loss of LMNA/C

results in prolonged expression of LBR in terminally differentiated cells (Solovei et al., 2013). Strong and persistent expression of LBR was also observed in IECs and polyps lacking LMNA/C. Since LBR is expressed in the crypts and transitional zones where GI cells are proliferating, our findings suggest that the slight increase in polyp size in $Lmna^{\Delta/\Delta/Vil\text{-}Cre}/Apc^{Min/+}$ mice may be due to the persistent expression of LBR, which otherwise would be suppressed by lamin A/C.

A recent study of human colon suggested that LMNA was expressed in colonic crypts and that LMNA could be a marker of adult human colonic stem cells (Willis et al., 2008). LGR5 positive cells are found in human GI and these cells give rise to multicellular organoids *ex vivo* indicating that they are pluripotent (Jung et al., 2011). Using a mouse strain expressing GFP specifically in Lgr5 positive intestinal stem cells, co-localization of LMNA/C with Lgr5 was not detected, indicating that LMNA/C positive cells in the crypts are not the stem cells that give rise to GI adenomas. In contrast to humans, LMNA/C may not be a marker for murine adult intestinal stem cells.

Chapter 6 – Determining the role of lamin A/C in skin development and carcinogenesis

6.1 <u>Structure and properties of skin and hair in human and mouse</u>

The skin is the largest organ of the human body and has important functions in providing of barrier to harmful organisms and substances, protection against ultraviolet radiation, as well as regulating water loss and body temperature (Blanpain and Fuchs, 2006). The skin is composed of 3 primary layers: the epidermis, dermis and hypodermis (Fig. 6.1A). The epidermis is further stratified into 4 sublayers with keratinocytes being the predominant cell type in all the sublayers. Above the basement membrane lies the basal cell layer (*stratum basale*) consisting of stem cells and transit amplifying cells that differentiate and move upwards into the suprabasal/spinous layer (*stratum spinosum*). Keratinocytes progressively flatten as they move apically. In the granular layer (*stratum granulosum*), keratinocytes further differentiate and eventually lose their nuclei. The outermost epidermal layer is the cornified layer (*stratum corneum*) and depending on their body location, consists of up to 30 layers of dead anucleated corneocytes. The mouse skin is a useful model for studying human skin, and is structurally similar. However, the number of epidermal layers can differ, with the epidermis of mouse body skin having only 1 to 2 cell layers and paw skin having up to 10 layers of epidermal cells.

The skin also contains important appendages such as hair follicles (HFs), nails and sebaceous glands. Mammalian hair is critical to regulating body heat and has significant sensory functions. The hair follicle (HF) is a specialized organ composed of several layers of epithelial cells (the root sheath) surrounding the hair shaft (Sperling, 1991). Specialized dermal papilla cells reside at the base of the HF and have significant roles in the postnatal regulation of hair growth (Jahoda et al., 1984). Throughout a mammal's lifetime, HFs cyclically degenerate and regenerate in three main phases: anagen as the growth phase, catagen as the apoptosis-driven regression phase and telogen as the resting phase (Fig. 6.1A) (Cotsarelis, 1997). While human HFs undergo asynchronous hair growth cycles throughout their lifespan (Xu et al., 2003), murine hair growth occurs in a wave-like pattern and is highly synchronized during the first two cycles (Muller-Rover et al., 2001).

In C57BL6 mice, HF morphogenesis starts during late embryogenesis and lasts until P14. After this period of rapid growth, HFs enter a catagen phase, a period of controlled regression that involves apoptosis of epithelial cells in the hair bulb and outer root sheath (ORS) (Lindner et al., 1997). At around P19, HFs enter the first postnatal hair cycle at telogen where they become dormant for a few days and await activation. The first postnatal anagen starts at P28 and HFs go through 2 weeks of rapid growth, after which they transit into a short catagen and then a resting telogen phase lasting 4 to 5 weeks. By P84, HFs re-enter anagen again and hair growth becomes random and asynchronous after this point (Fig. 6.1B) (Krause and Foitzik, 2006; Muller-Rover et al., 2001; Stenn and Paus, 2001).
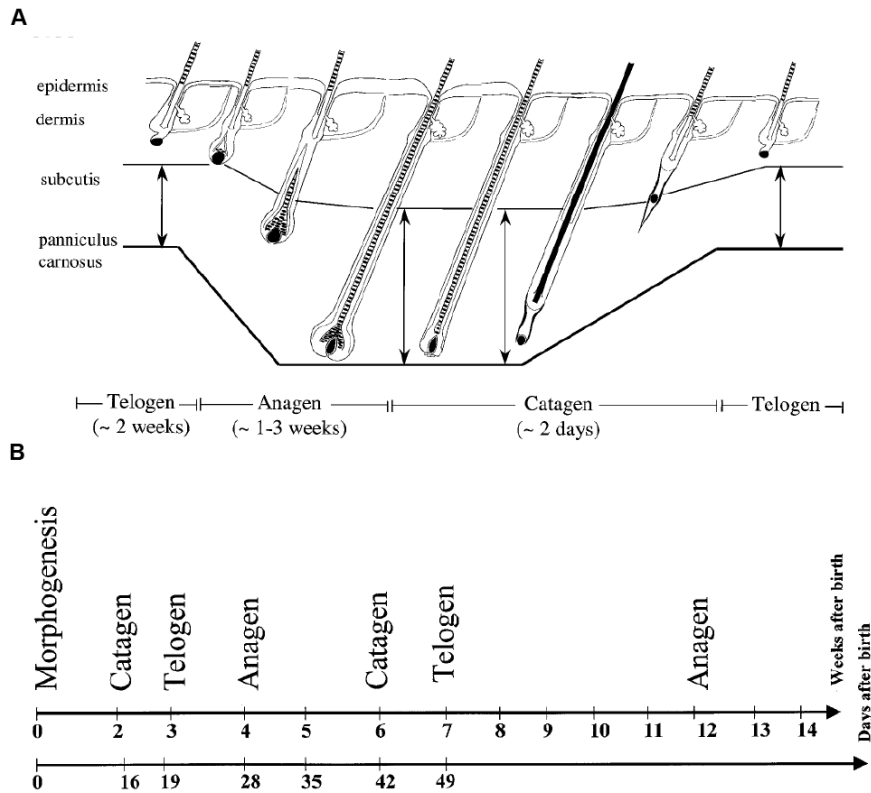
Figure 6.1: Hair cycling in C57BL6 mice. (A) The skin is a stratified organ comprising of epidermis, dermis, hypodermis (*subcutis*) made up of subcutaneous fat and a thin dermal muscle layer *panniculus carnosus*. Hair follicles (HFs) undergo cycles of hair growth in 3 distinct stages: telogen (rest), catagen (regression) and anagen (growth) phase. At each phase, the sublayers and HFs show distinct histomorphologies. (B) HFs in C57BL6 mice cycle in a synchronized manner for about 12 weeks after birth. First postnatal anagen phase starts around P28 and lasts for 1-2 weeks, followed by a short catagen phase and a longer telogen phase at P49. The second anagen starts at around P84. Illustration adapted with permission (Muller-Rover et al., 2001).

6.2 Key molecular mechanisms regulate skin and HF growth

Growth and differentiation of keratinocytes are influenced by a large number of factors. Several different cyclin-dependent kinases and growth factors such as epidermal growth factor (EGF), insulin-like growth factor-1 (IGF-1), keratinocyte growth factor (KGF) and TGF-β participate in enhancing or inhibiting keratinocyte proliferation (Gniadecki, 1998). TGF-β

125

belongs to BMP superfamily and is the most important inhibitor of keratinocyte growth (Glick, 2012). Low levels of TGF-β1 and TGF-β2 are usually found in keratinocytes of the suprabasal layer and enhanced levels of TGF-β can lead to epidermal atrophy in mice (Sellheyer et al., 1993).

Molecular signaling pathways involved in the formation, growth and cycling of HFs have been extensively studied. During hair morphogenesis, growth factors such as fibroblast growth factors (FGF), KGF and BMP-inhibitory factors determine the positions of hair placodes and specify their commitment (Mou et al., 2006; Petiot et al., 2003; Werner et al., 1994). During hair development, sonic hedgehog (*Shh*) is necessary for epithelial cells proliferation and formation of new HFs. Disruption of *Shh* results in impaired formation of HFs (St-Jacques et al., 1998; Wang et al., 2000) while ectopic expression of *Shh* induces quiescent HFs to enter anagen (Sato et al., 1999). Wnt/β-catenin signaling is also critical during HF induction and growth. Disruption of β-catenin or ectopic expression of Wnt inhibitor dickkopf-1 (Dkk1) in the epidermis resulted in impaired hair placodes formation (Andl et al., 2002; Huelsken et al., 2001). Constitutive expression of the stabilized form of β-catenin in the epidermis resulted in excess HF and hair tumours in mice (Gat et al., 1998; Lo Celso et al., 2004; Van Mater et al., 2003). During hair cycling, expression of TGF-β declines as HFs cycle from catagen to telogen. In mice, ectopic TGF-β expression causes premature catagen (Foitzik et al., 2000) whereas suppression of TGF-β signaling delays catagen (Tsuji et al., 2003). Taken together, these studies implicate various molecular signaling pathways play important roles in keratinocyte growth and hair cycling.

6.3 Expression and functions of lamins in skin and hair

While B-type lamins are expressed in all cells and are essential for normal embryogenesis (Vergnes et al., 2004), A-type lamins are found in more differentiated cells and may have more specialized tissue-specific functions (Goldman et al., 2002). In the human skin, this expression pattern is conserved. B-type lamins are expressed in all cell types of the human skin. *LMNB1*, but not *LMNB2*, declines as keratinocytes differentiate and migrate up the epidermal axis (Dreesen et al., 2013a). A-type lamins are highly expressed in dermal fibroblasts and epidermal suprabasal cells but absent in actively proliferating basal cells (Broers et al., 1997; Tilli et al., 2003; Venables et al., 2001).

In mice, expression of lamin A/C in skin starts at around E15 and persists postnatally through adulthood (Rober et al., 1989). During the different hair growth phases, differential levels of A- and B-type lamins were observed: expression of both A- and B-type lamins are strongest in basal keratinocytes, ORS of HFs and dermal papilla cells but lower in catagen hair bulbs and suprabasal cells in all stages (Hanif et al., 2009). During development and cellular differentiation, expression of LBR and LMNA/C is sequential and coordinated in keratinocytes (Solovei et al., 2013). In stratified epidermis of the skin, expression of LBR and LMNA/C is spatially and temporally coordinated: basal keratinocytes express higher levels of LBR while more differentiated suprabasal cells express higher levels of LMNA/C (Fig. 4.3). Matrix cells in the hair bulb express LBR (Cohen et al., 2008) but

not LMNA/C while differentiated keratinocytes along the edge of the hair bulb show strong LMNA/C expression (Fig. 4.4E) (Solovei et al., 2013).

A mouse line, harboring a spontaneous mutation in exon 1 of *Lmna* (*Lmna^Dhe^*), displayed severe abnormalities in skin, hair and bone structure. This missense mutation resulted in amino acid substitution (L52R) that destabilizes the coiled coil rod domain of lamin A/C, so potentially disrupting the functions of lamin A-interacting proteins. Besides defective skull growth and mineralization deficiencies, homozygous *Lmna^Dhe^* mice exhibit profound anomalies in the skin and hair such as thickened epidermis, multinucleated suprabasal keratinocytes, reduced hypodermis thickness, increased basal keratinocyte apoptosis, shorter length of anagen HFs and ulcerations in the oral mucosa. While homozygous *Lmna^Dhe^* mice die at P10, heterozygous mice have a lifespan comparable to WT mice. Heterozygous mice exhibit mild skin and hair anomalies such as smaller ear pinnae, flaky skin and sparse hair with accelerated greying (Odgren et al., 2010). In mice deficient in *Zmpste24*, the gene coding for the metalloproteinase required for the post-translational processing of lamin A, mice exhibit alopecia and apoptotic hair bulbs due to reduced Wnt signaling in their hair follicles (Espada et al., 2008).

In contrast, mice with a tissue-specific deletion of *Lmnb1* and *Lmnb2* in their keratinocytes did not present any overt pathology in their skin, hair and nails and histological analysis did not reveal abnormalities. *Lmnb*-null keratinocytes exhibited normal proliferation rates and chromosome numbers although a significant increase in occurrence of misshapen nuclei and blebs

was observed (Yang et al., 2011a). Hence, B-type lamins would appear to be dispensable in murine keratinocyte development and proliferation. In a follow up study, a mouse line was created where keratinocytes lack all nuclear lamins (*Lmna^{Sul}*, *Lmnb1* and *Lmnb2*). These mice exhibit morphological anomalies such as ichythosis, defective skin barrier function leading to severe dehydration, a thickened epidermis, lipid accumulation in the epidermis, defective hair placode development with the mice surviving only up to few days after birth. Lamin-deficient keratinocytes showed abnormal nucleoplasmic localization of emerin, intrusion of cytoplasmic fibers into the nucleus and incursion of nuclear and ER membranes into the chromatin, indicating that lamins are important in the formation of a "physical barrier" at the nuclear envelope to prevent invasion cytoplasmic organelles into the nucleoplasm. DNA synthesis and proliferation of lamins-deficient keratinocytes from P1 mice was not altered (Jung et al., 2014). Taken together, the complete absence of nuclear lamins in keratinocytes does not hinder embryonic skin formation, growth and differentiation, but A-type lamins may be more critical than B-type lamins in the postnatal regulation and maintenance of skin and HFs.

Mutations in lamins result in many diseases known as laminopathies. While many laminopathies affect skeletal and cardiac muscles, peripheral nerves and fat distribution, in 3 of the laminopathies the skin is also affected. HGPS patients exhibit accelerated aging symptoms and anomalies in skin and hair such as alopecia, scleroderma and thinning of epidermis (Sarkar and Shinton, 2001). Patients with mandibuloacral dysplasia also display alopecia,

skin atrophy and hyperpigmentation in their skin (Novelli et al., 2002). Loss of *Zmpste24* causes the very rare neonatal lethal disease RD where newborns exhibit tight erosive skin with hyperkeratosis, sparse eyebrows and hair (Navarro et al., 2005). The occurrence of these skin-related laminopathies indicates that *LMNA* has important tissue-specific functions in the development and homeostasis of skin and hair.

6.4 <u>Expression of lamins in skin cancers</u>

Lamins have important roles in maintenance of nuclear architecture, chromatin organization, apoptosis and genome stability (Broers et al., 2006; Foster et al., 2010; Gonzalez-Suarez et al., 2009a; Zink et al., 2004), all of which may contribute to tumourigenesis. Hence, mutations in lamins and changes in the nuclear lamina may contribute to cancer development and progression (Worman and Foisner, 2010). Indeed, aberrant expression and localization of lamins have been implicated in both hematopoietic and other cancers including those of the skin (Foster et al., 2010; Tilli et al., 2003; Venables et al., 2001).

The expression of LMNA generally marks non-proliferating differentiated cells while the absence of LMNA is associated with a more proliferative profile. In a study looking at human basal cell carcinoma (BCC), 10 out of 16 tumours that did not express LMNA showed enhanced proliferation, while tumours lacking LMNC displayed slower growth. This

observation suggests that lamin A, but not lamin C, may have tumour suppressing roles in BCC (Venables et al., 2001). However, in another study, LMNA was reported as being widely expressed in squamous cell carcinoma (SCC) and BCC, and 60% of actively proliferating cells in the tumours expressed LMNA. In normal human skin, LMNA is usually absent in the basal cells. However, LMNA was detected in the basal cells of epidermis overlying SCC and BCC, suggesting that lamin A may have a role in the primary processes of carcinogenesis. Hence, it was proposed that LMNA is absent in the early phase of BCC and SCC but as tumour progresses, the tumour cells differentiate with increasing LMNA expression (Tilli et al., 2003).

Using our $Lmna^{\Delta/\Delta K14\text{-}Cre}$ mouse model, I sought to study the effect of loss of *Lmna* in keratinocytes. I evaluated the roles which lamin A/C play in the development and homeostasis of murine skin and hair. In particular, I am interested in defining whether *Lmna* partakes in the processes involved in skin transformation.

6.5 Deleting *Lmna* in keratinocytes with *K14-Cre*

Lamins are abundantly expressed in the mouse skin. A-type lamins are expressed in the keratinocytes, dermal fibroblasts, sebaceous glands, inner and outer root sheath (ORS) of HFs, bulb and dermal papilla (Fig. 6.2A) (Hanif et al., 2009; Solovei et al., 2013). They are also expressed in the epithelial keratinocytes and striated muscles of the tongue (Fig. 6.2B).

To study the effect of loss of *Lmna* in highly proliferative epithelial cells in the skin, I use the *K14-Cre* line to delete *Lmna* specifically in the keratinocytes. *K14-Cre* driven β-galactosidase expression was observed in skin and tongue epithelium, HFs, and also at low levels in the uterus, liver and thymus (http:/cre.jax.org/Krt14/Krt14-creNano.html). *Lmna*^{Δ/ΔK14-Cre} mice are born at Mendelian ratios, and indistinguishable from their WT littermates. Skin tissues including the dorsal skin, ventral skin, paws and tongue were analyzed and keratinocyte-specific *Lmna* knockout mice (*Lmna*^{Δ/ΔK14-Cre}) do not express LMNA/C in the skin epidermis, ORS of HFs and tongue epithelium (Fig. 6.2A, B). The efficiency of deletion was near 100% and keratinocyte-specific.

Keratinocytes were harvested from WT (*Lmna*^{FL/FL}) and *Lmna*^{Δ/ΔK14-Cre} mice and analyzed via qRT-PCR, western analysis and immunofluorescence staining for LMNA/C. Similar to the *Zp3-Cre* driven global knockout *Lmna*^{Δ/Δ}, *Lmna* mRNA transcript levels at exons 9 to 10 are greatly depleted (~99%) while exons 3 to 4 show a ~50% reduction (Fig. 6.3A). LMNA/C protein expression was completely abolished in *Lmna*-null keratinocytes as demonstrated by western blot analysis and immunofluorescence staining (Fig. 6.3B, C).
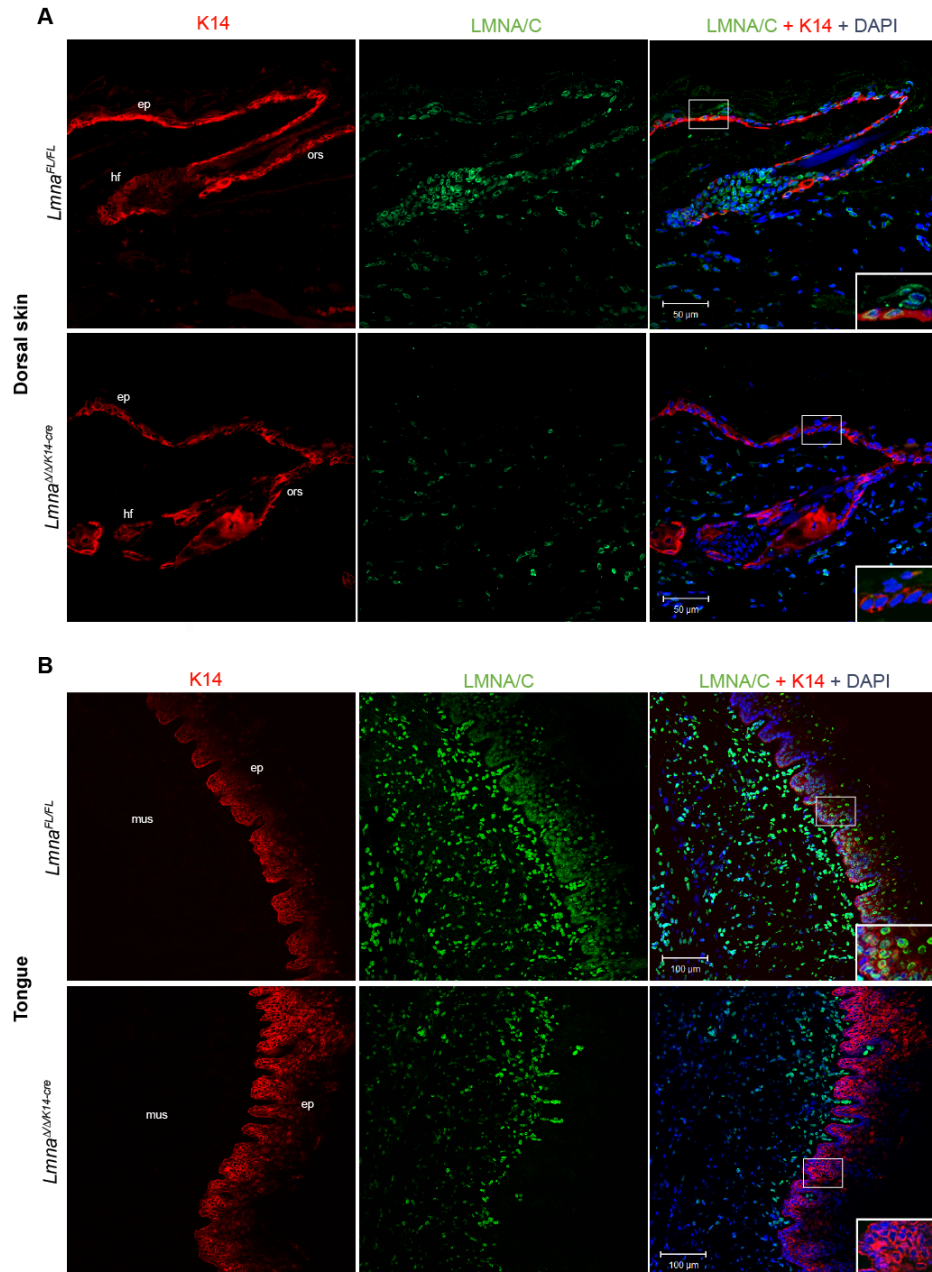
Figure 6.2: LMNA/C is widely expressed in skin and tongue. Upon introduction of *K14-Cre*, LMNA/C is abolished in keratinocytes in skin and tongue epithelium of *Lmna*^{Δ/ΔK14-Cre} mice. (A) In the dorsal skin, LMNA/C (green) is expressed in keratinocytes in the skin epidermis (ep) and hair follicles (hf), dermal fibroblasts in the dermis, and dermal papilla cells. K14 (red) is expressed in the basal cell layer and ORS of HFs. In the dorsal skin of *Lmna*^{Δ/ΔK14-Cre} mice, expression of LMNA/C is abolished in K14-expressing keratinocytes (red, see inset) but remains expressed in fibroblasts in the dermis (Scale bars, 50 µm). (B) In the tongue, LMNA/C is expressed in high levels in the muscular layer (mus) and in lower levels in the K14-expressing keratinocytes (ep) in the epithelium. In *Lmna*^{Δ/ΔK14-Cre} mice, expression of LMNA/C is completely abolished (Scale bars, 100 µm).

133
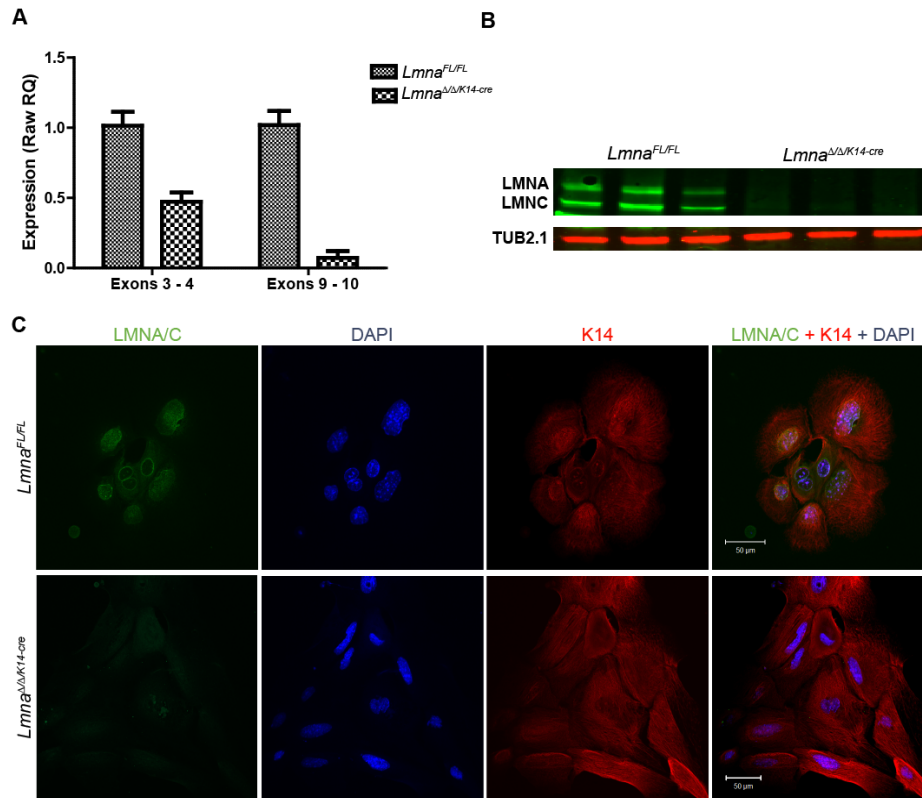
Figure 6.3: LMNA/C is abolished in keratinocytes of *Lmna*^{Δ/ΔK14-Cre} mice. Keratinocytes extracted from dorsal skin of *Lmna*^{Δ/ΔK14-Cre} mice confirm that (A) *Lmna* mRNA transcript levels are reduced by ~90% and ~50% at exons 9 to 10 and exons 3 to 4 respectively (n=3 biological samples; data represents mean ± SEM). At the protein level, LMNA/C cannot be detected by (B) western analysis (n=3 biological samples) and (C) immunofluorescence staining of *Lmna*-null keratinocytes. (Scale bars, 50 μm).

6.6 Loss of lamin A/C does not affect B-type lamins and other NE proteins

To study the effect of loss of *Lmna* on other components of the nuclear lamina, I studied the expression profiles of B-type lamins and NE components including emerin and LAP2α in *Lmna*-null keratinocytes. *Lmnb1* and *Lmnb2* mRNA levels are unchanged (Fig. 6.4A) and western analysis revealed that expression levels of LMNB1, LMNB2, emerin and LAP2α were not significantly altered (Fig. 6.4B). In the epidermis and HFs of *Lmna*^{Δ/ΔK14-Cre}

mice, there are more LMNA-null keratinocytes expressing LMNB1 but localization of LMNB1 was not altered (Fig. 6.4C). Contrary to previous reports from FVB/N mice (Hanif et al., 2009), I did not see differential expression of LMNA/C and LMNB in basal and suprabasal cells. In WT mice, expression of LMNA/C and LMNB1 is similar in both basal and suprabasal keratinocytes (Fig. 6.4C). On the other hand, expression of LBR was prolonged and enhanced in epidermis of $Lmna^{\Delta/\Delta K14-Cre}$ mice (Fig. 4.8) and this may be important in maintenance of heterochromatin positioning.

6.7 <u>Histological analysis of skin of $Lmna^{\Delta/\Delta K14-Cre}$ mice</u>

Histological examination of skin tissue sections from 10 weeks old mice (age and gender matched littermates) show thickened epidermis in the dorsal skin, ventral skin, and non-cornified layer of stratified squamous epithelial in the tongue of the $Lmna^{\Delta/\Delta K14-Cre}$ mice. Follicular hyperkeratosis and hyperplasia are also observed in $Lmna^{\Delta/\Delta K14-Cre}$ mice (Fig. 6.5, Appendix C – Pathology report).

The thickness of dorsal and ventral skin epidermis as well as tongue epithelium was measured. In $Lmna^{\Delta/\Delta K14-Cre}$ mice, the dorsal skin epidermis is 3.33-fold thicker than WT mice (23.37 ± 0.94 μm vs. 7.01 ± 0.22 μm), ventral skin is 1.77-fold thicker (21.56 ± 0.89 μm vs. 12.18 ± 0.52 μm) and tongue epithelium is 2.05-fold thicker (56.61 ± 2.09 μm vs. 27.57 ± 1.39 μm) (Fig

6.5). These results indicate that loss of *Lmna* leads to greater epidermal thickness possibly due to hyperproliferation of keratinocytes.
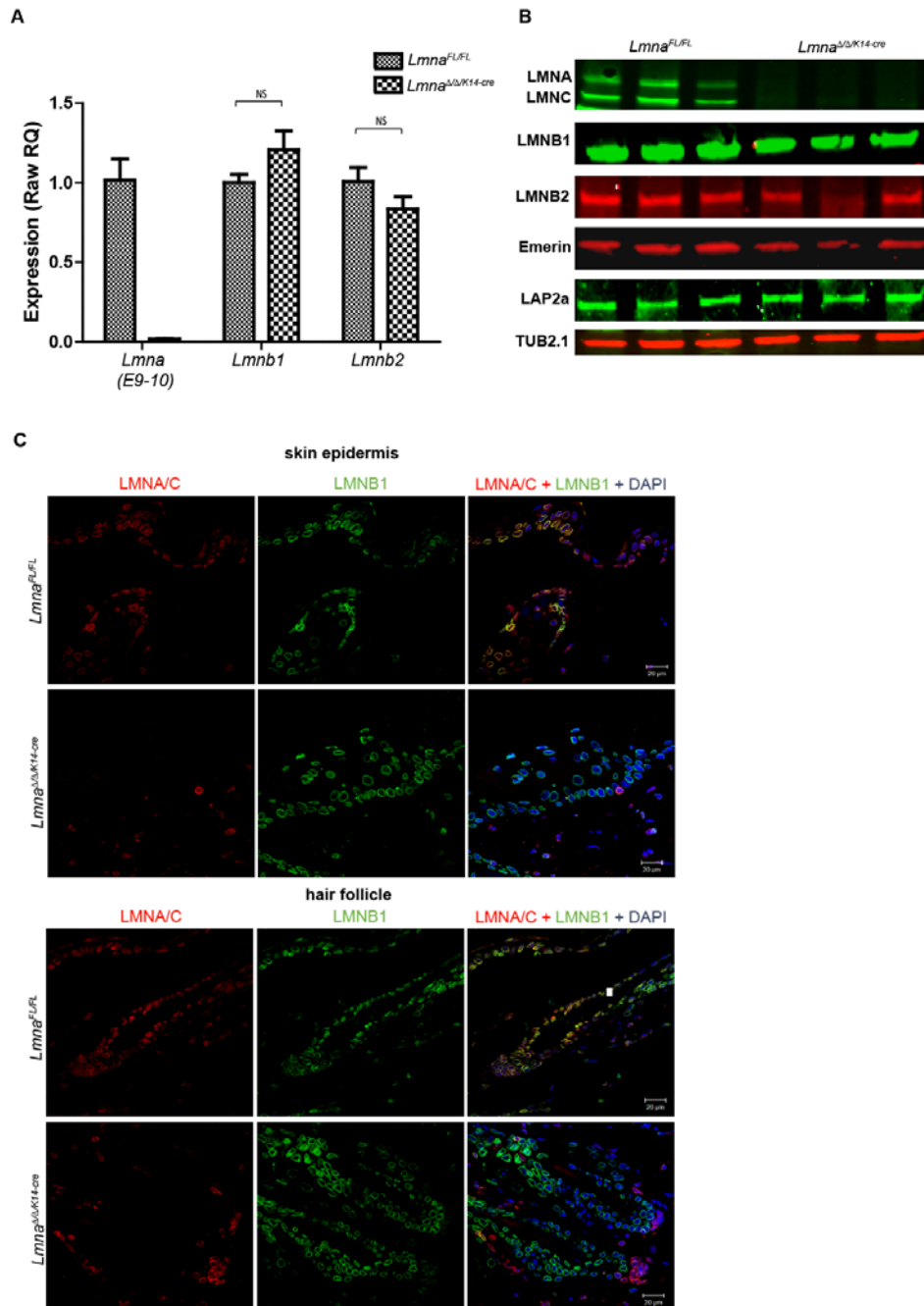
Figure 6.4: Expression of B-type lamins and other NE proteins is not affected in *Lmna*$^{\Delta/\Delta K14-Cre}$ mice. (A) Transcript levels of *Lmnb1* and *Lmnb2* are not changed in *Lmna*-null keratinocytes. (Data represents mean ± SEM). (B) Expression levels of B-type lamins and NE proteins such as emerin and LAP2α are not altered in *Lmna*-null

keratinocytes (n= 3 biological samples). (C) Expression and localization of lamin B1 (LMNB1) are not altered in dorsal skin epidermis and HFs of *Lmna*$^{\Delta/\Delta K14\text{-}Cre}$ mice. (Scale bars, 20 µm).
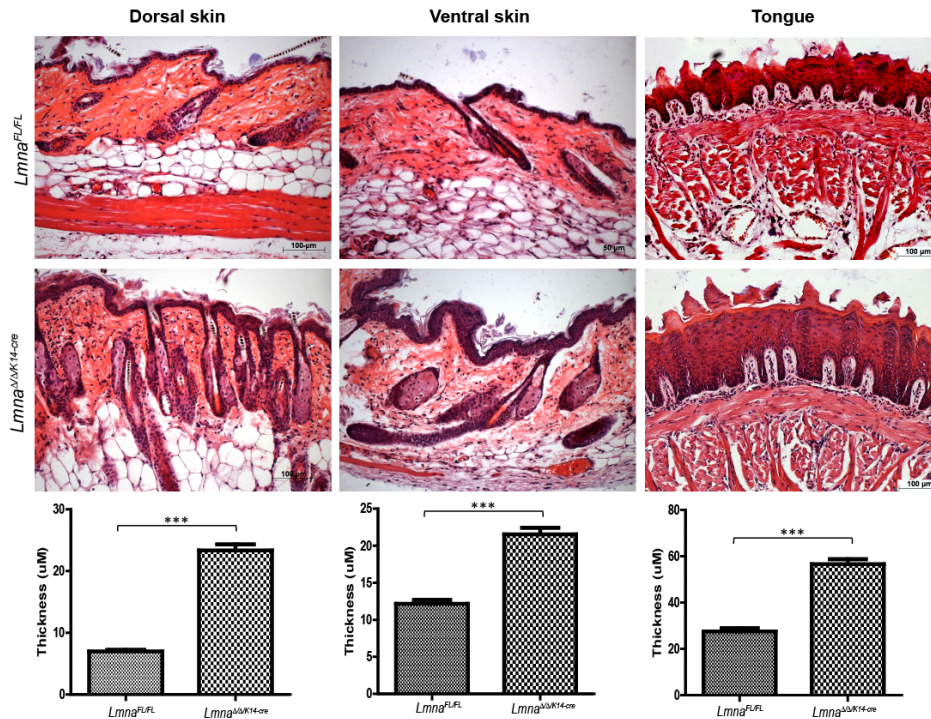
Figure 6.5: Histological examination of dorsal skin, ventral skin and tongue reveals epidermal thickening in *Lmna*$^{\Delta/\Delta K14\text{-}Cre}$ mice. An increased number and larger HFs are also observed in *Lmna*$^{\Delta/\Delta K14\text{-}Cre}$ mice. Data represents mean ± SEM. (*** p<0.0001) (Scale bars, 50/100 µm)

6.8 Epidermal thickness does not increase with age in *Lmna*$^{\Delta/\Delta K14\text{-}Cre}$ mice

Since defects in the nuclear lamina and increased genomic instability occur during normal cellular aging (Negrini et al., 2010; Scaffidi and Misteli, 2006), I analyzed older mice (6 and 18 months old) to investigate whether a prolonged lack of lamin A/C might have a stronger effect on epidermal thickening. I compared the thickness of epidermis of dorsal skin, ventral skin

and hind paw, as well as tongue epithelium and in 3, 6 and 18 month old *Lmna*$^{\Delta/\Delta K14\text{-}Cre}$ mice (Fig. 6.6B).

No gross abnormality in skin and hair, other than a decrease in subcutaneous fat was observed in 18 month old *Lmna*$^{\Delta/\Delta K14\text{-}Cre}$ mice. However, histological assessment revealed epidermal thickening and large hyperplastic HFs in their dorsal and ventral skin. A reduction in hypodermis thickness was also observed in *Lmna*$^{\Delta/\Delta K14\text{-}Cre}$ mice, which could be a secondary effect since *K14-Cre* is also active in the liver (http:/cre.jax.org/Krt14/Krt14-creNano.html). Paw and tongue epithelium also greatly increased in thickness. Furthermore, the tongue epithelium appeared to be more disorganized compared to WT mice (Fig. 6.6A).

To quantify the epidermal thickness in mice of different ages, I compared the epidermis thickness of 3, 6 and 18 month old WT and *Lmna*$^{\Delta/\Delta K14\text{-}Cre}$ mice (Fig. 6.6B). In general, epidermal thickness is significantly increased in all skin types (dorsal and ventral skin, tongue and paws) in *Lmna*$^{\Delta/\Delta K14\text{-}Cre}$ mice. However, even as the mice aged, the intensity of epidermal thickening does not change. Dorsal skin of *Lmna*$^{\Delta/\Delta K14\text{-}Cre}$ mice shows no change in epidermal thickness between 3 to 6 months, but is greatly reduced between 6 to 18 months. The thickness of epidermis in the ventral skin and tongue however was not significantly affected with age. In paw skin of *Lmna*$^{\Delta/\Delta K14\text{-}Cre}$ mice, epidermal thickening is greatly increased from 3 to 6 months, but do not change between 6 to 18 months. Taken together, I conclude

that loss of *Lmna* causes epidermal thickening in *Lmna*$^{\Delta/\Delta K14\text{-}Cre}$ mice, and this effect does not change as the mice age.

6.9 *Lmna*-null keratinocytes exhibit hyperproliferation

Since *Lmna*$^{\Delta/\Delta K14\text{-}Cre}$ mice exhibit thickened skin and tongue epithelia, I hypothesized that *Lmna*-null keratinocytes possess enhanced proliferative capacity rather than increase in size. The total number of cells in the epidermis was counted and a 1.36-fold increase in the total number of epidermal cells in *Lmna*$^{\Delta/\Delta K14\text{-}Cre}$ compared to WT mice in both dorsal skin and tongue was observed (Fig. 6.7A2, B2). Staining for the proliferation marker Ki-67 revealed that proliferating cells were largely located in the basal layer in dorsal skin and tongue epidermis (Fig. 6.7A1, B1). A 3-fold increase in Ki-67 positive cells was observed in dorsal skin and 1.97-fold increase in the tongue from *Lmna*$^{\Delta/\Delta K14\text{-}Cre}$ mice (Fig. 6.7A3, B3). These findings indicate that *Lmna*-null keratinocytes show greater proliferative capacity explaining the increased numbers of epidermal keratinocytes resulting in a thicker epidermis in *Lmna*$^{\Delta/\Delta K14\text{-}Cre}$ mice. Microarray gene expression analysis of *Lmna*-null keratinocytes identified more than 50 genes associated with cell proliferation and hyperplasia, as being altered in their expression levels (Fig. 6.14).
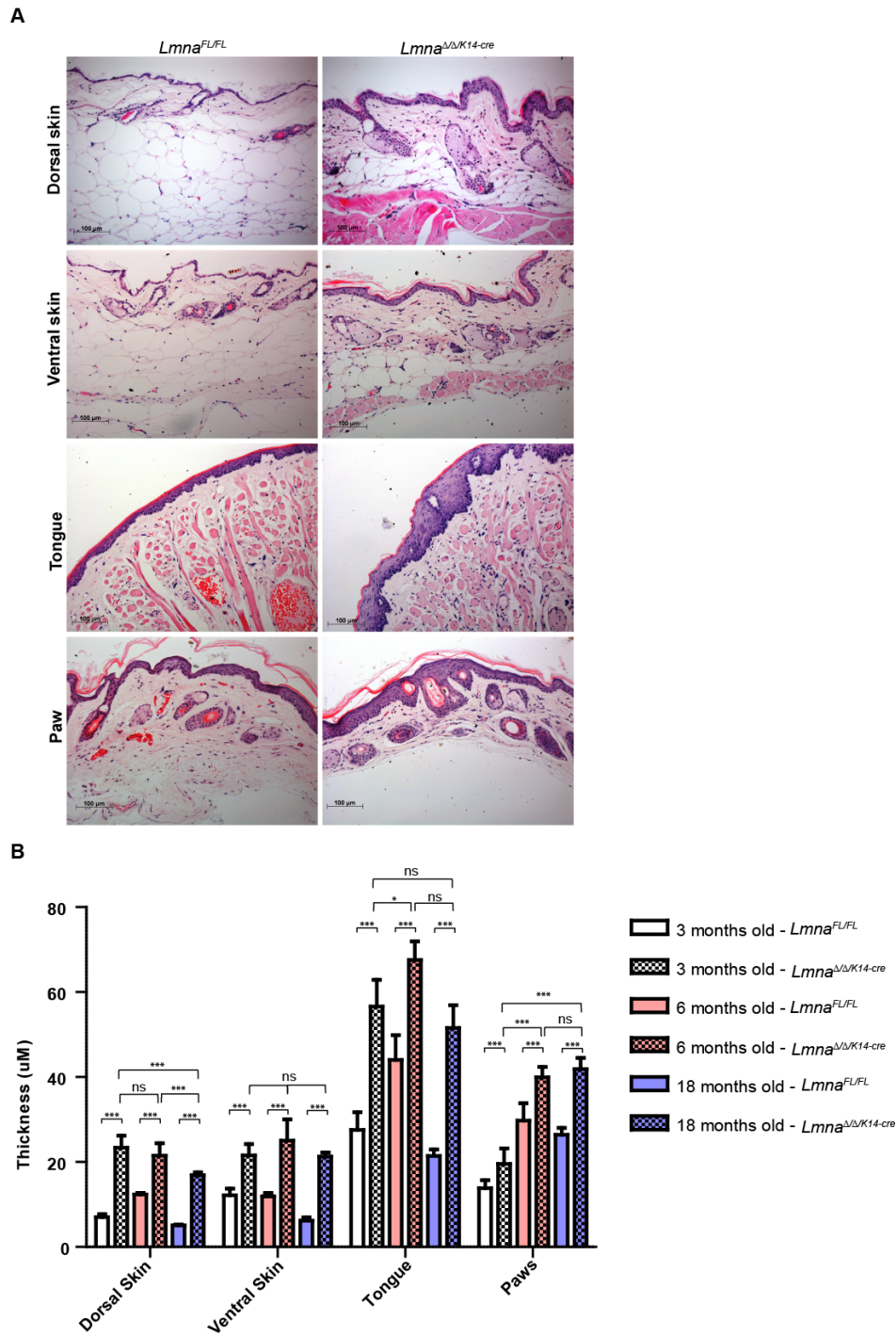
Figure 6.6: Epidermal thickening is observed in 18 month old $Lmna^{\Delta/\Delta K14\text{-}Cre}$ mice. (A) In dorsal and ventral skin, tongue and paw, epidermal thickening is observed in $Lmna^{\Delta/\Delta K14\text{-}Cre}$ mice. (Scale bars, 100 μm) (B) When comparing epidermis thickening in mice of 3,6 and 18 months old, epidermal thickening is observed in dorsal and ventral skin, tongue and paw of $Lmna^{\Delta/\Delta K14\text{-}Cre}$ mice Data represents mean ± SEM (*<0.05, *** p<0.0001, ns = not statistically significant).
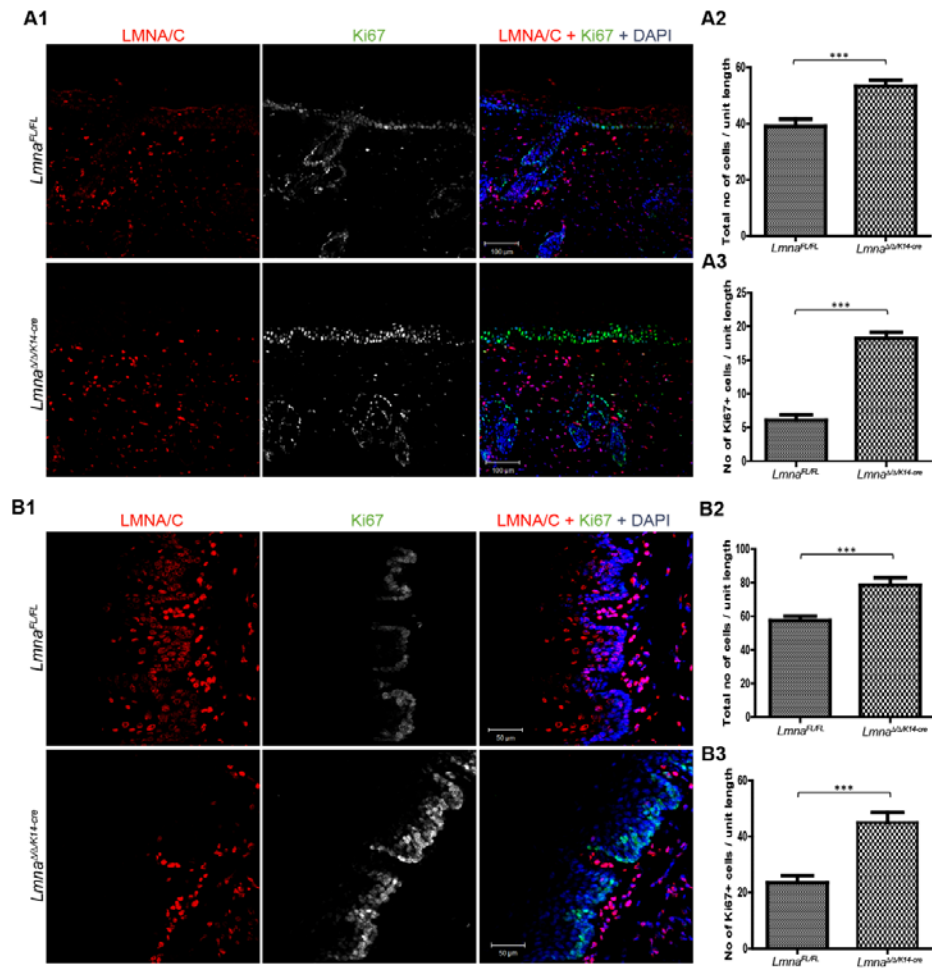
Figure 6.7: Keratinocytes of *Lmna*^{Δ/ΔK14-Cre} mice dorsal skin and tongue display hyperproliferation. (A1, B1) More Ki-67-positive cells (white/green) are detected in *Lmna*^{Δ/ΔK14-Cre} mice dorsal skin and tongue. (Scale bars, (A1) 100 μm; (B1) 50 μm). (A2, B2) There are more keratinocytes in the epidermis of dorsal skin and tongue in *Lmna*^{Δ/ΔK14-Cre} than WT mice. (A3, B3) There are more Ki-67-positive proliferating keratinocytes in *Lmna*^{Δ/ΔK14-Cre} dorsal skin and tongue compared to WT mice. Data represents mean ± SEM (*** $p<0.001$).

6.10 *Lmna*-null keratinocytes do not show defects in differentiation and stratification

Keratinocytes in the different epidermal sublayers express different markers. Actively proliferating basal keratinocytes directly above the dermal-epidermal junction express keratins 5 and 14 (K5, K14). As they differentiate and migrate apically, they occupy the spinous layer and express keratins 1 and 10 (K1, K10). As keratinocytes continue to differentiate, they occupy the granular layer and express differentiation markers including loricrin and filaggrin.

Since the expression of LMNA is regarded as a hallmark of differentiation, I investigated if the loss of *Lmna* would hinder the differentiation capacity of keratinocytes. Sections of dorsal skin and tongue were analyzed for the expression of skin differentiation markers including K14, K10 and loricrin. While K14 remains unchanged, expression of K10 appeared to be slightly increased in the dorsal skin of *Lmna*$^{\Delta/\Delta K14-Cre}$ mice (Fig. 6.8). Loricrin, the marker for the granular layer, was also greatly increased in dorsal skin and tongue epithelia of *Lmna*$^{\Delta/\Delta K14-Cre}$ mice (Fig. 6.9A, B). Increased expression of markers such as K10 and loricrin is most likely due to an increased number of keratinocytes in dorsal skin and tongue, and not due to an altered differentiation capacity of keratinocytes. Hence, these findings reveal that loss of *Lmna* does not prevent the keratinocytes from differentiating as they progress through the epidermal sublayers and in forming a functional skin barrier.
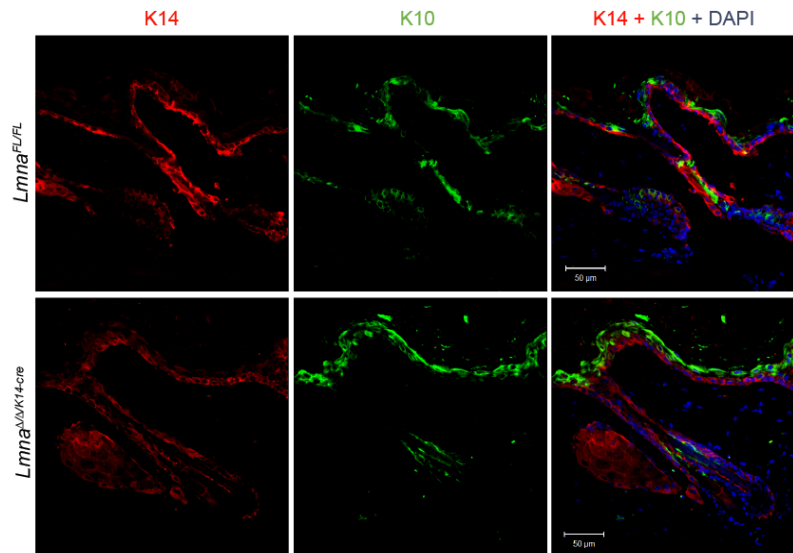
Figure 6.8: Keratin 10 (K10) is slightly increased in dorsal skin of *Lmna*$^{\Delta/\Delta K14\text{-}Cre}$ mice. The thickness of basal layer (K14, red) of dorsal skin epidermis is not altered in *Lmna*$^{\Delta/\Delta K14\text{-}Cre}$ mice, but thickness of spinous layer (K10, green) may be slightly increased, possibly due to the presence of more differentiated suprabasal keratinocytes located in this area. (Scale bars, 50 μm)
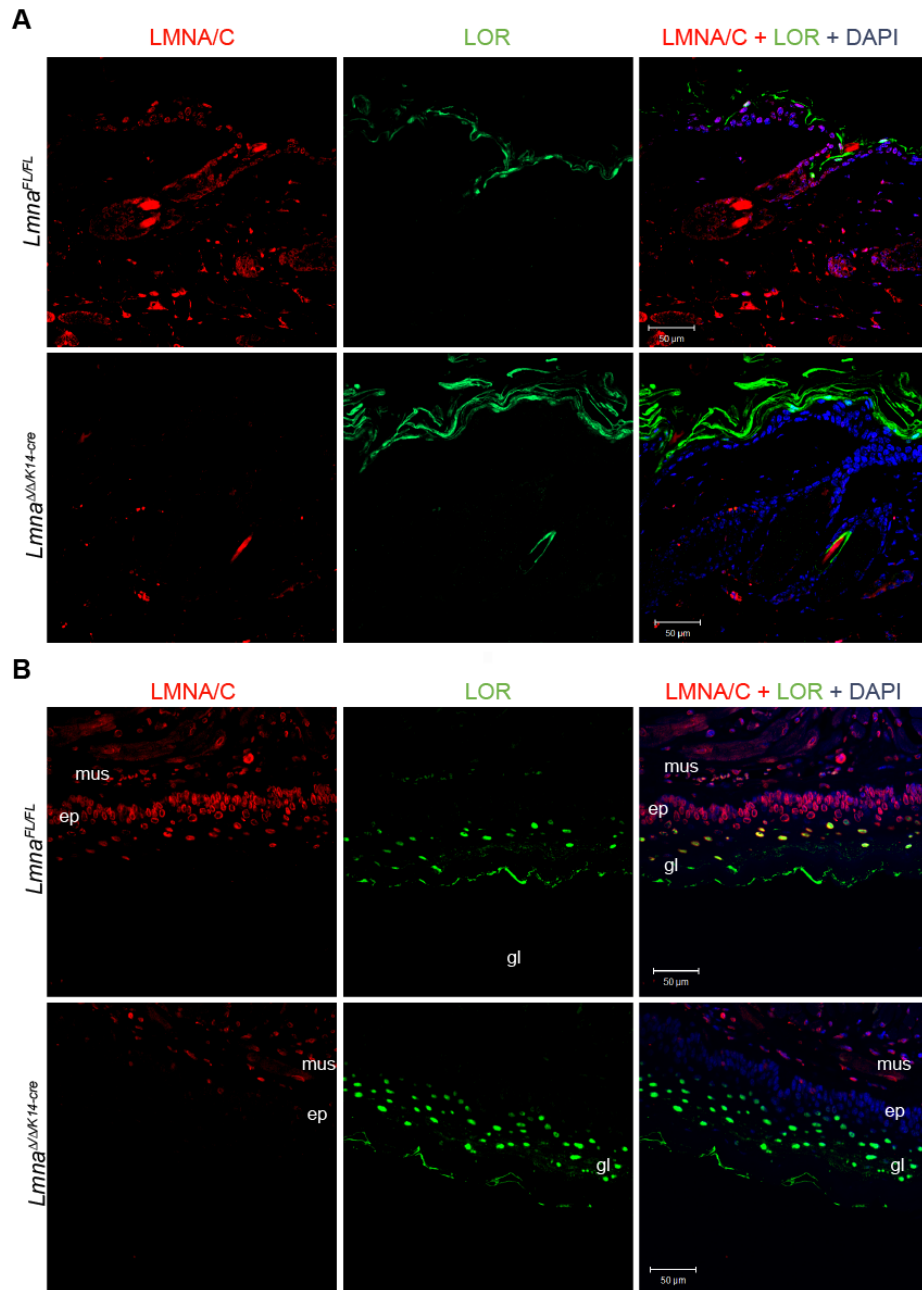
Figure 6.9: Expression of loricrin was increased in dorsal skin and tongue of *Lmna*$^{\Delta/\Delta K14\text{-}Cre}$ **mice.** Increase number of keratinocytes in the granular layer leads to elevated expression of loricrin (LOR, green) in (A) dorsal skin and (B) tongue epithelia. (Scale bars, 50 µm)

6.11 <u>Aberrant hair cycles in *Lmna*$^{\Delta/\Delta K14\text{-}Cre}$ mice</u>

Since hyperproliferation of keratinocytes was observed in *Lmna*$^{\Delta/\Delta K14\text{-}Cre}$ mice (Fig. 6.7, 6.15), I speculated that hair growth cycle may also be affected in the absence of *Lmna*. The hair growth profile of C57BL6 mice is well documented (Fig. 6.1B) and differs slightly between mice of different gender and ages (Muller-Rover et al., 2001). Consequently, only male littermates mice were aged to respective major time points of hair cycle and their dorsal skin collected for histomorphological examination of HFs (Fig. 6.10). As mice rarely have interfollicular epidermal pigmentation, the skin colour in mice closely correlates to hair cycle phases. For example, the colour of the skin changes from dark gray to black during anagen and pale pink by telogen (Muller-Rover et al., 2001). Therefore, to obtain a better understanding of the hair growth in *Lmna*$^{\Delta/\Delta K14\text{-}Cre}$ mice, hair coats of more than 50 P16 to P120 *Lmna*$^{FL/FL}$ and *Lmna*$^{\Delta/\Delta K14\text{-}Cre}$ mice (age- and gender-matched) were shaved and changes in their skin pigmentation and hair regrowth were recorded to complement the histomorphological classification of HFs (Fig 6.10).

At P16, mice of both genotypes have light grey skin. Histological analysis shows HFs characteristic of late anagen to catagen stage with *Lmna*$^{\Delta/\Delta K14\text{-}Cre}$ mice displaying a slight increase in number of HFs (Fig. 6.10A). At P21 corresponding to telogen, the skin colour in both genotypes turns pink. HFs appeared to be shortened in both genotypes but HFs in *Lmna*$^{\Delta/\Delta K14\text{-}Cre}$ mice appeared larger compared to WT HFs (Fig. 6.10B). No

obvious epidermal thickening is detected in P16 and P21 $Lmna^{\Delta/\Delta K14\text{-}Cre}$ mice (Fig. 6.10A, B). Interestingly, $Lmna^{\Delta/\Delta K14\text{-}Cre}$ mice display a pink skin colour for 1-3 days longer than WT mice, indicating that the telogen is slightly prolonged in $Lmna^{\Delta/\Delta K14\text{-}Cre}$ mice. After P21, WT mice skin colour greys earlier in comparison to $Lmna^{\Delta/\Delta K14\text{-}Cre}$ mice and by P30, WT mice exhibit visible hair growth but $Lmna^{\Delta/\Delta K14\text{-}Cre}$ mice continue to display strong pigmentation resulting in very dark grey skin colour although hair was not visible. At this stage, HFs in both genotypes are in anagen phase and appear as long shafts extending into the dermis with enlarged dermal papilla. The first sign of epidermal thickening is observed at this stage (Fig. 6.10C).

As hair growth continues, anagen HFs gradually enter a short catagen. At P42, HFs in WT mice show dramatic shortening and regression, with concomitant lightening of skin colour from grey to pink. In contrast, $Lmna^{\Delta/\Delta K14\text{-}Cre}$ mice continue to display larger HFs and darker skin colour compared to WT littermates (Fig. 6.10D), indicating that HFs in $Lmna^{\Delta/\Delta K14\text{-}Cre}$ mice remain in anagen longer and enter catagen later. This phenomenon extends until P49 where HFs in $Lmna^{\Delta/\Delta K14\text{-}Cre}$ mice are in catagen and the skin displays a darker pigmentation compared to WT littermates that have pink skin and HFs in telogen (Fig. 6.10E).

In the murine hair cycle, the second telogen usually lasts for 4 weeks. However in $Lmna^{\Delta/\Delta K14\text{-}Cre}$ mice, the telogen phase is shortened to 2 weeks and by around P67, while WT littermates still display pink skin with HFs in telogen phase, $Lmna^{\Delta/\Delta K14\text{-}Cre}$ mice have anagen HFs and up to 80% hair

regrowth (Fig. 6.10F). At P84, HFs in WT mice cycle into anagen while HFs in $Lmna^{\Delta/\Delta K14\text{-}Cre}$ mice regress (Fig. 6.10G). By P101, HFs in WT mice are in telogen while in $Lmna^{\Delta/\Delta K14\text{-}Cre}$ mice, there is a mix of HFs in catagen and anagen. A summary of the hair cycles is presented in Fig. 6.11.
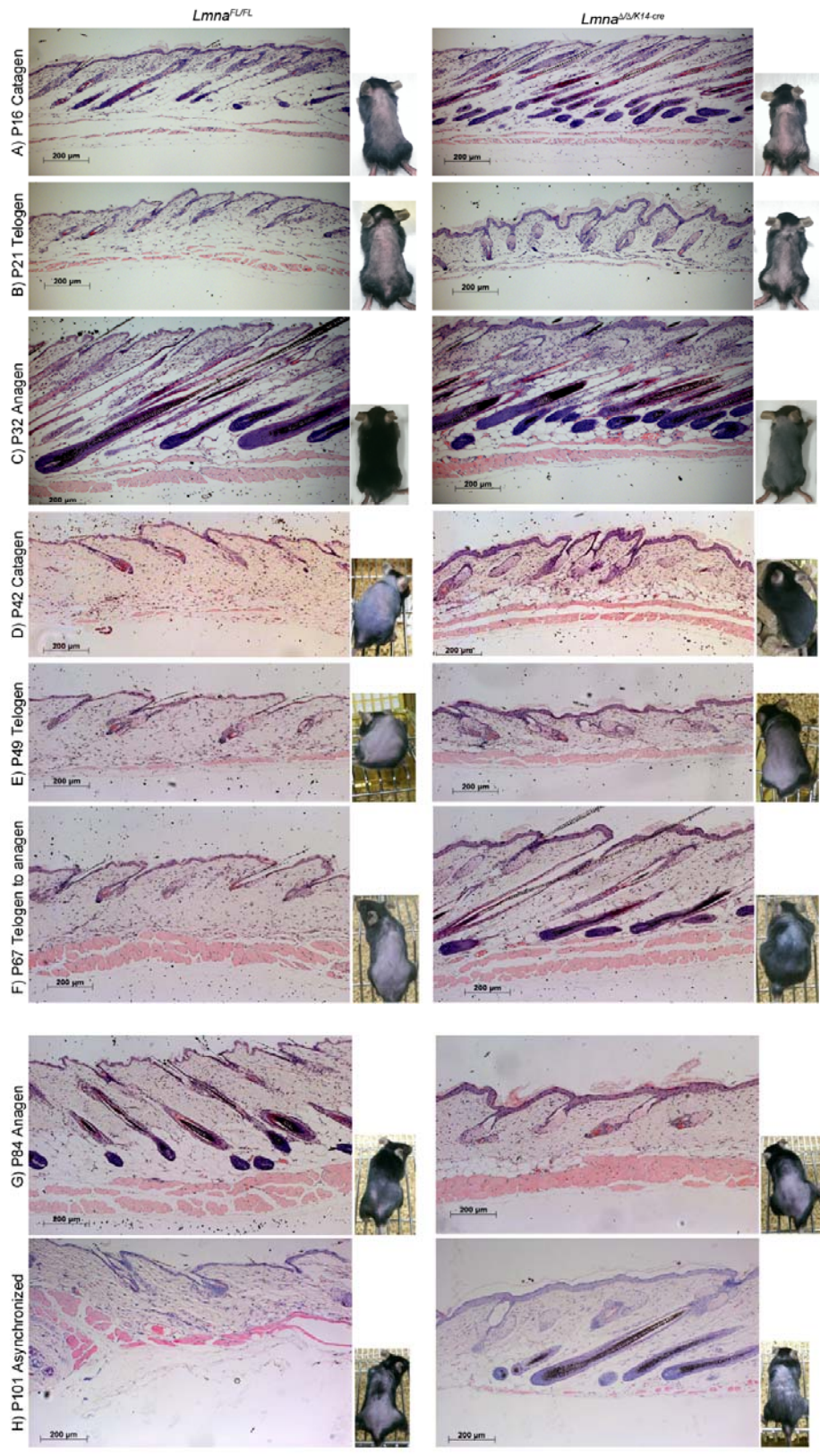
Figure 6.10: Hair growth cycles are altered in *Lmna*^{Δ/ΔK14-Cre} mice. At both P16 to P28, hair stages in mice of both genotypes are similar. However at P42 to P49, *Lmna*^{Δ/ΔK14-Cre} mice HFs remain in catagen but do not cycle into telogen phase. At P67, hair cycle in *Lmna*^{Δ/ΔK14-Cre} mice accelerates into anagen while HFs in WT mice remain in telogen. At P84, HFs in WT mice enter anagen while HFs in *Lmna*^{Δ/ΔK14-Cre} mice show signs of regression. At P101, HFs in WT are in telogen while in *Lmna*^{Δ/ΔK14-Cre} mice, there is a mix of catagen and anagen HFs. Epidermal thickening is not observed in P16 and P19 mice but become evident from P32 onwards. Compared to their WT littermates, HFs in *Lmna*^{Δ/ΔK14-Cre} mice are significantly larger. (Scale bars, 200 µm). Representative images of mice showing different skin pigmentation and hair growth corresponding to HF stages are shown on the right.
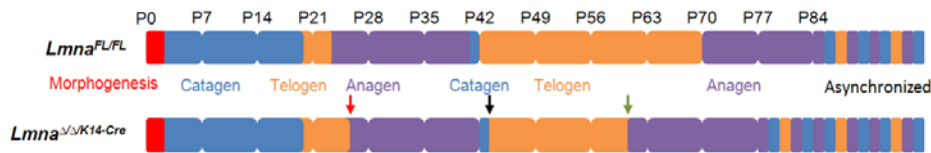
Figure 6.11: Summary of hair growth cycle in WT vs. *Lmna*^{Δ/ΔK14-Cre} mice. During the first hair cycle telogen (red arrow), *Lmna*^{Δ/ΔK14-Cre} mice display a slightly prolonged telogen and enter anagen phase later compared to WT mice. At P42, WT HFs enter catagen followed by telogen while *Lmna*^{Δ/ΔK14-Cre} mice HFs show delayed catagen and telogen (black arrow). HFs in WT mice stay in telogen phase for around 4 weeks, but HFs in *Lmna*^{Δ/ΔK14-Cre} mice cycle into anagen phase in 2 to 3 weeks (green arrow). Hair growth in both genotypes becomes asynchronized after the second anagen.

6.12 Accelerated wound healing in *Lmna*^{Δ/ΔK14-Cre} mice

Keratinocyte proliferation and migration are critical in cutaneous wound healing. To further evaluate the proliferative capacity of *Lmna*-null keratinocytes, *Lmna*^{Δ/ΔK14-Cre} mice and WT littermates were injured in their dorsal skin with a 4mm skin punch and after 2-3 days, skin surrounding the wound was harvested. Based on my observations of hair growth, I chose 7-weeks old mice since both WT and *Lmna*^{Δ/ΔK14-Cre} mice do not exhibit active hair growth. In general, *Lmna*^{Δ/ΔK14-Cre} mice showed accelerated healing leading to smaller wound size (Fig. 6.12) compared to WT mice.. Compared

149

to WT mice, $Lmna^{\Delta/\Delta K14\text{-}Cre}$ littermates had smaller wound area, an indication of better wound healing (5.759 ± 0.52 mm^2 vs. 7.898 ± 0.77 mm^2, p<0.05) (Fig 6.12B).
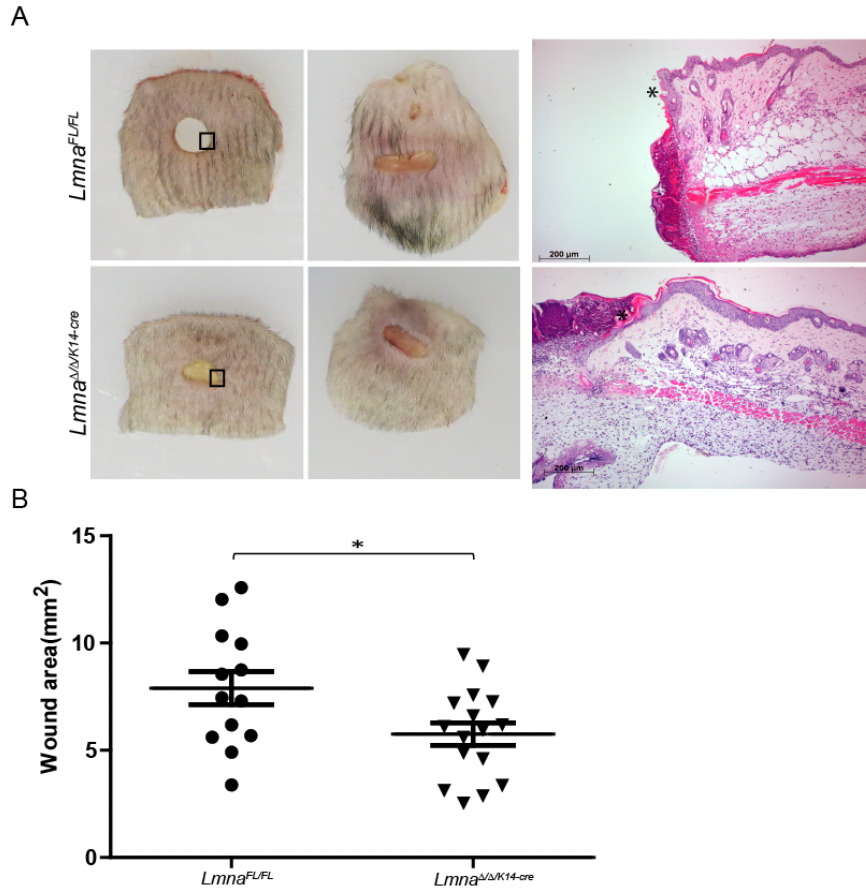
Figure 6.12: $Lmna^{\Delta/\Delta K14\text{-}Cre}$ mice display accelerated wound healing. (A) After skin injury, WT mice show slower repair of the skin wound while $Lmna^{\Delta/\Delta K14\text{-}Cre}$ mice show accelerated healing with smaller wound size. Histological analysis of skin wounds show greater inflammation and keratinocytes proliferation and migration at injury site (*) in $Lmna^{\Delta/\Delta K14\text{-}Cre}$ compared to WT mice. (B) Statistical analysis of the area of wound size confirms that $Lmna^{\Delta/\Delta K14\text{-}Cre}$ mice show better wound healing compared to their WT littermates ($Lmna^{Fl/FL}$ n=13, $Lmna^{\Delta/\Delta K14\text{-}Cre}$ n=16, * p = 0.027). Data represents mean ± SEM.

6.13 <u>**Genes associated with growth and proliferation are altered in *Lmna*-**</u>
<u>**null keratinocytes**</u>

Since *Lmna*$^{\Delta/\Delta K14\text{-}Cre}$ mice exhibit accelerated growth in their epidermal keratinocytes, I was interested in defining the molecular pathways associated with loss of *Lmna*. I used microarray gene expression analysis to determine changes in gene profiles in *Lmna*-null keratinocytes. RNA was extracted from keratinocytes of P120 *Lmna*$^{\Delta/\Delta K14\text{-}Cre}$ mice and their WT littermates. Principal component analysis (PCA) confirmed the integrity of the samples permitting analysis of inter-animal variation (Fig. 6.13A) while hierarchical clustering applied to the dataset showed that biological samples within each genotype display similar gene expression profiles. A total of 84 unique genes are downregulated and 103 unique genes are upregulated (fold change $\geq$ 1.5) in *Lmna*-null keratinocytes (Fig. 6.13B).

Lmna is downregulated by 3.04-fold in keratinocytes derived from *Lmna*$^{\Delta/\Delta K14\text{-}Cre}$ mice skin (Fig 6.14). Loss of *Lmna* in keratinocytes leads to alteration of 187 genes (Fig. 6.13B) in the nucleus, cytoplasm and plasma membrane. Of these, 49 molecules are involved in increased proliferation of epithelial (z-score = 2.27) and tumour (z-score = 3.155) cells (Fig. 6.14).

Figure 6.13: PCA analysis of microarray dataset confirms the integrity of samples and expression profiles of 187 unique genes are altered in *Lmna*$^{\Delta/\Delta K14\text{-}Cre}$ mice. (A) Spheres of each colour represent each mouse (biological sample) and from the PCA analysis, technical replicates cluster closely and keratinocytes from *Lmna*$^{FL/FL}$ (WT) and *Lmna*$^{\Delta/\Delta K14\text{-}Cre}$ mice (KO) are distinct. (B) Hierarchical cluster analysis of microarray dataset showed that *Lmna*$^{FL/FL}$ (WT, green) and *Lmna*$^{\Delta/\Delta K14\text{-}Cre}$ mice (KO, red) show similar expression profiles. In *Lmna*-null keratinocytes, 84 genes are downregulated (blue) and 103 genes are upregulated (red). Grey bars indicate unchanged genes.

Figure 6.14: Gene network of molecules associated with proliferation. 49 unique molecules are identified by microarray analysis of keratinocytes derived from *Lmna*$^{\Delta/\Delta K14\text{-}Cre}$ mice. *Lmna* (boxed) shows a 3-fold decrease in *Lmna*$^{\Delta/\Delta K14\text{-}Cre}$ mice. Pink (less extreme) to red (more extreme) represent upregulated genes while light green (less extreme) to dark green (more extreme) molecules are downregulated. Orange dashed lines indicate activation of cell proliferation, while yellow and grey dashed lines indicate that effects are inconsistent or not predicted respectively. The genes are also sub-divided into their cellular location.

Keratin 16 (*K16*), a well-documented marker for hyperproliferation (Jiang et al., 1993; Weiss et al., 1984), was also upregulated in *Lmna*-deficient keratinocytes (Fig. 6.14). Kallikrein-related peptidase 6 (*Klk6*) was the most upregulated gene, (8.96-fold increase). *Klk6* level was further validated by qRT-PCR of cDNA derived from *Lmna*-null keratinocytes and 2-fold increase was detected (Fig. 6.15). Upregulation in *KLK6* was reported in human SCC and also other epithelial tumours in the ovaries and colon (Klucky et al., 2007; Vakrakou et al., 2014). Ectopic *Klk6* expression in mouse keratinocyte cell lines resulted in reduced expression of cell adhesion protein E-cadherin and nuclear translocation of β-catenin which consequently promotes proliferation, migration, and invasion (Klucky et al., 2007). In *Lmna*-null keratinocytes, transcript levels of E-cadherin were downregulated but no change was observed in β-catenin (Fig. 6.15). Since measurements of mRNA transcript levels cannot differentiate between nuclear and cytoplasmic β-catenin, more work should be done to determine if β-catenin is altered in *Lmna*-null keratinocytes. Nevertheless, based on these data, it is possible that loss of *Lmna* results in acute increase in *Klk6* and decrease of cell adhesion molecule E-cadherin, resulting in keratinocytes displaying enhanced proliferation and migration properties, which are hallmarks of tumourigenesis.
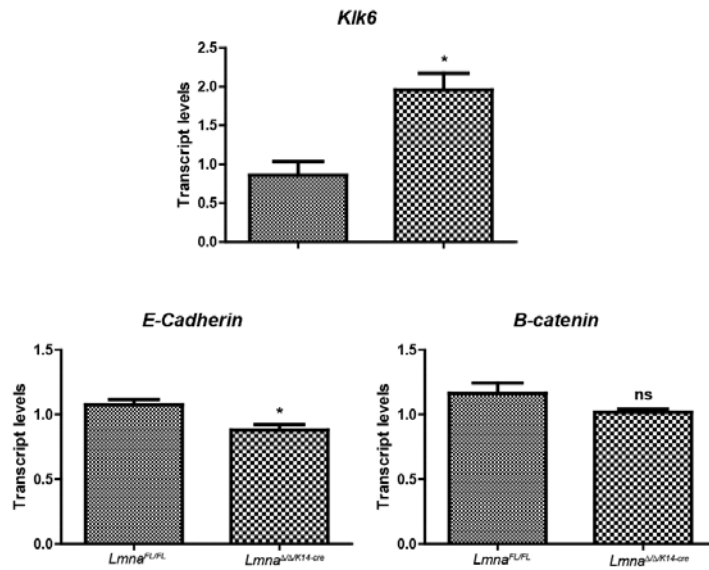
Figure 6.15: Enhanced *Klk6* in *Lmna*-null keratinocytes. Loss of *Lmna* resulted in increased *Klk6* transcript level leading to decreased E-cadherin but no change in β-catenin (n = 3 biological replicates, * p<0.05, ns = not statistically significant). Data represents mean ± SEM.

6.14 TGF-β signaling is affected in keratinocytes of *Lmna*$^{Δ/ΔK14-Cre}$ mice

TGF-β signaling is critical is homeostasis of the skin and influences various biological processes including morphogenesis, cell proliferation and differentiation (Moustakas et al., 2002). In particular, TGF-β1 serves as a potent growth inhibitor in keratinocytes (Anzano et al., 1982). TGF-β binds to type 2 TGF-β receptor (TGFβR2) that recruits and activates TGFβR1. This leads to binding and phosphorylation of receptor-regulated Smads (R-Smads) such as Smad2 or Smad3 (Massague et al., 2005). Smad2 and Smad3 form a complex with the co-Smad (Smad4). Subsequently the complex translocates to the nucleus and binds promoters to modulate expression of target genes (Lagna et al., 1996) such as p21, a cyclin-dependent kinase inhibitor, which lead to cell cycle arrest (Pardali et al., 2000). Furthermore, when TGF-β is

suppressed, it can delay the progression of catagen in mouse hair growth cycles (Tsuji et al., 2003).

Based on our observations that proliferation is enhanced in *Lmna*-null keratinocytes and delayed catagen and shortened telogen growth cycles of *Lmna*$^{\Delta/\Delta K14\text{-}Cre}$ mice, I hypothesize that TGF-β signaling may be altered in *Lmna*-null keratinocytes. TGF-β and TGFβR2 have been reported to promote a switch between proliferation to regression during hair cycling (Foitzik et al., 2000). BMP4, a member in the TGF-β superfamily was also downregulated by 2.17-fold in *Lmna*-null keratinocytes (Fig. 6.14). Hence, I analyzed the transcription profile of molecules of the TGF-β signaling pathway and found that in keratinocytes derived from *Lmna*$^{\Delta/\Delta K14\text{-}Cre}$ mice, transcript levels of *TGF-β1* and *TGF-β2* were downregulated (Fig. 6.16). However, expression levels of receptors such as *TGFβR1* and *TGFβR2* were not altered. *Smad2*, but not *Smad3* and *Smad4*, was also slightly downregulated in *Lmna*-null keratinocytes (Fig. 6.16). Loss of *Lmna* therefore results in downregulation of TGF-β and consequently, keratinocyte proliferation is not inhibited resulted in enhanced *Lmna*-null keratinocytes proliferation. TGF-β signaling is critical to skin and hair development and carcinogenesis (Andres and Gonzalez, 2009). For example, deregulation of members of the TGF-β family have been implicated in several cancers (Massague, 2008) including skin epithelial cancers such as SCC and BCC (Glick, 2012).
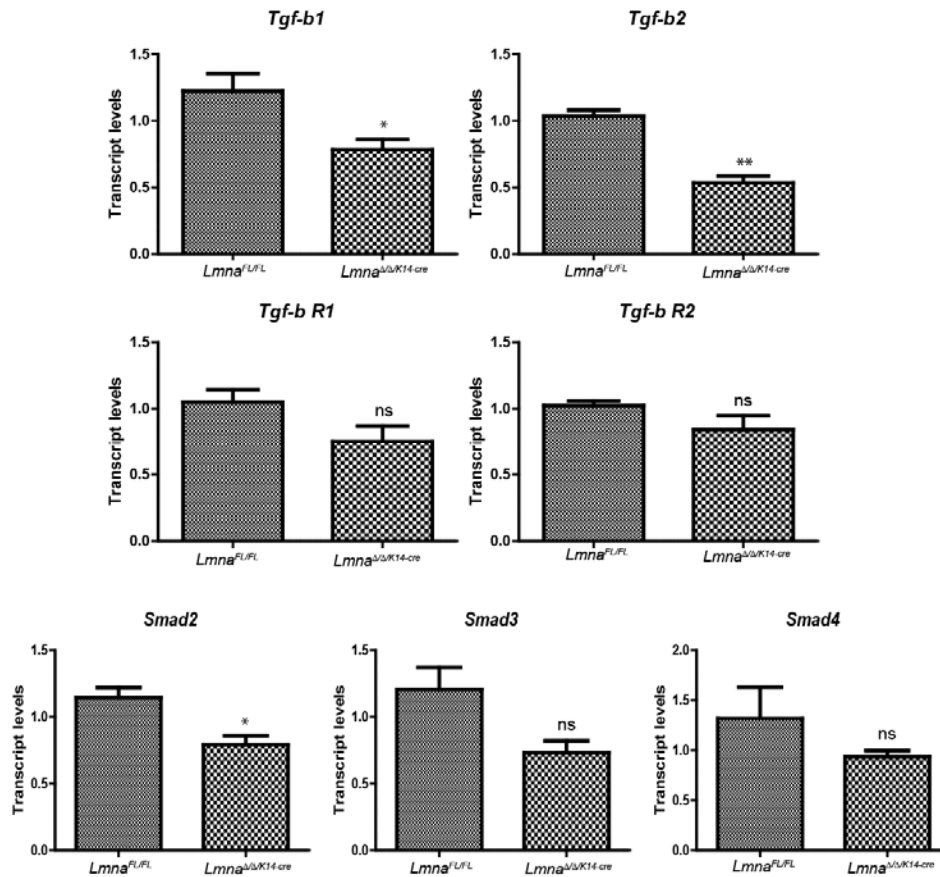
Figure 6.16: Altered TGF-β signaling in *Lmna*–null keratinocytes. Loss of *Lmna* results in reduced *TGF-β1* and *TGF-β2* transcript levels but no change in transcript levels of *TGF-βR1* and *TGF-βR2*. *Smad2* (* p<0.05), but not *Smad3* and *Smad4* (ns), is also reduced in *Lmna*-null keratinocytes. (n = 3 biological samples, * p<0.05, ** p<0.01, ns = not statistically significant). Data represents mean ± SEM.

6.15 <u>Accelerated hair growth in *Lmna*$^{Δ/ΔK14\text{-}Cre}$ FVB/N mice</u>

Since hyperproliferation and upregulation of cancer associated markers were observed in *Lmna*-null keratinocytes, I hypothesized that loss of *Lmna* in skin epidermis may predispose *Lmna*$^{Δ/ΔK14\text{-}Cre}$ mice to skin cancer. I sought to expose *Lmna*$^{Δ/ΔK14\text{-}Cre}$ mice to a well-documented cutaneous two-stage chemical carcinogenesis assay to study papillomas formation in *Lmna*$^{Δ/ΔK14\text{-}Cre}$ and WT mice. However, C57BL6 mice have been reported to be resistant to

the chemical carcinogenesis assay (Hennings et al., 1993), so I proceeded to cross our $Lmna^{\Delta/\Delta K14\text{-}Cre}$ mouse model onto a FVB/N background which are known to be good models for the study of skin papillomas induction (Abel et al., 2009).

As a convenient way to ensure the enhanced proliferative capacity of keratinocytes is still conserved in $Lmna^{\Delta/\Delta K14\text{-}Cre}$ FVB/N mice, I shaved littermate mice at their second telogen (P49) and observed for rate of hair regrowth. After 18 days, $Lmna^{\Delta/\Delta K14\text{-}Cre}$ mice displayed approximately 70 to 100% hair regrowth, while $Lmna^{FL/FL}$ mice did not show visible hair regrowth until 3 weeks later (Fig. 6.17). This indication of a shortened second telogen phase and early onset of anagen phase confirms that $Lmna^{\Delta/\Delta K14\text{-}Cre}$ mice on FVB/N background have the same proliferative profile as C57BL6 mice. I am currently in the process of inducing skin papillomas in the dorsal skin of $Lmna^{\Delta/\Delta K14\text{-}Cre}$ and WT mice.

Figure 6.17: *Lmna*$^{\Delta/\Delta K14\text{-}Cre}$ **mice on a FVB/N background exhibit shorter telogen phase and is a suitable model to study skin papilloma formation.** Dorsal hair of 7-weeks old *Lmna*$^{FL/FL}$ and *Lmna*$^{\Delta/\Delta K14\text{-}Cre}$ female littermates was shaved. After 18 days, *Lmna*$^{\Delta/\Delta K14\text{-}Cre}$ mice displayed at least 70% hair regrowth while *Lmna*$^{FL/FL}$ mice did not display any signs of hair regrowth.

6.16 Deriving *LMNA*^{KD} human N/TERT1 keratinocytes

To establish a human cell line of keratinocytes lacking *LMNA* (*LMNA*^{KD}), I employed lentiviral vectors expressing *LMNA* shRNA to knock down *LMNA* in human N/TERT1 keratinocytes using *shLMNA* (Dreesen et al., 2013b). Western blot analysis shows that both LMNA and LMNC protein levels were reduced by about 40% and 60% respectively in *LMNA*^{KD} keratinocytes (Fig. 6.18). I proceeded to use *LMNA*^{KD} cell lines to study proliferation profiles and gene expression due to loss of *LMNA*.
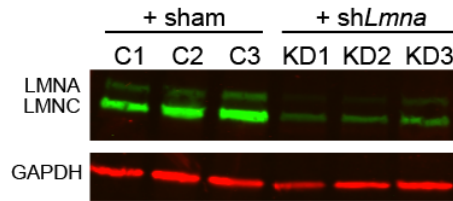
**Figure 6.18: LMNA and LMNC proteins are significantly reduced in *LMNA^KD*
keratinocytes.** Western blot analysis revealed that N/TERT keratinocytes infected
with *shLMNA* showed 40% reduction in LMNA and 60% reduction in LMNC.
GAPDH protein was used as loading control and normalization marker for
quantification of LMNA/C levels.

6.17 *LMNA^KD* keratinocytes exhibit accelerated proliferation

Since keratinocytes in $Lmna^{\Delta/\Delta K14\text{-}Cre}$ mice exhibited enhanced
proliferation *in vivo* (Fig. 6.7) and gene expression analysis presented
evidence of upregulation of hyperproliferation markers (Fig. 6.14), I was
interested in finding out if the loss of *LMNA* in human keratinocytes will also
elicit similar effects. Cell growth of $LMNA^{WT}$ and $LMNA^{KD}$ N/TERT1
keratinocytes was determined whereby cells attached to the bottom of
microelectrode assay plates transmit an electrical microimpedance signal. The
growth rate of $LMNA^{WT}$ and $LMNA^{KD}$ keratinocytes was measured over 8
days. $LMNA^{KD}$ keratinocytes proliferated faster compared to $LMNA^{WT}$
keratinocytes by ~70% (Fig 6.19A, B). These results are in sync with
enhanced proliferative capacity observed in keratinocytes of $Lmna^{\Delta/\Delta K14\text{-}Cre}$
mice. I then proceeded to measure transcript levels of TGF-β1 and TGF-β2 in
$LMNA^{WT}$ and $LMNA^{KD}$ keratinocytes. However, transcript levels of both TGF-
β1 and TGF-β2 are unaffected in $LMNA^{KD}$ keratinocytes (Fig. 6.20), possibly
due to incomplete loss of *LMNA* in the knockdown cell lines.
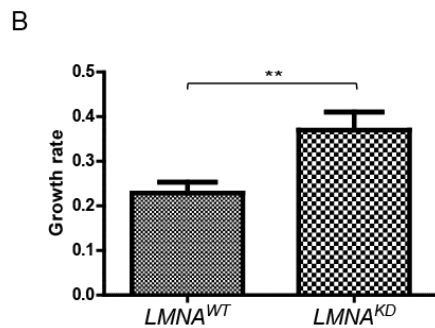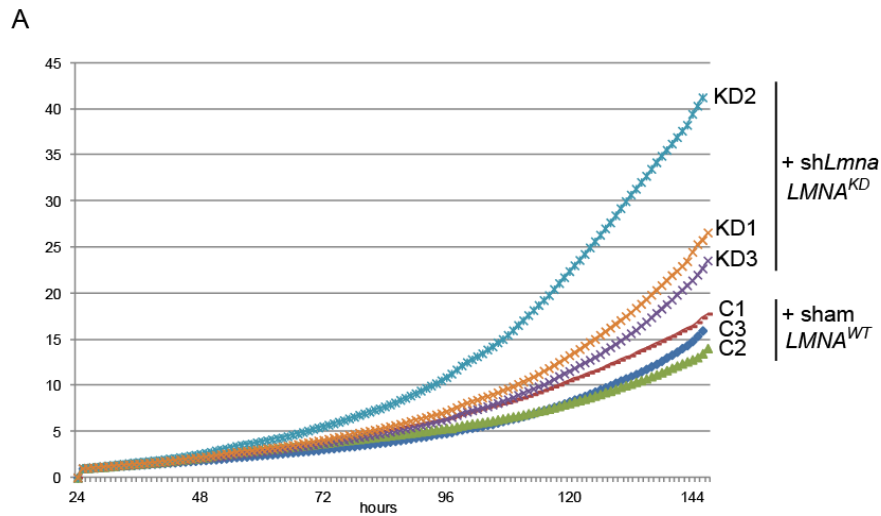
Figure 6.19: *LMNA^KD* keratinocytes exhibit accelerated proliferation rate compared to *LMNA^WT* keratinocytes. (A) Growth rate of N/TERT1 keratinocytes was observed and recorded. *LMNA^KD* keratinocytes showed a faster growth compared to *LMNA^WT* keratinocytes. (B) On average, *LMNA^KD* keratinocytes showed 70% increase in growth rate compared to *LMNA^WT* keratinocytes. Data represents mean ± SEM from 4 experiments. (n=3 for both *LMNA^WT* and *LMNA^KD* ** p = 0.0065).
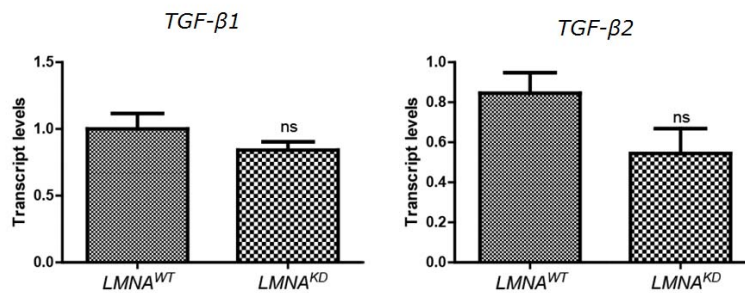
Figure 6.20: *TGF-β1* and *TGF-β2* transcript levels are not altered in *LMNA^KD* keratinocytes. No significant change was observed in levels of *TGF-β1* and *TGF-β2*, possibly due to incomplete loss of LMNA in keratinocytes. Data represents mean ± SEM. (n=3 for both *LMNA^WT* and *LMNA^KD*, ns = not statistically significant).

6.18 <u>Conclusions</u>

In summary, I have described the use of a tissue-specific knockout mouse model (*Lmna*$^{\Delta/\Delta K14\text{-}Cre}$) where lamin A/C is deleted in the keratinocytes of skin epidermis, ORS of HFs and tongue epithelium using a K14 promoter driven Cre recombinase. *Lmna*$^{\Delta/\Delta K14\text{-}Cre}$ mice exhibit a longer lifespan compared to other global *Lmna*-null mouse models (Stewart et al., 2007a; Zhang et al., 2013), allowing me to address the key issues that relate to the loss of *Lmna* in the skin such as postnatal maintenance and hair homeostasis and susceptibility to carcinogenesis.

Lmna$^{\Delta/\Delta K14\text{-}Cre}$ mice exhibit normal lifespan with no gross morphological abnormalities in their skin and hair coat. I demonstrated that *Lmna*-null keratinocytes in *Lmna*$^{\Delta/\Delta K14\text{-}Cre}$ mice proliferate, differentiate and migrate into the different epidermal sublayers and express markers such as K10 and loricrin characteristic of differentiated keratinocytes. In several *Lmna* mutant mouse models, thickened epidermis was reported in the paw epidermis (Naetar et al., 2008; Sullivan et al., 1999) and dorsal skin (Jung et al., 2014; Odgren et al., 2010). *Lmna*$^{\Delta/\Delta K14\text{-}Cre}$ mice (aged 1 to 18 months) display thickened epidermis in their skin and tongue, as well as hyperkeratosis and hyperplasia of HFs. Enhanced proliferation of *Lmna*-null keratinocytes was confirmed by increased Ki-67-positive cells in the basal layer of the skin and tongue epidermis of *Lmna*$^{\Delta/\Delta K14\text{-}Cre}$ mice. In the knockout mice where both A- and B-type lamins were depleted in the keratinocytes, no effect on cell proliferation was observed in embryos and P1 mice (Jung et al., 2014). Since

Lmna$^{\Delta/\Delta K14\text{-}Cre}$ mice do not show increase thickness in epidermis before P21, the requirement for lamin A/C may be more important in the postnatal control of keratinocyte growth.

Hyperproliferation of keratinocytes in *Lmna*$^{\Delta/\Delta K14\text{-}Cre}$ mice led me to speculate that their hair growth cycles may also be affected. Indeed, *Lmna*$^{\Delta/\Delta K14\text{-}Cre}$ mice exhibit earlier activation of the second anagen, causing hair to regrow faster post shaving. TGF-β is the most important growth inhibitor in keratinocytes (Gniadecki, 1998) and regulates cycling of HFs (Foitzik et al., 2000). In *Lmna*-null keratinocytes, I showed that *TGF-β1* and *TGF-β2*, along with *Smad2* transcript levels, which are associated with the TGF-β signaling pathway, were decreased. My preliminary data indicates that loss of *Lmna* impairs TGF-β signaling resulting in hyperproliferation of keratinocytes which consequently alters hair cycling in *Lmna*$^{\Delta/\Delta K14\text{-}Cre}$ mice.

To elucidate the molecular pathways involved in hyperproliferation in *Lmna*-null keratinocytes, I performed microarray analysis. Many of the altered molecules are associated with hyperproliferation of keratinocytes, such as *Klk6* (Klucky et al., 2007), *K16* (Jiang et al., 1993; Weiss et al., 1984) and *BMP4* (Huelsken et al., 2001). For instance, constitutive expression of *Klk6* resulted in enhanced wound healing in mice due to decreased cell adhesion molecule E-cadherin, resulting in increased cell migration and wound closure (Klucky et al., 2007). This corroborates my observations that loss of *Lmna* in *Lmna*$^{\Delta/\Delta K14\text{-}Cre}$ mice accelerates wound healing due to enhanced proliferation

of the keratinocytes as well as increased motility resulting from decreased expression of E-cadherin in *Lmna*-null keratinocytes.

A great body of evidence suggests that lamins can influence pathways implicated in cancer such as DNA replication (Johnson et al., 2004) and regulation of genomic stability (Gonzalez-Suarez et al., 2009b; Redwood et al., 2011), and therefore it is possible that alterations in lamin A/C expression could modify cancer development and progression (Prokocimer et al., 2009). Furthermore, altered levels of LMNA have been implicated in many cancers including skin epithelial cancers such as BCC and SCC (Tilli et al., 2003; Venables et al., 2001). Although no distinct pathway was suggested in the microarray analysis, a large number of genes associated with activation of proliferation and oncogenesis were altered, strongly suggesting that loss of *Lmna* in keratinocytes may lead to tumourigenesis. For instance, upregulation of *KLK*6 is reported in SCC (Klucky et al., 2007) and deregulation of *TGF-β* is associated with SCC and BCC (Glick, 2012). To further elucidate if loss of lamin A/C contributes to skin carcinogenesis, I am performing carcinogenesis studies on *Lmna*$^{Δ/ΔK14-Cre}$ mice. I hypothesize that absence of *Lmna* relieves the inhibition of keratinocyte growth due to decreased TGF-β levels, and when *Lmna*$^{Δ/ΔK14-Cre}$ mice are challenged with carcinogens, the mice may have increased tendency to form papillomas in their skin.

A-type lamins form an interconnected network with LEM domain proteins at the INM and mediate the localization of emerin, Lem2 and Lap2 to the INM (Brachner et al., 2005; Dechat et al., 2000a; Sullivan et al., 1999).

MAN1, an INM protein with a nucleoplasmic LEM domain (Lin et al., 2000), inhibits Smad2 and Smad3 activity so antagonizing TGF-β signaling (Bourgeois et al., 2013; Lin et al., 2005). Nucleoenvelopathies that arise due to mutations in *LEMD3* (MAN1) showed abnormalities in bone and skin and enhanced TGF-β activity (Hellemans et al., 2004). Overexpression of MAN1 leads to inhibition of BMP and TGF-β signaling (Hellemans et al., 2004) whereas loss of MAN1 results in Smad2/3 activation in mice (Bourgeois et al., 2013; Cohen et al., 2007; Lin et al., 2005). Emerin and MAN1 have essential and overlapping functions in chromosomal segregation during cell division (Liu et al., 2003). I speculate that since lamin A/C closely interacts with emerin, loss of *Lmna* may also affect the functions of MAN1 in keratinocytes.

Furthermore, as MAN1 can differentially regulate TGF-β and BMP, pathways important in skin homeostasis, it is possible that *Lmna* loss on keratinocytes and TGF-β signaling involves MAN1. Lem2 is a less studied INM LEM domain protein which interacts with and recruits A-type lamins, BAF, emerin and MAN1 (Brachner et al., 2005). Similar to emerin, lamin A/C also shows selective retention for Lem2 as loss of *Lmna* results in the redistribution of Lem2 throughout the ER (data not shown) (Brachner et al., 2005). Further studies and understanding of the roles of lamin A/C and other LEM domain proteins in the skin will shed light onto the mechanisms by which lamin A/C causes skin-related disorders in some laminopathies and also investigate its potential role in skin cancer.

Final conclusions and future work

Lamin A/C and its associated nuclear proteins have many significant functions. Mutations in *LMNA* result in at least thirteen different diseases collectively known as the laminopathies. Patients present clinical features in various tissues including the skeletal muscles, cardiac muscles, adipose tissues, bones and skin. This has led to the question of how different mutations in the single *LMNA* gene that is almost ubiquitously expressed in adult tissues leads to different tissue specific diseases. Moreover, mutations in *LMNA* affect a variety of processes that may impact cancer development and progression, such as changes in nuclear architecture, gene regulation, proliferation, apoptosis, chromatin organization and genome stability (Broers et al., 2006; Foster et al., 2010; Gonzalez-Suarez et al., 2009a; Zink et al., 2004). Colorectal, lung, skin, ovarian, breast and thyroid cancers as well as some leukemias, show altered levels of A-type lamins expression (Foster et al., 2010). However there has been little experimental investigation as to whether changes in LMNA expression contribute to the development of tumours. Mouse lines with constitutive *Lmna* mutations exhibit early postnatal lethality due to muscular dystrophy and cardiomyopathy. Therefore, it is essential to generate tissue-specific *Lmna* knockout mice that will live longer, to study the tissue-specific roles of lamin A/C as well as in the development of cancer.

In this thesis, I report a conditional *Lmna* knockout mouse model ($Lmna^{FL/FL}$), where exons 10 and 11 can be deleted by Cre recombinase. A constitutive *Lmna* knockout mouse line was obtained by crossing $Lmna^{FL/FL}$ to

Zp3-Cre mice, no full length *Lmna* transcripts or LMNA/C protein were detected in the *Lmna*$^{\Delta/\Delta}$ mice. These mice showed retarded postnatal growth and histological analysis of quadriceps muscles indicative of either delayed or defective muscle growth and maturation. This was probably a major contributory factor to the severe weight loss in the knockout mice. *Lmna*$^{\Delta/\Delta}$ mice had a shorter life span than the first constitutive *Lmna* mouse deletion (Sullivan *et al.*, 1999), perhaps due to differences in strain background and/or the absence of the low levels of the truncated LMNA/C fragment that had been reported as being present in these mice (Jahn et al., 2012).

Recently, a *Lmna* conditional mouse model which targets exon 2 of *Lmna* was reported. Constitutive deletion of *Lmna* using CMV-Cre results in functional deletion resulting in early death of the mice at P16-18 (Kim and Zheng, 2013). Our mouse line therefore provides an alternative to this line. The availability of a *Lmna* conditional model is especially important since the constitutive knockout models are early postnatal lethal, so preventing the study of the roles of LMNA/C in more mature tissues. The conditional *Lmna* knockout mouse lines, combined with different tissue-specific Cre lines, will be a powerful and essential tool to study the roles of LMNA/C in different tissues, cell types, and at different ages. This will be important for gaining further insight into how lamin A/C has a role in causing laminopathies and cancer. Using this conditional *Lmna* mouse line, I investigated the physiological roles of *Lmna* in two highly proliferative tissues: the skin and gastrointestinal tract. I also investigated the involvement of *Lmna* in the tumorigenesis of these two tissues.

166

Our $Lmna^{\Delta/\Delta/Vil\text{-}Cre}$ mouse line that lacks $Lmna$ in their intestinal epithelial cells (IECs) through the GI tract survives more than 1 year without presenting any gross abnormalities or decrease in lifespan. This allowed me to bypass the early lethality of global loss of LMNA/C to evaluate tissue-specific loss of $Lmna$ in the intestines and the consequences on disease progression. Our $Lmna^{\Delta/\Delta/Vil\text{-}Cre}/Apc^{Min/+}$ mice model showed that loss of $Lmna$ in the intestinal epithelium leads to an increased frequency of larger tumors. Although Willis and colleagues previously linked the over-expression of LMNA to increased progression of colorectal cancer (CRC) and tumor metastasis in humans (Willis et al., 2008), my data shows that loss of $Lmna$ may result in enhanced tumorigenesis in the intestines, indicating that lamin A/C may serve as a tumor suppressor gene. Based on our findings that both LBR and LMNA/C have a mutual and interactive role in regulating heterochromatin distribution, I found that the nuclei in IECs and polyps also expressed LBR, which may have compensated for the loss of LMNA/C. In turn, this suggested that $Lmna$-null cells may be in a less differentiated state, so contributing to the slight increase in polyp size in $Lmna^{\Delta/\Delta/Vil\text{-}Cre}/Apc^{Min/+}$ mice.

$Lmna^{\Delta/\Delta/K14\text{-}Cre}$ mice do not express LMNA/C in the keratinocytes of the skin epidermis and hair follicles as well as in the keratinocytes of the tongue epidermis. These mice show pronounced epidermal thickening in the skin with concomitant hyperproliferation of basal keratinocytes. Loss of $Lmna$ also resulted in accelerated hair growth, particularly during the second anagen of the hair cycle. While B-type lamins are dispensable in the proliferation of

murine keratinocytes and development of skin and hair in mice (Yang et al., 2011a), my data shows that lamin A/C is important in regulating epidermal proliferation and hair follicle growth. Furthermore, when lamin A is deleted in keratinocytes deficient for both *Lmnb* genes, the mice showed severe anomalies in the skin particularly in the formation of a proper skin barrier resulting in early postnatal death, probably due to dehydration (Jung et al., 2014). Taken together with my data, I propose that lamin A may play a more important role in postnatal skin and hair homeostasis in comparison to B-type lamins.

Further studies and understanding of the roles of lamin A/C in the skin are still required to fully understand the mechanisms by which mutations in *LMNA* cause skin-related disorders in some laminopathies. In addition, further work is needed to investigate a potential role of lamin A/C in skin cancer. Therefore, work beyond this thesis will mainly focus on defining the molecular mechanisms by which lamin A/C regulates cell proliferation. Microarray gene expression analysis of *Lmna*-null keratinocytes from P120 mice revealed upregulation of several genes associated with hyperproliferation such as *Klk6*, *K16* and *BMP4*. At P120, WT and *Lmna*$^{\Delta/\Delta K14\text{-}Cre}$ mice have asynchronized hair cycles. However, at around P70, *Lmna*$^{\Delta/\Delta K14\text{-}Cre}$ show accelerated hair growth compared to their WT littermates. Therefore, I will analyze the gene expression profiles of P70 *Lmna*-null keratinocytes, which will aid in understanding the mechanisms which lamin A/C has in the skin epidermis. Hopefully, this may identify regulatory pathways and how the loss of *Lmna* results in accelerated hair growth in *Lmna*$^{\Delta/\Delta K14\text{-}Cre}$ mice. RNA

sequencing (RNA-Seq) of WT and *Lmna*-null keratinocytes is currently in progress.

MAFs expressing laminA$^{\Delta 9}$, a truncated and farnesylated form of lamin A known as progerin, show reduced transcriptional activity of Wnt signaling components Tcf-1 and Lef1 hence slowing down cell proliferation (Hernandez et al., 2010). *Lmna*-null MEFs show disrupted NF-kB regulated gene transcription (Lammerding et al., 2004) and Rb signaling (Johnson et al., 2004; Markiewicz et al., 2002; Ozaki et al., 1994). Lamin A/C is also associated with Rb, Smad2 and nuclear protein phosphatase 2A (PP2A) to regulate gene expression downstream of TGF-β signaling (Van Berlo et al., 2005). TGF-β, a potent inhibitor of keratinocyte growth and hair cycling, is downregulated in *Lmna*-null keratinocytes. Deregulation of the TGF-β signaling pathway is often associated with squamous cell carcinoma (SCC) (Glick, 2012).

A-type lamins have important interactions with other INM proteins such as emerin, Lem2 and MAN1 (Brachner et al., 2005; Dechat et al., 2000a; Sullivan et al., 1999), all of which have been implicated in regulating major signaling pathways. Emerin participates in regulating Notch, Wnt, IGF and TGF-β signaling pathways to govern the proliferation and differentiation of myoblasts (Koch and Holaska, 2012). Emerin, as well as Lem2, also negatively regulates extracellular signal-regulated kinase (ERK) (Huber et al., 2009; Muchir et al., 2007a; Muchir et al., 2007b) . MAN1 has a major role in regulating TGF-β and BMP signaling by influencing Smad phosphorylation

(Bourgeois et al., 2013; Cohen et al., 2007; Hellemans et al., 2004; Lin et al., 2005). Therefore, loss of *Lmna* may alter the functions of these INM proteins in regulating these different but critical signaling pathways in keratinocyte proliferation and hair cycling (Fuchs, 2007; Lee and Tumbar, 2012).

Future work will analyze the interplay and molecular functions of lamin A/C, MAN1 and Lem2 in TGF-β signaling and possibly emerin in Wnt signaling, although *Emd*-null mice do not show any overt skin pathology (Melcon et al., 2006; Ozawa et al., 2006). Using human keratinocytes lines, my preliminary findings suggested an increase in proliferation rate when *LMNA* was knocked down. These cell lines will be helpful to study the molecular pathways which are altered in the event of reduced *LMNA*. In addition, I am also analyzing whether absence of *Lmna* predisposes *Lmna*$^{\Delta/\Delta/K14-Cre}$ mice to enhanced skin papilloma formation and ultimately hope to elucidate the role of lamin A/C in maintenance of genomic stability.

In collaboration with Dr. Irina Solovei and colleagues from Ludwig-Maximilians University Munich, we investigated the role of LBR and LMNA/C in heterochromatin tethering and their roles in regulating cellular differentiation. We showed that peripheral heterochromatin is maintained by two tethers: LBR or lamin A/C. In all mammalian cells, except rod photoreceptors, at least one of these tethers is present. Absence of both LBR and LMNA/C leads to the peripheral heterochromatin relocalizing to the nuclear centre and an inverted nuclear architecture. Myoblast transcriptome analysis indicated that the selective disruption of either the LBR- or LMNA/C-

dependent heterochromatin tether has inverse effects on the muscle gene expression, up- or downregulating them, respectively. These results show how developmental regulation of NE composition regulates global heterochromatin positioning, gene expression and cellular differentiation.

Since our data corroborates with published data and supports the notion that LEM-domain proteins cooperate with LMNA/C in tethering peripheral heterochromatin to the NE in mammals, we will continue to investigate the involvement of other LEM domain proteins such as Lem2 and MAN1 in mediating heterochromatin binding to LMNA/C. Since we have preliminary data that the localization of Lem2 is affected in the event of *Lmna* loss, we aim to investigate the nuclear architecture and chromatin organization in cells lacking Lem2. We plan to derive a conditional *Lemd2* knockout mouse line in the laboratory as embryonic stem (ES) cell clones with a conditional allele are available. The availability of a *Lemd2* knockout mouse model will provide further insight on the overall understanding of the nuclear envelope, and also help to define the composition of LMNA/C-dependent peripheral heterochromatin tether in mammalian cells.

In conclusion, the tissue-specific deletion of *Lmna* in mice has provided new insights in the requirement of lamin A/C in the intestinal epithelium and skin epidermis, and loss of *Lmna* results in defective proliferation. My studies show that lamin A/C, together with LBR and perhaps Lem2 and MAN1, have important functions in proliferation, cellular differentiation and chromatin organization. Future work mentioned above will

provide additional information on the signaling pathways implicated in the event of *Lmna* loss and nuclear lamin biology. Ultimately, I hope to provide new knowledge on nuclear lamins and contribute to improvement of therapeutic options of treatment of rare laminopathies and perhaps cancer.

BIBLIOGRAPHY

Abel, E.L., Angel, J.M., Kiguchi, K., and DiGiovanni, J. (2009). Multi-stage chemical carcinogenesis in mouse skin: fundamentals and applications. Nat Protoc *4*, 1350-1362.

Aebi, U., Cohn, J., Buhle, L., and Gerace, L. (1986). The nuclear lamina is a meshwork of intermediate-type filaments. Nature *323*, 560-564.

Agrelo, R., Setien, F., Espada, J., Artiga, M.J., Rodriguez, M., Perez-Rosado, A., Sanchez-Aguilera, A., Fraga, M.F., Piris, M.A., and Esteller, M. (2005). Inactivation of the lamin A/C gene by CpG island promoter hypermethylation in hematologic malignancies, and its association with poor survival in nodal diffuse large B-cell lymphoma. Journal of clinical oncology : official journal of the American Society of Clinical Oncology *23*, 3940-3947.

Akter, R., Rivas, D., Geneau, G., Drissi, H., and Duque, G. (2009). Effect of lamin A/C knockdown on osteoblast differentiation and function. Journal of bone and mineral research : the official journal of the American Society for Bone and Mineral Research *24*, 283-293.

Alsheimer, M., Fecher, E., and Benavente, R. (1998). Nuclear envelope remodelling during rat spermiogenesis: distribution and expression pattern of LAP2/thymopoietins. Journal of cell science *111 (Pt 15)*, 2227-2234.

Alsheimer, M., Liebe, B., Sewell, L., Stewart, C.L., Scherthan, H., and Benavente, R. (2004). Disruption of spermatogenesis in mice lacking A-type lamins. Journal of cell science *117*, 1173-1178.

Andl, T., Reddy, S.T., Gaddapara, T., and Millar, S.E. (2002). WNT signals are required for the initiation of hair follicle development. Dev Cell *2*, 643-653.

Andres, V., and Gonzalez, J.M. (2009). Role of A-type lamins in signaling, transcription, and chromatin organization. The Journal of cell biology *187*, 945-957.

Anzano, M.A., Roberts, A.B., Meyers, C.A., Komoriya, A., Lamb, L.C., Smith, J.M., and Sporn, M.B. (1982). Synergistic interaction of two classes of transforming growth factors from murine sarcoma cells. Cancer Res *42*, 4776-4778.

173

Araki, K., Imaizumi, T., Okuyama, K., Oike, Y., and Yamamura, K. (1997). Efficiency of recombination by Cre transient expression in embryonic stem cells: comparison of various promoters. Journal of biochemistry *122*, 977-982.

Arimura, T., Helbling-Leclerc, A., Massart, C., Varnous, S., Niel, F., Lacene, E., Fromes, Y., Toussaint, M., Mura, A.M., Keller, D.I.*, et al.* (2005). Mouse model carrying H222P-Lmna mutation develops muscular dystrophy and dilated cardiomyopathy similar to human striated muscle laminopathies. Human molecular genetics *14*, 155-169.

Barkan, R., Zahand, A.J., Sharabi, K., Lamm, A.T., Feinstein, N., Haithcock, E., Wilson, K.L., Liu, J., and Gruenbaum, Y. (2012). Ce-emerin and LEM-2: essential roles in Caenorhabditis elegans development, muscle function, and mitosis. Molecular biology of the cell *23*, 543-552.

Barker, N., van Es, J.H., Kuipers, J., Kujala, P., van den Born, M., Cozijnsen, M., Haegebarth, A., Korving, J., Begthel, H., Peters, P.J.*, et al.* (2007). Identification of stem cells in small intestine and colon by marker gene Lgr5. Nature *449*, 1003-1007.

Belt, E.J., Fijneman, R.J., van den Berg, E.G., Bril, H., Delis-van Diemen, P.M., Tijssen, M., van Essen, H.F., de Lange-de Klerk, E.S., Belien, J.A., Stockmann, H.B.*, et al.* (2011). Loss of lamin A/C expression in stage II and III colon cancer is associated with disease recurrence. Eur J Cancer *47*, 1837-1845.

Bengtsson, L. (2007). What MAN1 does to the Smads. TGFbeta/BMP signaling and the nuclear envelope. The FEBS journal *274*, 1374-1382.

Berger, R., Theodor, L., Shoham, J., Gokkel, E., Brok-Simoni, F., Avraham, K.B., Copeland, N.G., Jenkins, N.A., Rechavi, G., and Simon, A.J. (1996). The characterization and localization of the mouse thymopoietin/lamina-associated polypeptide 2 gene and its alternatively spliced products. Genome research *6*, 361-370.

Bertrand, A.T., Renou, L., Papadopoulos, A., Beuvin, M., Lacene, E., Massart, C., Ottolenghi, C., Decostre, V., Maron, S., Schlossarek, S.*, et al.* (2012). DelK32-lamin A/C has abnormal location and induces incomplete tissue maturation and severe metabolic defects leading to premature death. Human molecular genetics *21*, 1037-1048.

Best, S., Salvati, F., Kallo, J., Garner, C., Height, S., Thein, S.L., and Rees, D.C. (2003). Lamin B-receptor mutations in Pelger-Huet anomaly. Br J Haematol *123*, 542-544.

Bhaskara, S., Knutson, S.K., Jiang, G., Chandrasekharan, M.B., Wilson, A.J., Zheng, S., Yenamandra, A., Locke, K., Yuan, J.L., Bonine-Summers, A.R.*, et al.* (2010). Hdac3 is essential for the maintenance of chromatin structure and genome stability. Cancer Cell *18*, 436-447.

Biamonti, G., Giacca, M., Perini, G., Contreas, G., Zentilin, L., Weighardt, F., Guerra, M., Della Valle, G., Saccone, S., Riva, S.*, et al.* (1992). The gene for a novel human lamin maps at a highly transcribed locus of chromosome 19 which replicates at the onset of S-phase. Molecular and cellular biology *12*, 3499-3506.

Bione, S., Maestrini, E., Rivella, S., Mancini, M., Regis, S., Romeo, G., and Toniolo, D. (1994). Identification of a novel X-linked gene responsible for Emery-Dreifuss muscular dystrophy. Nature genetics *8*, 323-327.

Blanpain, C., and Fuchs, E. (2006). Epidermal stem cells of the skin. Annu Rev Cell Dev Biol *22*, 339-373.

Boguslavsky, R.L., Stewart, C.L., and Worman, H.J. (2006). Nuclear lamin A inhibits adipocyte differentiation: implications for Dunnigan-type familial partial lipodystrophy. Human molecular genetics *15*, 653-663.

Bonne, G., and Levy, N. (2003). LMNA mutations in atypical Werner's syndrome. Lancet *362*, 1585-1586; author reply 1586.

Bonne, G., Mercuri, E., Muchir, A., Urtizberea, A., Becane, H.M., Recan, D., Merlini, L., Wehnert, M., Boor, R., Reuner, U.*, et al.* (2000). Clinical and molecular genetic spectrum of autosomal dominant Emery-Dreifuss muscular dystrophy due to mutations of the lamin A/C gene. Ann Neurol *48*, 170-180.

Bourgeois, B., Gilquin, B., Tellier-Lebegue, C., Ostlund, C., Wu, W., Perez, J., El Hage, P., Lallemand, F., Worman, H.J., and Zinn-Justin, S. (2013). Inhibition of TGF-beta signaling at the nuclear envelope: characterization of interactions between MAN1, Smad2 and Smad3, and PPM1A. Sci Signal *6*, ra49.

Brachner, A., and Foisner, R. (2011). Evolvement of LEM proteins as chromatin tethers at the nuclear periphery. Biochem Soc Trans *39*, 1735-1741.

Brachner, A., Reipert, S., Foisner, R., and Gotzmann, J. (2005). LEM2 is a novel MAN1-related inner nuclear membrane protein associated with A-type lamins. Journal of cell science *118*, 5797-5810.

Bridger, J.M., and Kill, I.R. (2004). Aging of Hutchinson-Gilford progeria syndrome fibroblasts is characterised by hyperproliferation and increased apoptosis. Exp Gerontol *39*, 717-724.

Broers, J.L., Kuijpers, H.J., Ostlund, C., Worman, H.J., Endert, J., and Ramaekers, F.C. (2005). Both lamin A and lamin C mutations cause lamina instability as well as loss of internal nuclear lamin organization. Experimental cell research *304*, 582-592.

Broers, J.L., Machiels, B.M., Kuijpers, H.J., Smedts, F., van den Kieboom, R., Raymond, Y., and Ramaekers, F.C. (1997). A- and B-type lamins are differentially expressed in normal human tissues. Histochemistry and cell biology *107*, 505-517.

Broers, J.L., Ramaekers, F.C., Bonne, G., Yaou, R.B., and Hutchison, C.J. (2006). Nuclear lamins: laminopathies and their role in premature ageing. Physiological reviews *86*, 967-1008.

Broers, J.L., Raymond, Y., Rot, M.K., Kuijpers, H., Wagenaar, S.S., and Ramaekers, F.C. (1993). Nuclear A-type lamins are differentially expressed in human lung cancer subtypes. The American journal of pathology *143*, 211-220.

Burke, B., and Ellenberg, J. (2002). Remodelling the walls of the nucleus. Nature reviews Molecular cell biology *3*, 487-497.

Burke, B., and Stewart, C.L. (2002). Life at the edge: the nuclear envelope and human disease. Nature reviews Molecular cell biology *3*, 575-585.

Burke, B., and Stewart, C.L. (2006). The laminopathies: the functional architecture of the nucleus and its contribution to disease. Annual review of genomics and human genetics *7*, 369-405.

Burke, B., and Stewart, C.L. (2013). The nuclear lamins: flexibility in function. Nature reviews Molecular cell biology *14*, 13-24.

Burke, B., and Stewart, C.L. (2014). Functional architecture of the cell's nucleus in development, aging, and disease. Curr Top Dev Biol *109*, 1-52.

Butler, J.T., Hall, L.L., Smith, K.P., and Lawrence, J.B. (2009). Changing nuclear landscape and unique PML structures during early epigenetic transitions of human embryonic stem cells. Journal of cellular biochemistry *107*, 609-621.

Cabanillas, R., Cadinanos, J., Villameytide, J.A., Perez, M., Longo, J., Richard, J.M., Alvarez, R., Duran, N.S., Illan, R., Gonzalez, D.J*., et al.* (2011). Nestor-Guillermo progeria syndrome: a novel premature aging condition with early onset and chronic development caused by BANF1 mutations. American journal of medical genetics Part A *155A*, 2617-2625.

Cai, M., Huang, Y., Ghirlando, R., Wilson, K.L., Craigie, R., and Clore, G.M. (2001). Solution structure of the constant region of nuclear envelope protein LAP2 reveals two LEM-domain structures: one binds BAF and the other binds DNA. The EMBO journal *20*, 4399-4407.

Cao, H., and Hegele, R.A. (2000). Nuclear lamin A/C R482Q mutation in canadian kindreds with Dunnigan-type familial partial lipodystrophy. Human molecular genetics *9*, 109-112.

Capanni, C., Cenni, V., Mattioli, E., Sabatelli, P., Ognibene, A., Columbaro, M., Parnaik, V.K., Wehnert, M., Maraldi, N.M., Squarzoni, S*., et al.* (2003). Failure of lamin A/C to functionally assemble in R482L mutated familial partial lipodystrophy fibroblasts: altered intermolecular interaction with emerin and implications for gene transcription. Experimental cell research *291*, 122-134.

Capo-chichi, C.D., Cai, K.Q., Smedberg, J., Ganjei-Azar, P., Godwin, A.K., and Xu, X.X. (2011). Loss of A-type lamin expression compromises nuclear envelope integrity in breast cancer. Chinese journal of cancer *30*, 415-425.

Casey, P.J. (1992). Biochemistry of protein prenylation. J Lipid Res *33*, 1731-1740.

Casey, P.J., and Seabra, M.C. (1996). Protein prenyltransferases. J Biol Chem *271*, 5289-5292.

Chaouch, M., Allal, Y., De Sandre-Giovannoli, A., Vallat, J.M., Amer-el-Khedoud, A., Kassouri, N., Chaouch, A., Sindou, P., Hammadouche, T., Tazir,

M., *et al.* (2003). The phenotypic manifestations of autosomal recessive axonal Charcot-Marie-Tooth due to a mutation in Lamin A/C gene. Neuromuscular disorders : NMD *13*, 60-67.

Chen, C.Y., Chi, Y.H., Mutalif, R.A., Starost, M.F., Myers, T.G., Anderson, S.A., Stewart, C.L., and Jeang, K.T. (2012). Accumulation of the inner nuclear envelope protein Sun1 is pathogenic in progeric and dystrophic laminopathies. Cell *149*, 565-577.

Chen, L., Lee, L., Kudlow, B.A., Dos Santos, H.G., Sletvold, O., Shafeghati, Y., Botha, E.G., Garg, A., Hanson, N.B., Martin, G.M., *et al.* (2003). LMNA mutations in atypical Werner's syndrome. Lancet *362*, 440-445.

Chen, Y., Gelfond, J., McManus, L.M., and Shireman, P.K. (2011). Temporal microRNA expression during in vitro myogenic progenitor cell proliferation and differentiation: regulation of proliferation by miR-682. Physiol Genomics *43*, 621-630.

Cheung, A.F., Carter, A.M., Kostova, K.K., Woodruff, J.F., Crowley, D., Bronson, R.T., Haigis, K.M., and Jacks, T. (2010). Complete deletion of Apc results in severe polyposis in mice. Oncogene *29*, 1857-1864.

Cheung, T.H., Quach, N.L., Charville, G.W., Liu, L., Park, L., Edalati, A., Yoo, B., Hoang, P., and Rando, T.A. (2012). Maintenance of muscle stem-cell quiescence by microRNA-489. Nature *482*, 524-528.

Chi, Y.H., Cheng, L.I., Myers, T., Ward, J.M., Williams, E., Su, Q., Faucette, L., Wang, J.Y., and Jeang, K.T. (2009). Requirement for Sun1 in the expression of meiotic reproductive genes and piRNA. Development *136*, 965-973.

Chigira, M., Kato, K., Mashio, K., and Shinozaki, T. (1991). Symmetry of bone lesions in osteopoikilosis. Report of 4 cases. Acta Orthop Scand *62*, 495-496.

Clarke, S. (1992). Protein isoprenylation and methylation at carboxyl-terminal cysteine residues. Annu Rev Biochem *61*, 355-386.

Clements, L., Manilal, S., Love, D.R., and Morris, G.E. (2000). Direct interaction between emerin and lamin A. Biochemical and biophysical research communications *267*, 709-714.

Clowney, E.J., LeGros, M.A., Mosley, C.P., Clowney, F.G., Markenskoff-Papadimitriou, E.C., Myllys, M., Barnea, G., Larabell, C.A., and Lomvardas, S. (2012). Nuclear aggregation of olfactory receptor genes governs their monogenic expression. Cell *151*, 724-737.

Coffinier, C., Jung, H.J., Nobumori, C., Chang, S., Tu, Y., Barnes, R.H., 2nd, Yoshinaga, Y., de Jong, P.J., Vergnes, L., Reue, K.*, et al.* (2011). Deficiencies in lamin B1 and lamin B2 cause neurodevelopmental defects and distinct nuclear shape abnormalities in neurons. Molecular biology of the cell *22*, 4683-4693.

Cohen, T.V., Gnocchi, V.F., Cohen, J.E., Phadke, A., Liu, H., Ellis, J.A., Foisner, R., Stewart, C.L., Zammit, P.S., and Partridge, T.A. (2013). Defective skeletal muscle growth in lamin A/C-deficient mice is rescued by loss of Lap2alpha. Human molecular genetics *22*, 2852-2869.

Cohen, T.V., Klarmann, K.D., Sakchaisri, K., Cooper, J.P., Kuhns, D., Anver, M., Johnson, P.F., Williams, S.C., Keller, J.R., and Stewart, C.L. (2008). The lamin B receptor under transcriptional control of C/EBPepsilon is required for morphological but not functional maturation of neutrophils. Human molecular genetics *17*, 2921-2933.

Cohen, T.V., Kosti, O., and Stewart, C.L. (2007). The nuclear envelope protein MAN1 regulates TGFbeta signaling and vasculogenesis in the embryonic yolk sac. Development *134*, 1385-1395.

Columbaro, M., Capanni, C., Mattioli, E., Novelli, G., Parnaik, V.K., Squarzoni, S., Maraldi, N.M., and Lattanzi, G. (2005). Rescue of heterochromatin organization in Hutchinson-Gilford progeria by drug treatment. Cellular and molecular life sciences : CMLS *62*, 2669-2678.

Constantinescu, D., Gray, H.L., Sammak, P.J., Schatten, G.P., and Csoka, A.B. (2006). Lamin A/C expression is a marker of mouse and human embryonic stem cell differentiation. Stem cells *24*, 177-185.

Cotsarelis, G. (1997). The hair follicle: dying for attention. The American journal of pathology *151*, 1505-1509.

Cremer, T., and Cremer, M. (2010). Chromosome territories. Cold Spring Harbor perspectives in biology *2*, a003889.

Crisp, M., Liu, Q., Roux, K., Rattner, J.B., Shanahan, C., Burke, B., Stahl, P.D., and Hodzic, D. (2006). Coupling of the nucleus and cytoplasm: role of the LINC complex. The Journal of cell biology *172*, 41-53.

Croft, D.R., Coleman, M.L., Li, S., Robertson, D., Sullivan, T., Stewart, C.L., and Olson, M.F. (2005). Actin-myosin-based contraction is responsible for apoptotic nuclear disintegration. The Journal of cell biology *168*, 245-255.

Dafforn, A., Chen, P., Deng, G., Herrler, M., Iglehart, D., Koritala, S., Lato, S., Pillarisetty, S., Purohit, R., Wang, M.*, et al.* (2004). Linear mRNA amplification from as little as 5 ng total RNA for global gene expression analysis. Biotechniques *37*, 854-857.

Dassule, H.R., Lewis, P., Bei, M., Maas, R., and McMahon, A.P. (2000). Sonic hedgehog regulates growth and morphogenesis of the tooth. Development *127*, 4775-4785.

Davies, B.S., Fong, L.G., Yang, S.H., Coffinier, C., and Young, S.G. (2009). The posttranslational processing of prelamin A and disease. Annu Rev Genomics Hum Genet *10*, 153-174.

De Castro, S.C., Malhas, A., Leung, K.Y., Gustavsson, P., Vaux, D.J., Copp, A.J., and Greene, N.D. (2012). Lamin b1 polymorphism influences morphology of the nuclear envelope, cell cycle progression, and risk of neural tube defects in mice. PLoS Genet *8*, e1003059.

De Sandre-Giovannoli, A., Bernard, R., Cau, P., Navarro, C., Amiel, J., Boccaccio, I., Lyonnet, S., Stewart, C.L., Munnich, A., Le Merrer, M.*, et al.* (2003). Lamin a truncation in Hutchinson-Gilford progeria. Science *300*, 2055.

De Sandre-Giovannoli, A., Chaouch, M., Kozlov, S., Vallat, J.M., Tazir, M., Kassouri, N., Szepetowski, P., Hammadouche, T., Vandenberghe, A., Stewart, C.L.*, et al.* (2002). Homozygous defects in LMNA, encoding lamin A/C nuclear-envelope proteins, cause autosomal recessive axonal neuropathy in human (Charcot-Marie-Tooth disorder type 2) and mouse. American journal of human genetics *70*, 726-736.

de Vries, W.N., Binns, L.T., Fancher, K.S., Dean, J., Moore, R., Kemler, R., and Knowles, B.B. (2000). Expression of Cre recombinase in mouse oocytes: a means to study maternal effect genes. Genesis *26*, 110-112.

Dechat, T., Korbei, B., Vaughan, O.A., Vlcek, S., Hutchison, C.J., and Foisner, R. (2000a). Lamina-associated polypeptide 2alpha binds intranuclear A-type lamins. Journal of cell science *113 Pt 19*, 3473-3484.

Dechat, T., Shimi, T., Adam, S.A., Rusinol, A.E., Andres, D.A., Spielmann, H.P., Sinensky, M.S., and Goldman, R.D. (2007). Alterations in mitosis and cell cycle progression caused by a mutant lamin A known to accelerate human aging. Proceedings of the National Academy of Sciences of the United States of America *104*, 4955-4960.

Dechat, T., Vlcek, S., and Foisner, R. (2000b). Review: lamina-associated polypeptide 2 isoforms and related proteins in cell cycle-dependent nuclear structure dynamics. Journal of structural biology *129*, 335-345.

Demmerle, J., Koch, A.J., and Holaska, J.M. (2012). The nuclear envelope protein emerin binds directly to histone deacetylase 3 (HDAC3) and activates HDAC3 activity. The Journal of biological chemistry *287*, 22080-22088.

Ding, X., Xu, R., Yu, J., Xu, T., Zhuang, Y., and Han, M. (2007). SUN1 is required for telomere attachment to nuclear envelope and gametogenesis in mice. Developmental cell *12*, 863-872.

Donehower, L.A., Harvey, M., Slagle, B.L., McArthur, M.J., Montgomery, C.A., Jr., Butel, J.S., and Bradley, A. (1992). Mice deficient for p53 are developmentally normal but susceptible to spontaneous tumours. Nature *356*, 215-221.

Dorner, D., Gotzmann, J., and Foisner, R. (2007). Nucleoplasmic lamins and their interaction partners, LAP2alpha, Rb, and BAF, in transcriptional regulation. FEBS J *274*, 1362-1373.

Dreesen, O., Chojnowski, A., Ong, P.F., Zhao, T.Y., Common, J.E., Lunny, D., Lane, E.B., Lee, S.J., Vardy, L.A., Stewart, C.L.*, et al.* (2013a). Lamin B1 fluctuations have differential effects on cellular proliferation and senescence. The Journal of cell biology *200*, 605-617.

Dreesen, O., Ong, P.F., Chojnowski, A., and Colman, A. (2013b). The contrasting roles of lamin B1 in cellular aging and human disease. Nucleus *4*, 283-290.

Dreuillet, C., Tillit, J., Kress, M., and Ernoult-Lange, M. (2002). In vivo and in vitro interaction between human transcription factor MOK2 and nuclear lamin A/C. Nucleic acids research *30*, 4634-4642.

Dundr, M., and Misteli, T. (2001). Functional architecture in the cell nucleus. Biochem J *356*, 297-310.

Dwyer, N., and Blobel, G. (1976). A modified procedure for the isolation of a pore complex-lamina fraction from rat liver nuclei. The Journal of cell biology *70*, 581-591.

Eberhart, A., Kimura, H., Leonhardt, H., Joffe, B., and Solovei, I. (2012). Reliable detection of epigenetic histone marks and nuclear proteins in tissue cryosections. Chromosome Res *20*, 849-858.

Eden, E., Navon, R., Steinfeld, I., Lipson, D., and Yakhini, Z. (2009). GOrilla: a tool for discovery and visualization of enriched GO terms in ranked gene lists. BMC Bioinformatics *10*, 48.

Ellis, D.J., Jenkins, H., Whitfield, W.G., and Hutchison, C.J. (1997). GST-lamin fusion proteins act as dominant negative mutants in Xenopus egg extract and reveal the function of the lamina in DNA replication. Journal of cell science *110 (Pt 20)*, 2507-2518.

Eriksson, M., Brown, W.T., Gordon, L.B., Glynn, M.W., Singer, J., Scott, L., Erdos, M.R., Robbins, C.M., Moses, T.Y., Berglund, P*., et al.* (2003). Recurrent de novo point mutations in lamin A cause Hutchinson-Gilford progeria syndrome. Nature *423*, 293-298.

Espada, J., Varela, I., Flores, I., Ugalde, A.P., Cadinanos, J., Pendas, A.M., Stewart, C.L., Tryggvason, K., Blasco, M.A., Freije, J.M*., et al.* (2008). Nuclear envelope defects cause stem cell dysfunction in premature-aging mice. The Journal of cell biology *181*, 27-35.

Fairley, E.A., Kendrick-Jones, J., and Ellis, J.A. (1999). The Emery-Dreifuss muscular dystrophy phenotype arises from aberrant targeting and binding of emerin at the inner nuclear membrane. Journal of cell science *112 (Pt 15)*, 2571-2582.

Fatkin, D., MacRae, C., Sasaki, T., Wolff, M.R., Porcu, M., Frenneaux, M., Atherton, J., Vidaillet, H.J., Jr., Spudich, S., De Girolami, U*., et al.* (1999). Missense mutations in the rod domain of the lamin A/C gene as causes of

dilated cardiomyopathy and conduction-system disease. The New England journal of medicine *341*, 1715-1724.

Favreau, C., Higuet, D., Courvalin, J.C., and Buendia, B. (2004). Expression of a mutant lamin A that causes Emery-Dreifuss muscular dystrophy inhibits in vitro differentiation of C2C12 myoblasts. Molecular and cellular biology *24*, 1481-1492.

Fearon, E.R., and Vogelstein, B. (1990). A genetic model for colorectal tumorigenesis. Cell *61*, 759-767.

Fernandez, P., Scaffidi, P., Markert, E., Lee, J.H., Rane, S., and Misteli, T. (2014). Transformation Resistance in a Premature Aging Disorder Identifies a Tumor-Protective Function of BRD4. Cell reports *9*, 248-260.

Finlan, L.E., Sproul, D., Thomson, I., Boyle, S., Kerr, E., Perry, P., Ylstra, B., Chubb, J.R., and Bickmore, W.A. (2008). Recruitment to the nuclear periphery can alter expression of genes in human cells. PLoS Genet *4*, e1000039.

Fisher, D.Z., Chaudhary, N., and Blobel, G. (1986). cDNA sequencing of nuclear lamins A and C reveals primary and secondary structural homology to intermediate filament proteins. Proceedings of the National Academy of Sciences of the United States of America *83*, 6450-6454.

Foisner, R., and Gerace, L. (1993). Integral membrane proteins of the nuclear envelope interact with lamins and chromosomes, and binding is modulated by mitotic phosphorylation. Cell *73*, 1267-1279.

Foitzik, K., Lindner, G., Mueller-Roever, S., Maurer, M., Botchkareva, N., Botchkarev, V., Handjiski, B., Metz, M., Hibino, T., Soma, T.*, et al.* (2000). Control of murine hair follicle regression (catagen) by TGF-beta1 in vivo. FASEB J *14*, 752-760.

Fong, L.G., Ng, J.K., Lammerding, J., Vickers, T.A., Meta, M., Cote, N., Gavino, B., Qiao, X., Chang, S.Y., Young, S.R.*, et al.* (2006). Prelamin A and lamin A appear to be dispensable in the nuclear lamina. The Journal of clinical investigation *116*, 743-752.

Foster, C.R., Przyborski, S.A., Wilson, R.G., and Hutchison, C.J. (2010). Lamins as cancer biomarkers. Biochem Soc Trans *38*, 297-300.

Frangioni, J.V., and Neel, B.G. (1993). Use of a general purpose mammalian expression vector for studying intracellular protein targeting: identification of critical residues in the nuclear lamin A/C nuclear localization signal. Journal of cell science *105 (Pt 2)*, 481-488.

Fuchs, E. (2007). Scratching the surface of skin development. Nature *445*, 834-842.

Furukawa, K., Fritze, C.E., and Gerace, L. (1998). The major nuclear envelope targeting domain of LAP2 coincides with its lamin binding region but is distinct from its chromatin interaction domain. The Journal of biological chemistry *273*, 4213-4219.

Furukawa, K., and Hotta, Y. (1993). cDNA cloning of a germ cell specific lamin B3 from mouse spermatocytes and analysis of its function by ectopic expression in somatic cells. The EMBO journal *12*, 97-106.

Furukawa, K., Inagaki, H., and Hotta, Y. (1994). Identification and cloning of an mRNA coding for a germ cell-specific A-type lamin in mice. Experimental cell research *212*, 426-430.

Galiova, G., Bartova, E., Raska, I., Krejci, J., and Kozubek, S. (2008). Chromatin changes induced by lamin A/C deficiency and the histone deacetylase inhibitor trichostatin A. European journal of cell biology *87*, 291-303.

Gant, T.M., Harris, C.A., and Wilson, K.L. (1999). Roles of LAP2 proteins in nuclear assembly and DNA replication: truncated LAP2beta proteins alter lamina assembly, envelope formation, nuclear size, and DNA replication efficiency in Xenopus laevis extracts. The Journal of cell biology *144*, 1083-1096.

Gat, U., DasGupta, R., Degenstein, L., and Fuchs, E. (1998). De Novo hair follicle morphogenesis and hair tumors in mice expressing a truncated beta-catenin in skin. Cell *95*, 605-614.

Gaudy-Marqueste, C., Roll, P., Esteves-Vieira, V., Weiller, P.J., Grob, J.J., Cau, P., Levy, N., and De Sandre-Giovannoli, A. (2010). LBR mutation and nuclear envelope defects in a patient affected with Reynolds syndrome. J Med Genet *47*, 361-370.

Gerace, L., and Blobel, G. (1980). The nuclear envelope lamina is reversibly depolymerized during mitosis. Cell *19*, 277-287.

Gerace, L., and Burke, B. (1988). Functional organization of the nuclear envelope. Annual review of cell biology *4*, 335-374.

Gerace, L., Comeau, C., and Benson, M. (1984). Organization and modulation of nuclear lamina structure. Journal of cell science Supplement *1*, 137-160.

Gerace, L., and Huber, M.D. (2012). Nuclear lamina at the crossroads of the cytoplasm and nucleus. Journal of structural biology *177*, 24-31.

Glick, A.B. (2012). The Role of TGFbeta Signaling in Squamous Cell Cancer: Lessons from Mouse Models. J Skin Cancer *2012*, 249063.

Gniadecki, R. (1998). Regulation of keratinocyte proliferation. Gen Pharmacol *30*, 619-622.

Goecks, J., Nekrutenko, A., and Taylor, J. (2010). Galaxy: a comprehensive approach for supporting accessible, reproducible, and transparent computational research in the life sciences. Genome Biol *11*, R86.

Goldman, R.D., Gruenbaum, Y., Moir, R.D., Shumaker, D.K., and Spann, T.P. (2002). Nuclear lamins: building blocks of nuclear architecture. Genes & development *16*, 533-547.

Goldman, R.D., Shumaker, D.K., Erdos, M.R., Eriksson, M., Goldman, A.E., Gordon, L.B., Gruenbaum, Y., Khuon, S., Mendez, M., Varga, R.*, et al.* (2004). Accumulation of mutant lamin A causes progressive changes in nuclear architecture in Hutchinson-Gilford progeria syndrome. Proceedings of the National Academy of Sciences of the United States of America *101*, 8963-8968.

Gonzalez-Suarez, I., Redwood, A.B., and Gonzalo, S. (2009a). Loss of A-type lamins and genomic instability. Cell Cycle *8*, 3860-3865.

Gonzalez-Suarez, I., Redwood, A.B., Perkins, S.M., Vermolen, B., Lichtensztejin, D., Grotsky, D.A., Morgado-Palacin, L., Gapud, E.J., Sleckman, B.P., Sullivan, T.*, et al.* (2009b). Novel roles for A-type lamins in telomere biology and the DNA damage response pathway. EMBO J *28*, 2414-2427.

Gotic, I., and Foisner, R. (2010). Multiple novel functions of lamina associated polypeptide 2alpha in striated muscle. Nucleus *1*, 397-401.

Gotic, I., Schmidt, W.M., Biadasiewicz, K., Leschnik, M., Spilka, R., Braun, J., Stewart, C.L., and Foisner, R. (2010). Loss of LAP2 alpha delays satellite cell differentiation and affects postnatal fiber-type determination. Stem cells *28*, 480-488.

Goto, M., Miller, R.W., Ishikawa, Y., and Sugano, H. (1996). Excess of rare cancers in Werner syndrome (adult progeria). Cancer Epidemiol Biomarkers Prev *5*, 239-246.

Gotzmann, J., and Foisner, R. (2006). A-type lamin complexes and regenerative potential: a step towards understanding laminopathic diseases? Histochemistry and cell biology *125*, 33-41.

Greco, V., and Guo, S. (2010). Compartmentalized organization: a common and required feature of stem cell niches? Development *137*, 1586-1594.

Gros-Louis, F., Dupre, N., Dion, P., Fox, M.A., Laurent, S., Verreault, S., Sanes, J.R., Bouchard, J.P., and Rouleau, G.A. (2007). Mutations in SYNE1 lead to a newly discovered form of autosomal recessive cerebellar ataxia. Nature genetics *39*, 80-85.

Grossman, E., Medalia, O., and Zwerger, M. (2012). Functional architecture of the nuclear pore complex. Annu Rev Biophys *41*, 557-584.

Gruber, J., Lampe, T., Osborn, M., and Weber, K. (2005). RNAi of FACE1 protease results in growth inhibition of human cells expressing lamin A: implications for Hutchinson-Gilford progeria syndrome. Journal of cell science *118*, 689-696.

Hafner, M., Wenk, J., Nenci, A., Pasparakis, M., Scharffetter-Kochanek, K., Smyth, N., Peters, T., Kess, D., Holtkotter, O., Shephard, P*., et al.* (2004). Keratin 14 Cre transgenic mice authenticate keratin 14 as an oocyte-expressed protein. Genesis *38*, 176-181.

Han, X., Feng, X., Rattner, J.B., Smith, H., Bose, P., Suzuki, K., Soliman, M.A., Scott, M.S., Burke, B.E., and Riabowol, K. (2008). Tethering by lamin A stabilizes and targets the ING1 tumour suppressor. Nature cell biology *10*, 1333-1340.

Hanif, M., Rosengardten, Y., Sagelius, H., Rozell, B., and Eriksson, M. (2009). Differential expression of A-type and B-type lamins during hair cycling. PLoS One *4*, e4114.

Haque, F., Lloyd, D.J., Smallwood, D.T., Dent, C.L., Shanahan, C.M., Fry, A.M., Trembath, R.C., and Shackleton, S. (2006). SUN1 interacts with nuclear lamin A and cytoplasmic nesprins to provide a physical connection between the nuclear lamina and the cytoskeleton. Molecular and cellular biology *26*, 3738-3751.

Harborth, J., Elbashir, S.M., Bechert, K., Tuschl, T., and Weber, K. (2001). Identification of essential genes in cultured mammalian cells using small interfering RNAs. Journal of cell science *114*, 4557-4565.

Hegele, R.A., Cao, H., Liu, D.M., Costain, G.A., Charlton-Menys, V., Rodger, N.W., and Durrington, P.N. (2006). Sequencing of the reannotated LMNB2 gene reveals novel mutations in patients with acquired partial lipodystrophy. American journal of human genetics *79*, 383-389.

Helfand, B.T., Wang, Y., Pfleghaar, K., Shimi, T., Taimen, P., and Shumaker, D.K. (2012). Chromosomal regions associated with prostate cancer risk localize to lamin B-deficient microdomains and exhibit reduced gene transcription. The Journal of pathology *226*, 735-745.

Hellemans, J., Preobrazhenska, O., Willaert, A., Debeer, P., Verdonk, P.C., Costa, T., Janssens, K., Menten, B., Van Roy, N., Vermeulen, S.J.*, et al.* (2004). Loss-of-function mutations in LEMD3 result in osteopoikilosis, Buschke-Ollendorff syndrome and melorheostosis. Nature genetics *36*, 1213-1218.

Hennings, H., Glick, A.B., Lowry, D.T., Krsmanovic, L.S., Sly, L.M., and Yuspa, S.H. (1993). FVB/N mice: an inbred strain sensitive to the chemical induction of squamous cell carcinomas in the skin. Carcinogenesis *14*, 2353-2358.

Hernandez, L., Roux, K.J., Wong, E.S., Mounkes, L.C., Mutalif, R., Navasankari, R., Rai, B., Cool, S., Jeong, J.W., Wang, H.*, et al.* (2010). Functional coupling between the extracellular matrix and nuclear lamina by Wnt signaling in progeria. Dev Cell *19*, 413-425.

Herrmann, H., and Aebi, U. (2004). Intermediate filaments: molecular structure, assembly mechanism, and integration into functionally distinct intracellular Scaffolds. Annu Rev Biochem *73*, 749-789.

Hirano, Y., Hizume, K., Kimura, H., Takeyasu, K., Haraguchi, T., and Hiraoka, Y. (2012). Lamin B receptor recognizes specific modifications of histone H4 in heterochromatin formation. The Journal of biological chemistry *287*, 42654-42663.

Hoffmann, K., Dreger, C.K., Olins, A.L., Olins, D.E., Shultz, L.D., Lucke, B., Karl, H., Kaps, R., Muller, D., Vaya, A*., et al.* (2002). Mutations in the gene encoding the lamin B receptor produce an altered nuclear morphology in granulocytes (Pelger-Huet anomaly). Nature genetics *31*, 410-414.

Hoffmann, K., Sperling, K., Olins, A.L., and Olins, D.E. (2007). The granulocyte nucleus and lamin B receptor: avoiding the ovoid. Chromosoma *116*, 227-235.

Hoger, T.H., Krohne, G., and Franke, W.W. (1988). Amino acid sequence and molecular characterization of murine lamin B as deduced from cDNA clones. Eur J Cell Biol *47*, 283-290.

Holmer, L., Pezhman, A., and Worman, H.J. (1998). The human lamin B receptor/sterol reductase multigene family. Genomics *54*, 469-476.

Holtz, D., Tanaka, R.A., Hartwig, J., and McKeon, F. (1989). The CaaX motif of lamin A functions in conjunction with the nuclear localization signal to target assembly to the nuclear envelope. Cell *59*, 969-977.

Horn, H.F., Brownstein, Z., Lenz, D.R., Shivatzki, S., Dror, A.A., Dagan-Rosenfeld, O., Friedman, L.M., Roux, K.J., Kozlov, S., Jeang, K.T*., et al.* (2013a). The LINC complex is essential for hearing. The Journal of clinical investigation *123*, 740-750.

Horn, H.F., Kim, D.I., Wright, G.D., Wong, E.S., Stewart, C.L., Burke, B., and Roux, K.J. (2013b). A mammalian KASH domain protein coupling meiotic chromosomes to the cytoskeleton. The Journal of cell biology *202*, 1023-1039.

Huber, M.D., Guan, T., and Gerace, L. (2009). Overlapping functions of nuclear envelope proteins NET25 (Lem2) and emerin in regulation of extracellular signal-regulated kinase signaling in myoblast differentiation. Molecular and cellular biology *29*, 5718-5728.

Huelsken, J., Vogel, R., Erdmann, B., Cotsarelis, G., and Birchmeier, W. (2001). beta-Catenin controls hair follicle morphogenesis and stem cell differentiation in the skin. Cell *105*, 533-545.

Hutchison, C.J. (2002). Lamins: building blocks or regulators of gene expression? Nature reviews Molecular cell biology *3*, 848-858.

Hutchison, C.J., Alvarez-Reyes, M., and Vaughan, O.A. (2001). Lamins in disease: why do ubiquitously expressed nuclear envelope proteins give rise to tissue-specific disease phenotypes? Journal of cell science *114*, 9-19.

Ikegami, K., Egelhofer, T.A., Strome, S., and Lieb, J.D. (2010). Caenorhabditis elegans chromosome arms are anchored to the nuclear membrane via discontinuous association with LEM-2. Genome Biol *11*, R120.

Ishimura, A., Chida, S., and Osada, S. (2008). Man1, an inner nuclear membrane protein, regulates left-right axis formation by controlling nodal signaling in a node-independent manner. Dev Dyn *237*, 3565-3576.

Ishimura, A., Ng, J.K., Taira, M., Young, S.G., and Osada, S. (2006). Man1, an inner nuclear membrane protein, regulates vascular remodeling by modulating transforming growth factor beta signaling. Development *133*, 3919-3928.

Ivorra, C., Kubicek, M., Gonzalez, J.M., Sanz-Gonzalez, S.M., Alvarez-Barrientos, A., O'Connor, J.E., Burke, B., and Andres, V. (2006). A mechanism of AP-1 suppression through interaction of c-Fos with lamin A/C. Genes & development *20*, 307-320.

Jacks, T., Remington, L., Williams, B.O., Schmitt, E.M., Halachmi, S., Bronson, R.T., and Weinberg, R.A. (1994). Tumor spectrum analysis in p53-mutant mice. Curr Biol *4*, 1-7.

Jahn, D., Schramm, S., Schnolzer, M., Heilmann, C.J., de Koster, C.G., Schutz, W., Benavente, R., and Alsheimer, M. (2012). A truncated lamin A in the Lmna -/- mouse line: implications for the understanding of laminopathies. Nucleus *3*, 463-474.

Jahoda, C.A., Horne, K.A., and Oliver, R.F. (1984). Induction of hair growth by implantation of cultured dermal papilla cells. Nature *311*, 560-562.

Jensen, K.B., Driskell, R.R., and Watt, F.M. (2010). Assaying proliferation and differentiation capacity of stem cells using disaggregated adult mouse epidermis. Nat Protoc *5*, 898-911.

Jiang, C.K., Magnaldo, T., Ohtsuki, M., Freedberg, I.M., Bernerd, F., and Blumenberg, M. (1993). Epidermal growth factor and transforming growth factor alpha specifically induce the activation- and hyperproliferation-associated keratins 6 and 16. Proceedings of the National Academy of Sciences of the United States of America *90*, 6786-6790.

Johnson, B.R., Nitta, R.T., Frock, R.L., Mounkes, L., Barbie, D.A., Stewart, C.L., Harlow, E., and Kennedy, B.K. (2004). A-type lamins regulate retinoblastoma protein function by promoting subnuclear localization and preventing proteasomal degradation. Proceedings of the National Academy of Sciences of the United States of America *101*, 9677-9682.

Jung, H.J., Tatar, A., Tu, Y., Nobumori, C., Yang, S.H., Goulbourne, C.N., Herrmann, H., Fong, L.G., and Young, S.G. (2014). An absence of nuclear lamins in keratinocytes leads to ichthyosis, defective epidermal barrier function, and intrusion of nuclear membranes and endoplasmic reticulum into the nuclear chromatin. Molecular and cellular biology.

Jung, P., Sato, T., Merlos-Suarez, A., Barriga, F.M., Iglesias, M., Rossell, D., Auer, H., Gallardo, M., Blasco, M.A., Sancho, E*., et al.* (2011). Isolation and in vitro expansion of human colonic stem cells. Nature medicine *17*, 1225-1227.

Kaufmann, S.H. (1992). Expression of nuclear envelope lamins A and C in human myeloid leukemias. Cancer research *52*, 2847-2853.

Kelley, R.I. (2000). Inborn errors of cholesterol biosynthesis. Adv Pediatr *47*, 1-53.

Kennedy, B.K., Barbie, D.A., Classon, M., Dyson, N., and Harlow, E. (2000). Nuclear organization of DNA replication in primary mammalian cells. Genes & development *14*, 2855-2868.

Kim, Y., Sharov, A.A., McDole, K., Cheng, M., Hao, H., Fan, C.M., Gaiano, N., Ko, M.S., and Zheng, Y. (2011). Mouse B-type lamins are required for proper organogenesis but not by embryonic stem cells. Science *334*, 1706-1710.

Kim, Y., Zheng, X., and Zheng, Y. (2013). Proliferation and differentiation of mouse embryonic stem cells lacking all lamins. Cell Res *23*, 1420-1423.

Kim, Y., and Zheng, Y. (2013). Generation and characterization of a conditional deletion allele for Lmna in mice. Biochemical and biophysical research communications *440*, 8-13.

Kizilyaprak, C., Spehner, D., Devys, D., and Schultz, P. (2011). The linker histone H1C contributes to the SCA7 nuclear phenotype. Nucleus *2*, 444-454.

Klucky, B., Mueller, R., Vogt, I., Teurich, S., Hartenstein, B., Breuhahn, K., Flechtenmacher, C., Angel, P., and Hess, J. (2007). Kallikrein 6 induces E-cadherin shedding and promotes cell proliferation, migration, and invasion. Cancer Res *67*, 8198-8206.

Koch, A.J., and Holaska, J.M. (2012). Loss of emerin alters myogenic signaling and miRNA expression in mouse myogenic progenitors. PLoS One *7*, e37262.

Kongkanuntn, R., Bubb, V.J., Sansom, O.J., Wyllie, A.H., Harrison, D.J., and Clarke, A.R. (1999). Dysregulated expression of beta-catenin marks early neoplastic change in Apc mutant mice, but not all lesions arising in Msh2 deficient mice. Oncogene *18*, 7219-7225.

Korfali, N., Wilkie, G.S., Swanson, S.K., Srsen, V., de Las Heras, J., Batrakou, D.G., Malik, P., Zuleger, N., Kerr, A.R., Florens, L.*, et al.* (2012). The nuclear envelope proteome differs notably between tissues. Nucleus *3*, 552-564.

Krause, K., and Foitzik, K. (2006). Biology of the hair follicle: the basics. Seminars in cutaneous medicine and surgery *25*, 2-10.

Krimm, I., Ostlund, C., Gilquin, B., Couprie, J., Hossenlopp, P., Mornon, J.P., Bonne, G., Courvalin, J.C., Worman, H.J., and Zinn-Justin, S. (2002). The Ig-like structure of the C-terminal domain of lamin A/C, mutated in muscular dystrophies, cardiomyopathy, and partial lipodystrophy. Structure *10*, 811-823.

Kubben, N., Adriaens, M., Meuleman, W., Voncken, J.W., van Steensel, B., and Misteli, T. (2012). Mapping of lamin A- and progerin-interacting genome regions. Chromosoma *121*, 447-464.

Kubben, N., Voncken, J.W., Konings, G., van Weeghel, M., van den Hoogenhof, M.M., Gijbels, M., van Erk, A., Schoonderwoerd, K., van den Bosch, B., Dahlmans, V.*, et al.* (2011). Post-natal myogenic and adipogenic developmental: defects and metabolic impairment upon loss of A-type lamins. Nucleus *2*, 195-207.

Kumaran, R.I., Muralikrishna, B., and Parnaik, V.K. (2002). Lamin A/C speckles mediate spatial organization of splicing factor compartments and RNA polymerase II transcription. The Journal of cell biology *159*, 783-793.

Kumaran, R.I., and Spector, D.L. (2008). A genetic locus targeted to the nuclear periphery in living cells maintains its transcriptional competence. The Journal of cell biology *180*, 51-65.

Lagna, G., Hata, A., Hemmati-Brivanlou, A., and Massague, J. (1996). Partnership between DPC4 and SMAD proteins in TGF-beta signalling pathways. Nature *383*, 832-836.

Lammerding, J., Fong, L.G., Ji, J.Y., Reue, K., Stewart, C.L., Young, S.G., and Lee, R.T. (2006). Lamins A and C but not lamin B1 regulate nuclear mechanics. The Journal of biological chemistry *281*, 25768-25780.

Lammerding, J., Schulze, P.C., Takahashi, T., Kozlov, S., Sullivan, T., Kamm, R.D., Stewart, C.L., and Lee, R.T. (2004). Lamin A/C deficiency causes defective nuclear mechanics and mechanotransduction. The Journal of clinical investigation *113*, 370-378.

Lee, J., and Tumbar, T. (2012). Hairy tale of signaling in hair follicle development and cycling. Semin Cell Dev Biol *23*, 906-916.

Lee, K.K., Haraguchi, T., Lee, R.S., Koujin, T., Hiraoka, Y., and Wilson, K.L. (2001). Distinct functional domains in emerin bind lamin A and DNA-bridging protein BAF. Journal of cell science *114*, 4567-4573.

Lee, K.K., and Wilson, K.L. (2004). All in the family: evidence for four new LEM-domain proteins Lem2 (NET-25), Lem3, Lem4 and Lem5 in the human genome. Symposia of the Society for Experimental Biology, 329-339.

Lenz-Bohme, B., Wismar, J., Fuchs, S., Reifegerste, R., Buchner, E., Betz, H., and Schmitt, B. (1997). Insertional mutation of the Drosophila nuclear lamin Dm0 gene results in defective nuclear envelopes, clustering of nuclear pore complexes, and accumulation of annulate lamellae. The Journal of cell biology *137*, 1001-1016.

Lin, F., Blake, D.L., Callebaut, I., Skerjanc, I.S., Holmer, L., McBurney, M.W., Paulin-Levasseur, M., and Worman, H.J. (2000). MAN1, an inner nuclear membrane protein that shares the LEM domain with lamina-associated

polypeptide 2 and emerin. The Journal of biological chemistry *275*, 4840-4847.

Lin, F., Morrison, J.M., Wu, W., and Worman, H.J. (2005). MAN1, an integral protein of the inner nuclear membrane, binds Smad2 and Smad3 and antagonizes transforming growth factor-beta signaling. Human molecular genetics *14*, 437-445.

Lin, F., and Worman, H.J. (1993). Structural organization of the human gene encoding nuclear lamin A and nuclear lamin C. The Journal of biological chemistry *268*, 16321-16326.

Lindeman, R.E., and Pelegri, F. (2012). Localized products of futile cycle/lrmp promote centrosome-nucleus attachment in the zebrafish zygote. Curr Biol *22*, 843-851.

Lindner, G., Botchkarev, V.A., Botchkareva, N.V., Ling, G., van der Veen, C., and Paus, R. (1997). Analysis of apoptosis during hair follicle regression (catagen). The American journal of pathology *151*, 1601-1617.

Liu, B., Wang, J., Chan, K.M., Tjia, W.M., Deng, W., Guan, X., Huang, J.D., Li, K.M., Chau, P.Y., Chen, D.J.*, et al.* (2005). Genomic instability in laminopathy-based premature aging. Nature medicine *11*, 780-785.

Liu, B., Wang, Z., Ghosh, S., and Zhou, Z. (2013). Defective ATM-Kap-1-mediated chromatin remodeling impairs DNA repair and accelerates senescence in progeria mouse model. Aging Cell *12*, 316-318.

Liu, J., Lee, K.K., Segura-Totten, M., Neufeld, E., Wilson, K.L., and Gruenbaum, Y. (2003). MAN1 and emerin have overlapping function(s) essential for chromosome segregation and cell division in Caenorhabditis elegans. Proceedings of the National Academy of Sciences of the United States of America *100*, 4598-4603.

Liu, J., Rolef Ben-Shahar, T., Riemer, D., Treinin, M., Spann, P., Weber, K., Fire, A., and Gruenbaum, Y. (2000). Essential roles for Caenorhabditis elegans lamin gene in nuclear organization, cell cycle progression, and spatial organization of nuclear pore complexes. Molecular biology of the cell *11*, 3937-3947.

Lloyd, D.J., Trembath, R.C., and Shackleton, S. (2002). A novel interaction between lamin A and SREBP1: implications for partial lipodystrophy and other laminopathies. Human molecular genetics *11*, 769-777.

Lo Celso, C., Prowse, D.M., and Watt, F.M. (2004). Transient activation of beta-catenin signalling in adult mouse epidermis is sufficient to induce new hair follicles but continuous activation is required to maintain hair follicle tumours. Development *131*, 1787-1799.

Loewinger, L., and McKeon, F. (1988). Mutations in the nuclear lamin proteins resulting in their aberrant assembly in the cytoplasm. The EMBO journal *7*, 2301-2309.

Luxton, G.W., Gomes, E.R., Folker, E.S., Vintinner, E., and Gundersen, G.G. (2010). Linear arrays of nuclear envelope proteins harness retrograde actin flow for nuclear movement. Science *329*, 956-959.

Machiels, B.M., Broers, J.L., Raymond, Y., de Ley, L., Kuijpers, H.J., Caberg, N.E., and Ramaekers, F.C. (1995). Abnormal A-type lamin organization in a human lung carcinoma cell line. Eur J Cell Biol *67*, 328-335.

Machiels, B.M., Zorenc, A.H., Endert, J.M., Kuijpers, H.J., van Eys, G.J., Ramaekers, F.C., and Broers, J.L. (1996). An alternative splicing product of the lamin A/C gene lacks exon 10. The Journal of biological chemistry *271*, 9249-9253.

Madison, B.B., Dunbar, L., Qiao, X.T., Braunstein, K., Braunstein, E., and Gumucio, D.L. (2002). Cis elements of the villin gene control expression in restricted domains of the vertical (crypt) and horizontal (duodenum, cecum) axes of the intestine. The Journal of biological chemistry *277*, 33275-33283.

Maison, C., Pyrpasopoulou, A., Theodoropoulos, P.A., and Georgatos, S.D. (1997). The inner nuclear membrane protein LAP1 forms a native complex with B-type lamins and partitions with spindle-associated mitotic vesicles. The EMBO journal *16*, 4839-4850.

Makatsori, D., Kourmouli, N., Polioudaki, H., Shultz, L.D., McLean, K., Theodoropoulos, P.A., Singh, P.B., and Georgatos, S.D. (2004). The inner nuclear membrane protein lamin B receptor forms distinct microdomains and links epigenetically marked chromatin to the nuclear envelope. The Journal of biological chemistry *279*, 25567-25573.

Malhas, A., Lee, C.F., Sanders, R., Saunders, N.J., and Vaux, D.J. (2007). Defects in lamin B1 expression or processing affect interphase chromosome position and gene expression. The Journal of cell biology *176*, 593-603.

Mansharamani, M., and Wilson, K.L. (2005). Direct binding of nuclear membrane protein MAN1 to emerin in vitro and two modes of binding to barrier-to-autointegration factor. The Journal of biological chemistry *280*, 13863-13870.

Marino, S., Vooijs, M., van Der Gulden, H., Jonkers, J., and Berns, A. (2000). Induction of medulloblastomas in p53-null mutant mice by somatic inactivation of Rb in the external granular layer cells of the cerebellum. Genes & development *14*, 994-1004.

Markiewicz, E., Dechat, T., Foisner, R., Quinlan, R.A., and Hutchison, C.J. (2002). Lamin A/C binding protein LAP2alpha is required for nuclear anchorage of retinoblastoma protein. Molecular biology of the cell *13*, 4401-4413.

Martin, L., Crimaudo, C., and Gerace, L. (1995). cDNA cloning and characterization of lamina-associated polypeptide 1C (LAP1C), an integral protein of the inner nuclear membrane. The Journal of biological chemistry *270*, 8822-8828.

Martins, S.B., Eide, T., Steen, R.L., Jahnsen, T., Skalhegg, B.S., and Collas, P. (2000). HA95 is a protein of the chromatin and nuclear matrix regulating nuclear envelope dynamics. Journal of cell science *113 Pt 21*, 3703-3713.

Massague, J. (2008). TGFbeta in Cancer. Cell *134*, 215-230.

Massague, J., Seoane, J., and Wotton, D. (2005). Smad transcription factors. Genes & development *19*, 2783-2810.

Mattout, A., Pike, B.L., Towbin, B.D., Bank, E.M., Gonzalez-Sandoval, A., Stadler, M.B., Meister, P., Gruenbaum, Y., and Gasser, S.M. (2011). An EDMD mutation in C. elegans lamin blocks muscle-specific gene relocation and compromises muscle integrity. Curr Biol *21*, 1603-1614.

Maunoury, R., Robine, S., Pringault, E., Leonard, N., Gaillard, J.A., and Louvard, D. (1992). Developmental regulation of villin gene expression in the epithelial cell lineages of mouse digestive and urogenital tracts. Development *115*, 717-728.

Meaburn, K.J., Cabuy, E., Bonne, G., Levy, N., Morris, G.E., Novelli, G., Kill, I.R., and Bridger, J.M. (2007). Primary laminopathy fibroblasts display altered genome organization and apoptosis. Aging cell *6*, 139-153.

Meier, J., Campbell, K.H., Ford, C.C., Stick, R., and Hutchison, C.J. (1991). The role of lamin LIII in nuclear assembly and DNA replication, in cell-free extracts of Xenopus eggs. Journal of cell science *98 (Pt 3)*, 271-279.

Melcon, G., Kozlov, S., Cutler, D.A., Sullivan, T., Hernandez, L., Zhao, P., Mitchell, S., Nader, G., Bakay, M., Rottman, J.N*., et al.* (2006). Loss of emerin at the nuclear envelope disrupts the Rb1/E2F and MyoD pathways during muscle regeneration. Human molecular genetics *15*, 637-651.

Mendez-Lopez, I., and Worman, H.J. (2012). Inner nuclear membrane proteins: impact on human disease. Chromosoma *121*, 153-167.

Merideth, M.A., Gordon, L.B., Clauss, S., Sachdev, V., Smith, A.C., Perry, M.B., Brewer, C.C., Zalewski, C., Kim, H.J., Solomon, B*., et al.* (2008). Phenotype and course of Hutchinson-Gilford progeria syndrome. The New England journal of medicine *358*, 592-604.

Moir, R.D., Montag-Lowy, M., and Goldman, R.D. (1994). Dynamic properties of nuclear lamins: lamin B is associated with sites of DNA replication. The Journal of cell biology *125*, 1201-1212.

Moir, R.D., Spann, T.P., Herrmann, H., and Goldman, R.D. (2000). Disruption of nuclear lamin organization blocks the elongation phase of DNA replication. The Journal of cell biology *149*, 1179-1192.

Mosley-Bishop, K.L., Li, Q., Patterson, L., and Fischer, J.A. (1999). Molecular analysis of the klarsicht gene and its role in nuclear migration within differentiating cells of the Drosophila eye. Current biology : CB *9*, 1211-1220.

Mou, C., Jackson, B., Schneider, P., Overbeek, P.A., and Headon, D.J. (2006). Generation of the primary hair follicle pattern. Proceedings of the National Academy of Sciences of the United States of America *103*, 9075-9080.

Mounkes, L.C., Kozlov, S., Hernandez, L., Sullivan, T., and Stewart, C.L. (2003). A progeroid syndrome in mice is caused by defects in A-type lamins. Nature *423*, 298-301.

Mounkes, L.C., Kozlov, S.V., Rottman, J.N., and Stewart, C.L. (2005). Expression of an LMNA-N195K variant of A-type lamins results in cardiac conduction defects and death in mice. Human molecular genetics *14*, 2167-2180.

Moustakas, A., Pardali, K., Gaal, A., and Heldin, C.H. (2002). Mechanisms of TGF-beta signaling in regulation of cell growth and differentiation. Immunol Lett *82*, 85-91.

Muchir, A., Bonne, G., van der Kooi, A.J., van Meegen, M., Baas, F., Bolhuis, P.A., de Visser, M., and Schwartz, K. (2000). Identification of mutations in the gene encoding lamins A/C in autosomal dominant limb girdle muscular dystrophy with atrioventricular conduction disturbances (LGMD1B). Human molecular genetics *9*, 1453-1459.

Muchir, A., Pavlidis, P., Bonne, G., Hayashi, Y.K., and Worman, H.J. (2007a). Activation of MAPK in hearts of EMD null mice: similarities between mouse models of X-linked and autosomal dominant Emery Dreifuss muscular dystrophy. Human molecular genetics *16*, 1884-1895.

Muchir, A., Pavlidis, P., Decostre, V., Herron, A.J., Arimura, T., Bonne, G., and Worman, H.J. (2007b). Activation of MAPK pathways links LMNA mutations to cardiomyopathy in Emery-Dreifuss muscular dystrophy. The Journal of clinical investigation *117*, 1282-1293.

Muchir, A., and Worman, H.J. (2007). Emery-Dreifuss muscular dystrophy. Curr Neurol Neurosci Rep *7*, 78-83.

Muller-Rover, S., Handjiski, B., van der Veen, C., Eichmuller, S., Foitzik, K., McKay, I.A., Stenn, K.S., and Paus, R. (2001). A comprehensive guide for the accurate classification of murine hair follicles in distinct hair cycle stages. The Journal of investigative dermatology *117*, 3-15.

Naetar, N., and Foisner, R. (2009). Lamin complexes in the nuclear interior control progenitor cell proliferation and tissue homeostasis. Cell cycle *8*, 1488-1493.

Naetar, N., Korbei, B., Kozlov, S., Kerenyi, M.A., Dorner, D., Kral, R., Gotic, I., Fuchs, P., Cohen, T.V., Bittner, R.*, et al.* (2008). Loss of nucleoplasmic LAP2alpha-lamin A complexes causes erythroid and epidermal progenitor hyperproliferation. Nat Cell Biol *10*, 1341-1348.

Nagy, A. (2000). Cre recombinase: the universal reagent for genome tailoring. Genesis *26*, 99-109.

Navarro, C.L., Cadinanos, J., De Sandre-Giovannoli, A., Bernard, R., Courrier, S., Boccaccio, I., Boyer, A., Kleijer, W.J., Wagner, A., Giuliano, F*., et al.* (2005). Loss of ZMPSTE24 (FACE-1) causes autosomal recessive restrictive dermopathy and accumulation of Lamin A precursors. Human molecular genetics *14*, 1503-1513.

Navarro, C.L., De Sandre-Giovannoli, A., Bernard, R., Boccaccio, I., Boyer, A., Genevieve, D., Hadj-Rabia, S., Gaudy-Marqueste, C., Smitt, H.S., Vabres, P*., et al.* (2004). Lamin A and ZMPSTE24 (FACE-1) defects cause nuclear disorganization and identify restrictive dermopathy as a lethal neonatal laminopathy. Hum Mol Genet *13*, 2493-2503.

Neamati, N., Fernandez, A., Wright, S., Kiefer, J., and McConkey, D.J. (1995). Degradation of lamin B1 precedes oligonucleosomal DNA fragmentation in apoptotic thymocytes and isolated thymocyte nuclei. Journal of immunology *154*, 3788-3795.

Negrini, S., Gorgoulis, V.G., and Halazonetis, T.D. (2010). Genomic instability--an evolving hallmark of cancer. Nature reviews Molecular cell biology *11*, 220-228.

Newport, J.W., Wilson, K.L., and Dunphy, W.G. (1990). A lamin-independent pathway for nuclear envelope assembly. The Journal of cell biology *111*, 2247-2259.

Nikolova, V., Leimena, C., McMahon, A.C., Tan, J.C., Chandar, S., Jogia, D., Kesteven, S.H., Michalicek, J., Otway, R., Verheyen, F*., et al.* (2004). Defects in nuclear structure and function promote dilated cardiomyopathy in lamin A/C-deficient mice. The Journal of clinical investigation *113*, 357-369.

Novelli, G., Muchir, A., Sangiuolo, F., Helbling-Leclerc, A., D'Apice, M.R., Massart, C., Capon, F., Sbraccia, P., Federici, M., Lauro, R*., et al.* (2002). Mandibuloacral dysplasia is caused by a mutation in LMNA-encoding lamin A/C. American journal of human genetics *71*, 426-431.

Oberhammer, F.A., Hochegger, K., Froschl, G., Tiefenbacher, R., and Pavelka, M. (1994). Chromatin condensation during apoptosis is accompanied by degradation of lamin A+B, without enhanced activation of cdc2 kinase. The Journal of cell biology *126*, 827-837.

Odgren, P.R., Pratt, C.H., Mackay, C.A., Mason-Savas, A., Curtain, M., Shopland, L., Ichicki, T., Sundberg, J.P., and Donahue, L.R. (2010). Disheveled hair and ear (Dhe), a spontaneous mouse Lmna mutation modeling human laminopathies. PLoS One *5*, e9959.

Olins, A.L., Rhodes, G., Welch, D.B., Zwerger, M., and Olins, D.E. (2010). Lamin B receptor: multi-tasking at the nuclear envelope. Nucleus *1*, 53-70.

Oosterwijk, J.C., Mansour, S., van Noort, G., Waterham, H.R., Hall, C.M., and Hennekam, R.C. (2003). Congenital abnormalities reported in Pelger-Huet homozygosity as compared to Greenberg/HEM dysplasia: highly variable expression of allelic phenotypes. J Med Genet *40*, 937-941.

Osada, S., Ohmori, S.Y., and Taira, M. (2003). XMAN1, an inner nuclear membrane protein, antagonizes BMP signaling by interacting with Smad1 in Xenopus embryos. Development *130*, 1783-1794.

Ozaki, T., Saijo, M., Murakami, K., Enomoto, H., Taya, Y., and Sakiyama, S. (1994). Complex formation between lamin A and the retinoblastoma gene product: identification of the domain on lamin A required for its interaction. Oncogene *9*, 2649-2653.

Ozawa, R., Hayashi, Y.K., Ogawa, M., Kurokawa, R., Matsumoto, H., Noguchi, S., Nonaka, I., and Nishino, I. (2006). Emerin-lacking mice show minimal motor and cardiac dysfunctions with nuclear-associated vacuoles. The American journal of pathology *168*, 907-917.

Padiath, Q.S., Saigoh, K., Schiffmann, R., Asahara, H., Yamada, T., Koeppen, A., Hogan, K., Ptacek, L.J., and Fu, Y.H. (2006). Lamin B1 duplications cause autosomal dominant leukodystrophy. Nat Genet *38*, 1114-1123.

Padmakumar, V.C., Libotte, T., Lu, W., Zaim, H., Abraham, S., Noegel, A.A., Gotzmann, J., Foisner, R., and Karakesisoglou, I. (2005). The inner nuclear membrane protein Sun1 mediates the anchorage of Nesprin-2 to the nuclear envelope. Journal of cell science *118*, 3419-3430.

Pan, D., Estevez-Salmeron, L.D., Stroschein, S.L., Zhu, X., He, J., Zhou, S., and Luo, K. (2005). The integral inner nuclear membrane protein MAN1 physically interacts with the R-Smad proteins to repress signaling by the transforming growth factor-{beta} superfamily of cytokines. The Journal of biological chemistry *280*, 15992-16001.

Pardali, K., Kurisaki, A., Moren, A., ten Dijke, P., Kardassis, D., and Moustakas, A. (2000). Role of Smad proteins and transcription factor Sp1 in p21(Waf1/Cip1) regulation by transforming growth factor-beta. The Journal of biological chemistry *275*, 29244-29256.

Park, Y.E., Hayashi, Y.K., Goto, K., Komaki, H., Hayashi, Y., Inuzuka, T., Noguchi, S., Nonaka, I., and Nishino, I. (2009). Nuclear changes in skeletal muscle extend to satellite cells in autosomal dominant Emery-Dreifuss muscular dystrophy/limb-girdle muscular dystrophy 1B. Neuromuscular disorders : NMD *19*, 29-36.

Paulin-Levasseur, M., Blake, D.L., Julien, M., and Rouleau, L. (1996). The MAN antigens are non-lamin constituents of the nuclear lamina in vertebrate cells. Chromosoma *104*, 367-379.

Pegoraro, G., Kubben, N., Wickert, U., Gohler, H., Hoffmann, K., and Misteli, T. (2009). Ageing-related chromatin defects through loss of the NURD complex. Nature cell biology *11*, 1261-1267.

Pekovic, V., Harborth, J., Broers, J.L., Ramaekers, F.C., van Engelen, B., Lammens, M., von Zglinicki, T., Foisner, R., Hutchison, C., and Markiewicz, E. (2007). Nucleoplasmic LAP2alpha-lamin A complexes are required to maintain a proliferative state in human fibroblasts. The Journal of cell biology *176*, 163-172.

Pekovic, V., and Hutchison, C.J. (2008). Adult stem cell maintenance and tissue regeneration in the ageing context: the role for A-type lamins as intrinsic modulators of ageing in adult stem cells and their niches. Journal of anatomy *213*, 5-25.

Pendas, A.M., Zhou, Z., Cadinanos, J., Freije, J.M., Wang, J., Hultenby, K., Astudillo, A., Wernerson, A., Rodriguez, F., Tryggvason, K*., et al.* (2002). Defective prelamin A processing and muscular and adipocyte alterations in Zmpste24 metalloproteinase-deficient mice. Nature genetics *31*, 94-99.

Petiot, A., Conti, F.J., Grose, R., Revest, J.M., Hodivala-Dilke, K.M., and Dickson, C. (2003). A crucial role for Fgfr2-IIIb signalling in epidermal development and hair follicle patterning. Development *130*, 5493-5501.

Porter, F.D. (2003). Human malformation syndromes due to inborn errors of cholesterol synthesis. Curr Opin Pediatr *15*, 607-613.

Powell, L., and Burke, B. (1990). Internuclear exchange of an inner nuclear membrane protein (p55) in heterokaryons: in vivo evidence for the interaction of p55 with the nuclear lamina. The Journal of cell biology *111*, 2225-2234.

Prokocimer, M., Davidovich, M., Nissim-Rafinia, M., Wiesel-Motiuk, N., Bar, D.Z., Barkan, R., Meshorer, E., and Gruenbaum, Y. (2009). Nuclear lamins: key regulators of nuclear structure and activities. Journal of cellular and molecular medicine *13*, 1059-1085.

Puente, X.S., Quesada, V., Osorio, F.G., Cabanillas, R., Cadinanos, J., Fraile, J.M., Ordonez, G.R., Puente, D.A., Gutierrez-Fernandez, A., Fanjul-Fernandez, M.*, et al.* (2011). Exome sequencing and functional analysis identifies BANF1 mutation as the cause of a hereditary progeroid syndrome. American journal of human genetics *88*, 650-656.

Raharjo, W.H., Enarson, P., Sullivan, T., Stewart, C.L., and Burke, B. (2001). Nuclear envelope defects associated with LMNA mutations cause dilated cardiomyopathy and Emery-Dreifuss muscular dystrophy. Journal of cell science *114*, 4447-4457.

Rao, L., Perez, D., and White, E. (1996). Lamin proteolysis facilitates nuclear events during apoptosis. The Journal of cell biology *135*, 1441-1455.

Rapaport, D.H., Wong, L.L., Wood, E.D., Yasumura, D., and LaVail, M.M. (2004). Timing and topography of cell genesis in the rat retina. J Comp Neurol *474*, 304-324.

Reddy, K.L., Zullo, J.M., Bertolino, E., and Singh, H. (2008). Transcriptional repression mediated by repositioning of genes to the nuclear lamina. Nature *452*, 243-247.

Redwood, A.B., Perkins, S.M., Vanderwaal, R.P., Feng, Z., Biehl, K.J., Gonzalez-Suarez, I., Morgado-Palacin, L., Shi, W., Sage, J., Roti-Roti, J.L.*, et al.* (2011). A dual role for A-type lamins in DNA double-strand break repair. Cell cycle *10*, 2549-2560.

Rober, R.A., Weber, K., and Osborn, M. (1989). Differential timing of nuclear lamin A/C expression in the various organs of the mouse embryo and the young animal: a developmental study. Development *105*, 365-378.

Robinson, A., Partridge, D., Malhas, A., De Castro, S.C., Gustavsson, P., Thompson, D.N., Vaux, D.J., Copp, A.J., Stanier, P., Bassuk, A.G.*, et al.*

(2013). Is LMNB1 a susceptibility gene for neural tube defects in humans? Birth Defects Res A Clin Mol Teratol *97*, 398-402.

Ronneberger, O., Baddeley, D., Scheipl, F., Verveer, P.J., Burkhardt, H., Cremer, C., Fahrmeir, L., Cremer, T., and Joffe, B. (2008). Spatial quantitative analysis of fluorescently labeled nuclear structures: problems, methods, pitfalls. Chromosome Res *16*, 523-562.

Rosario, G.X., Hondo, E., Jeong, J.W., Mutalif, R., Ye, X., Yee, L.X., and Stewart, C.L. (2014). The LIF-Mediated Molecular Signature Regulating Murine Embryo Implantation. Biology of reproduction *91*, 66.

Roux, K.J., Crisp, M.L., Liu, Q., Kim, D., Kozlov, S., Stewart, C.L., and Burke, B. (2009). Nesprin 4 is an outer nuclear membrane protein that can induce kinesin-mediated cell polarization. Proceedings of the National Academy of Sciences of the United States of America *106*, 2194-2199.

Roux, K.J., Kim, D.I., Raida, M., and Burke, B. (2012). A promiscuous biotin ligase fusion protein identifies proximal and interacting proteins in mammalian cells. J Cell Biol *196*, 801-810.

Rowat, A.C., Jaalouk, D.E., Zwerger, M., Ung, W.L., Eydelnant, I.A., Olins, D.E., Olins, A.L., Herrmann, H., Weitz, D.A., and Lammerding, J. (2013). Nuclear envelope composition determines the ability of neutrophil-type cells to passage through micron-scale constrictions. The Journal of biological chemistry *288*, 8610-8618.

Rozencwaig, R., Wilson, M.R., and McFarland, G.B., Jr. (1997). Melorheostosis. Am J Orthop (Belle Mead NJ) *26*, 83-89.

Sabatelli, P., Lattanzi, G., Ognibene, A., Columbaro, M., Capanni, C., Merlini, L., Maraldi, N.M., and Squarzoni, S. (2001). Nuclear alterations in autosomal-dominant Emery-Dreifuss muscular dystrophy. Muscle & nerve *24*, 826-829.

Sarkar, P.K., and Shinton, R.A. (2001). Hutchinson-Guilford progeria syndrome. Postgraduate medical journal *77*, 312-317.

Sato, A., Isaac, B., Phillips, C.M., Rillo, R., Carlton, P.M., Wynne, D.J., Kasad, R.A., and Dernburg, A.F. (2009). Cytoskeletal forces span the nuclear envelope to coordinate meiotic chromosome pairing and synapsis. Cell *139*, 907-919.

Sato, N., Leopold, P.L., and Crystal, R.G. (1999). Induction of the hair growth phase in postnatal mice by localized transient expression of Sonic hedgehog. The Journal of clinical investigation *104*, 855-864.

Sauer, B., and Henderson, N. (1988). Site-specific DNA recombination in mammalian cells by the Cre recombinase of bacteriophage P1. Proceedings of the National Academy of Sciences of the United States of America *85*, 5166-5170.

Scaffidi, P., and Misteli, T. (2005). Reversal of the cellular phenotype in the premature aging disease Hutchinson-Gilford progeria syndrome. Nature medicine *11*, 440-445.

Scaffidi, P., and Misteli, T. (2006). Lamin A-dependent nuclear defects in human aging. Science *312*, 1059-1063.

Scaffidi, P., and Misteli, T. (2008). Lamin A-dependent misregulation of adult stem cells associated with accelerated ageing. Nature cell biology *10*, 452-459.

Schirmer, E.C., Florens, L., Guan, T., Yates, J.R., 3rd, and Gerace, L. (2003). Nuclear membrane proteins with potential disease links found by subtractive proteomics. Science *301*, 1380-1382.

Sellheyer, K., Bickenbach, J.R., Rothnagel, J.A., Bundman, D., Longley, M.A., Krieg, T., Roche, N.S., Roberts, A.B., and Roop, D.R. (1993). Inhibition of skin development by overexpression of transforming growth factor beta 1 in the epidermis of transgenic mice. Proceedings of the National Academy of Sciences of the United States of America *90*, 5237-5241.

Shackleton, S., Lloyd, D.J., Jackson, S.N., Evans, R., Niermeijer, M.F., Singh, B.M., Schmidt, H., Brabant, G., Kumar, S., Durrington, P.N.*, et al.* (2000). LMNA, encoding lamin A/C, is mutated in partial lipodystrophy. Nature genetics *24*, 153-156.

Shin, J.Y., Mendez-Lopez, I., Wang, Y., Hays, A.P., Tanji, K., Lefkowitch, J.H., Schulze, P.C., Worman, H.J., and Dauer, W.T. (2013). Lamina-associated polypeptide-1 interacts with the muscular dystrophy protein emerin and is essential for skeletal muscle maintenance. Dev Cell *26*, 591-603.

Shultz, L.D., Lyons, B.L., Burzenski, L.M., Gott, B., Samuels, R., Schweitzer, P.A., Dreger, C., Herrmann, H., Kalscheuer, V., Olins, A.L.*, et al.* (2003). Mutations at the mouse ichthyosis locus are within the lamin B receptor gene:

a single gene model for human Pelger-Huet anomaly. Human molecular genetics *12*, 61-69.

Shumaker, D.K., Dechat, T., Kohlmaier, A., Adam, S.A., Bozovsky, M.R., Erdos, M.R., Eriksson, M., Goldman, A.E., Khuon, S., Collins, F.S.*, et al.* (2006). Mutant nuclear lamin A leads to progressive alterations of epigenetic control in premature aging. Proceedings of the National Academy of Sciences of the United States of America *103*, 8703-8708.

Shumaker, D.K., Lee, K.K., Tanhehco, Y.C., Craigie, R., and Wilson, K.L. (2001). LAP2 binds to BAF.DNA complexes: requirement for the LEM domain and modulation by variable regions. The EMBO journal *20*, 1754-1764.

Silve, S., Dupuy, P.H., Ferrara, P., and Loison, G. (1998). Human lamin B receptor exhibits sterol C14-reductase activity in Saccharomyces cerevisiae. Biochim Biophys Acta *1392*, 233-244.

Smythe, C., Jenkins, H.E., and Hutchison, C.J. (2000). Incorporation of the nuclear pore basket protein nup153 into nuclear pore structures is dependent upon lamina assembly: evidence from cell-free extracts of Xenopus eggs. The EMBO journal *19*, 3918-3931.

Solovei, I., Kreysing, M., Lanctot, C., Kosem, S., Peichl, L., Cremer, T., Guck, J., and Joffe, B. (2009). Nuclear architecture of rod photoreceptor cells adapts to vision in mammalian evolution. Cell *137*, 356-368.

Solovei, I., Wang, A.S., Thanisch, K., Schmidt, C.S., Krebs, S., Zwerger, M., Cohen, T.V., Devys, D., Foisner, R., Peichl, L.*, et al.* (2013). LBR and lamin A/C sequentially tether peripheral heterochromatin and inversely regulate differentiation. Cell *152*, 584-598.

Sosa, B.A., Demircioglu, F.E., Chen, J.Z., Ingram, J., Ploegh, H., and Schwartz, T.U. (2014). How lamina-associated polypeptide 1 (LAP1) activates Torsin. Elife, e03239.

Sosa, B.A., Kutay, U., and Schwartz, T.U. (2013). Structural insights into LINC complexes. Curr Opin Struct Biol *23*, 285-291.

Sosa, B.A., Rothballer, A., Kutay, U., and Schwartz, T.U. (2012). LINC complexes form by binding of three KASH peptides to domain interfaces of trimeric SUN proteins. Cell *149*, 1035-1047.

Spann, T.P., Goldman, A.E., Wang, C., Huang, S., and Goldman, R.D. (2002). Alteration of nuclear lamin organization inhibits RNA polymerase II-dependent transcription. The Journal of cell biology *156*, 603-608.

Spann, T.P., Moir, R.D., Goldman, A.E., Stick, R., and Goldman, R.D. (1997). Disruption of nuclear lamin organization alters the distribution of replication factors and inhibits DNA synthesis. The Journal of cell biology *136*, 1201-1212.

Sperling, L.C. (1991). Hair anatomy for the clinician. J Am Acad Dermatol *25*, 1-17.

St-Jacques, B., Dassule, H.R., Karavanova, I., Botchkarev, V.A., Li, J., Danielian, P.S., McMahon, J.A., Lewis, P.M., Paus, R., and McMahon, A.P. (1998). Sonic hedgehog signaling is essential for hair development. Curr Biol *8*, 1058-1068.

Starr, D.A., and Fischer, J.A. (2005). KASH 'n Karry: the KASH domain family of cargo-specific cytoskeletal adaptor proteins. Bioessays *27*, 1136-1146.

Starr, D.A., and Han, M. (2002). Role of ANC-1 in tethering nuclei to the actin cytoskeleton. Science *298*, 406-409.

Stenn, K.S., and Paus, R. (2001). Controls of hair follicle cycling. Physiological reviews *81*, 449-494.

Sternberg, N., and Hamilton, D. (1981). Bacteriophage P1 site-specific recombination. I. Recombination between loxP sites. J Mol Biol *150*, 467-486.

Stewart, C., and Burke, B. (1987). Teratocarcinoma stem cells and early mouse embryos contain only a single major lamin polypeptide closely resembling lamin B. Cell *51*, 383-392.

Stewart, C.L., Kozlov, S., Fong, L.G., and Young, S.G. (2007a). Mouse models of the laminopathies. Experimental cell research *313*, 2144-2156.

Stewart, C.L., Roux, K.J., and Burke, B. (2007b). Blurring the boundary: the nuclear envelope extends its reach. Science *318*, 1408-1412.

Stierle, V., Couprie, J., Ostlund, C., Krimm, I., Zinn-Justin, S., Hossenlopp, P., Worman, H.J., Courvalin, J.C., and Duband-Goulet, I. (2003). The carboxyl-terminal region common to lamins A and C contains a DNA binding domain. Biochemistry *42*, 4819-4828.

Stuurman, N., Heins, S., and Aebi, U. (1998). Nuclear lamins: their structure, assembly, and interactions. Journal of structural biology *122*, 42-66.

Su, L.K., Kinzler, K.W., Vogelstein, B., Preisinger, A.C., Moser, A.R., Luongo, C., Gould, K.A., and Dove, W.F. (1992). Multiple intestinal neoplasia caused by a mutation in the murine homolog of the APC gene. Science *256*, 668-670.

Subramanian, A., Tamayo, P., Mootha, V.K., Mukherjee, S., Ebert, B.L., Gillette, M.A., Paulovich, A., Pomeroy, S.L., Golub, T.R., Lander, E.S.*, et al.* (2005). Gene set enrichment analysis: a knowledge-based approach for interpreting genome-wide expression profiles. Proceedings of the National Academy of Sciences of the United States of America *102*, 15545-15550.

Sullivan, T., Escalante-Alcalde, D., Bhatt, H., Anver, M., Bhat, N., Nagashima, K., Stewart, C.L., and Burke, B. (1999). Loss of A-type lamin expression compromises nuclear envelope integrity leading to muscular dystrophy. The Journal of cell biology *147*, 913-920.

Swift, J., Ivanovska, I.L., Buxboim, A., Harada, T., Dingal, P.C., Pinter, J., Pajerowski, J.D., Spinler, K.R., Shin, J.W., Tewari, M.*, et al.* (2013). Nuclear lamin-A scales with tissue stiffness and enhances matrix-directed differentiation. Science *341*, 1240104.

Tang, C.W., Maya-Mendoza, A., Martin, C., Zeng, K., Chen, S., Feret, D., Wilson, S.A., and Jackson, D.A. (2008). The integrity of a lamin-B1-dependent nucleoskeleton is a fundamental determinant of RNA synthesis in human cells. Journal of cell science *121*, 1014-1024.

Tifft, K.E., Bradbury, K.A., and Wilson, K.L. (2009). Tyrosine phosphorylation of nuclear-membrane protein emerin by Src, Abl and other kinases. Journal of cell science *122*, 3780-3790.

Tilli, C.M., Ramaekers, F.C., Broers, J.L., Hutchison, C.J., and Neumann, H.A. (2003). Lamin expression in normal human skin, actinic keratosis, squamous cell carcinoma and basal cell carcinoma. The British journal of dermatology *148*, 102-109.

Towbin, B.D., Gonzalez-Aguilera, C., Sack, R., Gaidatzis, D., Kalck, V., Meister, P., Askjaer, P., and Gasser, S.M. (2012). Step-wise methylation of histone H3K9 positions heterochromatin at the nuclear periphery. Cell *150*, 934-947.

Trapnell, C., Pachter, L., and Salzberg, S.L. (2009). TopHat: discovering splice junctions with RNA-Seq. Bioinformatics *25*, 1105-1111.

Trapnell, C., Williams, B.A., Pertea, G., Mortazavi, A., Kwan, G., van Baren, M.J., Salzberg, S.L., Wold, B.J., and Pachter, L. (2010). Transcript assembly and quantification by RNA-Seq reveals unannotated transcripts and isoform switching during cell differentiation. Nat Biotechnol *28*, 511-515.

Tsai, L.H., and Gleeson, J.G. (2005). Nucleokinesis in neuronal migration. Neuron *46*, 383-388.

Tsuji, Y., Denda, S., Soma, T., Raftery, L., Momoi, T., and Hibino, T. (2003). A potential suppressor of TGF-beta delays catagen progression in hair follicles. J Investig Dermatol Symp Proc *8*, 65-68.

Tunnah, D., Sewry, C.A., Vaux, D., Schirmer, E.C., and Morris, G.E. (2005). The apparent absence of lamin B1 and emerin in many tissue nuclei is due to epitope masking. J Mol Histol *36*, 337-344.

Tzur, Y.B., Wilson, K.L., and Gruenbaum, Y. (2006). SUN-domain proteins: 'Velcro' that links the nucleoskeleton to the cytoskeleton. Nature reviews Molecular cell biology *7*, 782-788.

Utomo, A.R., Nikitin, A.Y., and Lee, W.H. (1999). Temporal, spatial, and cell type-specific control of Cre-mediated DNA recombination in transgenic mice. Nat Biotechnol *17*, 1091-1096.

Vakrakou, A., Devetzi, M., Papachristopoulou, G., Malachias, A., Scorilas, A., Xynopoulos, D., and Talieri, M. (2014). Kallikrein-related peptidase 6 (KLK6) expression in the progression of colon adenoma to carcinoma. Biol Chem *395*, 1105-1117.

Van Berlo, J.H., Voncken, J.W., Kubben, N., Broers, J.L., Duisters, R., van Leeuwen, R.E., Crijns, H.J., Ramaekers, F.C., Hutchison, C.J., and Pinto, Y.M. (2005). A-type lamins are essential for TGF-beta1 induced PP2A to dephosphorylate transcription factors. Human molecular genetics *14*, 2839-2849.

Van Mater, D., Kolligs, F.T., Dlugosz, A.A., and Fearon, E.R. (2003). Transient activation of beta -catenin signaling in cutaneous keratinocytes is sufficient to trigger the active growth phase of the hair cycle in mice. Genes & development *17*, 1219-1224.

Vasioukhin, V., Degenstein, L., Wise, B., and Fuchs, E. (1999). The magical touch: genome targeting in epidermal stem cells induced by tamoxifen application to mouse skin. Proc Natl Acad Sci U S A *96*, 8551-8556.

Vaughan, A., Alvarez-Reyes, M., Bridger, J.M., Broers, J.L., Ramaekers, F.C., Wehnert, M., Morris, G.E., Whitfield, W.G.F., and Hutchison, C.J. (2001). Both emerin and lamin C depend on lamin A for localization at the nuclear envelope. Journal of cell science *114*, 2577-2590.

Venables, R.S., McLean, S., Luny, D., Moteleb, E., Morley, S., Quinlan, R.A., Lane, E.B., and Hutchison, C.J. (2001). Expression of individual lamins in basal cell carcinomas of the skin. British journal of cancer *84*, 512-519.

Vergnes, L., Peterfy, M., Bergo, M.O., Young, S.G., and Reue, K. (2004). Lamin B1 is required for mouse development and nuclear integrity. Proceedings of the National Academy of Sciences of the United States of America *101*, 10428-10433.

Verhagen, A.M., de Graaf, C.A., Baldwin, T.M., Goradia, A., Collinge, J.E., Kile, B.T., Metcalf, D., Starr, R., and Hilton, D.J. (2012). Reduced lymphocyte longevity and homeostatic proliferation in lamin B receptor-deficient mice results in profound and progressive lymphopenia. J Immunol *188*, 122-134.

Vigouroux, C., Magre, J., Vantyghem, M.C., Bourut, C., Lascols, O., Shackleton, S., Lloyd, D.J., Guerci, B., Padova, G., Valensi, P*., et al.* (2000). Lamin A/C gene: sex-determined expression of mutations in Dunnigan-type familial partial lipodystrophy and absence of coding mutations in congenital and acquired generalized lipoatrophy. Diabetes *49*, 1958-1962.

Walter, J., Joffe, B., Bolzer, A., Albiez, H., Benedetti, P.A., Muller, S., Speicher, M.R., Cremer, T., Cremer, M., and Solovei, I. (2006). Towards many colors in FISH on 3D-preserved interphase nuclei. Cytogenet Genome Res *114*, 367-378.

Wang, L.C., Liu, Z.Y., Gambardella, L., Delacour, A., Shapiro, R., Yang, J., Sizing, I., Rayhorn, P., Garber, E.A., Benjamin, C.D*., et al.* (2000). Regular articles: conditional disruption of hedgehog signaling pathway defines its

critical role in hair development and regeneration. The Journal of investigative dermatology *114*, 901-908.

Warren, D.T., Zhang, Q., Weissberg, P.L., and Shanahan, C.M. (2005). Nesprins: intracellular scaffolds that maintain cell architecture and coordinate cell function? Expert reviews in molecular medicine *7*, 1-15.

Waterham, H.R., Koster, J., Mooyer, P., Noort Gv, G., Kelley, R.I., Wilcox, W.R., Wanders, R.J., Hennekam, R.C., and Oosterwijk, J.C. (2003). Autosomal recessive HEM/Greenberg skeletal dysplasia is caused by 3 beta-hydroxysterol delta 14-reductase deficiency due to mutations in the lamin B receptor gene. American journal of human genetics *72*, 1013-1017.

Weber, K., Plessmann, U., and Traub, P. (1989). Maturation of nuclear lamin A involves a specific carboxy-terminal trimming, which removes the polyisoprenylation site from the precursor; implications for the structure of the nuclear lamina. FEBS letters *257*, 411-414.

Weiss, R.A., Eichner, R., and Sun, T.T. (1984). Monoclonal antibody analysis of keratin expression in epidermal diseases: a 48- and 56-kdalton keratin as molecular markers for hyperproliferative keratinocytes. The Journal of cell biology *98*, 1397-1406.

Werner, S., Smola, H., Liao, X., Longaker, M.T., Krieg, T., Hofschneider, P.H., and Williams, L.T. (1994). The function of KGF in morphogenesis of epithelium and reepithelialization of wounds. Science *266*, 819-822.

Willis, N.D., Cox, T.R., Rahman-Casans, S.F., Smits, K., Przyborski, S.A., van den Brandt, P., van Engeland, M., Weijenberg, M., Wilson, R.G., de Bruine, A.*, et al.* (2008). Lamin A/C is a risk biomarker in colorectal cancer. PLoS One *3*, e2988.

Wilson, K.L., and Foisner, R. (2010). Lamin-binding Proteins. Cold Spring Harbor perspectives in biology *2*, a000554.

Wolf, C.M., Wang, L., Alcalai, R., Pizard, A., Burgon, P.G., Ahmad, F., Sherwood, M., Branco, D.M., Wakimoto, H., Fishman, G.I.*, et al.* (2008). Lamin A/C haploinsufficiency causes dilated cardiomyopathy and apoptosis-triggered cardiac conduction system disease. Journal of molecular and cellular cardiology *44*, 293-303.

Worman, H.J. (2012). Nuclear lamins and laminopathies. J Pathol *226*, 316-325.

Worman, H.J., and Bonne, G. (2007). "Laminopathies": a wide spectrum of human diseases. Exp Cell Res *313*, 2121-2133.

Worman, H.J., and Foisner, R. (2010). The nuclear envelope from basic biology to therapy. Biochem Soc Trans *38*, 253-256.

Worman, H.J., Ostlund, C., and Wang, Y. (2010). Diseases of the nuclear envelope. Cold Spring Harbor perspectives in biology *2*, a000760.

Worman, H.J., Yuan, J., Blobel, G., and Georgatos, S.D. (1988). A lamin B receptor in the nuclear envelope. Proceedings of the National Academy of Sciences of the United States of America *85*, 8531-8534.

Xu, X., Lyle, S., Liu, Y., Solky, B., and Cotsarelis, G. (2003). Differential expression of cyclin D1 in the human hair follicle. The American journal of pathology *163*, 969-978.

Yang, L., Guan, T., and Gerace, L. (1997). Lamin-binding fragment of LAP2 inhibits increase in nuclear volume during the cell cycle and progression into S phase. The Journal of cell biology *139*, 1077-1087.

Yang, S.H., Chang, S.Y., Yin, L., Tu, Y., Hu, Y., Yoshinaga, Y., de Jong, P.J., Fong, L.G., and Young, S.G. (2011a). An absence of both lamin B1 and lamin B2 in keratinocytes has no effect on cell proliferation or the development of skin and hair. Human molecular genetics *20*, 3537-3544.

Yang, S.H., Jung, H.J., Coffinier, C., Fong, L.G., and Young, S.G. (2011b). Are B-type lamins essential in all mammalian cells? Nucleus *2*, 562-569.

Yang, S.H., Meta, M., Qiao, X., Frost, D., Bauch, J., Coffinier, C., Majumdar, S., Bergo, M.O., Young, S.G., and Fong, L.G. (2006). A farnesyltransferase inhibitor improves disease phenotypes in mice with a Hutchinson-Gilford progeria syndrome mutation. The Journal of clinical investigation *116*, 2115-2121.

Yao, J., Fetter, R.D., Hu, P., Betzig, E., and Tjian, R. (2011). Subnuclear segregation of genes and core promoter factors in myogenesis. Genes & development *25*, 569-580.

Ye, Q., Callebaut, I., Pezhman, A., Courvalin, J.C., and Worman, H.J. (1997). Domain-specific interactions of human HP1-type chromodomain proteins and inner nuclear membrane protein LBR. The Journal of biological chemistry *272*, 14983-14989.

Zammit, P.S., Partridge, T.A., and Yablonka-Reuveni, Z. (2006). The skeletal muscle satellite cell: the stem cell that came in from the cold. J Histochem Cytochem *54*, 1177-1191.

Zewe, M., Hoger, T.H., Fink, T., Lichter, P., Krohne, G., and Franke, W.W. (1991). Gene structure and chromosomal localization of the murine lamin B2 gene. Eur J Cell Biol *56*, 342-350.

Zhang, H., Kieckhaefer, J.E., and Cao, K. (2013). Mouse models of laminopathies. Aging cell *12*, 2-10.

Zhang, J., Lian, Q., Zhu, G., Zhou, F., Sui, L., Tan, C., Mutalif, R.A., Navasankari, R., Zhang, Y., Tse, H.F.*, et al.* (2011). A human iPSC model of Hutchinson Gilford Progeria reveals vascular smooth muscle and mesenchymal stem cell defects. Cell Stem Cell *8*, 31-45.

Zhang, Q., Ragnauth, C.D., Skepper, J.N., Worth, N.F., Warren, D.T., Roberts, R.G., Weissberg, P.L., Ellis, J.A., and Shanahan, C.M. (2005). Nesprin-2 is a multi-isomeric protein that binds lamin and emerin at the nuclear envelope and forms a subcellular network in skeletal muscle. Journal of cell science *118*, 673-687.

Zhang, Q., Skepper, J.N., Yang, F., Davies, J.D., Hegyi, L., Roberts, R.G., Weissberg, P.L., Ellis, J.A., and Shanahan, C.M. (2001). Nesprins: a novel family of spectrin-repeat-containing proteins that localize to the nuclear membrane in multiple tissues. Journal of cell science *114*, 4485-4498.

Zhang, X., Lei, K., Yuan, X., Wu, X., Zhuang, Y., Xu, T., Xu, R., and Han, M. (2009). SUN1/2 and Syne/Nesprin-1/2 complexes connect centrosome to the nucleus during neurogenesis and neuronal migration in mice. Neuron *64*, 173-187.

Zhang, X., Xu, R., Zhu, B., Yang, X., Ding, X., Duan, S., Xu, T., Zhuang, Y., and Han, M. (2007). Syne-1 and Syne-2 play crucial roles in myonuclear anchorage and motor neuron innervation. Development *134*, 901-908.

Zhang, Y.Q., and Sarge, K.D. (2008). Sumoylation regulates lamin A function and is lost in lamin A mutants associated with familial cardiomyopathies. The Journal of cell biology *182*, 35-39.

Zheng, R., Ghirlando, R., Lee, M.S., Mizuuchi, K., Krause, M., and Craigie, R. (2000). Barrier-to-autointegration factor (BAF) bridges DNA in a discrete, higher-order nucleoprotein complex. Proceedings of the National Academy of Sciences of the United States of America *97*, 8997-9002.

Zink, D., Fischer, A.H., and Nickerson, J.A. (2004). Nuclear structure in cancer cells. Nature reviews Cancer *4*, 677-687.

Zullo, J.M., Demarco, I.A., Pique-Regi, R., Gaffney, D.J., Epstein, C.B., Spooner, C.J., Luperchio, T.R., Bernstein, B.E., Pritchard, J.K., Reddy, K.L.*, et al.* (2012). DNA sequence-dependent compartmentalization and silencing of chromatin at the nuclear lamina. Cell *149*, 1474-1487.

Zwerger, M., Jaalouk, D.E., Lombardi, M.L., Isermann, P., Mauermann, M., Dialynas, G., Herrmann, H., Wallrath, L.L., and Lammerding, J. (2013). Myopathic lamin mutations impair nuclear stability in cells and tissue and disrupt nucleo-cytoskeletal coupling. Human molecular genetics *22*, 2335-2349.

APPENDICES

Expression (FPKM) of Genes
Covered by GOC GO:0008307
Structural Constituent of Muscle, Related to Figures 4.8
only genes with non-zero expression are shown

	Myoblasts					Limb muscles		
	Lmna		*Lbr*			*Lmna*		*Lbr*
	KO	WT	KO	WT		KO	WT	KO
Actn2	0.59	3.39	6.10	1.97		940.06	609.04	622.49
Actn3	1.24	4.54	8.00	3.00		1073.66	1206.24	1171.46
Ankrd2	0.10	0.22	0.88	0.23		83.81	32.32	36.71
Asph	29.93	28.84	36.07	34.73		184.44	165.27	175.48
Capn3	0.05	0.58	2.20	0.46		23.57	33.97	29.86
Dag1	68.52	61.61	58.41	54.30		50.99	47.06	38.57
Dmd	7.91	7.01	7.95	8.60		48.25	43.60	42.84
Jph1	2.21	2.10	3.41	2.67		40.22	40.87	36.33
Krt19	26.25	17.33	7.44	5.45		0.49	0.99	0.78
Mybpc1	0.11	1.74	4.39	1.29		508.70	263.51	298.83
Mybpc2	0.02	0.05	0.13	0.06		731.24	991.51	1152.91
Mybph	0.50	9.31	9.08	4.43		103.91	204.25	152.98
Myh11	15.68	14.34	13.76	11.61		23.68	26.03	18.73
Myh2	0.06	0.77	1.43	0.60		710.92	589.01	617.86
Myh4	0.04	0.61	1.55	0.55		9782.86	12587.00	13015.30
Myh6	0.03	0.13	0.07	0.05		9.30	19.10	22.17
Myh7	0.07	0.79	0.92	0.39		99.28	130.29	148.25
Myh8	0.43	4.94	13.39	3.67		617.67	580.59	480.81
Myl1	3.43	31.99	61.29	20.12		15323.10	17287.30	20558.90
Myl2	0.27	1.17	1.03	0.19		127.31	220.80	270.21
Myl4	8.10	46.73	74.36	23.31		8.94	11.50	10.76
Myl6	283.98	245.45	152.79	135.19		208.72	265.15	250.32
Myl6b	9.74	16.89	22.15	10.88		46.88	38.52	43.86
Myl9	1064.41	807.9	495.5	461.1		95.54	191.28	183.77

		3	9	0				
Mylpf	18.69	119.06	195.72	57.53		6090.17	7984.37	8909.78
Myom1	5.00	5.72	3.52	3.79		209.33	175.56	156.56
Myom2	0.02	0.80	1.81	0.50		361.25	313.96	331.71
Myot	0.07	0.72	1.51	0.43		509.58	299.01	336.97
Neb	1.44	3.27	9.38	3.78		1018.04	1044.35	1107.44
Nebl	0.37	0.48	0.37	0.61		0.46	0.41	0.16
Nexn	24.66	28.10	44.52	42.72		126.76	140.47	179.70
Obscn	0.02	0.13	0.32	0.09		90.80	67.53	62.48
Pdlim3	1.06	5.28	8.29	3.08		243.15	221.76	256.16
Plec	50.58	48.81	41.58	44.52		133.32	96.67	91.53
Smtn	55.78	53.66	39.44	38.76		40.29	49.27	41.45
Sorbs2	2.29	2.06	2.85	1.85		5.24	4.54	3.59
Synm	0.34	0.57	0.51	0.80		24.05	25.24	28.12
Tcap	0.13	1.01	2.08	0.39		423.62	216.30	266.53
Tpm2	739.47	705.35	460.99	485.72		3426.35	2937.79	3198.86
Tpm3	183.94	177.29	169.51	145.75		73.44	68.06	80.54
Ttn	0.19	0.95	2.13	0.75		862.21	940.31	920.35

Appendix A: Gene list of structural constituent of muscle (GO: 0008307).

Expression (FPKM) of Genes
Covered by GOC GO:0051146
Striated Muscle Cell Differentiation, Related to Figures 4.8
only genes with non-zero expression are shown

	Myoblasts					Limb muscles		
	Lmna		*Lbr*			*Lmna*		
	KO	WT	KO	WT		KO	WT	*Lbr* KO
Acadm	10.73	10.18	12.72	13.44		46.09	82.57	52.23
Acta1	32.47	52.60	62.51	25.55		16909.60	13887.00	17214.80
Actc1	24.91	77.96	146.81	36.67		4741.20	1642.43	6500.62
Actg1	1144.69	1051.84	777.98	733.65		222.22	209.26	245.47
Afg3l2	25.11	22.95	22.86	22.04		23.73	24.20	24.43
Agrn	9.62	9.68	7.50	8.24		4.38	5.73	3.72
Agt	0.18	0.10	0.14	0.03		6.24	8.12	4.35
Akt1	91.26	93.20	70.79	78.99		35.02	28.60	29.15
Als2	5.50	4.16	4.75	5.17		4.28	5.36	3.64
App	151.61	147.76	147.92	136.28		51.17	59.77	53.67
Atg5	10.53	9.66	10.45	9.74		3.07	3.86	3.47
Atg7	6.39	5.17	4.73	4.25		2.06	2.32	3.04
Bcl2	6.19	5.55	5.33	5.02		2.52	2.40	1.49
Bcl9	9.58	7.40	8.73	10.20		2.13	2.35	1.41
Bcl9l	22.85	21.83	17.85	20.38		7.93	8.31	5.41
Bhlhe41	3.05	2.70	2.72	2.87		0.94	0.72	1.59
Bmp2	0.10	0.20	0.27	0.17		0.65	0.70	0.85
Bmp4	4.78	5.37	12.62	3.73		1.69	1.28	2.57
Bnip2	98.89	96.88	100.06	103.20		32.52	26.74	32.04
Boc	6.50	6.46	4.86	4.69		2.53	3.32	2.39

Btg1	10.50	10.01	9.66	8.36	6.44	6.68	5.07
Cacnb4	0.58	0.40	0.36	0.51	0.28	0.45	0.28
Cacybp	31.42	34.67	40.49	44.21	7.59	8.87	10.74
Capn2	290.93	278.61	205.21	263.00	31.58	33.92	36.63
Capn3	0.05	0.58	2.06	0.46	33.97	23.57	29.86
Casp1	2.17	3.62	3.80	1.15	1.02	1.43	0.60
Cav2	8.07	7.51	8.28	8.61	21.17	27.86	24.60
Cav3	0.38	3.55	4.35	1.56	112.06	92.77	102.04
Cby1	8.51	7.53	5.79	5.10	3.82	3.73	3.52
Cdh2	57.37	54.78	45.69	54.80	2.43	2.53	2.32
Cdon	12.37	12.84	15.57	15.50	6.71	6.11	6.32
Chrna1	2.67	9.69	14.13	6.48	8.22	6.68	6.12
Chrnb1	4.22	4.10	5.03	3.52	29.95	26.60	34.58
Chuk	11.60	12.26	19.63	18.97	4.52	7.63	4.95
Col4a1	149.47	122.62	105.40	86.12	101.83	95.94	101.60
Col4a5	7.98	6.30	5.70	5.45	1.37	1.16	1.23
Cxadr	1.29	1.27	5.37	2.28	0.57	0.69	0.59
Ddx17	74.96	82.07	102.25	103.56	58.32	65.36	49.45
Dicer1	10.68	9.91	14.01	14.46	6.47	5.93	6.05
Dmpk	5.48	5.42	5.50	3.13	93.92	100.11	94.08
Dnaja3	12.17	12.76	11.67	11.43	42.01	40.70	47.48
Dner	0.57	0.19	0.52	0.30	0.43	0.31	0.68
Dok7	0.08	0.19	0.27	0.09	1.55	2.28	1.53
Dvl1	6.67	7.03	5.87	5.50	22.97	23.49	21.47
Dyrk1b	3.05	2.98	3.18	2.49	37.29	31.19	25.88

Edn1	13.56	5.99	4.54	5.19		1.49	2.81	1.39
Emd	87.38	75.02	53.37	51.55		3.53	2.22	3.73
Epc1	12.83	13.67	15.40	15.47		9.75	11.10	7.70
Erbb2	7.95	8.25	7.02	7.40		1.51	1.92	1.44
Ezh2	27.09	26.09	27.58	27.04		5.98	5.30	4.35
F2r	278.13	214.60	287.10	221.24		10.05	11.72	8.65
Fbxo22	37.71	39.19	36.74	37.60		15.71	17.99	17.19
Fdps	21.65	16.40	17.49	15.68		18.71	14.31	19.79
Fgfr2	8.15	7.88	7.54	7.28		0.54	0.97	0.61
Fhod3	0.28	0.47	0.57	0.36		5.36	4.50	7.35
Flnc	39.18	29.89	25.32	24.36		53.21	71.76	58.96
Foxp1	22.67	22.68	29.82	31.88		4.59	4.72	3.03
Gata6	3.55	2.19	6.35	3.01		1.02	0.85	1.03
Gphn	4.88	5.80	7.10	6.76		10.63	10.58	10.29
Gpx1	274.67	254.86	170.95	150.88		92.10	86.25	86.35
Gsk3a	29.69	26.79	23.81	25.20		24.13	27.49	19.77
Gsk3b	39.41	42.37	48.37	53.10		5.65	6.46	5.82
Hdac4	6.94	6.20	6.94	6.53		12.23	9.29	9.30
Hdac5	8.13	7.46	7.89	7.30		13.68	19.04	10.56
Hdac9	0.61	0.60	1.27	0.61		2.60	2.65	2.38
Hey2	1.98	2.67	1.34	2.25		0.84	0.98	0.80
Hmgb1	24.73	26.72	32.34	32.40		44.89	44.85	43.37
Homer1	6.07	5.63	8.33	7.61		17.93	17.87	20.52
Hopx	0.33	0.29	0.32	0.34		7.32	5.54	6.93
Igf1	16.86	17.26	20.23	10.37		18.22	13.55	15.92

Igf2	114.41	63.06	171.07	72.85	437.45	495.32	395.91
Igf2bp3	11.77	9.94	12.70	11.30	2.22	1.33	1.53
Igfbp5	32.87	28.92	32.83	44.53	196.17	60.85	155.54
Ilk	236.63	202.28	164.70	154.50	39.58	36.67	36.45
Itgb1	400.30	392.16	402.26	444.74	71.21	74.33	62.72
Itgb1bp3	0.11	0.87	0.60	0.20	23.20	27.13	24.69
Kras	28.19	32.11	45.47	37.76	8.00	7.98	7.38
Krt19	26.25	17.33	7.44	5.45	0.99	0.49	0.78
Ky	0.02	0.06	0.08	0.04	50.06	23.75	40.62
Lamb2	15.83	17.61	12.22	12.48	23.59	23.75	18.39
Lef1	2.56	2.83	1.46	1.84	1.20	0.84	0.25
Lemd2	9.65	8.72	8.03	7.24	9.38	9.95	7.37
Lemd3	3.40	4.14	4.52	4.87	2.30	3.12	2.43
Lrp4	1.20	1.02	1.61	1.54	4.62	6.04	3.75
Lrrk2	6.03	6.08	9.07	11.55	2.14	3.14	2.21
Maml1	15.54	15.29	14.71	13.10	3.16	3.28	2.81
Mamstr	0.34	0.25	0.51	0.26	19.97	14.14	18.33
Mapk14	34.05	30.82	26.36	25.42	31.36	32.03	28.27
Mbnl3	3.83	3.49	7.81	6.31	1.33	1.08	1.09
Mef2a	20.31	20.23	36.63	29.05	16.70	18.02	14.23
Mef2c	2.50	5.45	13.29	6.62	71.18	67.40	69.06
Met	4.90	4.52	6.45	6.61	2.60	3.05	2.61
Msx1	1.52	1.77	0.88	1.95	1.32	1.75	1.28
Murc	2.80	6.03	12.21	6.00	78.30	76.54	75.38
Musk	0.14	0.64	2.00	0.86	6.58	6.79	4.99

Myh10	52.35	55.55	64.40	65.10	9.15	11.83	11.52
Myh11	15.68	14.34	13.76	11.61	26.03	23.68	18.73
Myh6	0.03	0.13	0.07	0.05	19.10	9.30	22.17
Myh9	269.81	251.20	223.55	251.97	55.35	54.26	45.18
Myl2	0.27	1.17	1.03	0.19	220.80	127.31	270.21
Mylk2	0.54	0.39	0.45	0.54	56.96	106.74	57.04
Myo18b	0.06	0.23	0.39	0.14	62.25	71.82	64.65
Myocd	2.37	1.95	1.21	1.39	0.64	1.11	0.26
Myod1	2.09	5.35	5.51	2.46	17.83	16.44	18.13
Myog	2.89	7.47	10.50	2.94	48.62	28.69	42.89
Mypn	0.09	0.66	1.28	0.27	93.07	89.00	79.05
Neb	1.44	3.27	9.38	3.78	1044.35	1018.04	1107.44
Nebl	0.37	0.48	0.37	0.61	0.41	0.46	0.16
Neo1	39.86	38.59	34.94	36.00	11.36	11.60	8.47
Neurl2	0.92	0.94	0.74	0.48	14.71	15.07	20.51
Notch1	5.73	4.67	4.37	4.16	5.80	5.95	4.85
Ntn3	0.04	0.29	0.08	0.10	0.37	0.29	0.31
Nupr1	81.34	66.17	48.14	42.87	26.43	29.40	16.94
Pak1	18.50	18.80	22.98	22.09	71.59	38.37	55.26
Pdgfra	10.81	9.53	17.71	14.13	8.99	9.09	6.95
Pdgfrb	71.12	68.08	71.20	66.08	13.58	14.76	10.80
Pdzrn3	49.40	41.77	65.51	66.46	7.50	8.34	7.75
Pik3r1	12.69	12.11	17.89	16.46	7.78	7.14	5.04
Pitx2	0.56	0.66	1.72	1.31	4.83	7.20	6.17
Plcb1	0.74	1.06	1.29	1.92	2.23	2.25	1.89

Ppp3ca	23.83	23.45	41.89	38.82	29.40	33.96	31.17
Prl2c2	0.96	0.71	1.08	1.96	1.14	1.41	1.13
Prox1	0.67	0.69	1.36	0.80	4.29	3.01	2.94
Ptcd2	14.29	16.31	14.67	13.26	21.56	18.79	23.64
Rara	28.82	26.62	20.86	21.98	8.96	9.07	7.62
Rarb	1.47	1.01	2.23	1.20	2.01	1.89	2.24
Rbm24	0.84	2.05	4.70	1.59	32.86	41.92	32.46
Rbm38	3.96	3.08	2.93	1.81	43.08	57.69	38.80
Rcan1	14.32	14.20	13.78	16.00	15.29	21.40	26.10
Rxra	9.92	8.77	7.15	7.45	10.53	11.62	7.97
Rxrb	5.34	5.16	4.81	3.97	5.10	6.75	3.12
Ryr1	0.12	0.53	1.00	0.26	198.72	236.35	168.19
S100b	0.86	0.70	0.88	0.35	3.26	1.44	2.94
Shox2	11.83	8.13	9.58	9.21	1.14	1.49	0.98
Sik1	8.97	6.93	8.28	6.81	5.99	5.66	4.61
Ski	45.16	47.41	42.76	43.28	21.75	22.21	16.54
Slc8a1	1.92	2.24	2.52	2.11	1.53	1.49	1.64
Snta1	9.93	9.34	8.79	9.13	53.79	76.61	47.46
Sort1	2.02	1.31	2.00	1.41	13.85	10.91	10.87
Sox8	1.57	2.04	1.41	1.69	5.86	3.76	5.05
Sox9	9.87	6.56	7.55	8.89	0.80	1.12	1.35
Srf	27.64	19.64	13.41	13.43	7.70	7.43	6.70
Tbx3	13.51	12.61	11.25	14.32	1.86	1.86	1.74
Tbx5	1.24	1.70	1.64	3.22	0.15	0.12	0.22
Tcap	0.13	1.01	2.08	0.39	216.30	423.62	266.53

Tgfb1	18.64	16.85	16.16	15.75	5.18	5.74	3.61
Thra	5.12	4.50	5.52	4.39	15.57	20.59	11.91
Tmod1	0.99	1.84	2.51	1.44	145.34	107.20	136.14
Tnc	456.17	300.75	296.64	285.28	4.66	7.79	6.53
Tnnt2	10.75	33.62	71.27	22.50	26.35	22.29	27.71
Tsc1	3.98	3.70	4.63	3.81	4.21	6.00	4.72
Ttn	0.19	0.95	2.13	0.75	940.31	862.21	920.35
Utrn	31.13	26.39	36.47	36.45	20.80	20.11	16.71
Vegfa	57.25	55.25	56.66	60.81	42.23	54.55	45.93
Xirp1	0.31	1.54	2.79	1.17	18.80	37.79	31.14
Ybx1	296.54	274.56	282.49	281.50	98.91	99.38	94.24
Zfhx3	17.12	17.72	19.46	19.34	2.65	2.77	2.47

Appendix B: Gene list of striated muscle cell differentiation (GO: 0051146).

PATHOLOGY REPORT

Company/ RI_Colin Stewart/IMB_____ Requestor _Audrey Wang_____

Study Number_____ Histology Number_0101-13_____

Study Title_____

SUMMARY

Four mouse skin slides (including one wild type) stained with H&E were histopathologically evaluated. Compared to the skin of the wild type littermate, all three skin samples from knockout (KO) mice revealed similar histopathological changes. In general, there was diffuse epidermal thickening (an average of 2 to 3-fold) with basophilia of epithelial cells (hyperplasia) and occasional mitosis (No 238). Diffusely, there was sebaceous gland hyperplasia leading to expansion of the dermis. The hyperplastic sebaceous glands were well differentiated and did not exhibit glandular atypia or dysplasia. The hair follicles in the KO mice were either in the early stage of telogen-anagen transition or in anagen phase. Compared to telogen hair follicle in wild type, the hair follicles in telogen-anagen transition phase were present in deep dermis or reaching the junction with subcutis in KO mice. In two KO mice (No. 235 and 237), the hair follicles are multifocally in anagen phase and residing mainly in the subcutis.

COMMENTS

In addition to the above mentioned changes, the hair follicles appeared prominent in KO mice. This change could be due to the active status of the hair follicle in these animals.

_____   19/02/13

Dr Muthafar Al-Haddawi BVM&S, MSc, DVSc, PhD, Diplomate ACVP   Date
Senior Veterinary Pathologist

Appendix C: Pathology report on skin and hair histomorphology of $Lmna^{\Delta/\Delta K14\text{-}Cre}$ mice.